

Aus dem Institut für Pathologie
der Medizinischen Fakultät Charité – Universitätsmedizin Berlin

DISSERTATION

Understanding treatment resistance in head and neck cancer,
lymphoma and neuroblastoma through omics data analysis in
a translational oncology setting.

Charakterisierung der Behandlungsresistenz bei Kopf- und Halskrebs,
Lymphomen und Neuroblastomen
durch die Analyse von Omics-Daten.

zur Erlangung des akademischen Grades

Doctor rerum medicinalium (Dr. rer. medic.)

vorgelegt der Medizinischen Fakultät
Charité – Universitätsmedizin Berlin

von

Clemens Messerschmidt

Erstbetreuung: Prof. Dr. Nils Blüthgen

Datum der Promotion: 29.11.2024

Contents

List of Abbreviations	i
List of Figures	iii
List of Tables	v
Abstract	1
Zusammenfassung	3
1 Introduction	5
1.1 Precision medicine in oncology	5
1.1.1 Cancer treatment	5
1.1.2 Making cancer treatment decisions	6
1.2 Treatment resistance	6
1.3 Biomarkers	7
1.3.1 Omics data analysis	7
1.3.2 Small somatic variants	8
1.3.3 Copy number variation	8
1.3.4 Signatures	8
1.4 Translational research enables better precision medicine	9
1.4.1 Cancer models	9
2 Distinct immune evasion in APOBEC-enriched, HPV-negative HNSCC	11
2.1 Introduction	11
2.1.1 Overview and contributions	11
2.1.2 Head and neck squamous cell cancer	12
2.1.3 Immune checkpoint inhibition	12
2.1.4 APOBEC3 enzymes and their mutational patterns	12
2.1.5 Signatures for mutational processes	13
2.2 Data	13
2.2.1 The Cancer Genome Atlas: HNSCC cohort	13
2.2.2 DKTK Master cohort	15
2.2.3 Single cell transcriptomics dataset	15
2.3 Methods	15
2.3.1 HPV status	15
2.3.2 TCW mutation enrichment	15
2.3.3 Inflammation scoring of tumors	16

2.3.4	Differential expression analysis	16
2.3.5	Analysis of immunotherapy relevant genes	16
2.3.6	Single cell transcriptomics analysis	16
2.4	Results	16
2.5	Discussion	22
3	Acquired resistance to DZNep-mediated apoptosis is associated with copy number gains of AHCY in a B-cell lymphoma model	23
3.1	Introduction	23
3.1.1	Overview and contributions	23
3.1.2	Molecular characteristics of Burkitt lymphoma	23
3.1.3	EZH2 inhibition	24
3.2	Data and Methods	25
3.2.1	Generation of a DZnep resistant cell line	25
3.2.2	Whole-exome sequencing analysis	25
3.2.3	Copy number analysis	25
3.3	Results	25
3.4	Discussion	27
4	Neuroblastoma signaling models unveil combination therapies targeting feedback-mediated resistance	29
4.1	Introduction	29
4.1.1	Overview and contributions	29
4.1.2	Neuroblastoma	29
4.1.3	The Ras/MAPK pathway	30
4.1.4	Mutations in MAPK signaling in high risk neuroblastoma	31
4.1.5	Cell line identification	31
4.2	Methods	31
4.2.1	Cell lines	31
4.2.2	Sequencing	32
4.2.3	Read mapping and variant calling	32
4.2.4	Matching cell lines with public databases	32
4.2.5	Prioritization of cancer-related variants	32
4.2.6	Drug sensitivity screen and signaling modeling	32
4.3	Results	33
4.4	Discussion	34
5	Extended Discussion	37
5.1	Translation in precision oncology	37
5.2	Reproducibility in translational research	38
5.2.1	Open research: open access, open data, open source	38
	References	41
	Eidesstattliche Versicherung	57
	Anteilerklärung an den aufgelisteten Publikationen	59
	Publikation 1	59
	Publikation 2	59

<i>CONTENTS</i>	iii
Publikation 3	60
Druckexemplar der Publikation Messerschmidt et al. 2020	61
Druckexemplar der Publikation Akpa et al. 2020	73
Druckexemplar der Publikation Dorel et al. 2021	87
Lebenslauf	115
Komplette Publikationsliste	117
Danksagung	119

List of Abbreviations

Abbreviation	Definition
AHCY	Adenosylhomocysteinase
ALK	Anaplastic Lymphoma Kinase
APOBEC	Apolipoprotein B mRNA Editing Catalytic Polypeptide-like
CNV	Copy Number Variant
DKTK	Deutsches Konsortium für Translationale Krebsforschung
DZnep	3-Deazaneplanocin A
EGF	Epidermal Growth Factor
ENA	European Nucleotide Archive
ER	Estrogen Receptor
EZH2	Enhancer Of Zeste 2 Polycomb Repressive Complex 2 Subunit
FDA	Food and Drug Administration
GEO	Gene Expression Omnibus
HNSCC	Head and Neck Squamous Cell Carcinoma
HPV	Human Papillomavirus
ICI	Immune Checkpoint Inhibition
ICMJE	International Committee of Medical Journal Editors
MAPK	Mitogen-Activated Protein Kinase
MTB	Molecular Tumor Board
PCAWG	Pan-Cancer Analysis of Whole Genomes
PDX	Patient Derived Xenograft
SAH	S-adenosylhomocysteine
TCGA	The Cancer Genome Atlas
TERT	Telomerase Reverse Transcriptase
TMB	Tumor Mutational Burden
VCF	Variant Call File
WES	Whole-exome Sequencing
WGS	Whole-genome Sequencing

List of Figures

2.1	Sketch of a simple model of APOBEC3 activation as a self-reinforcing process.	13
2.2	Mutational probabilities for signature 2 from COSMIC mutational signatures.	14
2.3	Mutational probabilities for signature 13 from COSMIC mutational signatures.	14
2.4	IFNG signature score is not associated with number of total mutations, but with number of TCW mutations in the TCGA HNSCC cohort.	17
2.5	HPV status is an important variable in HNSCC.	18
2.6	HPV-negative/APOBEC3-enriched tumors show higher inflammation, differential checkpoint inhibition when compared to other HPV-negative tumors. .	20
2.7	Single cell expression data from an independent cohort demonstrates APOBEC3 expression in tumor cells.	21
2.8	Analysis of IFNG score by APOBEC status in HPV-negative DKTK Master patients.	22
3.1	Structural similarity of a DZnep and b S-adenosylhomocysteine (SAH). . . .	24
3.2	<i>AHCY</i> copy number amplification found in the DZnep-resistant cell culture.	26
4.1	Ras/MAPK pathway representation extracted from the literature for modeling.	33
4.2	Mutations insufficiently explain drug sensitivity in high risk neuroblastoma cell lines.	35

List of Tables

- 2.1 Results of Fisher exact tests for enrichment of mutations in immunotherapy-relevant genes as defined by Patel et al., once with HLA genes and once without to exclude possible false positive variant calls in these loci. 18
- 4.1 Top Uniquorn results for cell line LAN6 when compared to the COSMIC cell line database. 33

Abstract

In this thesis, I present my contributions to three publications in the field of translational precision oncology. What all three presented studies have in common is that they elucidate mechanisms that influence drug resistance, which is one of the major reasons why cancer ultimately proves lethal. Through technical and methodical advances, understanding of the inner workings of cancer cells is continuously improving even after decades of research. This progress allows for better treatment, tailored specifically for every patient. But as treatment puts pressure onto a tumor, resistance might eventually develop and the tumor relapses. For optimal treatment outcome, it is therefore important to use an effective drug while at the same time monitoring for the emergence of resistance and counteract it.

The first publication, *Distinct immune evasion in APOBEC-enriched, HPV-negative HNSCC*, is the result of our interest in identifying possible markers for immune checkpoint inhibition in head and neck tumors, an area of study at Charité Comprehensive Cancer Center. Using open data from TCGA, we analyzed 496 tumors and evaluated their HPV status, mutational signatures, gene expression signatures as well as mutational load. We were able to define a subgroup with a distinct immune profile in HPV-negative tumors that shows increased inflammation, which correlates with the footprint of APOBEC3-associated single-nucleotide mutations. Further, in these tumors we observed a higher frequency in mutations that allow immune-evasion. In a separate single cell expression dataset, we show mRNA expression of APOBEC3 family members in tumor cells for the first time. Previously, it was not clear if APOBEC3 was expressed by the tumor cells or only in the surrounding tumor micro-environment, as APOBEC3 proteins are notoriously difficult to stain with antibodies.

The publication by Akpa et al., *Acquired resistance to DZNep-mediated apoptosis is associated with copy number gains of AHCY in a B-cell lymphoma model*, describes how we engineered a B-cell lymphoma cell line to become resistant against the drug DZnep. By analyzing whole-exome data and comparing the resistant with sensitive cells, we were able to pinpoint a gene amplification of the gene AHCY, which is exactly the gene inhibited by DZnep. Thus, we have shown one possible avenue for development of resistance even before DZnep has been used in clinical studies.

The final publication by Dorel et al., *Neuroblastoma signaling models unveil combination therapies targeting feedback-mediated resistance*, describes our efforts to model Ras/MAPK pathway activity in a panel of nine cell lines representative of high risk neuroblastoma. Through molecular characterization and pathway modeling on perturbation-response data we were able to formulate new treatment strategies that work by vertical inhibition on multiple pathway targets. By combining targeted drugs in such a deliberate manner, treatment outcomes will improve in the future.

Zusammenfassung

In dieser Arbeit stelle ich meine Beiträge zu drei Veröffentlichungen im Bereich der translationalen Präzisionsonkologie vor. Allen drei Studien ist gemeinsam, dass sie Mechanismen aufklären, die Arzneimittelresistenzen beeinflussen. Durch technische und methodische Fortschritte wird das Wissen über das Innenleben von Krebszellen auch nach Jahrzehnten der Forschung immer besser. Dieser Fortschritt ermöglicht eine Behandlung, die speziell auf jeden Patienten zugeschnitten ist. Da die Behandlung jedoch Druck auf den Tumor ausübt, kann sich schließlich eine Resistenz entwickeln. Für ein optimales Behandlungsergebnis ist es daher wichtig, ein wirksames Medikament einzusetzen und gleichzeitig die Entstehung von Resistenzen zu überwachen und ihnen entgegenzuwirken.

Die erste Publikation, *Distinct immune evasion in APOBEC-enriched, HPV-negative HNSCC*, beschreibt einen möglichen Marker für die Antwort auf Immun-Checkpoint-Inhibition bei Kopf-Hals-Tumoren. Wir analysierten 496 Tumore und werteten ihren HPV-Status, Mutationssignaturen, Genexpressionssignaturen sowie die Mutationslast aus. Wir definieren eine Untergruppe mit einem ausgeprägten Immunprofil in HPV-negativen Tumoren, die erhöhte Entzündungswerte aufweist, welche mit APOBEC3-assoziierten Einzelnukleotidmutationen korreliert. Außerdem beobachteten wir in diesen Tumoren eine höhere Häufigkeit von Mutationen, die eine Umgehung des Immunsystems ermöglichen. In einem separaten single-cell Datensatz zeigen wir mRNA-Expression von APOBEC3 in Tumorzellen. Bisher war nicht klar, ob APOBEC3 von den Tumorzellen oder nur in der Tumorumgebung exprimiert wird, da APOBEC3-Proteine mit Antikörpern schwer zu färben sind.

Die Veröffentlichung von Akpa et al, *Erworbene Resistenz gegen DZNep-vermittelte Apoptose steht in Verbindung mit Kopienzahlgewinnen von AHCY in einem B-Zell-Lymphom-Modell*, beschreibt, wie wir eine B-Zell-Lymphom-Zelllinie so verändert haben, dass sie gegen das Medikament DZnep resistent wurde. Durch die Analyse von Whole-Exom-Daten und den Vergleich der resistenten mit den empfindlichen Zellen konnten wir eine Genamplifikation des Gens AHCY nachweisen, das genau das Gen ist, das von DZnep gehemmt wird. Damit haben wir einen möglichen Weg für die Entwicklung einer Resistenz aufgezeigt, noch bevor DZnep in klinischen Studien eingesetzt wurde.

Die letzte Veröffentlichung von Dorel et al, *Neuroblastoma signaling models unveil combination therapies targeting feedback-mediated resistance*, beschreibt unsere Bemühungen, die Aktivität des Ras/MAPK-Signalwegs in einer Gruppe von neun Zelllinien zu modellieren, die für das Hochrisiko-Neuroblastom repräsentativ sind. Durch molekulare Charakterisierung und Modellierung der Signalwege auf der Grundlage von Perturbationsdaten waren wir in der Lage, neue Behandlungsstrategien zu formulieren, die durch vertikale Hemmung mehrerer Targets wirken. Durch eine solche gezielte Kombination von Medikamenten werden sich die Behandlungsergebnisse in Zukunft verbessern.

Chapter 1

Introduction

In this dissertation, I present my contributions to three publications in the field of translational precision medicine where omics data analysis was used to pinpoint characteristics of cancer cells to help understand treatment resistance. In this chapter, I introduce key concepts and methods in precision oncology (Sec. 1.1), treatment resistance (Sec. 1.2), biomarkers (Sec. 1.3), and translational research (Sec. 1.4). Then follow three chapters, each based on a peer-reviewed publication. In Chapter 2, we show how a subgroup of HPV-negative tumors of the head and neck have high proportions of APOBEC3-associated mutations that potentially influence sensitivity to immunotherapy. In Chapter 3, we discuss how analysis of whole-exome data helped to identify an escape mechanism to EZH2 inhibition treatment in a lymphoma cell line. In Chapter 4, I present my contributions to a study concerning the genetic makeup of neuroblastoma cell lines and how it influences treatment response for a selected panel of drugs targeting the Ras/MAPK pathway. The final chapter concludes the thesis with an extended discussion.

1.1 Precision medicine in oncology

Precision medicine in the context of oncology means to treat each patient's tumor based on its respective characteristics such as mutations, fusion genes, or hyper-active pathways. While these aberrations give the tumor its vigor in the first place, they can also be prime targets for treatment (Lassen et al., 2021). This approach requires interdisciplinary decision making and close collaboration between oncologists, pathologists, molecular biologists, and more recently, bioinformaticians. This team effort is necessary because how to treat a cancer patient is not an easy decision to take. Primarily, for optimal outcome, one wants to select the treatment that works best, e.g. the one with the highest chance to either cure the cancer, shrink the tumor or stop progression. Secondly, drugs have unwanted side-effects, so one would only chose a drug if one can be reasonably sure that the advantages outweigh the downsides. And lastly, time is of the essence. It is a waste of money, and worse, the patient's time, to try a drug that does not work. Even giving the "correct" drug later will not correct the outcome as disease will have progressed.

1.1.1 Cancer treatment

Over time, the preferred cancer treatment options have shifted from unspecific cytostatic or cytotoxic agents, colloquially called chemotherapy, to targeted drugs (Kummar et al., 2006).

One drawback of unspecific agents is that they usually have more side effects and higher toxicity as they affect both healthy and tumor cells. On the other hand, targeted agents interfere with a molecular target that is in some way involved in processes such as cancer growth, survival, or metabolism (Hanahan and Weinberg, 2000). In other words, it means to attack a process that is vital for one tumor specifically.

To name one example, the first targeted drug approved by the U.S. Food and Drug Administration (FDA) was Tamoxifen (Yan et al., 2011). It competes with estrogen when binding to the estrogen receptor (ER). For breast cancer, depending on the cohort between ca. 65 and 80 percent of tumors are estrogen receptor-positive (Kohler et al., 2015), which makes these tumors susceptible to treatment with Tamoxifen. On the other hand, tumors that are not addicted to the constant signaling downstream of ER should be treated differently. It is therefore imperative to match known biomarkers of each tumor with available drugs for optimal treatment responses. A dedicated section on biomarkers (sec. 1.3) gives a formal definition of what a biomarker is and discusses which types of biomarkers are commonly used in the clinic.

1.1.2 Making cancer treatment decisions

To understand why researchers try to find new biomarkers, it is beneficial to briefly look at the treatment decision process in practice. We have documented our own experience on how to support decision making at the Molecular Tumor Board (MTB) of the Charité Comprehensive Cancer Center (Lamping et al., 2020), and I want to give a brief summary here. During our meetings, for every patient known tumor characteristics were presented, e.g. surgical and pathology reports as well as molecular readouts. This was followed by a discussion on which treatment course to choose. The following steps had to be completed to arrive at a recommendation:

- 1) Identify molecular aberrations in the tumor.
- 2) Match all identified aberrations to drugs, including information on sensitivity or resistance based on prior knowledge.
- 3) Discuss and rank all options and decide which drug to give.

Generally, based on whole-exome sequencing data, most tumors show a large number of mutations or copy number changes that do not have corresponding information in any of the consulted databases yet. Without this information, aberrations cannot be used in decision making yet.

1.2 Treatment resistance

Treatment resistance in the context of cancer means that the tumor is or becomes tolerant to the treatment, rendering it ineffective. This means that the disease will progress and that other options will need to be pursued, given that not all alternatives have been exhausted already. As discussed in the ER example (sec. 1.1.1), it is imperative to pick a treatment that has a high chance of success in the first place, given everything one knows about a particular tumor. While most tumors respond at first, they are a dynamic system that can and will evolve under pressure to escape treatment (Haider et al., 2020). This is called “acquired resistance” and the theory of its origin draws from ideas developed in evolutionary biology,

cf. the landmark paper by Nowell (1976). Every tumor consists of an ecosystem of cells that appear similar when compared to normal cells of the respective tissue, but they will not be genetically identical. Some cells for instance will share mutations picked up by an ancestor that other tumor cells might not carry. Given this genetic diversity, selection processes such as pressure from the immune system or drug treatment will select populations of cells that carry mutations that increase their fitness in this environment (Greaves and Maley, 2012). Unsurprisingly, tumors with a high level of heterogeneity tend to have worse clinical outcomes due to development of drug resistance (Crucitta et al., 2022; Dagogo-Jack and Shaw, 2018). Common mechanisms of drug resistance include increased drug efflux, mutations of the drug target, activation of survival, and inactivation of apoptotic pathways (Bukowski et al., 2020; Housman et al., 2014). Indeed, resistance and relapse are major barriers to curing cancer (Vasan et al., 2019). Therefore, we need to understand better what drives resistance, how to monitor for its emergence and lastly, what to do when it happens.

1.3 Biomarkers

The Biomarkers Definitions Working Group defines a biomarker as follows (Atkinson et al., 2001):

“Biological marker (biomarker): A characteristic that is objectively measured and evaluated as an indicator of normal biological processes, pathogenic processes, or pharmacologic responses to a therapeutic intervention.”

While biomarkers in medicine can also be of physiologic, histologic or radiographic nature, precision oncology is dominated by molecular biomarkers. Further, biomarkers are commonly grouped into different categories based on what they are useful for. The FDA-NIH Biomarker Working Group gives the following definitions:

“Diagnostic biomarker: A biomarker used to detect or confirm presence of a disease or condition of interest or to identify individuals with a subtype of the disease.” (FDA-NIH Biomarker Working Group, 2016a)

“Prognostic biomarker: A biomarker used to identify likelihood of a clinical event, disease recurrence or progression in patients who have the disease or medical condition of interest.” (FDA-NIH Biomarker Working Group, 2016b)

“Predictive biomarker: A biomarker used to identify individuals who are more likely than similar individuals without the biomarker to experience a favorable or unfavorable effect from exposure to a medical product or an environmental agent.” (FDA-NIH Biomarker Working Group, 2016c)

Although Sechidis et al. (2018) argue that most biomarkers have prognostic as well as predictive value to some extent, the work we have published is clearly concerned with predictive biomarkers, i.e. we want to predict the effectiveness of a treatment given some knowledge about the tumor like genomic or transcriptomic changes.

1.3.1 Omics data analysis

Commonly used types of omics data in translational cancer research are genomics and transcriptomics data, with other approaches that require mass spectrometry being less common. In each of the three studies that I will present, we analyzed whole-exome data

generated on sequencing machines manufactured by Illumina as well as RNA-seq data for two of the studies (Dorel et al., 2021; Messerschmidt et al., 2020). The concrete analysis steps are described in the methods section of the respective chapters. Below, I will discuss some general points concerning small somatic variants (Sec. 1.3.2), copy number variation (Sec. 1.3.3), and two types of signatures (Sec. 1.3.4).

1.3.2 Small somatic variants

Small somatic variants are genomic changes where only one or a few base pairs are changed compared to a reference, i.e. the healthy normal control in the case of cancer cells. Single nucleotide variants (SNVs) and small insertions or deletions (Indels) might only change a tiny fraction of the DNA sequence, but these changes can have dramatic effects downstream. Drawing from the Pan-Cancer Analysis of Whole Genomes (PCAWG) study (Campbell et al., 2020), the most recurrent SNVs in this cohort are in the tumor suppressor gene TP53 (33.6 %) and in the proto-oncogene KRAS (10.2 %, according to cbiportal.org, accessed 2022-06-07). To find small somatic variants, researchers use software methods to compare sequencing data from a tumor to a reference of the same patient. The latter is often derived from white blood cells (“buffy coat”) as they are easily accessible, or from non-cancerous tissue parts of a tumor biopsy (“near tumor normal”).

1.3.3 Copy number variation

Healthy somatic human cells have a diploid genome. That means that each cell has two homologous copies of each autosomes, one from the mother and one from the father. In cancer, this balance is often destabilized, leading to either losses or gains of stretches of DNA, together with the genes encoded on them (Shlien and Malkin, 2009). Gene expression is tightly regulated in normal cells, and having fewer or more copies of certain genes can be a survival advantage for the cell that carries them. Because beneficial copy number variations (CNVs) are selected for, specific recurrent CNVs can be observed in most cancer entities (Harbers et al., 2021). One example is the amplification of the transcription factor *MYCN* in high risk neuroblastoma, discussed in more depth in Sec. 4.1.2. How CNV calling was used in one of our projects is described in Sec. 3.2.2.

1.3.4 Signatures

The term “signature” is not always clearly defined and has different meanings depending on the context. We made use of two different classes of signatures for the project presented in Chapter 2. We used a so-called mutational signature to assess the activity of a mutational process, in this case of the AID/APOBEC family of enzymes. For a more in-depth overview, see Sec. 2.1.4 and Sec. 2.1.5.

Another type of signature we used is the IFN- γ signature to assess inflammation in tumors, i.e. a gene expression signature. This is a score based on gene expression measurements in a sample, based on a gene set. Gene sets have been defined for many processes and pathways (Liberzon et al., 2015; Schubert et al., 2018) and have been quite popular since the introduction of gene set enrichment analysis (Subramanian et al., 2005). In this setting, the coordinated expression of some genes might be considered a signature for a process or biological state.

1.4 Translational research enables better precision medicine

Translational research aims to bring new insights generated by basic research into practical clinical application. Here, often the slogan “From the bench to the bedside” is cited, presumably used for the first time by Spencer B. King III (1996). Feedback from bedside back to bench is a crucial feature (Cohrs et al., 2015). The discovery of new biomarkers is one application where insights from basic research can be used to improve treatment of patients (Hartl et al., 2021). Marrying the two concepts of precision medicine and translational research, the community aims to

1. Select the best treatment based on the available information on the patient and the tumor.
2. Introduce new biomarkers (cf. sec. 1.3) into the clinical practice to help with 1.

Research by Dubois and Kyle (2016) shows that novel cancer treatments are associated with a decline in mortality. Additionally, biomarker testing and a greater selection of treatment options improve survival of patients (D’Avo Luís and Seo, 2021).

1.4.1 Cancer models

Model organisms are the most studied organisms in biology, e.g. *Drosophila melanogaster*, *Arabidopsis thaliana*, *Caenorhabditis elegans*, and *Mus musculus*. Insights from experiments in models are assumed to translate to other related organisms. For example, mouse experiments might be used if such research would be unethical or not practical in humans. Knock-out experiments come to mind or other forms of genome editing. However, models also have drawbacks as they are not the entity that they represent, and crucial differences remain between mice and men (Junhee Seok et al., 2013; Perlman, 2016).

Models also exist for cancer, among them cancer cell lines, organoids or mice harboring a tumor, e.g. from a patient-derived xenograft (PDX). The simplest model are cancer cell lines, which are cultures of cancer cells derived from tumors growing and dividing in a dish in a laboratory. Kept under the right conditions, these cells are immortal - consider the HeLa cell line, which was derived from cervical cancer cells of Henrietta Lacks in 1951 (Skloot, 2011). Obvious drawbacks of cancer cell lines are the lack of heterogeneity and cell hierarchy as well as the missing tumor micro-environment. In vivo, immune cells and stromal cells interact with the tumor and vice versa. Nevertheless, these models can be studied to gain new insights as in the experiments described in chapters 3 and 4. By correlating drug sensitivity with readouts of accompanying omics datasets, researchers are able to find new biomarkers that can then be studied in more elaborate models and finally in patient cohorts and in clinical trials.

Chapter 2

Distinct immune evasion in APOBEC-enriched, HPV-negative HNSCC

2.1 Introduction

2.1.1 Overview and contributions

The following chapter is based on the work published by Messerschmidt et al. (2020) in the International Journal of Cancer. In this paper, we delineate a subgroup of human papilloma virus-negative squamous cell tumors of the head and neck that exhibit an enrichment of mutations associated with activity of the family of APOBEC3 enzymes. This subgroup exhibits a number of characteristics that make it an interesting target to study in the context of immune checkpoint inhibitors, as these tumors show higher inflammation, more immune escape variants and higher expression of important checkpoint genes.

My contributions to the publication were as follows:

- I contributed to conception and planning of the project.
- I co-developed the in-house bioinformatics pipeline called snappy for the analysis of high-throughput sequencing data.
- I executed the complete bioinformatics analysis of all data from the TCGA and DKTK Master cohorts.
- I contributed to the single cell transcriptomics analysis.
- I created Figures 1A, 1B, 2, 3, 4, 5A, 6.
- I created Table 1.
- I co-wrote the manuscript and was responsible for all communication with the editor during the submission and the revision process.

This paper won a prize for re-use of open data, awarded by the QUEST center for Responsible Research of the Berlin Institute of Health.

2.1.2 Head and neck squamous cell cancer

The term “head and neck cancer” refers to a diverse set of tumors that develop from tissue of the lip, mouth, throat or skin. The majority of these tumors are originating from squamous cells (Chow, 2020), in contrast to rarer tumors originating for instance from the salivary glands (Son et al., 2018). Squamous cells are a cell type that can be found on the surface of skin, and the lining of inner organs. A common abbreviation of head and neck squamous cell carcinoma is HNSCC, as used in The Cancer Genome Atlas (Lawrence et al., 2015).

One well known cause of cell transformation of squamous cells is infection with human papilloma virus (HPV), where the virus proteins E6 and E7 act as oncoproteins (Yim and Park, 2005). Compared to patients with HPV-negative tumors, those with HPV-positive tumors are generally younger and have no history of smoking, but statistically had a higher number of sex partners (Young et al., 2015). For HPV-negative head and neck tumors, tobacco and alcohol are among the known risk factors, as well as betel quid chewing as practiced in some areas of Asia (Su et al., 2016). Although originating from the same tissue, it is known that HPV-positive and HPV-negative tumors are quite different in their characteristics (Rieke et al., 2016). Their respective expression patterns are specific, as well as clinical outcomes as HPV-positive patients have more favorable survival rates (Keck et al., 2015).

2.1.3 Immune checkpoint inhibition

One relatively recent treatment option with great promise are immune-checkpoint inhibitors (ICI), sometimes called immune-checkpoint blockade. ICI therapies work through monoclonal antibodies targeting surface proteins on either immune or tumor cells that mediate the suppression of the immune response against the tumor. These surface proteins are called immune checkpoints. For the basic research enabling these therapies, James Allison and Tasuku Honjo received the Nobel Prize in Physiology or Medicine (2018). Ferris et al. (2016) showed that ICI results in significantly longer overall survival compared to standard therapy. However, it is not entirely clear which patients will benefit from the treatment. Because treatment costs are high, selecting likely responders upfront is an active topic of research. In previous publications, different biomarkers for ICI response were proposed, for example tumor mutational burden (Cristescu et al., 2018; Van Allen et al., 2015), inflammation (Ayers et al., 2017; Seiwert et al., 2016), and expression of the immune checkpoint PD-L1 (Bila et al., 2022; Ferris et al., 2016). It remains unclear which of the proposed biomarkers offers the best predictive performance, however (Oliva et al., 2019).

2.1.4 APOBEC3 enzymes and their mutational patterns

The enzymes of the APOBEC3 (apolipoprotein B mRNA editing enzyme, catalytic polypeptide-like 3) family, i.e. APOBEC3A, APOBEC3B, APOBEC3C, APOBEC3D, APOBEC3F, APOBEC3G, and APOBEC3H, possess the ability to deaminate cytidine to uridine in single stranded DNA. They are part of the innate response to infection with retroviruses (Uriu et al., 2021). Due to replication stress, cells in some tumors exhibit elevated levels of single stranded DNA (Trenner and Sartori, 2019), which is the substrate of APOBEC3. The genomes of those tumor cells then bear traces of APOBEC3 mutational activity. This phenomenon can sometimes be observed even independently of viral infection (Burns et al., 2013). What currently remains unclear is why APOBEC3 might get activated in these cases, as no causal insult is known yet (cf. Fig. 2.1).

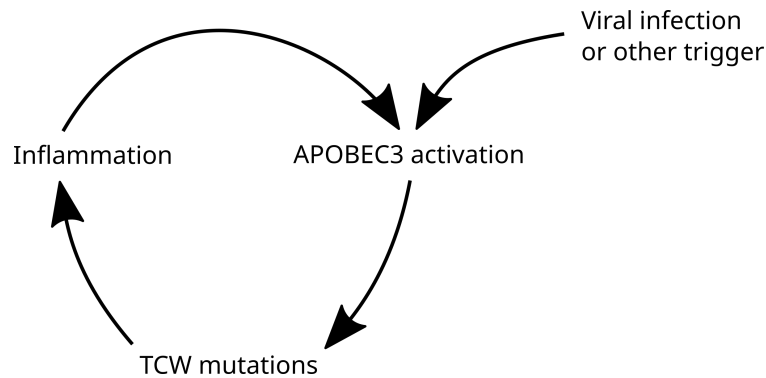


Figure 2.1: Sketch of a simple model of APOBEC3 activation as a self-reinforcing process. After APOBEC3 expression is activated by a trigger such as viral infection, immunogenic TCW mutations lead to inflammation, which in turn upregulates APOBEC3 expression.

APOBEC3-catalyzed mutations are usually single base changes from cytosine to either guanine or thymine. Importantly, the context of the mutations is mostly either TCT or TCA, which can be shortened to TCW in IUPAC notation. An accumulation of mutations in this TCW motif can be used to identify tumors with high APOBEC3 activity.

2.1.5 Signatures for mutational processes

In 2013, Alexandrov et al. (2013) published a seminal study in *Cell Reports*, describing an approach to decipher mutational signatures from catalogs of somatic variants. A signature based on single nucleotide variants describes the respective percentages of six substitution subtypes, i.e. C>A, C>G, C>T, T>A, T>C, and T>G, for every possible combination of preceding (5') and succeeding (3') bases - 96 classes in total. The base change is represented by the pyrimidine base of the DNA, so C>A is equivalent to a G>T substitution. Alexandrov et al. found signatures that can be attributed to effects such as aging, exposure to UV light, alcohol and tobacco use, and APOBEC3 activity. Their method further enables researchers to assign contribution scores of mutagenic processes to a tumor mutational profile. An extension of the initial method to estimate per-signature error bars through bootstrapping of the input profile that we developed is available as an R package (Schumann et al., 2019).

Two signatures in the corpus of signatures published by Cosmic (https://cancer.sanger.ac.uk/signatures/signatures_v2/) are currently attributed to APOBEC activity. Those are signature 2 (cf. Fig. 2.2, C>T preference) and signature 13 (cf. Fig. 2.3, C>G preference).

2.2 Data

In total, data from three different sources were used. The main findings were generated using data from the HNSCC cohort of TCGA, while data from the German DKTK Master cohort and from a single cell dataset from the BROAD Institute were analyzed to support the findings.

2.2.1 The Cancer Genome Atlas: HNSCC cohort

The Cancer Genome Atlas (TCGA) includes the largest HNSCC cohort publicly available for researchers. At the time of analysis, the cohort comprised of 502 patients, with 496 having

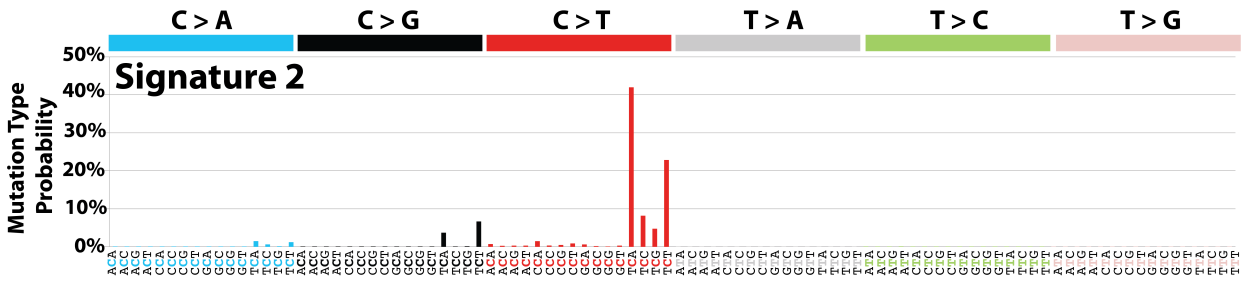


Figure 2.2: Mutational probabilities for signature 2 from COSMIC mutational signatures, with enrichment of C>T variants in the TCW motif and attributed to APOBEC3 activity. From https://cancer.sanger.ac.uk/signatures/signatures_v2. Reprinted with permission.

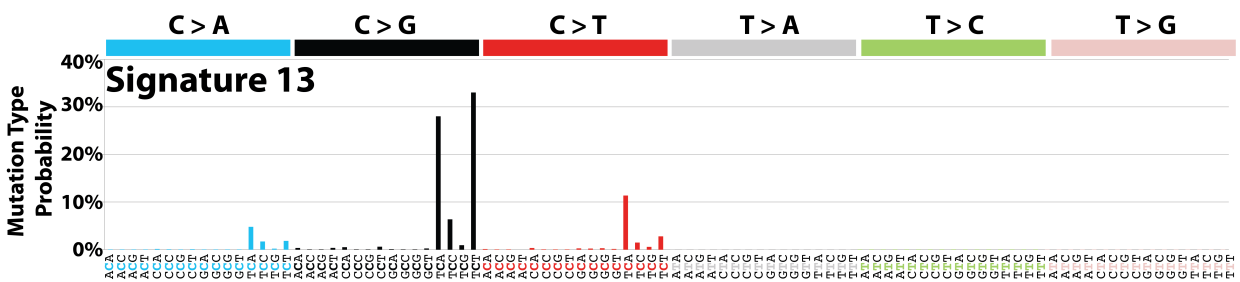


Figure 2.3: Mutational probabilities for signature 13 from COSMIC mutational signatures, with enrichment of C>G variants in the TCW motif and attributed to APOBEC3 activity. From https://cancer.sanger.ac.uk/signatures/signatures_v2. Reprinted with permission.

complete sequencing profiles of whole-exome sequencing (WES) for tumor and normal and tumor mRNA-seq.

Data were downloaded from a range of sources. Non-aggregated mRNA-seq data (bam files) were downloaded from the Genomic Data Commons Data Portal (<https://portal.gdc.cancer.gov>). Variant calls were downloaded from BROAD firehose portal (<https://gdac.broadinstitute.org>) in MAF format. Aggregated expression data for select genes were additionally downloaded from cbioportal.org (Gao et al., 2013).

2.2.2 DKTK Master cohort

The “MASTER” programme of DKTK (Deutsches Konsortium für Translationale Krebsforschung) aims to support treatment decision making by offering molecular insights for each tumor. For this project, we used data from all patients with squamous cell head and neck tumors who had WES and mRNA-seq data available at the time of analysis ($n = 10$). Raw sequencing data were downloaded from the sequencing facility in Heidelberg and processed using our in-house pipeline, consisting of read mapping, somatic variant calling and annotation as well as gene expression quantification for mRNA data.

2.2.3 Single cell transcriptomics dataset

Transcriptome profiling data of ca. 6000 cells from 18 HNSCC patients were published by Puram et al. (2017). The data also contain cell type annotations and another coarser level, defining malignant and non-malignant cells. Data were downloaded from Gene Expression Omnibus (GEO) under accession ID GSE103322.

2.3 Methods

2.3.1 HPV status

To assign HPV status to each sample in TCGA, we used the mRNA-seq data of each patient. As cells infected with HPV show expression of viral genes, we assigned HPV status based on the presence of HPV transcripts that were detectable besides all transcripts of human origin. For that, we collected the number of transcripts mapping to the most common HPV genomes that were included in genome release 38. If a sample had more than 3500 reads mapping to HPV, we labeled it HPV-positive. Note that the distribution of viral reads in the cohort is bimodal, i.e. negative samples have fewer than 10 reads.

To check for correctness, we compared the results to prior work by (Tang et al., 2013), TCGA clinical meta data and a published HPV gene expression signature (Buitrago-Pérez et al., 2009), which were in agreement for the samples shared.

2.3.2 TCW mutation enrichment

As the proportion of contribution of each signature reported by the method of Alexandrov et al. (2013) is hard to compare between samples, we opted for another simpler procedure. The method has been previously used by Roberts et al. (Roberts et al., 2013) and looks at the proportion of all TCW mutations to C mutations compared to the occurrence of C's and the motif TCW in the genome. Then, we use a Fisher's exact test to determine if the

number of C mutations in the TCW context is bigger than expected by chance. P-values were Holm-Bonferroni corrected and all samples with $p' < 0.05$ were labeled APOBEC-enriched.

2.3.3 Inflammation scoring of tumors

A gene expression signature, also called a “gene set”, consists of a list of genes, a label, and optionally, weights for each gene. The final signature score might be computed as the (weighted) sum or mean of expression values for all genes in the list. To assess inflammation in tumor samples, we used a published gene expression signature, termed IFN- γ or IFNG signature (Ayers et al., 2017). This gene set consists of IFNG, IDO1, CXCL9, CXCL10, HLA-DRA, and STAT1. To compute the IFNG signature score, we used the TPM values (labeled “RNA Seq V2 RSEM”) downloaded from cbiportal.org for the TCGA HNSCC cohort as the mean of the log2-transformed expression values per sample.

2.3.4 Differential expression analysis

Expression data (“RNA-seq V2 RSEM” from cbiportal.org) was subset to all samples with mutational data and differential expression analyzed for groups of interest using a Wilcoxon rank test in R for immune checkpoint genes CD274, CTLA4, LAG3, PDCD1 and VTCN1. To compare APOBEC3 expression between groups, expression values of all APOBEC3 genes were summed up before testing.

2.3.5 Analysis of immunotherapy relevant genes

A list of immunotherapy-relevant genes has been published by Patel et al. (2017). They used a two cell type (2CT) CRISPR assay. The assay consisted of melanoma cells and engineered CD8+ cells targeting HLA-A*02-restricted antigen. In a genome-wide CRISPR screen, genes that led to significantly improved survival of the melanoma cells when knocked out were included as relevant for immunotherapy success. The final list consists of 554 genes.

To identify an over-representation of mutations in immunotherapy-relevant genes, we used a Fisher’s exact test, comparing the sum of mutations in each subgroup and the number of cases, respectively.

2.3.6 Single cell transcriptomics analysis

Based on the digital expression matrix provided by Puram et al., cells were visualized with t-distributed stochastic neighbor embedding (t-SNE). Cells were colored either by the malignant/non-malignant annotation provided by the authors or by APOBEC3 expression.

2.4 Results

The first question we wanted to look at was if total mutational burden (TMB) was associated with inflammation in HNSCC as it has been proposed as a marker for ICI response before. In the TCGA cohort, no correlation was observed between these two measures (Fig. 2.4A). However, the number of TCW mutations shows a positive correlation with inflammation, but only in the group of HPV-negative samples (Fig. 2.4B).

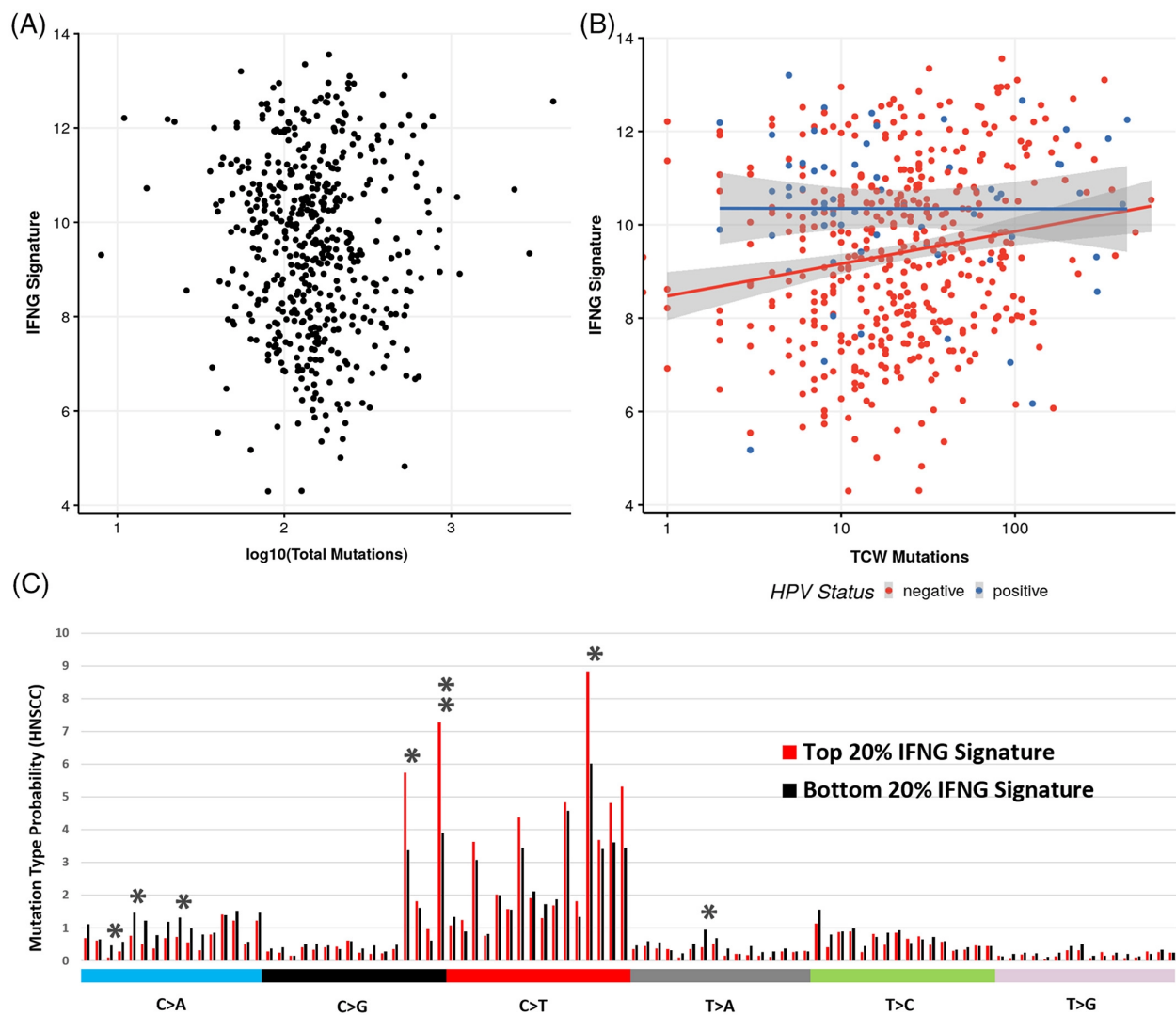


Figure 2.4: IFNG signature score is not associated with number of total mutations, but with number of TCW mutations in the TCGA HNSCC cohort. **A** Scatter plot of the 6-gene IFNG signature score and \log_{10} of total mutations ($n = 496$). No significant correlation was found. **B** Scatter plot of the IFNG signature score and number of TCW mutations by HPV status (red: HPV-negative, $n = 423$, blue: HPV-positive, $n = 64$). A significant Pearson correlation was identified ($p = 1 * 10^{-4}$). **C** The frequency of base exchanges of the 96 possible mutations types was compared between samples of the highest and lowest quintile of the IFNG signature score. The top 20 percent showed preference for the APOBEC3-associated TCW mutations. Figure from “Distinct immune evasion in APOBEC-enriched, HPV-negative HNSCC” by Messerschmidt et al. (2020), licensed under CC BY 4.0 (<https://creativecommons.org/licenses/by/4.0/>)

Comparing HPV-positive vs HPV-negative cases, we reproduced a set of known differences. Firstly, HPV-negative cases tend to have more point mutations overall ($p = 0.00017$, Fig. 2.5A). On the other hand, HPV-positive cases had higher inflammation as measured by IFNG signature ($p = 3.7e-05$, Fig. 2.5B). And finally, HPV-positive samples have a higher share of TCW mutations ($p = 0.0026$, Fig. 2.5C).

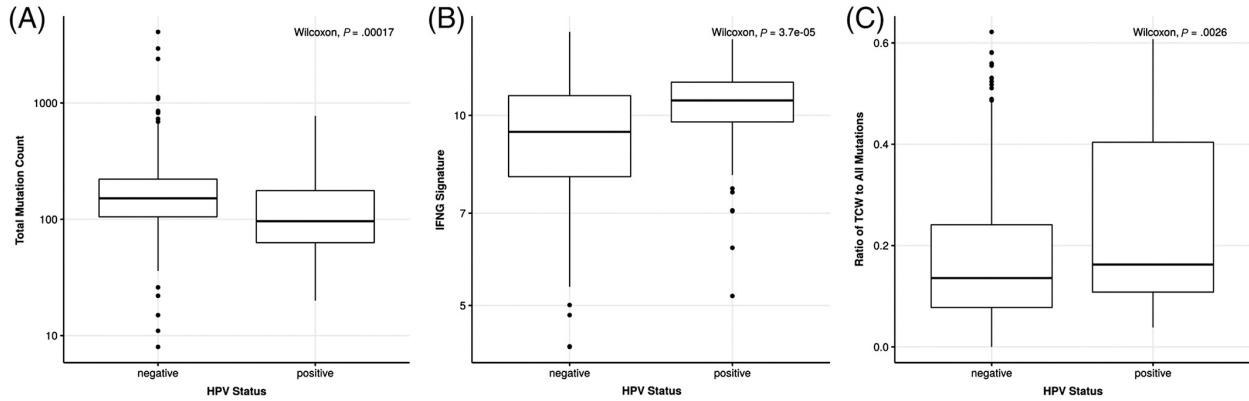


Figure 2.5: HPV status is an important variable in HNSCC. **A** HPV-negative tumors have higher total mutation count ($p = 1.7 * 10^{-4}$). **B** HPV-positive tumors show higher inflammation as measured by IFNG signature score ($p = 3.7 * 10^{-5}$). **C** HPV-positive tumors have a higher ratio of TCW to all mutations ($p = 2.6 * 10^{-3}$). Figure from “Distinct immune evasion in APOBEC-enriched, HPV-negative HNSCC” by Messerschmidt et al. (2020), licensed under CC BY 4.0 (<https://creativecommons.org/licenses/by/4.0/>)

To group HPV-negative samples regarding their APOBEC activity, we used a Fisher’s exact test to find all samples that had a higher proportion of TCW mutations than expected. These samples were labeled HPV-negative/APOBEC-enriched. The other remaining subgroup was labeled HPV-negative/APOBEC-negative. Comparing the new subgroups, we show three key observations that make the HPV-negative/APOBEC-enriched group special. Not only does the group have higher inflammation on average (Fig. 2.6A), but it also exhibits differential expression in key checkpoint genes (Fig. 2.6B). Further, we observe significantly more mutations in genes that are immuno-therapy relevant as previously identified by Patel et al. (2017), cf. Tbl. 2.1.

Table 2.1: Results of Fisher exact tests for enrichment of mutations in immunotherapy-relevant genes as defined by Patel et al., once with HLA genes and once without to exclude possible false positive variant calls in these loci.

	HPV-negative/ APOBEC- enriched	HPV-negative/ APOBEC- negative	P- Value
No. of Cases	84	348	
No. of hits (collapsed to genes)/No. of cases	7.6 (638 total)	4.7 (1643 total)	1.80E-04
No. of hits with functional impact (collapsed to genes)/No. of cases	5.7 (476 total)	3.7 (1277 total)	8.80E-04

	HPV-negative/ APOBEC- enriched	HPV-negative/ APOBEC- negative	P- Value
No. of hits (collapsed to genes), without HLA genes/No. of cases	7.3 (617 total)	4.7 (1623 total)	4.10E-04
No. of hits with functional impact (collapsed to genes, without HLA genes)/No. of cases	5.5 (461 total)	3.6 (1259 total)	1.60E-03

To replicate our findings in an independent cohort, we collected data from all HPV-negative HNSCC patients in the DKTK Master study ($n = 10$). Samples were annotated with HPV and APOBEC status as described above for TCGA. IFNG scores were computed as for TCGA, i.e. the mean of $\log_2(TPM + 1)$ of the six genes in the signature. TPM values were generated with salmon (Patro et al., 2017). There was only one case qualifying as HPV-negative/APOBEC-enriched, but among the ten samples it had the highest IFNG score (cf. Fig. 2.8).

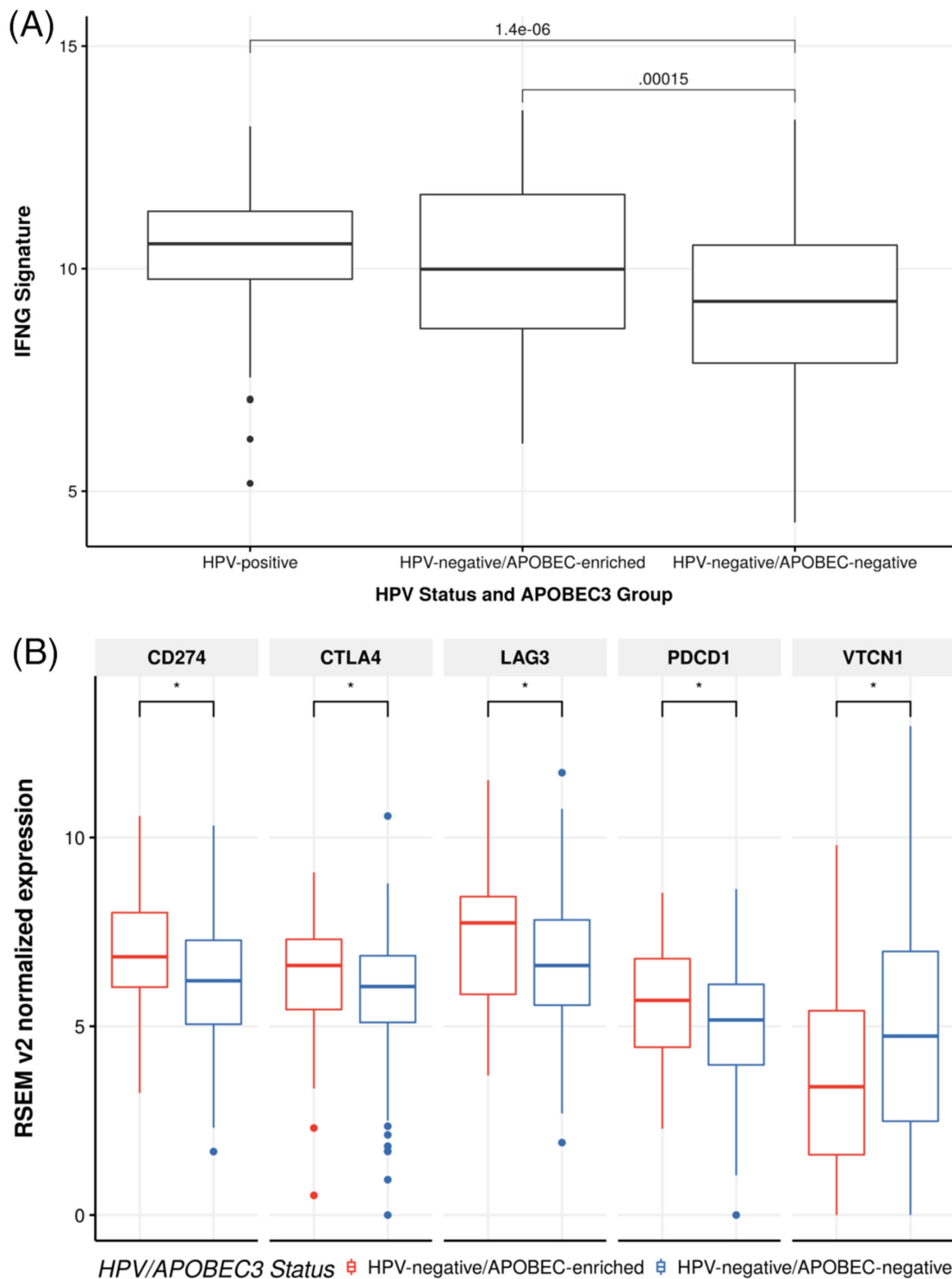


Figure 2.6: HPV-negative/APOBEC3-enriched tumors show higher inflammation, differential checkpoint inhibition when compared to other HPV-negative tumors. **A** Boxplot of IGFN signature score, grouped by HPV and APOBEC3 status. HPV-negative/APOBEC3-enriched tumors show higher inflammation compared to HPV-negative/APOBEC3-negative tumors ($p = 1.5 \times 10^{-4}$). No significant difference was observed between HPV-positive and HPV-negative/APOBEC3-enriched tumors. **B** Gene expression of five immune checkpoints was compared between HPV-negative/APOBEC3-enriched and HPV-negative/APOBEC3-negative tumors. CD274, CTLA4, LAG3 and PDCD1 were higher expressed in APOBEC3-enriched cases, VTCN1 in APOBEC3-negative cases ($p < 0.05$ after Bonferroni correction.) Figure from “Distinct immune evasion in APOBEC-enriched, HPV-negative HNSCC” by Messerschmidt et al. (2020), licensed under CC BY 4.0 (<https://creativecommons.org/licenses/by/4.0/>)

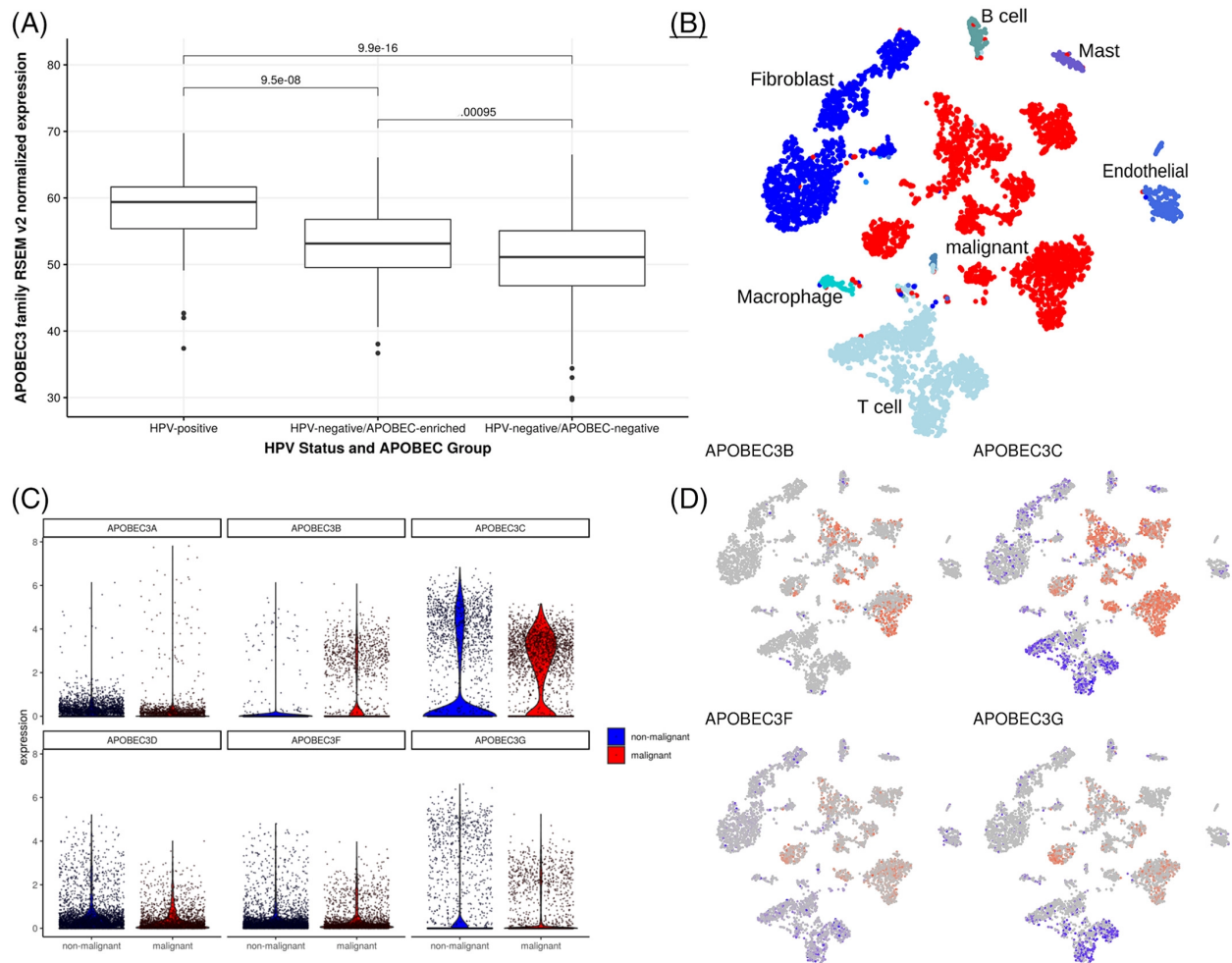


Figure 2.7: Single cell expression data from an independent cohort demonstrates APOBEC3 expression in tumor cells. **A** Aggregated APOBEC3 expression by group for HPV-positive, APOBEC-enriched/HPV-negative cases, and APOBEC-negative/HPV-negative cases from TCGA. While HPV-positive cases have the highest expression, APOBEC3-enriched cases have higher expression among HPV-negative tumors. **B** tSNE projection of all cells from 17 donors profiled by Puram et al., annotated as malignant (red) or non-malignant (blue). **C** Violin plots of six APOBEC3 genes, comparing malignant (red) and non-malignant (blue) cells. **D** tSNE projections of all cells as in **B**. APOBEC3B, APOBEC3C, APOBEC3F, APOBEC3G expression strength indicated by color intensity, with malignant cells in red, non-malignant in blue and gray cells having no expression. Figure from “Distinct immune evasion in APOBEC-enriched, HPV-negative HNSCC” by Messerschmidt et al. (2020), licensed under CC BY 4.0 (<https://creativecommons.org/licenses/by/4.0/>)

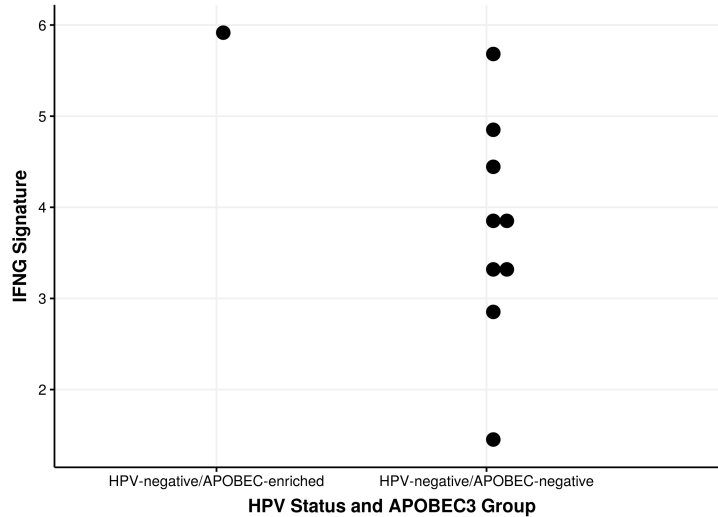


Figure 2.8: Analysis of IFNG score by APOBEC status in HPV-negative DKTK Master patients. The one identified APOBEC3-enriched case showed the highest IFNG signature score. Figure from “Distinct immune evasion in APOBEC-enriched, HPV-negative HNSCC” by Messerschmidt et al. (2020), licensed under CC BY 4.0 (<https://creativecommons.org/licenses/by/4.0/>)

2.5 Discussion

In this publication, we defined a subgroup of HPV-negative tumors that show higher inflammation, enrichment of APOBEC3-associated mutations in the exome, significantly more mutations in immunotherapy-relevant genes, and differential expression in some key checkpoint genes such as CD274, CTLA4 and PDCD1. Taken together, these findings suggest differences in ICI response when compared to the HPV-negative, APOBEC3-negative subgroup. The main limitation of this study is that we did not have response data for immune checkpoint inhibition, but that we had to rely on the IFNG signature as proxy for tumor inflammation and T-cell infiltration. Further, it was difficult to acquire the data necessary for validation in a ICI-treated cohort and we had to rely on a small cohort from DKTK Master.

The most important question remaining is which among all proposed biomarkers for ICI response does perform best in practice. For instance, both a T-cell inflamed phenotype and a high mutational burden have been linked to ICI response (Ayers et al., 2017; Van Allen et al., 2015). Yet, in our analysis we found no significant correlation between the two. Early evidence suggests that tumors with APOBEC activity respond better to ICI (Miao et al., 2018; Wang et al., 2018). APOBEC activation without viral infection is proposed to occur later in the tumor life cycle, inducing branched evolution in lung cancer (McGranahan et al., 2015). It is unclear what drives APOBEC activation in these cases, but elevated levels of single stranded DNA are a candidate. Ultimately, we hope that the APOBEC3 status of a HPV-negative head and neck tumor can be used to direct ICI treatment in the future.

Chapter 3

Acquired resistance to DZNep-mediated apoptosis is associated with copy number gains of *AHCY* in a B-cell lymphoma model

3.1 Introduction

3.1.1 Overview and contributions

The following chapter is based on the work published by Akpa et al. in *BMC Cancer* (2020), where we found an acquired copy number change in the gene *AHCY* that was the cause for resistance to DZnep treatment in a B-cell lymphoma cell line. For this work, I contributed the following:

- I analyzed the whole-exome sequencing data, including quality control of raw sequencing data and read alignment on genome reference GRCh37.
- I called and annotated copy number variants genome-wide and suggested the *AHCY* amplification as the likeliest candidate for the acquisition of DZNep resistance.
- I created Figure 2A and wrote the manuscript sections describing the whole-exome analysis and reviewed the final manuscript.

3.1.2 Molecular characteristics of Burkitt lymphoma

Lymphoma are a type of tumor that arise from a transformed population of lymphocytes. Depending on which cell type gave rise to this population, lymphoma can be coarsely grouped into subclasses like B-cell or T-cell lymphoma, which in turn can be subdivided again into multiple specific subtypes. The cell line analyzed in this project is a model for Burkitt lymphoma, a type of B-cell lymphoma that was first described by Denis Burkitt (1958).

The common aberration that all Burkitt lymphoma share is dysregulation of the gene *MYC* (*MYC* Proto-Oncogene, BHLH Transcription Factor) (Nguyen et al., 2017). This is most commonly caused by a genetic variant called (chromosomal) translocation where parts of a chromosome relocate to a different position by breaking off and reattaching somewhere

else, e.g. another chromosome. The majority of Burkitt lymphoma tumors harbor a t(8;14) translocation, linking *MYC* to the *IgH* (immunoglobulin heavy chain) locus on chromosome 14 (Hoffman et al., 2017). As a consequence, expression of *MYC* is not controlled by regulatory elements on chromosome 8 as in healthy cells anymore, but will be regulated like the Ig heavy chain gene, which is strongly expressed in antibody-producing B cells. This genetic change leads to overexpression of *MYC* in these cells specifically. Because *MYC* is a transcription factor, its overexpression has consequences on the cellular level, among them increased proliferation (Bretones et al., 2015), changes in metabolism (Miller et al., 2012) and apoptosis (Hoffman and Liebermann, 2008). While *MYC* is also deregulated in many other cancer types, specific treatments that directly target *MYC* are currently not available (Chen et al., 2018), although work in this area is ongoing (Duffy et al., 2021).

3.1.3 EZH2 inhibition

EZH2 inhibition is another recently proposed treatment option for B-cell lymphoma. The drug 3-Deazaneplanocin A (DZnep) has been shown to inhibit cancer growth in vitro in a number of cancer entities like Burkitt Lymphoma and DLBCL (Akpa et al., 2019). DZnep indirectly targets EZH2 (Enhancer of zeste homolog 2), which is part of polycomb repressor complex 2 (PRC2) (Kim and Roberts, 2016). EZH2 is a histone methyltransferase, i.e. an enzyme that can catalyze the trimethylation of lysine 27 on histone 3 (H3K27me3). H3K27me3 is a repressive histone modification, and generally leads to downregulation of gene expression through denser packaging of DNA (Francis et al., 2004). This way, it is possible to repress genes like tumor suppressors that regulate apoptosis, cell cycle or differentiation (Gan et al., 2018; Tian et al., 2016). By counteracting this gene repression, DZnep is acting on the epigenetic level and reprogramming the transcriptome.

On the biochemical level, DZnep inhibits another enzyme called AHCY (S-Adenosyl-L-Homocysteine Hydrolase, also Adenosylhomocysteinase). AHCY catalyzes the reversible hydrolysis of S-adenosylhomocysteine (SAH) to adenosine and L-homocysteine, and thereby regulates SAH concentration in the cell. When this reaction is inhibited, SAH accumulates and this causes inhibition of methyltransferases like EZH2 because SAH is also a product of the methylation reaction (cf. Fig. 3.1 for the structural similarities between DZnep and SAH).

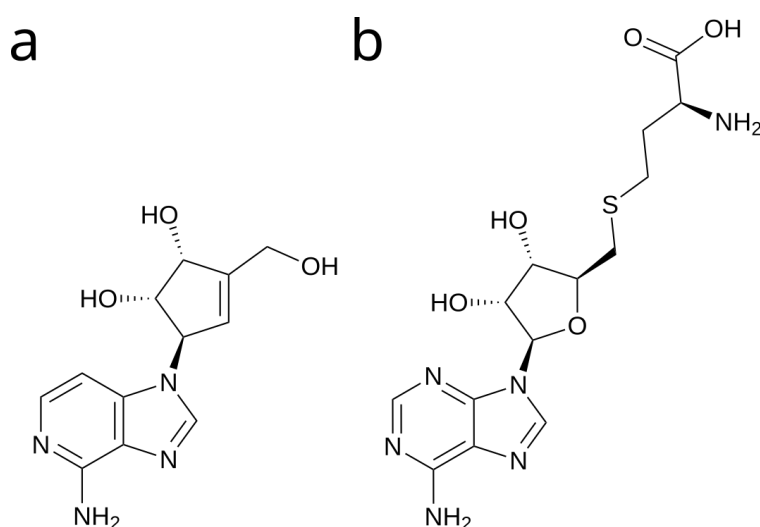


Figure 3.1: Structural similarity of **a** DZnep and **b** S-adenosylhomocysteine (SAH).

Given that DZnep is used in preclinical trials and could be used as a cancer treatment in the future (Kim and Roberts, 2016), it is valuable to explore possible resistance mechanisms that would allow a tumor to escape the treatment. Our aim is to find a plausible mechanism for engineered EZH2 inhibition resistance in vitro.

3.2 Data and Methods

3.2.1 Generation of a DZnep resistant cell line

A culture of a cancer cell line called BLUE-1 (sporadic Burkitt lymphoma) was split into a control culture and a treatment culture. The treatment culture was then over the course of seven months treated with DZnep, while increasing concentration of the drug from 200 nM to 2000 nM (cf. Fig. 1 in the original publication). Finally, we arrived at two cell cultures, a DZnep-sensitive one cultured in parallel (“K10”) as well as the resistant one, labeled “R10”. The exact protocol is described in detail in the methods section of our paper.

3.2.2 Whole-exome sequencing analysis

After genomic DNA was isolated from the respective cell cultures, libraries were generated with the SureSelect XT Human All Exon v4 kit by Agilent and sequenced on a Illumina HiSeq 2000 machine. Reads were aligned using BWA-mem version 0.7.12 (Li, 2013) against reference genome GRCh37 with decoy sequences (hs37d5.fa). Samblaster version 0.1.22 (Faust and Hall, 2014) was used to mark duplicate reads.

3.2.3 Copy number analysis

We used the software CNVkit version 0.7.10 (Talevich et al., 2016) to compare the read depth profiles of R10 vs K10, using the alignment files as inputs. CNV segments were annotated with genes as described in the CNVkit manual. Copy number variants were prioritized according to their log2 fold change and plots generated with CNVkit. To estimate the average copy number per cell given the log2 fold change, the following formula was used:

$$\log_2 FC = \log_2 \left(\frac{p * n + (1 - p) * 2}{2} \right) \quad (3.1)$$

where p is the purity or fraction of cancer cells in a sample and n the average number of copies of a gene or segment in the cancer cells. We assume the ploidy of healthy cells to be 2.

3.3 Results

Two segments in particular showed prominent copy number changes with log2 fold changes of ca. 4.9, on chromosome 6 and 20, respectively (cf. Fig. 3.2a for the CNV on chromosome 20). The amplified segments were circa 1.5 Mb and 150 kb in size, respectively.

To estimate the copy number n from the log2 fold change of 4.9, we re-arrange eq. 3.1 and set $p = 1$ as we assume the cell culture to be clonal.

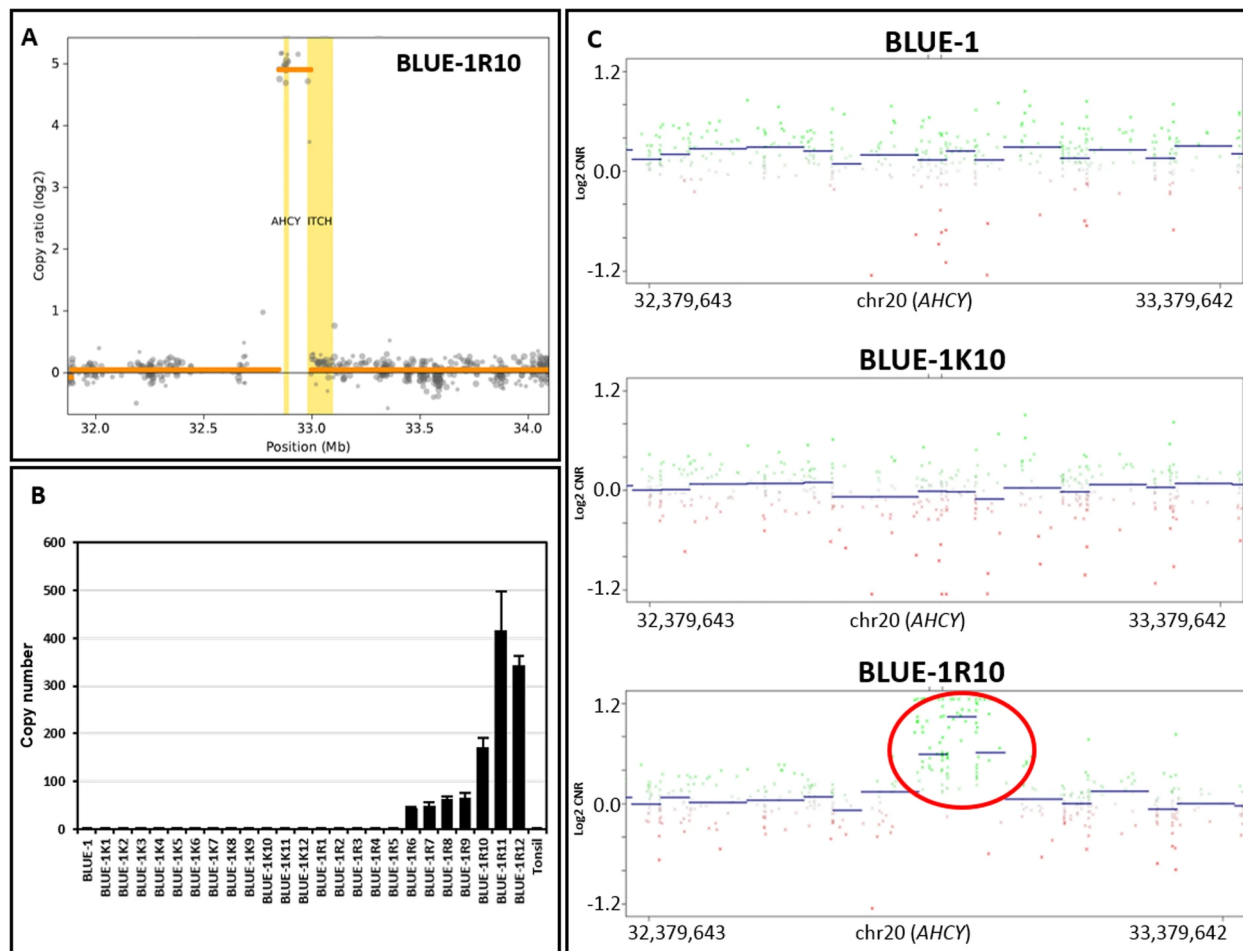


Figure 3.2: *AHCY* copy number amplification found in the DZnep-resistant cell culture. **A** Copy number profile of Blue1-R10 when compared to Blue1-K10 around the *AHCY* locus. The normalized ratio of reads is shown on log₂ scale, with gray dots depicting bins, orange lines segments and yellow stripes annotated genes. **B** Evolution of the copy number amplification through succession of culture generation for K and R based on TaqMan assay. Beginning with culture Blue1-R6, the copy number amplification around *AHCY* can be observed. **C** Validation of *AHCY* copy number gain, circled in red, using methylation arrays. Figure from “Acquired resistance to DZNep-mediated apoptosis is associated with copy number gains of *AHCY* in a B-cell lymphoma model” by Akpa et al. (2020), licensed under CC BY 4.0 (<https://creativecommons.org/licenses/by/4.0/>)

$$\log_2 FC \approx 4.9$$

$$2^{4.9} \approx \frac{n}{2}$$

$$n \approx 60$$

We arrive at an estimated average copy number of ~ 60 for the gene *AHCY* and the proximal part of the gene *ITCH*. The same applies to the genes *SNHG5*, *SMIM11P1*, *HTR1E*, and *CGA* on chromosome 6. As discussed in sec. 3.1.3, *AHCY* is the enzyme that is inhibited by DZnep. Therefore, it was the primary target for validation of the WES results. We were able to recapitulate the copy number amplification of *AHCY* with a TaqMan assay. Beginning with culture R6 after 5 months of DZnep treatment, we observe high levels of *AHCY* amplification in the range of 50 copies (cf. Fig. 3.2b). Subsequent cultures (R11, R12) show up to 400 copies in this assay. We further showed that mRNA expression and protein expression are also elevated to similar levels as predicted by the copy number analysis (Fig. 3b and Fig. 4 in the original publication).

3.4 Discussion

For this publication, we engineered a DZnep-resistant cell culture and proposed that the most likely cause for resistance was a prominent focal copy number amplification and overexpression of *AHCY*, which is the enzyme inhibited by DZnep. This suggests that cancer cells can successfully regulate SAH concentration even in the presence of DZnep when expressing *AHCY* in large enough levels.

CNVs have long been recognized for the role they sometimes play when cells develop drug resistance (Corcoran et al., 2010; Schinke et al., 1978). Krijgsman et al. (2014) propose that focal CNVs are especially significant as they are the results of many selection events during tumor evolution, giving these cells a fitness advantage. One example has been demonstrated by Beroukhi et al. (2010), who showed that focal amplification of anti-apoptotic genes *MCL1* and *BCL2L1* would lead to increased expression of these genes and protected tumor cells from chemotherapy.

While we found one plausible mechanism for DZnep resistance, others might be possible. We do not know which mechanism will arise in tumors in vivo when treated with DZnep. These data will only be forthcoming if DZnep is used in more trials in the future. Our findings suggest that *AHCY* status could be monitored during treatment with DZnep to catch development of resistance in clinical practice, but it remains unclear how treatment should be changed when observing such an event, i.e. which alternative agents to follow up with. Optimizing treatment schedule thus remains an open question.

Chapter 4

Neuroblastoma signaling models unveil combination therapies targeting feedback-mediated resistance

4.1 Introduction

4.1.1 Overview and contributions

The following chapter is based on the work published by Dorel et al. in PLoS Computational Biology (2021). In this paper, we molecularly characterized a panel of nine high risk neuroblastoma cell lines and analyzed their sensitivity to agents targeting the Ras/MAPK pathway. Using mathematical modeling based on perturbation data as well as phosphoproteomics data, we found two possible modes of MEK inhibitor resistance. Depending on the routing of the feedback in the signaling network, MEK inhibition might be combined with inhibition of either RAF or IGFR to overcome resistance. The predictions were tested experimentally and predictions were found to be correct in 2 out of 3 cases.

For this work, I contributed the following:

- I analyzed the whole-exome sequencing data, including quality control of raw sequencing data, read alignment on genome reference GRCh37, variant calling, variant annotation and variant prioritization.
- I uploaded these results to our self-hosted cbiportal instance to make them conveniently accessible for collaborators.
- I compared the mutation profile of each cell line with public databases to make sure that cell lines identities were correct and matched prior knowledge regarding driver mutations.

4.1.2 Neuroblastoma

Neuroblastoma is a pediatric cancer that develops from cells of the sympathetic nervous system. The disease has large variability in outcome, ranging from spontaneous regression to death. Tumors are grouped into risk categories (low, intermediate, high), taking into account a number of parameters like stage, age, tumor differentiation, MYCN (MYCN

Proto-Oncogene, BHLH Transcription Factor) status, or TERT status. The outlook for patients with low-risk neuroblastoma is rather good. They have a 5-year survival rate of greater than 95 percent and usually receive surgery only. On the other end of the spectrum, high risk neuroblastoma are much more challenging to treat and are responsible for up to 15 percent of total childhood cancer deaths (Park et al., 2008). Understanding the disease on a molecular level is therefore important, as this influences optimal treatment and prognosis.

There are two well known molecular biomarkers whose importance for neuroblastoma classification is established in the field. Most important is the *MYCN* amplification status, which is also a parameter in risk classification. *MYCN*, like *MYC*, is a master transcription factor and its copy number amplification has consequences for many downstream processes, as discussed in sec. 3.1.2. Therefore, its importance has long been recognized (Brodeur et al., 1984).

Another feature that influences a tumor cell's fitness is how well they can maintain telomere length. The telomeres are particular sections of DNA at the end of each chromosome arm. Like a protection cap, they ensure the integrity of the chromosome. Additionally, each cell division leads to slightly shorter telomeres in healthy somatic cells. Demonstrated by Leonard Hayflick (1961), human fetal cells in culture would divide ca. 40 to 60 times before entering senescence. This phenomenon was termed the "Hayflick limit" or "Hayflick hypothesis". To keep proliferating, cancer cells can acquire traits found in stem cells to maintain telomere length. One way, found in high risk neuroblastoma, are structural rearrangements of *TERT* (Telomerase Reverse Transcriptase), leading to overexpression of TERT (Peifer et al., 2015). While TERT is normally repressed in somatic cells, this deregulation allows telomere maintenance in cancer cells.

4.1.3 The Ras/MAPK pathway

Familiar to any cancer researcher, the Ras/MAPK pathway is among the most important and well studied signaling pathways. The pathway is regulating several cellular response programs such as proliferation, differentiation, and apoptosis (Mlakar et al., 2021). Variants in the Ras/MAPK pathway have recently attracted attention from neuroblastoma researchers as its permanent activation is a well-known cancer driver.

Conceptually, a signaling pathway works by propagating a stimulus, e.g. from a receptor on the cell surface, through a network of proteins. The final recipient of the signal might then be a transcription factor in the nucleus like c-MYC, which in turn initiates transcription of genes that promote cell growth. Most building blocks of a signaling cascade are protein kinases. They are enzymes that modify the confirmation and activity of other proteins by adding phosphate groups to phosphorylation sites. For instance in the Ras/MAPK pathway, the following steps might occur for a signal from the cell membrane to reach the nucleus: A ligand like Epidermal growth factor (EGF) binds to the epidermic growth factor receptor (EGFR, also called ErbB1). This leads to dimerization of the receptor, which in turn allows for kinase activity and autophosphorylation near the C-terminus (Downward et al., 1984). The adaptor protein Grb2 then recruits guanine nucleotide exchange factors (GEFs) such as Sos to the cell membrane. This close contact allows activation of Ras proteins (KRAS, HRAS, NRAS) by releasing GDP for GTP (Molina and Adjei, 2006). Ras activation leads to Raf recruitment and binding. The Raf family comprises of A-RAF, B-RAF and c-Raf, which are so-called MAP kinase kinases (MAP3K). That means that they phosphorylate MAP kinase kinases (MAP2K) like MAP2K1 (MEK1) or MAP1K2 (MEK2), which in turn phosphorylate MAP kinases (MAPK) like extracellular signal-regulated kinase 1 (ERK1) or

2 (ERK2).

However, the preceding description glances over one important aspect, i.e. that the signal is not just propagated from top to bottom like in a waterfall, but the pathway is a network with feedback loops (cf. Fig. 4.1). For example, ERK inhibits Raf upstream (Lake et al., 2016). This feedback can lead to signaling reactivation when MEK is inhibited (Fritsche-Guenther et al., 2011), leading to resistance.

4.1.4 Mutations in MAPK signaling in high risk neuroblastoma

For signaling to become corrupted, usually one of the kinases involved either acquires an activating mutation or is overexpressed due to a copy number amplification of the respective gene. Just to put into perspective how often such events occur, consider the frequency with which mutations in the RAS gene family occur. Taking a pan-cancer view, Prior et al. estimate that ca. 18.7 percent of cancer patients will have a tumor with a KRAS, HRAS or NRAS mutation, i.e. over 260 000 patients annually in the United States alone (Prior et al., 2020).

Mutations that affect the Ras/MAPK signaling pathway also occur in a subset of high risk neuroblastoma, with an enrichment after relapse as shown by Eleveld et al. (2015), who observed such events in 18 out of 23 relapsed tumors. Another kinase upstream of the Ras/MAPK axis is Anaplastic lymphoma kinase (ALK). In high risk neuroblastoma, one review estimated that ca. 14 % of tumors harbor a gain-of-function mutation in ALK (Trigg and Turner, 2018). These findings provide a strong rationale for targeted treatment approaches in high risk neuroblastoma harboring alterations in the Ras/MAPK pathway. However, over many years of investigation it has become clear that there will be no easy success stories, as the development of resistance leads to relapse (Mlakar et al., 2021). Thus, better approaches to target the Ras/MAPK pathway are still needed.

4.1.5 Cell line identification

One of the risks that researchers face when working with cancer cell lines is misidentification or contamination. It is therefore important to make sure that one is indeed working with the correct cells, because otherwise findings are baseless. One famous example is the confusion regarding the cell line MDA-MB-435, which was in fact derived from melanoma cells when researchers were using it as a model for breast cancer (Rae et al., 2007). It is therefore critical that all cell cultures used in a study are identified correctly.

4.2 Methods

4.2.1 Cell lines

A panel of nine cell lines, representative for high risk neuroblastoma, was selected. We chose the following cell lines: LAN6, SKNSH, NBEB1, IMR32, N206, SKNAS, KELLY, NGP, CHP212. Cultures of the cell lines were obtained as part of the Terminate-NB project.

4.2.2 Sequencing

Before sequencing, DNA was extracted from the respective cell line cultures. Libraries were prepared with Agilent Human All Exon v7 kit and sequenced on Illumina HiSeq 4000 or Novaseq 6000 machines. Sequencing data quality control was done using FASTQC (Andrews et al., 2010). The raw sequencing data is available from the European Nucleotide Archive (ENA) under Project ID PRJEB40670.

4.2.3 Read mapping and variant calling

FASTQ files were aligned to the human genome (versions GRCh37 and GRCh38) with BWA-mem (Li, 2013) and duplicates removed with Sambaster (Faust and Hall, 2014). Single nucleotide variants were called with Strelka (Kim et al., 2018).

4.2.4 Matching cell lines with public databases

Public databases like the Broad Institute's Cancer Cell Line Encyclopedia (CCLE, Barretina et al. (2012)) or the Cell Line Project (CLP, Tate et al. (2019)) by the Wellcome Sanger Institute collect extensive information on most cell lines used in cancer research. By using the genomic variants published, researchers can make sure that they are indeed working with the correct cells in culture.

One method to match variants from a cell line with the databases mentioned above is called Uniquorn (Otto et al., 2019). After variant calling, the genomic variants of each cell lines in the form of a variant call file (VCF) are given to Uniquorn as input, with tables denoting the best matching cell lines in the catalog as outputs.

4.2.5 Prioritization of cancer-related variants

Contrary to most settings where a normal sample can be used to filter germline variants from the tumor sample, this is not possible with cell lines. Variant calling will produce a list of variants with a mix of germline and somatic ones. Most of these variants will be of germline origin and thus not interesting for this research topic. To find cancer-related genes, there are typically two approaches: Firstly, prioritize all variants annotated in databases as cancer-specific drivers, e.g. using Cosmic (Tate et al., 2019) or CIViC (Griffith et al., 2017). Or secondly, filter out all variants that occur with greater frequency than some very low frequency, e.g. $> .01\%$, in a cohort of healthy people. The reasoning behind the second approach is that a variant that is prevalent in healthy people cannot be pathogenic (on its own). For so-called driver mutations like in the Ras/MAPK pathway, the first approach is more direct though, as most are known already. We used both approaches consecutively to generate a list of putative driver mutations impacting the Ras/MAPK pathway. Besides making variant calls available in VCF format, I also provided an accessible way to explore the data in our in-house cbiportal instance for all collaborators.

4.2.6 Drug sensitivity screen and signaling modeling

We selected 6 of 9 cell lines and designed perturbation-response experiments. These included stimulation for 30 minutes with 4 different growth factors (IGF1, EGF, NGF, and PDGF) and inhibition of ASK1, AKT, mTORC, MEK, RAF, PI3K for 90 minutes with 7 different agents. Activation of six different phosphoproteins (AKT, MEK, ERK, S6K, cJUN, p38)

was measured, yielding 240 data points per cell line (cf. Fig 2c in the original publication). These data were used to model signaling responses with the R package STASNet (Dorel et al., 2018) based on a literature pathway map (Fig. 4.1).

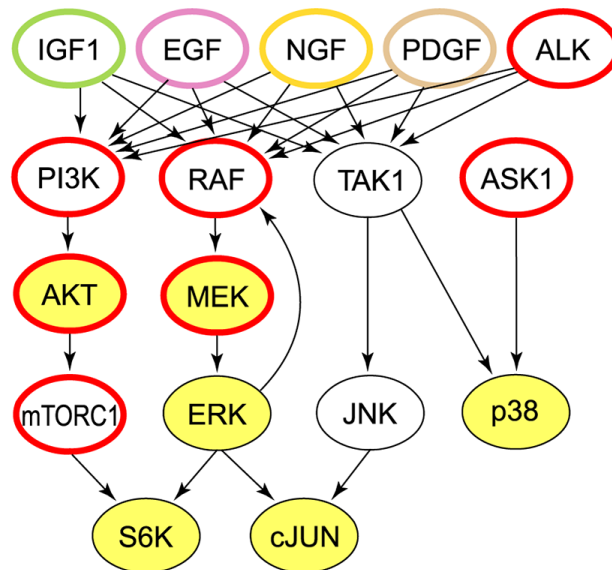


Figure 4.1: Ras/MAPK pathway representation extracted from the literature for modeling. IGF1, EGF, NGF and PDGF were used for stimulation of cells, red circles denote inhibited kinases and yellow fill denotes measured phosphoproteins in our perturbation experiments. Figure from “Neuroblastoma signaling models unveil combination therapies targeting feedback-mediated resistance” by Dorel et al. (2021), licensed under CC BY 4.0 (<https://creativecommons.org/licenses/by/4.0/>).

4.3 Results

We used Uniquorn to match all variant profiles to the Cosmic database of somatic mutations in cancer (Tate et al., 2019). For 5 out of 9 cell lines, we were able to confirm their identity, while NBEBC1, N206, NGP, CHP212 were not part of the databases used for identification. One exemplary output table generated with Uniquorn for the cell line LAN6 is shown in Tbl. 4.1. Using the cellosaurus web tool (<https://web.expasy.org/cellosaurus/>), we additionally checked that driver mutations matched public knowledge.

Table 4.1: Top Uniquorn results for cell line LAN6 when compared to the COSMIC cell line database.

Cancer Cell Line	Matches	Library
LAN-6	316	COSMIC
CA46	3	COSMIC
PC-3	2	COSMIC
ML-2	2	COSMIC
OS-RC-2	2	COSMIC
STS-0421	2	COSMIC

Cancer Cell Line	Matches	Library
HDQ-P1	2	COSMIC

We found that each cell line in our panel harbored at least one mutation in genes of the Ras/MAPK pathway (Fig. 4.2A). Most prevalently were mutations in ATRX (67 % of cell lines), followed by ALK, ATM, KRAS, NF1, NRAS and PRKDC, which were each mutated in 3 cell lines. Results of the drug sensitivity screens showed that response to the MEK inhibitor AZD6244 was the most variable (Fig. 4.2B) along with Rapamycin. We observe 6 cell lines being resistant ($IC_{50} > 10\mu\text{M}$) to AZD6244, with the 3 remaining ones being sensitive (Fig. 4.2C). We found no significant associations when correlating drug sensitivity of AZD6244 with mutations.

4.4 Discussion

Many high risk neuroblastoma tumors rely on increased signaling in the Ras/MAPK pathway. Our analysis of nine neuroblastoma cell lines showed that each had at least one mutation in the Ras/MAPK pathway. We observed that the mutational profile was not sufficient to explain drug response to MEK inhibition. Using mathematical modeling on drug perturbation data, we showed that negative feedback loops explain pathway re-activation and propose cell line specific combinatorial treatments.

One limitation of the study is that the response-perturbation data only was measured at one time point close to intervention. However, previous work showed these results to be transferable to chronic tumors (Schubert et al., 2018). Based on the literature network, signaling differences will be attributed to apparent feedback within the network, without consideration for other effects like non-linear interactions or cross-talk.

Future work might investigate if results hold up in vivo when tumors relapse on treatment. The mechanistic insights presented here can be used to design new trials with combinatorial treatments, i.e. multiple inhibitors. For clinical application, finding the optimal combination of drugs in high risk, Ras/MAPK active neuroblastoma without pathway readouts upon perturbation will be challenging. The application of ex-vivo models, so-called avatars might be needed in practice to test treatment options as proposed by Saez-Rodriguez and Blüthgen (2020).

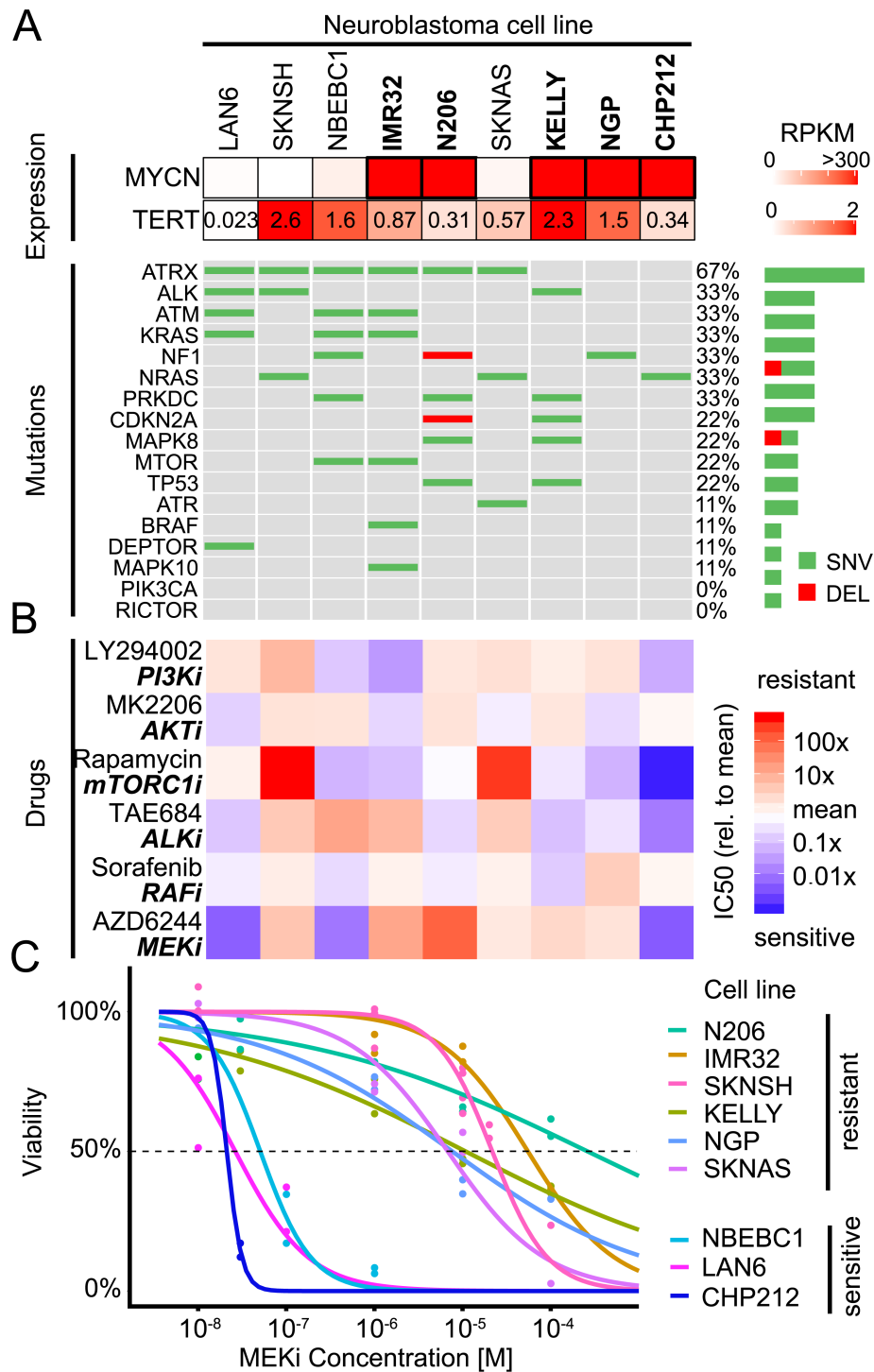


Figure 4.2: Mutations insufficiently explain drug sensitivity in high risk neuroblastoma cell lines. **A** Oncoprint for driver mutations in nine neuroblastoma cell lines. MYCN and TERT status based on mRNA expression. **B** Heatmap of relative IC₅₀ values for six drugs from the same cell lines. **C** Cell viability assay curves for the MEK inhibitor AZD6244. Intersection of each fitted curve with the dotted line (50 % viability) represents the IC₅₀. Figure from “Neuroblastoma signaling models unveil combination therapies targeting feedback-mediated resistance” by Dorel et al. (2021), licensed under CC BY 4.0 (<https://creativecommons.org/licenses/by/4.0/>)

Chapter 5

Extended Discussion

In this thesis, I presented my contributions to three publications in the field of translational precision oncology. The projects covered different cancer entities, i.e. head and neck squamous cell carcinoma, Burkitt lymphoma and neuroblastoma, respectively. In each setting, we sought to discover molecular biomarkers that would explain resistance against a specific drug or class of drugs. In Chapter 2, I presented our evidence for potentially distinct immune evasion in a subgroup of APOBEC-enriched, HPV-negative HNSCC based on our publication in the *International Journal of Cancer* (Messerschmidt et al., 2021). Chapter 3 covers our analysis of a lymphoma cell line engineered for resistance against the drug DZnep, where we found a copy number amplification of the gene *AHCY*, which is the target of DZnep. Finally, Chapter 4 gives an overview of our work on modeling the signaling dynamics in the Ras/MAPK pathway of high risk neuroblastoma cell lines given perturbation-response data.

5.1 Translation in precision oncology

In day-to-day practice, challenges in preclinical translational research are often the same as in basic research. Incomplete datasets, incomplete or incompatible metadata variables, or limited availability of specimen clashing with experimental design considerations are among the problems that researchers encounter. These problems are often less severe when working with tumor models, where sample availability might be constrained by time or money only. Getting data from human tumors can be considerably harder, to the point where either the data does not exist, one does not know it exists or one cannot get access to it. Unsurprisingly, among all sequencing data that were used in the three projects only ten datasets (matched WES and RNA-seq per tumor) were from cancer patients in Germany as part of DKTK Master. For the rest of our analyses, we relied on data from cancer cell cultures and open data (cf. Sec. 5.2.1).

Each of our projects was set at a different stage of the translational setting, although all were preclinical. Furthest from clinical application is our work in lymphoma (Akpa et al., 2020). Although we have found a new mechanism for cancer cells to become resistant to DZnep, it remains unclear if this is how a tumor would evolve in practice. One of the reasons is that a tumor has many possibilities to escape the treatment as discussed in Sec. 1.2. Therefore, we need more evidence of an *AHCY* amplification in other systems and ultimately in real tumors treated with DZnep in clinical trials.

Closer to clinical practice were our contributions in Messerschmidt et al. (2021) and Dorel et al. (2021), which do enable planning of prospective clinical trials for the biomarkers identified. To collect more evidence regarding our hypothesis of an association between the APOBEC3-induced mutation pattern, an analysis of a ICI-treated cohort with available genomic sequencing data would have been necessary. For this project, we tried actively to get access to an independent validation cohort, which we knew existed at a US-American university. Most researchers in the field are quite protective of the data they generate, especially before publishing on it themselves. Ultimately, no agreement could be reached and we proceeded with our own cohort of ten patients. At the time of writing, our work has not been cited in publication trying to validate our findings, but was picked up in a number of review articles (Affolter et al., 2022; Stampe et al., 2021; Warren et al., 2022). At least theoretically, the path forward is clear and analyses can be conducted as more data becomes available. DKTK Master continuously adds more data, so that now 68 cases with either HNSCC or salivary gland carcinoma are available for analysis (Horak et al., 2021).

What makes adoption of the mathematical model in Dorel et al. in a routine clinical setting hard is the need for perturbation experiments on patient-derived models. This is still a hurdle, as it takes not only time and money, but additionally needs established processes and interfaces to work. The use of short-term cell cultures to explore sensitivity to drug combinations remains an area of active research (Bosdriesz et al., 2022) that is likely to make its way into clinical practice at some point.

5.2 Reproducibility in translational research

Translational medicine is not immune to the problem known as the reproducibility crisis, sometimes also called replication crisis. In an alarming publication, researchers at Bayer showed that only 20 to 25% of selected studies on drug targets could be replicated in-house (Prinz et al., 2011). Another current meta-analysis of 193 experiments in preclinical cancer biology from 53 publications showed that information was only sufficient to repeat 50 experiments and of those, the median effect sizes were 85% lower than initially reported (Errington et al., 2021).

In translational cancer research, work might be done initially in cell lines, organoids, or other models like tumors in immunosuppressed mice. These models are compromised regarding the degree to which they can represent a real tumor. In vivo tumors can take years or decades to grow for instance (Fearon and Vogelstein, 1990), which means that tumor models have entirely different time-scales and dynamics. They also interface with the immune system and adjacent normal cells, which means the complexity is higher than in tumor models (Bożyk et al., 2022). Additionally, no tumor is clonal, i.e. there often is a considerable degree of genetic heterogeneity between tumor cells (McGranahan et al., 2015). What is therefore needed is not just reproducibility of an experiment, but generalization (Yarkoni, 2022). A gene or signature that is proposed as a biomarker in cancer needs to be predictive not only in cell cultures, organoids or mice, but in multiple cohorts, possibly in multiple (related) tumor entities, before it should be considered a good candidate for application in the clinic.

5.2.1 Open research: open access, open data, open source

Making data available to other researchers as part of a publication is important because it allows for three things. First, it makes the data that led to the conclusions in the paper part

of the scientific record. That in turn allows others to replicate the analysis. Finally, these data can be incorporated into new analyses or used as validation data in other studies. The gold standard for open data is described in the FAIR Guiding Principles (Wilkinson et al., 2016). FAIR stands for **F**indable, **A**ccessible, **I**nteroperable, and **R**eusable. Making data user-friendly to access and re-use, these principles go beyond open data. Initiatives such as The Cancer Genome Atlas show how much value accessible data can generate, as its data has been used in countless publications to this day and will in the future. National initiatives in Germany such as GHGA (“The german human genome-phenome archive,” 2020) and genomDE (“genomDE - nationale strategie für genommedizin,” 2022) will establish central repositories for medical data that offer researchers access to medical data for their research.

Showing our commitment to the principles of open research, the three selected publications presented in this dissertation were published open access, i.e. under the CC-BY 4 license by Creative Commons (creativecommons.org). The sequencing data for the panel of neuroblastoma cell lines is available from the European Sequencing Archive (ENA) under accession PRJEB40670 for other researchers to download and re-use.

The third component of open research in addition to open access publication and open data is software and code. By sharing the code that their analyses relied on, researchers are enabling others to follow and comprehend each step unambiguously, which would not be the case when reading a description of said software in the methods part of a publication. Further, Vandewalle (2012) could show that sharing code was associated with research impact. In this spirit, we try to make most of the software we develop at the BIH Core Unit Bioinformatics publicly available, such as our pipeline snappy for processing of high-throughput sequencing data (<https://github.com/bihealth/snappy-pipeline>), our tool to detect sample swaps based on HLA types (<https://github.com/bihealth/hlama>, Messerschmidt et al. (2017)) or our system to demultiplex Illumina sequencing data (<https://github.com/bihealth/digestiflow-demux>, Holtgrewe et al. (2019)).

References

- Affolter, A., Kern, J., Bieback, K., Scherl, C., Rotter, N., Lammert, A., 2022. Biomarkers and 3D models predicting response to immune checkpoint blockade in head and neck cancer (Review). *International Journal of Oncology* 61, 1–22. <https://doi.org/10.3892/IJ O.2022.5378/HTML>
- Akpa, C.A., Kleo, K., Lenze, D., Oker, E., Dimitrova, L., Hummel, M., 2019. DZNep-mediated apoptosis in B-cell lymphoma is independent of the lymphoma type, EZH2 mutation status and MYC, BCL2 or BCL6 translocations. *PLoS ONE* 14. <https://doi.org/10.1371/journal.pone.0220681>
- Akpa, C.A., Kleo, K., Oker, E., Tomaszewski, N., Messerschmidt, C., López, C., Wagener, R., Oehl-Huber, K., Dettmer, K., Schoeler, A., Others, 2020. Acquired resistance to DZNep-mediated apoptosis is associated with copy number gains of AHCY in a B-cell lymphoma model. *BMC cancer* 20, 1–12.
- Alexandrov, L.B., Nik-Zainal, S., Wedge, D.C., Aparicio, S.A.J.R., Behjati, S., Biankin, A.V., Bignell, G.R., Bolli, N., Borg, A., Børresen-Dale, A.-L., Boyault, S., Burkhardt, B., Butler, A.P., Caldas, C., Davies, H.R., Desmedt, C., Eils, R., Eyfjörd, J.E., Foekens, J.A., Greaves, M., Hosoda, F., Hutter, B., Ilicic, T., Imbeaud, S., Imielinski, M., Jäger, N., Jones, D.T.W., Jones, D., Knappskog, S., Kool, M., Lakhani, S.R., López-Otín, C., Martin, S., Munshi, N.C., Nakamura, H., Northcott, P.A., Pajic, M., Papaemmanuil, E., Paradiso, A., Pearson, J.V., Puente, X.S., Raine, K., Ramakrishna, M., Richardson, A.L., Richter, J., Rosenstiel, P., Schlesner, M., Schumacher, T.N., Span, P.N., Teague, J.W., Totoki, Y., Tutt, A.N.J., Valdés-Mas, R., Buuren, M.M. van, van 't Veer, L., Vincent-Salomon, A., Waddell, N., Yates, L.R., Zucman-Rossi, J., Andrew Futreal, P., McDermott, U., Lichter, P., Meyerson, M., Grimmond, S.M., Siebert, R., Campo, E., Shibata, T., Pfister, S.M., Campbell, P.J., Stratton, M.R., Shibata, T., Pfister, S.M., Campbell, P.J., Stratton, M.R., 2013. Signatures of mutational processes in human cancer. *Nature* 500, 415–421. <https://doi.org/10.1038/nature12477>
- Andrews, S., others, 2010. FastQC: A quality control tool for high throughput sequence data.
- Atkinson, A.J., Colburn, W.A., DeGruttola, V.G., DeMets, D.L., Downing, G.J., Hoth, D.F., Oates, J.A., Peck, C.C., Schooley, R.T., Spilker, B.A., Woodcock, J., Zeger, S.L., 2001. Biomarkers and surrogate endpoints: Preferred definitions and conceptual framework. *Clinical Pharmacology and Therapeutics* 69, 89–95. <https://doi.org/10.1067/mcp.2001.113989>
- Ayers, M., Lunceford, J., Nebozhyn, M., Murphy, E., Loboda, A., Kaufman, D.R., Albright, A., Cheng, J.D., Kang, S.P., Shankaran, V., Piha-Paul, S.A., Yearley, J., Seiwert, T.Y., Ribas, A., McClanahan, T.K., 2017. IFN- γ -related mRNA profile predicts clinical response to PD-1 blockade. *The Journal of Clinical Investigation* 127, 2930–2940. <https://doi.org/10.1172/JCI91190>
- Barretina, J., Caponigro, G., Stransky, N., Venkatesan, K., Margolin, A.A., Kim, S., Wilson,

- C.J., Lehár, J., Kryukov, G.V., Sonkin, D., Reddy, A., Liu, M., Murray, L., Berger, M.F., Monahan, J.E., Morais, P., Meltzer, J., Korejwa, A., Jané-Valbuena, J., Mapa, F.A., Thibault, J., Bric-Furlong, E., Raman, P., Shipway, A., Engels, I.H., Cheng, J., Yu, G.K., Yu, J., Aspesi, P., De Silva, M., Jagtap, K., Jones, M.D., Wang, L., Hatton, C., Palescandolo, E., Gupta, S., Mahan, S., Sougnez, C., Onofrio, R.C., Liefeld, T., MacConaill, L., Winckler, W., Reich, M., Li, N., Mesirov, J.P., Gabriel, S.B., Getz, G., Ardlie, K., Chan, V., Myer, V.E., Weber, B.L., Porter, J., Warmuth, M., Finan, P., Harris, J.L., Meyerson, M., Golub, T.R., Morrissey, M.P., Sellers, W.R., Schlegel, R., Garraway, L.A., 2012. The Cancer Cell Line Encyclopedia enables predictive modelling of anticancer drug sensitivity. *Nature* 483, 603–607. <https://doi.org/10.1038/NATURE11003>
- Beroukhir, R., Mermel, C.H., Porter, D., Wei, G., Raychaudhuri, S., Donovan, J., Barretina, J., Boehm, J.S., Dobson, J., Urashima, M., McHenry, K.T., Pinchback, R.M., Ligon, A.H., Cho, Y.J., Haery, L., Greulich, H., Reich, M., Winckler, W., Lawrence, M.S., Weir, B.A., Tanaka, K.E., Chiang, D.Y., Bass, A.J., Loo, A., Hoffman, C., Prensner, J., Liefeld, T., Gao, Q., Yecies, D., Signoretti, S., Maher, E., Kaye, F.J., Sasaki, H., Tepper, J.E., Fletcher, J.A., Tabernero, J., Baselga, J., Tsao, M.S., Demichelis, F., Rubin, M.A., Janne, P.A., Daly, M.J., Nucera, C., Levine, R.L., Ebert, B.L., Gabriele, S., Rustgi, A.K., Antonescu, C.R., Ladanyi, M., Letai, A., Garraway, L.A., Loda, M., Beer, D.G., True, L.D., Okamoto, A., Pomeroy, S.L., Singer, S., Golub, T.R., Lander, E.S., Getz, G., Sellers, W.R., Meyerson, M., 2010. The landscape of somatic copy-number alteration across human cancers. *Nature* 463, 899–905. <https://doi.org/10.1038/NATURE08822>
- Bila, M., Van Dessel, J., Smeets, M., Vander Poorten, V., Nuyts, S., Meulemans, J., Clement, P.M., 2022. A Retrospective Analysis of a Cohort of Patients Treated With Immune Checkpoint Blockade in Recurrent/Metastatic Head and Neck Cancer. *Frontiers in Oncology* 12, 1. <https://doi.org/10.3389/fonc.2022.761428>
- Bosdriesz, E., Fernandes Neto, J.M., Sieber, A., Bernards, R., Blüthgen, N., Wessels, L.F.A., 2022. Identifying mutant-specific multi-drug combinations using comparative network reconstruction. *iScience* 25. <https://doi.org/10.1016/j.isci.2022.104760>
- Bożyk, A., Wojas-Krawczyk, K., Krawczyk, P., Milanowski, J., 2022. Tumor Microenvironment—A Short Review of Cellular and Interaction Diversity. *Biology* 11. <https://doi.org/10.3390/biology11060929>
- Bretones, G., Delgado, M.D., León, J., 2015. Myc and cell cycle control. *Biochimica et Biophysica Acta - Gene Regulatory Mechanisms* 1849, 506–516. <https://doi.org/10.1016/j.bbagr.2014.03.013>
- Brodeur, G.M., Seeger, R.C., Schwab, M., Varmus, H.E., Michael Bishop, J., 1984. Amplification of N-myc in untreated human neuroblastomas correlates with advanced disease stage. *Science* 224, 1121–1124. <https://doi.org/10.1126/science.6719137>
- Buitrago-Pérez, A., Garaulet, G., Vázquez-Carballo, A., Paramio, J.M., García-Escudero, R., 2009. Molecular Signature of HPV-Induced Carcinogenesis: pRb, p53 and Gene Expression Profiling. *Current genomics* 10, 26–34. <https://doi.org/10.2174/138920209787581235>
- Bukowski, K., Kciuk, M., Kontek, R., 2020. Mechanisms of multidrug resistance in cancer chemotherapy. <https://doi.org/10.3390/ijms21093233>
- Burkitt, D., 1958. A sarcoma involving the jaws in african children. *British Journal of Surgery* 46, 218–223. <https://doi.org/10.1002/bjs.18004619704>
- Burns, M.B., Temiz, N.A., Harris, R.S., 2013. Evidence for APOBEC3B mutagenesis in multiple human cancers. *Nature Genetics* 45, 977–983. <https://doi.org/10.1038/ng.2701>
- Campbell, P.J., Getz, G., Korb, J.O., Stuart, J.M., Jennings, J.L., Stein, L.D., Perry, M.D., Nahal-Bose, H.K., Ouellette, B.F.F., Li, C.H., Rheinbay, E., Nielsen, G.P., Sgroi, D.C.,

Wu, C.L., Faquin, W.C., Deshpande, V., Boutros, P.C., Lazar, A.J., Hoadley, K.A., Louis, D.N., Dursi, L.J., Yung, C.K., Bailey, M.H., Saksena, G., Raine, K.M., Buchhalter, I., Kleinheinz, K., Schlesner, M., Zhang, J., Wang, W., Wheeler, D.A., Ding, L., Simpson, J.T., O'Connor, B.D., Yakneen, S., Ellrott, K., Miyoshi, N., Butler, A.P., Royo, R., Shorser, S.I., Vazquez, M., Rausch, T., Tiao, G., Waszak, S.M., Rodriguez-Martin, B., Shringarpure, S., Wu, D.Y., Demidov, G.M., Delaneau, O., Hayashi, S., Imoto, S., Habermann, N., Segre, A.V., Garrison, E., Cafferkey, A., Alvarez, E.G., Heredia-Genestar, J.M., Muyas, F., Drechsel, O., Bruzos, A.L., Temes, J., Zamora, J., Baez-Ortega, A., Kim, H.L., Mashl, R.J., Ye, K., DiBiase, A., Huang, K. lin, Letunic, I., McLellan, M.D., Newhouse, S.J., Shmaya, T., Kumar, S., Wedge, D.C., Wright, M.H., Yellapantula, V.D., Gerstein, M., Khurana, E., Marques-Bonet, T., Navarro, A., Bustamante, C.D., Siebert, R., Nakagawa, H., Easton, D.F., Ossowski, S., Tubio, J.M.C., De La Vega, F.M., Estivill, X., Yuen, D., Mihaiescu, G.L., Omberg, L., Ferretti, V., Sabarinathan, R., Pich, O., Gonzalez-Perez, A., Taylor-Weiner, A., Fittall, M.W., Demeulemeester, J., Tarabichi, M., Roberts, N.D., Van Loo, P., Cortés-Ciriano, I., Urban, L., Park, P., Zhu, B., Pitkänen, E., Li, Y., Saini, N., Klimczak, L.J., Weischenfeldt, J., Sidiropoulos, N., Alexandrov, L.B., Rabionet, R., Escaramis, G., Bosio, M., Holik, A.Z., Susak, H., Prasad, A., Erkek, S., Calabrese, C., Raeder, B., Harrington, E., Mayes, S., Turner, D., Juul, S., Roberts, S.A., Song, L., Koster, R., Mirabello, L., Hua, X., Tanskanen, T.J., Tojo, M., Chen, J., Aaltonen, L.A., Rättsch, G., Schwarz, R.F., Butte, A.J., Brazma, A., Chanock, S.J., Chatterjee, N., Stegle, O., Harismendy, O., Bova, G.S., Gordenin, D.A., Haan, D., Sieverling, L., Feuerbach, L., Chalmers, D., Joly, Y., Knoppers, B.M., Molnár-Gábor, F., Phillips, M., Thorogood, A., Townend, D., Goldman, M., Fonseca, N.A., Xiang, Q., Craft, B., Piñeiro-Yáñez, E., Muñoz, A., Petryszak, R., Füllgrabe, A., Al-Shahrour, F., Keays, M., Haussler, D., Weinstein, J.N., Huber, W., Valencia, A., Papatheodorou, I., Zhu, J., Fan, Y., Torrents, D., Bieg, M., Chen, K., Chong, Z., Cibulskis, K., Eils, R., Fulton, R.S., Gelpi, J.L., Gonzalez, S., Gut, I.G., Hach, F., Heinold, M., Hu, T., Huang, V., Hutter, B., Jäger, N., Jung, J., Kumar, Y., Lalansingh, C., Leshchiner, I., Livitz, D., Ma, E.Z., Maruvka, Y.E., Milovanovic, A., Nielsen, M.M., Paramasivam, N., Pedersen, J.S., Puiggròs, M., Sahinalp, S.C., Sarrafi, I., Stewart, C., Stobbe, M.D., Wala, J.A., Wang, J., Wendl, M., Werner, J., Wu, Z., Xue, H., Yamaguchi, T.N., Yellapantula, V., Davis-Dusenbery, B.N., Grossman, R.L., Kim, Y., Heinold, M.C., Hinton, J., Jones, D.R., Menzies, A., Stebbings, L., Hess, J.M., Rosenberg, M., Dunford, A.J., Gupta, M., Imielinski, M., Meyerson, M., Beroukhim, R., Reimand, J., Dhingra, P., Favero, F., Dentro, S., Wintersinger, J., Rudneva, V., Park, J.W., Hong, E.P., Heo, S.G., Kahles, A., Lehmann, K.V., Soulette, C.M., Shiraishi, Y., Liu, F., He, Y., Demircioğlu, D., Davidson, N.R., Greger, L., Li, S., Liu, D., Stark, S.G., Zhang, F., Amin, S.B., Bailey, P., Chateigner, A., Frenkel-Morgenstern, M., Hou, Y., Huska, M.R., Kilpinen, H., Lamaze, F.C., Li, C., Li, X., Li, X., Liu, X., Marin, M.G., Markowski, J., Nandi, T., Ojesina, A.I., Pan-Hammarström, Q., Park, P.J., Pedomallu, C.S., Su, H., Tan, P., Teh, B.T., Wang, J., Xiong, H., Ye, C., Yung, C., Zhang, X., Zheng, L., Zhu, S., Awadalla, P., Creighton, C.J., Wu, K., Yang, H., Göke, J., Zhang, Z., Brooks, A.N., Fittall, M.W., Martincorena, I., Rubio-Perez, C., Juul, M., Schumacher, S., Shapira, O., Tamborero, D., Mularoni, L., Hornshøj, H., Deu-Pons, J., Muiños, F., Bertl, J., Guo, Q., Gonzalez-Perez, A., Xiang, Q., Bazant, W., Barrera, E., Al-Sedairy, S.T., Aretz, A., Bell, C., Betancourt, M., Buchholz, C., Calvo, F., Chomienne, C., Dunn, M., Edmonds, S., Green, E., Gupta, S., Hutter, C.M., Jegalian, K., Jones, N., Lu, Y., Nakagama, H., Nettekoven, G., Planko, L., Scott, D., Shibata, T., Shimizu, K., Stratton, M.R., Yagawa, T., Tortora, G., VijayRaghavan,

K., Zenklusen, J.C., Townend, D., Aminou, B., Bartolome, J., Boroevich, K.A., Boyce, R., Buchanan, A., Byrne, N.J., Chen, Z., Cho, S., Choi, W., Clapham, P., Dow, M.T., Dursi, L.J., Eils, J., Farcas, C., Fayzullaev, N., Flicek, P., Heath, A.P., Hofmann, O., Hong, J.H., Hudson, T.J., Hübschmann, D., Ivkovic, S., Jeon, S.H., Jiao, W., Kabbe, R., Kahles, A., Kerssemakers, J.N.A., Kim, H., Kim, J., Koscher, M., Koures, A., Kovacevic, M., Lawerenz, C., Liu, J., Mijalkovic, S., Mijalkovic-Lazic, A.M., Miyano, S., Nastic, M., Nicholson, J., Ocana, D., Ohi, K., Ohno-Machado, L., Pihl, T.D., Prinz, M., Radovic, P., Short, C., Sofia, H.J., Spring, J., Struck, A.J., Tijanic, N., Vicente, D., Wang, Z., Williams, A., Woo, Y., Wright, A.J., Yang, L., Hamilton, M.P., Johnson, T.A., Kahraman, A., Kellis, M., Polak, P., Sallari, R., Sinnott-Armstrong, N., Mering, C. von, Beltran, S., Gerhard, D.S., Gut, M., Trotta, J.R., Whalley, J.P., Niu, B., Espiritu, S.M.G., Gao, S., Huang, Y., Lalansingh, C.M., Teague, J.W., Wendl, M.C., Abascal, F., Bader, G.D., Bandopadhyay, P., Barenboim, J., Brunak, S., Carlevaro-Fita, J., Chakravarty, D., Chan, C.W.Y., Choi, J.K., Diamanti, K., Fink, J.L., Frigola, J., Gambacorti-Passerini, C., Garsed, D.W., Haradhvala, N.J., Harmanci, A.O., Helmy, M., Herrmann, C., Hobolth, A., Hodzic, E., Hong, C., Isaev, K., Izarzugaza, J.M.G., Johnson, R., Juul, R.I., Kim, J., Kim, J.K., Jan Komorowski, Lanzós, A., Larsson, E., Lee, D., Li, S., Li, X., Lin, Z., Liu, E.M., Lochovsky, L., Lou, S., Madsen, T., Marchal, K., Martinez-Fundichely, A., McGillivray, P.D., Meyerson, W., Paczkowska, M., Park, K., Park, K., Pons, T., Pulido-Tamayo, S., Reyes-Salazar, I., Reyna, M.A., Rubin, M.A., Salichos, L., Sander, C., Schumacher, S.E., Shackleton, M., Shen, C., Shrestha, R., Shuai, S., Tsunoda, T., Umer, H.M., Uusküla-Reimand, L., Verbeke, L.P.C., Wadelius, C., Wadi, L., Warrell, J., Wu, G., Yu, J., Zhang, J., Zhang, X., Zhang, Y., Zhao, Z., Zou, L., Lawrence, M.S., Raphael, B.J., Bailey, P.J., Craft, D., Goldman, M.J., Aburatani, H., Binder, H., Dinh, H.Q., Heath, S.C., Hoffmann, S., Imbusch, C.D., Kretzmer, H., Laird, P.W., Martin-Subero, J.I., Nagae, G., Shen, H., Wang, Q., Weichenhan, D., Zhou, W., Berman, B.P., Brors, B., Plass, C., Akdemir, K.C., Bowtell, D.D.L., Burns, K.H., Busanovich, J., Chan, K., Dueso-Barroso, A., Edwards, P.A., Etemadmoghadam, D., Haber, J.E., Jones, D.T.W., Ju, Y.S., Kazanov, M.D., Koh, Y., Kumar, K., Lee, E.A., Lee, J.J.K., Lynch, A.G., Macintyre, G., Markowitz, F., Navarro, F.C.P., Pearson, J.V., Rippe, K., Scully, R., Villasante, I., Waddell, N., Yang, L., Yao, X., Yoon, S.S., Zhang, C.Z., Bergstrom, E.N., Boot, A., Covington, K., Fujimoto, A., Huang, M.N., Islam, S.M.A., McPherson, J.R., Morganella, S., Mustonen, V., Ng, A.W.T., Prokopec, S.D., Vázquez-García, I., Wu, Y., Yousif, F., Yu, W., Rozen, S.G., Rudneva, V.A., Shringarpure, S.S., Turner, D.J., Xia, T., Atwal, G., Chang, D.K., Cooke, S.L., Faltas, B.M., Haider, S., Kaiser, V.B., Karlić, R., Kato, M., Kübler, K., Margolin, A., Martin, S., Nik-Zainal, S., P'ng, C., Semple, C.A., Smith, J., Sun, R.X., Thai, K., Wright, D.W., Yuan, K., Biankin, A.V., Garraway, L., Grimmond, S.M., Adams, D.J., Anur, P., Cao, S., Christie, E.L., Cmero, M., Cun, Y., Dawson, K.J., Dentre, S.C., Deshwar, A.G., Donmez, N., Drews, R.M., Gerstung, M., Ha, G., Haase, K., Jerman, L., Ji, Y., Jolly, C., Lee, J., Lee-Six, H., Malikić, S., Mitchell, T.J., Morris, Q.D., Oesper, L., Peifer, M., Peto, M., Rosebrock, D., Rubanova, Y., Salcedo, A., Sengupta, S., Shi, R., Shin, S.J., Spiro, O., Vembu, S., Wintersinger, J.A., Yang, T.P., Yu, K., Zhu, H., Spellman, P.T., Chen, Y., Fujita, M., Han, L., Hasegawa, T., Komura, M., Li, J., Mizuno, S., Shimizu, E., Wang, Y., Xu, Y., Yamaguchi, R., Yang, F., Yang, Y., Yoon, C.J., Yuan, Y., Liang, H., Alawi, M., Borozan, I., Brewer, D.S., Cooper, C.S., Desai, N., Grundhoff, A., Iskar, M., Su, X., Zapatka, M., Lichter, P., Alsop, K., Bruxner, T.J.C., Christ, A.N., Cordner, S.M., Cowin, P.A., Drapkin, R., Fereday, S., George, J., Hamilton, A., Holmes, O., Hung, J.A., Kassahn, K.S., Kazakoff, S.H., Kennedy, C.J.,

Leonard, C.R., Mileskin, L., Miller, D.K., Arnau, G.M., Mitchell, C., Newell, F., Nones, K., Patch, A.M., Quinn, M.C., Taylor, D.F., Thorne, H., Traficante, N., Vedururu, R., Waddell, N.M., Waring, P.M., Wood, S., Xu, Q., DeFazio, A., Anderson, M.J., Antonello, D., Barbour, A.P., Bassi, C., Bersani, S., Cataldo, I., Chantrill, L.A., Chiew, Y.E., Chou, A., Cingarlini, S., Cloonan, N., Corbo, V., Davi, M.V., Duthie, F.R., Gill, A.J., Graham, J.S., Harliwong, I., Jamieson, N.B., Johns, A.L., Kench, J.G., Landoni, L., Lawlor, R.T., Mafficini, A., Merrett, N.D., Miotto, M., Musgrove, E.A., Nagrial, A.M., Oien, K.A., Pajic, M., Pinese, M., Robertson, A.J., Rومان, I., Rusev, B.C., Samra, J.S., Scardoni, M., Scarlett, C.J., Scarpa, A., Sereni, E., Sikora, K.O., Simbolo, M., Taschuk, M.L., Toon, C.W., Vicentini, C., Wu, J., Zeps, N., Behren, A., Burke, H., Cebon, J., Dagg, R.A., De Paoli-Iseppi, R., Dutton-Regester, K., Field, M.A., Fitzgerald, A., Hersey, P., Jakrot, V., Johansson, P.A., Kakavand, H., Kefford, R.F., Lau, L.M.S., Long, G.V., Pickett, H.A., Pritchard, A.L., Pupo, G.M., Saw, R.P.M., Schramm, S.J., Shang, C.A., Shang, P., Spillane, A.J., Stretch, J.R., Tembe, V., Thompson, J.F., Vilain, R.E., Wilmott, J.S., Yang, J.Y., Hayward, N.K., Mann, G.J., Scolyer, R.A., Bartlett, J., Bavi, P., Chadwick, D.E., Chan-Seng-Yue, M., Cleary, S., Connor, A.A., Czajka, K., Denroche, R.E., Dhani, N.C., Eagles, J., Gallinger, S., Grant, R.C., Hedley, D., Hollingsworth, M.A., Jang, G.H., Johns, J., Kalimuthu, S., Liang, S.B., Lungu, I., Luo, X., Mbabaali, F., McPherson, T.A., Miller, J.K., Moore, M.J., Notta, F., Pasternack, D., Petersen, G.M., Roehrl, M.H.A., Sam, M., Selander, I., Serra, S., Shahabi, S., Thayer, S.P., Timms, L.E., Wilson, G.W., Wilson, J.M., Wouters, B.G., McPherson, J.D., Beck, T.A., Bhandari, V., Collins, C.C., Fleshner, N.E., Fox, N.S., Fraser, M., Heisler, L.E., Lalonde, E., Livingstone, J., Meng, A., Sabelnykova, V.Y., Shiah, Y.J., Van der Kwast, T., Bristow, R.G., Ding, S., Fan, D., Li, L., Nie, Y., Xiao, X., Xing, R., Yang, S., Yu, Y., Zhou, Y., Banks, R.E., Bourque, G., Brennan, P., Letourneau, L., Riazalhosseini, Y., Scelo, G., Vasudev, N., Viksna, J., Lathrop, M., Tost, J., Ahn, S.M., Aparicio, S., Arnould, L., Aure, M.R., Bhosle, S.G., Birney, E., Borg, A., Boyault, S., Brinkman, A.B., Brock, J.E., Broeks, A., Børresen-Dale, A.L., Caldas, C., Chin, S.F., Davies, H., Desmedt, C., Dirix, L., Dronov, S., Ehinger, A., Eyfjord, J.E., Fatima, A., Foekens, J.A., Futreal, P.A., Garred, Ø., Giri, D.D., Glodzik, D., Grabau, D., Hilmarsdottir, H., Hooijer, G.K., Jacquemier, J., Jang, S.J., Jonasson, J.G., Jonkers, J., Kim, H.Y., King, T.A., Knappskog, S., Kong, G., Krishnamurthy, S., Lakhani, S.R., Langerød, A., Larsimont, D., Lee, H.J., Lee, J.Y., Lee, M.T.M., Lingjærde, O.C., MacGrogan, G., Martens, J.W.M., O'Meara, S., Pauporté, I., Pinder, S., Pivot, X., Provenzano, E., Purdie, C.A., Ramakrishna, M., Ramakrishnan, K., Reis-Filho, J., Richardson, A.L., Ringnér, M., Rodriguez, J.B., Rodríguez-González, F.G., Romieu, G., Salgado, R., Sauer, T., Shepherd, R., Sieuwerts, A.M., Simpson, P.T., Smid, M., Sotiriou, C., Span, P.N., Stefánsson, Ó.A., Stenhouse, A., Stunnenberg, H.G., Sweep, F., Tan, B.K.T., Thomas, G., Thompson, A.M., Tommasi, S., Treilleux, I., Tutt, A., Ueno, N.T., Van Laere, S., Van den Eynden, G.G., Vermeulen, P., Viari, A., Vincent-Salomon, A., Wong, B.H., Yates, L., Zou, X., Deurzen, C.H.M. van, Vijver, M.J. van de, Veer, L. van't, Ammerpohl, O., Aukema, S., Bergmann, A.K., Bernhart, S.H., Borkhardt, A., Borst, C., Burkhardt, B., Claviez, A., Goebler, M.E., Haake, A., Haas, S., Hansmann, M., Hoell, J.I., Hummel, M., Karsch, D., Klapper, W., Kneba, M., Kreuz, M., Kube, D., Küppers, R., Lenze, D., Loeffler, M., López, C., Mantovani-Löffler, L., Möller, P., Ott, G., Radlwimmer, B., Richter, J., Rohde, M., Rosenstiel, P.C., Rosenwald, A., Schilhabel, M.B., Schreiber, S., Stadler, P.F., Staib, P., Stilgenbauer, S., Sungalee, S., Szczepanowski, M., Toprak, U.H., Trümper, L.H.P., Wagener, R., Zenz, T., Hovestadt, V., Kalle, C. von, Kool, M., Korshunov, A., Landgraf, P., Lehrach, H., Northcott, P.A., Pfister, S.M., Reifenberger, G.,

- Warnatz, H.J., Wolf, S., Yaspo, M.L., Assenov, Y., Gerhauser, C., Minner, S., Schlomm, T., Simon, R., Sauter, G., Sülmann, H., Biswas, N.K., Maitra, A., Majumder, P.P., Sarin, R., Barbi, S., Bonizzato, G., Cantù, C., Dei Tos, A.P., Fassan, M., Grimaldi, S., Luchini, C., Malleo, G., Marchegiani, G., Milella, M., Paiella, S., Pea, A., Pederzoli, P., Ruzzenente, A., Salvia, R., Sperandio, N., Arai, Y., Hama, N., Hiraoka, N., Hosoda, F., Nakamura, H., Ojima, H., Okusaka, T., Totoki, Y., Urushidate, T., Fukayama, M., Ishikawa, S., Katai, H., Katoh, H., Komura, D., Rokutan, H., Saito-Adachi, M., Suzuki, A., Taniguchi, H., Tatsuno, K., Ushiku, T., Yachida, S., Yamamoto, S., Aikata, H., Arihiro, K., Ariizumi, S. ichi, Chayama, K., Furuta, M., Gotoh, K., Hayami, S., Hirano, S., Kawakami, Y., Maejima, K., Nakamura, T., Nakano, K., Ohdan, H., Sasaki-Oku, A., Tanaka, H., Ueno, M., Yamamoto, M., Yamaue, H., Choo, S.P., Cutcutache, I., Khuntikeo, N., Ong, C.K., Pairojkul, C., Popescu, I., Ahn, K.S., Aymerich, M., Lopez-Guillermo, A., López-Otín, C., Puente, X.S., Campo, E., Amary, F., Baumhoer, D., Behjati, S., Bjerkehagen, B., Futreal, P.A., Myklebost, O., Pillay, N., Tarpey, P., Tirabosco, R., Zaikova, O., Flanagan, A.M., Boulton, J., Bowen, D.T., Cazzola, M., Green, A.R., Hellstrom-Lindberg, E., Malcovati, L., Nangalia, J., Papaemmanuil, E., Vyas, P., Ang, Y., Barr, H., Beardsmore, D., Eldridge, M., Gossage, J., Grehan, N., Hanna, G.B., Hayes, S.J., Hupp, T.R., Khoo, D., Lagergren, J., Lovat, L.B., MacRae, S., O'Donovan, M., O'Neill, J.R., Parsons, S.L., Preston, S.R., Puig, S., Roques, T., Sanders, G., Sothi, S., Tavaré, S., Tucker, O., Turkington, R., Underwood, T.J., Welch, I., Fitzgerald, R.C., Berney, D.M., De Bono, J.S., Cahill, D., Camacho, N., Dennis, N.M., Dudderidge, T., Edwards, S.E., Fisher, C., Foster, C.S., Ghori, M., Gill, P., Gnanapragasam, V.J., Gundem, G., Hamdy, F.C., Hawkins, S., Hazell, S., Howat, W., Isaacs, W.B., Karaszi, K., Kay, J.D., Khoo, V., Kote-Jarai, Z., Kremeyer, B., Kumar, P., Lambert, A., Leongamornlert, D.A., Livni, N., Lu, Y.J., Luxton, H.J., Marsden, L., Massie, C.E., Matthews, L., Mayer, E., McDermott, U., Merson, S., Neal, D.E., Ng, A., Nicol, D., Ogden, C., Rowe, E.W., Shah, N.C., Thomas, S., Thompson, A., Verrill, C., Visakorpi, T., Warren, A.Y., Whitaker, H.C., Zhang, H., As, N. van, Eeles, R.A., Abeshouse, A., Agrawal, N., Akbani, R., Al-Ahmadie, H., Albert, M., Aldape, K., Ally, A., Appelbaum, E.L., Armenia, J., Asa, S., Auman, J.T., Balasundaram, M., Balu, S., Barnholtz-Sloan, J., Bathe, O.F., Baylin, S.B., Benz, C., Berchuck, A., Berrios, M., Bigner, D., Birrer, M., Bodenheimer, T., Boice, L., Bootwalla, M.S., Bosenberg, M., Bowlby, R., Boyd, J., Broaddus, R.R., Brock, M., Brooks, D., Bullman, S., Caesar-Johnson, S.J., Carey, T.E., Carlsen, R., Cerfolio, R., Chandan, V.S., Chen, H.W., Cherniack, A.D., Chien, J., Cho, J., Chuah, E., Cibulskis, C., Cope, L., Cordes, M.G., Curley, E., Czerniak, B., Danilova, L., Davis, I.J., Defreitas, T., Demchok, J.A., Dhalla, N., Dhir, R., Doddapaneni, H.V., El-Naggar, A., Felau, I., Ferguson, M.L., Finocchiaro, G., Fong, K.M., Frazer, S., Friedman, W., Fronick, C.C., Fulton, L.A., Gabriel, S.B., Gao, J., Gehlenborg, N., Gershenwald, J.E., Ghossein, R., Giama, N.H., Gibbs, R.A., Gomez, C., Govindan, R., Hayes, D.N., Hegde, A.M., Heiman, D.I., Heins, Z., Hepperla, A.J., Holbrook, A., Holt, R.A., Hoyle, A.P., Hruban, R.H., Hu, J., Huang, M., Huntsman, D., Huse, J., Iacobuzio-Donahue, C.A., Ittmann, M., Jayaseelan, J.C., Jefferys, S.R., Jones, C.D., Jones, S.J.M., Juhl, H., Kang, K.J., Karlan, B., Kasaian, K., Kebebew, E., Kim, H.K., Korchina, V., Kundra, R., Lai, P.H., Lander, E., Le, X., Lee, D., Levine, D.A., Lewis, L., Ley, T., Li, H.I., Lin, P., Linehan, W.M., Liu, F.F., Lu, Y., Lype, L., Ma, Y., Maglinte, D.T., Mardis, E.R., Marks, J., Marra, M.A., Matthew, T.J., Mayo, M., McCune, K., Meier, S.R., Meng, S., Mieczkowski, P.A., Mikkelsen, T., Miller, C.A., Mills, G.B., Moore, R.A., Morrison, C., Mose, L.E., Moser, C.D., Mungall, A.J., Mungall, K., Mutch, D., Muzny, D.M., Myers, J., Newton, Y., Noble, M.S., O'Donnell, P., O'Neill,

- B.P., Ochoa, A., Park, J.W., Parker, J.S., Pass, H., Pastore, A., Pennell, N.A., Perou, C.M., Petrelli, N., Potapova, O., Rader, J.S., Ramalingam, S., Rathmell, W.K., Reuter, V., Reynolds, S.M., Ringel, M., Roach, J., Roberts, L.R., Robertson, A.G., Sadeghi, S., Saller, C., Sanchez-Vega, F., Schandorf, D., Schein, J.E., Schmidt, H.K., Schultz, N., Seethala, R., Senbabaoglu, Y., Shelton, T., Shi, Y., Shih, J., Shmulevich, I., Shriver, C., Signoretti, S., Simons, J.V., Singer, S., Sipahimalani, P., Skelly, T.J., Smith-McCune, K., Succi, N.D., Soloway, M.G., Sood, A.K., Tam, A., Tan, D., Tarnuzzer, R., Thiessen, N., Thompson, R.H., Thorne, L.B., Tsao, M., Umbricht, C., Van Den Berg, D.J., Van Meir, E.G., Veluvolu, U., Voet, D., Wang, L., Weinberger, P., Weisenberger, D.J., Wagle, D., Wilkerson, M.D., Wilson, R.K., Winterhoff, B., Wiznerowicz, M., Wong, T., Wong, W., Xi, L., Yau, C., Zhang, H., Zhang, H., Zhang, J., 2020. Pan-cancer analysis of whole genomes. *Nature* 2020 578:7793 578, 82–93. <https://doi.org/10.1038/s41586-020-1969-6>
- Chen, H., Liu, H., Qing, G., 2018. Targeting oncogenic Myc as a strategy for cancer treatment. *Signal Transduction and Targeted Therapy* 3, 1–7. <https://doi.org/10.1038/s41392-018-0008-7>
- Chow, L.Q.M., 2020. Head and Neck Cancer. *The New England journal of medicine* 382, 60–72. <https://doi.org/10.1056/NEJMRA1715715>
- Cohrs, R.J., Martin, T., Ghahramani, P., Bidaut, L., Higgins, P.J., Shahzad, A., 2015. Translational medicine definition by the European society for translational medicine. *New Horizons in Translational Medicine* 2, 86–88. <https://doi.org/10.1016/J.NHTM.2014.12.002>
- Corcoran, R.B., Dias-Santagata, D., Bergethon, K., Iafrate, A.J., Settleman, J., Engelman, J.A., 2010. BRAF gene amplification can promote acquired resistance to MEK inhibitors in cancer cells harboring the BRAF V600E mutation. *Science signaling* 3. <https://doi.org/10.1126/SCISIGNAL.2001148>
- Cristescu, R., Mogg, R., Ayers, M., Albright, A., Murphy, E., Yearley, J., Sher, X., Liu, X.Q., Lu, H., Nebozhyn, M., Zhang, C., Lunceford, J.K., Joe, A., Cheng, J., Webber, A.L., Ibrahim, N., Plimack, E.R., Ott, P.A., Seiwert, T.Y., Ribas, A., McClanahan, T.K., Tomassini, J.E., Loboda, A., Kaufman, D., 2018. Pan-tumor genomic biomarkers for PD-1 checkpoint blockade-based immunotherapy. *Science* 362, eaar3593. <https://doi.org/10.1126/science.aar3593>
- Crucitta, S., Cucchiara, F., Mathijssen, R., Mateo, J., Jager, A., Joosse, A., Passaro, A., Attili, I., Petrini, I., Schaik, R. van, Danesi, R., Del Re, M., 2022. Treatment-driven tumour heterogeneity and drug resistance: Lessons from solid tumours. <https://doi.org/10.1016/j.ctrv.2022.102340>
- D’Avo Luís, A.B., Seo, M.K., 2021. Has the development of cancer biomarkers to guide treatment improved health outcomes? *The European Journal of Health Economics* 22, 789. <https://doi.org/10.1007/S10198-021-01290-4>
- Dagogo-Jack, I., Shaw, A.T., 2018. Tumour heterogeneity and resistance to cancer therapies. <https://doi.org/10.1038/nrclinonc.2017.166>
- Dorel, M., Klinger, B., Gross, T., Sieber, A., Prahallad, A., Bosdriesz, E., Wessels, L.F.A., Blüthgen, N., 2018. Modelling signalling networks from perturbation data. *Bioinformatics* 34, 4079–4086. <https://doi.org/10.1093/BIOINFORMATICS/BTY473>
- Dorel, M., Klinger, B., Mari, T., Toedling, J., Blanc, E., Messerschmidt, C., Nadler-Holly, M., Ziehm, M., Sieber, A., Hertwig, F., Beule, D., Eggert, A., Schulte, J.H., Selbach, M., Blüthgen, N., 2021. Neuroblastoma signalling models unveil combination therapies targeting feedback-mediated resistance. *PLOS Computational Biology* 17, e1009515. <https://doi.org/10.1371/journal.pcbi.1009515>

- Downward, J., Yarden, Y., Mayes, E., Scrace, G., Totty, N., Stockwell, P., Ullrich, A., Schlessinger, J., Waterfield, M.D., 1984. Close similarity of epidermal growth factor receptor and v-erb-B oncogene protein sequences. *Nature* 307, 521–527. <https://doi.org/10.1038/307521a0>
- Dubois, P., Kyle, M., 2016. The Effects of Pharmaceutical Innovation on Cancer Mortality Rates.
- Duffy, M.J., O’Grady, S., Tang, M., Crown, J., 2021. MYC as a target for cancer treatment. *Cancer Treatment Reviews* 94, 102154. <https://doi.org/10.1016/j.ctrv.2021.102154>
- Eleveld, T.F., Oldridge, D.A., Bernard, V., Koster, J., Daage, L.C., Diskin, S.J., Schild, L., Bentahar, N.B., Bellini, A., Chicard, M., Lapouble, E., Combaret, V., Legoux-Né, P., Michon, J., Pugh, T.J., Hart, L.S., Rader, J., Attiyeh, E.F., Wei, J.S., Zhang, S., Naranjo, A., Gastier-Foster, J.M., Hogarty, M.D., Asgharzadeh, S., Smith, M.A., Guidry Auvil, J.M., Watkins, T.B.K., Zwijnenburg, D.A., Ebus, M.E., Van Sluis, P., Hakkert, A., Van Wezel, E., Van Der Schoot, C.E., Westerhout, E.M., Schulte, J.H., Tytgat, G.A., Dolman, M.E.M., Janoueix-Lerosey, I., Gerhard, D.S., Caron, H.N., Delattre, O., Khan, J., Versteeg, R., Schleiermacher, G., Molenaar, J.J., Maris, J.M., 2015. Relapsed neuroblastomas show frequent RAS-MAPK pathway mutations. *Nature Genetics* 47, 864–871. <https://doi.org/10.1038/ng.3333>
- Errington, T.M., Mathur, M., Soderberg, C.K., Denis, A., Perfito, N., Iorns, E., Nosek, B.A., 2021. Investigating the replicability of preclinical cancer biology. *eLife* 10. <https://doi.org/10.7554/ELIFE.71601>
- Faust, G.G., Hall, I.M., 2014. SAMBLASTER: Fast duplicate marking and structural variant read extraction. *Bioinformatics* 30, 2503–2505. <https://doi.org/10.1093/bioinformatics/btu314>
- FDA-NIH Biomarker Working Group, 2016a. Diagnostic biomarker [WWW Document]. URL <https://www.ncbi.nlm.nih.gov/books/NBK402285/> (accessed 5.28.2022).
- FDA-NIH Biomarker Working Group, 2016b. Prognostic biomarker [WWW Document]. URL <https://www.ncbi.nlm.nih.gov/books/NBK402289/> (accessed 5.28.2022).
- FDA-NIH Biomarker Working Group, 2016c. Predictive biomarker [WWW Document]. URL <https://www.ncbi.nlm.nih.gov/books/NBK402283/> (accessed 5.28.2022).
- Fearon, E.R., Vogelstein, B., 1990. A genetic model for colorectal tumorigenesis. *Cell* 61, 759–767. [https://doi.org/10.1016/0092-8674\(90\)90186-I](https://doi.org/10.1016/0092-8674(90)90186-I)
- Ferris, R.L., Blumenschein, G., Fayette, J., Guigay, J., Colevas, A.D., Licitra, L., Harrington, K., Kasper, S., Vokes, E.E., Even, C., Worden, F., Saba, N.F., Iglesias Docampo, L.C., Haddad, R., Rordorf, T., Kiyota, N., Tahara, M., Monga, M., Lynch, M., Geese, W.J., Kopit, J., Shaw, J.W., Gillison, M.L., 2016. Nivolumab for Recurrent Squamous-Cell Carcinoma of the Head and Neck. *New England Journal of Medicine* 375, 1856–1867. <https://doi.org/10.1056/NEJMoa1602252>
- Francis, N.J., Kingston, R.E., Woodcock, C.L., 2004. Chromatin compaction by a polycomb group protein complex. *Science (New York, N.Y.)* 306, 1574–1577. <https://doi.org/10.1126/SCIENCE.1100576>
- Fritsche-Guenther, R., Witzel, F., Sieber, A., Herr, R., Schmidt, N., Braun, S., Brummer, T., Sers, C., Blüthgen, N., 2011. Strong negative feedback from Erk to Raf confers robustness to MAPK signalling. *Molecular Systems Biology* 7, 489. <https://doi.org/10.1038/msb.2011.27>
- Gan, L., Yang, Y., Li, Q., Feng, Y., Liu, T., Guo, W., 2018. Epigenetic regulation of cancer progression by EZH2: From biological insights to therapeutic potential. *Biomarker Research* 6, 1–10. <https://doi.org/10.1186/s40364-018-0122-2>

- Gao, J., Aksoy, B.A., Dogrusoz, U., Dresdner, G., Gross, B., Sumer, S.O., Sun, Y., Jacobsen, A., Sinha, R., Larsson, E., Cerami, E., Sander, C., Schultz, N., 2013. Integrative Analysis of Complex Cancer Genomics and Clinical Profiles Using the cBioPortal. *Science Signaling* 6, p11–p11. <https://doi.org/10.1126/scisignal.2004088>
- genomDE - nationale strategie für genommedizin [WWW Document], 2022. URL <https://www.bundesgesundheitsministerium.de/themen/gesundheitswesen/personalisierte-medicin/genomde-de.html>
- Greaves, M., Maley, C.C., 2012. Clonal evolution in cancer. <https://doi.org/10.1038/nature10762>
- Griffith, M., Spies, N.C., Krysiak, K., McMichael, J.F., Coffman, A.C., Danos, A.M., Ainscough, B.J., Ramirez, C.A., Rieke, D.T., Kujan, L., Barnell, E.K., Wagner, A.H., Skidmore, Z.L., Wollam, A., Liu, C.J., Jones, M.R., Bilski, R.L., Lesurf, R., Feng, Y.Y., Shah, N.M., Bonakdar, M., Trani, L., Matlock, M., Ramu, A., Campbell, K.M., Spies, G.C., Graubert, A.P., Gangavarapu, K., Eldred, J.M., Larson, D.E., Walker, J.R., Good, B.M., Wu, C., Su, A.I., Dienstmann, R., Margolin, A.A., Tamborero, D., Lopez-Bigas, N., Jones, S.J.M., Bose, R., Spencer, D.H., Wartman, L.D., Wilson, R.K., Mardis, E.R., Griffith, O.L., 2017. CIViC is a community knowledgebase for expert crowdsourcing the clinical interpretation of variants in cancer. *Nature Genetics* 49, 170–174. <https://doi.org/10.1038/ng.3774>
- Haider, T., Pandey, V., Banjare, N., Gupta, P.N., Soni, V., 2020. Drug resistance in cancer: mechanisms and tackling strategies. *Pharmacological Reports* 2020 72:5 72, 1125–1151. <https://doi.org/10.1007/S43440-020-00138-7>
- Hanahan, D., Weinberg, R.A., 2000. The Hallmarks of Cancer. *Cell* 100, 57–70. [https://doi.org/10.1016/S0092-8674\(00\)81683-9](https://doi.org/10.1016/S0092-8674(00)81683-9)
- Harbers, L., Agostini, F., Nicos, M., Poddighe, D., Bienko, M., Crosetto, N., 2021. Somatic Copy Number Alterations in Human Cancers: An Analysis of Publicly Available Data From The Cancer Genome Atlas. *Frontiers in Oncology* 11, 2877. <https://doi.org/10.3389/FONC.2021.700568/BIBTEX>
- Hartl, D., Luca, V. de, Kostikova, A., Laramie, J., Kennedy, S., Ferrero, E., Siegel, R., Fink, M., Ahmed, S., Millholland, J., Schuhmacher, A., Hinder, M., Piali, L., Roth, A., 2021. Translational precision medicine: an industry perspective. *Journal of Translational Medicine* 19, 1–14. <https://doi.org/10.1186/s12967-021-02910-6>
- Hayflick, L., Moorhead, P.S., 1961. The serial cultivation of human diploid cell strains. *Experimental Cell Research* 25, 585–621. [https://doi.org/10.1016/0014-4827\(61\)90192-6](https://doi.org/10.1016/0014-4827(61)90192-6)
- Hoffman, B., Liebermann, D.A., 2008. Apoptotic signaling by c-MYC. *Oncogene* 27, 6462–6472. <https://doi.org/10.1038/onc.2008.312>
- Hoffman, R., Benz, E.J., Silberstein, L.E., Heslop, H.E., Weitz, J.I., Anastasi, J., Salama, M.E., Abutalib, S., 2017. *Hematology: Basic principles and practice*. Elsevier Inc. <https://doi.org/10.1016/C2013-0-23355-9>
- Holtgrewe, M., Messerschmidt, C., Nieminen, M., Beule, D., 2019. Digestiflow: from BCL to FASTQ with ease. *Bioinformatics* 36, 1983–1985. <https://doi.org/10.1093/bioinformatics/btz850>
- Horak, P., Heining, C., Kreutzfeldt, S., Hutter, B., Mock, A., Hüllelin, J., Fröhlich, M., Uhrig, S., Jahn, A., Rump, A., Gieldon, L., Möhrmann, L., Hanf, D., Teleanu, V., Heilig, C.E., Lipka, D.B., Allgäuer, M., Ruhnke, L., Laßmann, A., Endris, V., Neumann, O., Penzel, R., Beck, K., Richter, D., Winter, U., Wolf, S., Pfütze, K., Geörg, C., Meißburger, B., Buchhalter, I., Augustin, M., Aulitzky, W.E., Hohenberger, P., Kroiss, M., Schirmacher, P., Schlenk, R.F., Keilholz, U., Klauschen, F., Folprecht, G., Bauer,

- S., Siveke, J.T., Brandts, C.H., Kindler, T., Boerries, M., Illert, A.L., Von Bubnoff, N., Jost, P.J., Spiekermann, K., Bitzer, M., Schulze-Osthoff, K., Von Kalle, C., Klink, B., Brors, B., Stenzinger, A., Schröck, E., Hübschmann, D., Weichert, W., Glimm, H., Fröhling, S., 2021. Comprehensive genomic and transcriptomic analysis for guiding therapeutic decisions in patients with rare cancers. *Cancer Discovery* 11, 2780–2795. <https://doi.org/10.1158/2159-8290.CD-21-0126/673850/AM/COMPREHENSIVE-GENOMIC-AND-TRANSCRIPTOMIC-ANALYSIS>
- Housman, G., Byler, S., Heerboth, S., Lapinska, K., Longacre, M., Snyder, N., Sarkar, S., 2014. Drug resistance in cancer: an overview. *Cancers* 6, 1769–1792. <https://doi.org/10.3390/CANCERS6031769>
- Junhee Seok, H. Shaw Warren, Alex, G.C., Michael, N.M., Henry, V.B., Xu, W., Richards, D.R., McDonald-Smith, G.P., Gao, H., Hennessy, L., Finnerty, C.C., López, C.M., Honari, S., Moore, E.E., Minei, J.P., Cuschieri, J., Bankey, P.E., Johnson, J.L., Sperry, J., Nathens, A.B., Billiar, T.R., West, M.A., Jeschke, M.G., Klein, M.B., Gamelli, R.L., Gibran, N.S., Brownstein, B.H., Miller-Graziano, C., Calvano, S.E., Mason, P.H., Cobb, J.P., Rahme, L.G., Lowry, S.F., Maier, R.V., Moldawer, L.L., Herndon, D.N., Davis, R.W., Xiao, W., Tompkins, R.G., 2013. Genomic responses in mouse models poorly mimic human inflammatory diseases. *Proceedings of the National Academy of Sciences of the United States of America* 110, 3507–3512. <https://doi.org/10.1073/pnas.1222878110>
- Keck, M.K., Zuo, Z., Khattri, A., Stricker, T.P., Brown, C.D., Imanguli, M., Rieke, D., Endhardt, K., Fang, P., Gelmann, J.B., DeBoer, R., El-Dinali, M., Aktolga, S., Lei, Z., Tan, P., Rozen, S.G., Salgia, R., Weichselbaum, R.R., Lingen, M.W., Story, M.D., Ang, K.K., Cohen, E.E.W., White, K.P., Vokes, E.E., Seiwert, T.Y., 2015. Integrative analysis of head and neck cancer identifies two biologically distinct HPV and three non-HPV subtypes. *Clinical Cancer Research* 21, 870–881. <https://doi.org/10.1158/1078-0432.CCR-14-2481>
- Kim, K.H., Roberts, C.W.M., 2016. Targeting EZH2 in cancer. *Nature Medicine* 22:2 22, 128–134. <https://doi.org/10.1038/nm.4036>
- Kim, S., Scheffler, K., Halpern, A.L., Bekritsky, M.A., Noh, E., Källberg, M., Chen, X., Kim, Y., Beyter, D., Krusche, P., Saunders, C.T., 2018. Strelka2: fast and accurate calling of germline and somatic variants. *Nature Methods* 15, 591–594. <https://doi.org/10.1038/s41592-018-0051-x>
- King, S.B., 1996. Angioplasty from bench to bedside to bench. <https://doi.org/10.1161/01.CIR.93.9.1621>
- Kohler, B.A., Sherman, R.L., Howlader, N., Jemal, A., Ryerson, A.B., Henry, K.A., Boscoe, F.P., Cronin, K.A., Lake, A., Noone, A.M., Henley, S.J., Ehemann, C.R., Anderson, R.N., Penberthy, L., 2015. Annual Report to the Nation on the Status of Cancer, 1975–2011, Featuring Incidence of Breast Cancer Subtypes by Race/Ethnicity, Poverty, and State. *Journal of the National Cancer Institute* 107. <https://doi.org/10.1093/JNCI/DJV048>
- Krijgsman, O., Carvalho, B., Meijer, G.A., Steenbergen, R.D.M., Ylstra, B., 2014. Focal chromosomal copy number aberrations in cancer—Needles in a genome haystack. *Biochimica et Biophysica Acta (BBA) - Molecular Cell Research* 1843, 2698–2704. <https://doi.org/10.1016/J.BBAMCR.2014.08.001>
- Kummar, S., Gutierrez, M., Doroshow, J.H., Murgo, A.J., 2006. Drug development in oncology: classical cytotoxics and molecularly targeted agents. *British Journal of Clinical Pharmacology* 62, 15. <https://doi.org/10.1111/J.1365-2125.2006.02713.X>
- Lake, D., Corrêa, S.A.L., Müller, J., 2016. Negative feedback regulation of the ERK1/2 MAPK pathway. *Cellular and Molecular Life Sciences* 73, 4397–4413. <https://doi.org/10.1007/s00018-016-2297-8>

- Lamping, M., Benary, M., Leyvraz, S., Messerschmidt, C., Blanc, E., Kessler, T., Schütte, M., Lenze, D., Jöhrens, K., Burock, S., Others, 2020. Support of a molecular tumour board by an evidence-based decision management system for precision oncology. *European Journal of Cancer* 127, 41–51.
- Lassen, U.N., Makaroff, L.E., Stenzinger, A., Italiano, A., Vassal, G., Garcia-Foncillas, J., Avouac, B., 2021. Precision oncology: A clinical and patient perspective. *Future Oncology* 17, 3995–4009. <https://doi.org/10.2217/FON-2021-0688>/ASSET/IMAGES/LARGE/FIGURE1.JPEG
- Lawrence, M.S., Sougnez, C., Lichtenstein, L., Cibulskis, K., Lander, E., Gabriel, S.B., Getz, G., Ally, A., Balasundaram, M., Birol, I., Bowlby, R., Brooks, D., Butterfield, Y.S.N., Carlsen, R., Cheng, D., Chu, A., Dhalla, N., Guin, R., Holt, R.A., Jones, S.J.M., Lee, D., Li, H.I., Marra, M.A., Mayo, M., Moore, R.A., Mungall, A.J., Robertson, A.G., Schein, J.E., Sipahimalani, P., Tam, A., Thiessen, N., Wong, T., Protopopov, A., Santoso, N., Lee, S., Parfenov, M., Zhang, J., Mahadeshwar, H.S., Tang, J., Ren, X., Seth, S., Haseley, P., Zeng, D., Yang, L., Xu, A.W., Song, X., Pantazi, A., Bristow, C.A., Hadjipanayis, A., Seidman, J., Chin, L., Park, P.J., Kucherlapati, R., Akbani, R., Casasent, T., Liu, W., Lu, Y., Mills, G., Motter, T., Weinstein, J., Diao, L., Wang, J., Hong Fan, Y., Liu, J., Wang, K., Auman, J.T., Balu, S., Bodenheimer, T., Buda, E., Hayes, D.N., Hoadley, K.A., Hoyle, A.P., Jefferys, S.R., Jones, C.D., Kimes, P.K., Liu, Y., Marron, J.S., Meng, S., Mieczkowski, P.A., Mose, L.E., Parker, J.S., Perou, C.M., Prins, J.F., Roach, J., Shi, Y., Simons, J.V., Singh, D., Soloway, M.G., Tan, D., Veluvolu, U., Walter, V., Waring, S., Wilkerson, M.D., Wu, J., Zhao, N., Cherniack, A.D., Hammerman, P.S., Tward, A.D., Pedamallu, C.S., Saksena, G., Jung, J., Ojesina, A.I., Carter, S.L., Zack, T.I., Schumacher, S.E., Beroukhim, R., Freeman, S.S., Meyerson, M., Cho, J., Noble, M.S., DiCara, D., Zhang, H., Heiman, D.I., Gehlenborg, N., Voet, D., Lin, P., Frazer, S., Stojanov, P., Liu, Y., Zou, L., Kim, J., Muzny, D., Doddapaneni, H.V., Kovar, C., Reid, J., Morton, D., Han, Y., Hale, W., Chao, H., Chang, K., Drummond, J.A., Gibbs, R.A., Kakkar, N., Wheeler, D., Xi, L., Ciriello, G., Ladanyi, M., Lee, W., Ramirez, R., Sander, C., Shen, R., Sinha, R., Weinhold, N., Taylor, B.S., Aksoy, B.A., Dresdner, G., Gao, J., Gross, B., Jacobsen, A., Reva, B., Schultz, N., Sumer, S.O., Sun, Y., Chan, T.A., Morris, L.G., Stuart, J., Benz, S., Ng, S., Benz, C., Yau, C., Baylin, S.B., Cope, L., Danilova, L., Herman, J.G., Bootwalla, M., Maglinte, D.T., Laird, P.W., Triche, T., Weisenberger, D.J., Van Den Berg, D.J., Agrawal, N., Bishop, J., Boutros, P.C., Bruce, J.P., Byers, L.A., Califano, J., Carey, T.E., Chen, Z., Cheng, H., Chiosea, S.I., Cohen, E., Diergaarde, B., Egloff, A.M., El-Naggar, A.K., Ferris, R.L., Frederick, M.J., Grandis, J.R., Guo, Y., Haddad, R.I., Harris, T., Hui, A.B.Y., Lee, J.J., Lippman, S.M., Liu, F.F., McHugh, J.B., Myers, J., Ng, P.K.S., Perez-Ordóñez, B., Pickering, C.R., Prystowsky, M., Romkes, M., Saleh, A.D., Sartor, M.A., Seethala, R., Seiwert, T.Y., Si, H., Van Waes, C., Waggott, D.M., Wiznerowicz, M., Yarbrough, W.G., Zhang, J., Zuo, Z., Burnett, K., Crain, D., Gardner, J., Lau, K., Mallery, D., Morris, S., Paulauskis, J., Penny, R., Shelton, C., Shelton, T., Sherman, M., Yena, P., Black, A.D., Bowen, J., Frick, J., Gastier-Foster, J.M., Harper, H.A., Leraas, K., Lichtenberg, T.M., Ramirez, N.C., Wise, L., Zmuda, E., Baboud, J., Jensen, M.A., Kahn, A.B., Pihl, T.D., Pot, D.A., Srinivasan, D., Walton, J.S., Wan, Y., Burton, R.A., Davidsen, T., Demchok, J.A., Eley, G., Ferguson, M.L., Mills Shaw, K.R., Ozenberger, B.A., Sheth, M., Sofia, H.J., Tarnuzzer, R., Wang, Z., Yang, L., Zenklusen, J.C., Saller, C., Tarvin, K., Chen, C., Bollag, R., Weinberger, P., Golusiński, W., Golusiński, P., Ibbs, M., Korski, K., Mackiewicz, A., Suchorska, W., Szybiak, B., Curley, E., Beard, C., Mitchell, C., Sandusky, G., Ahn, J., Khan, Z., Irish, J., Waldron,

- J., William, W.N., Egea, S., Gomez-Fernandez, C., Herbert, L., Bradford, C.R., Chepeha, D.B., Haddad, A.S., Jones, T.R., Komarck, C.M., Malakh, M., Moyer, J.S., Nguyen, A., Peterson, L.A., Prince, M.E., Rozek, L.S., Taylor, E.G., Walline, H.M., Wolf, G.T., Boice, L., Chera, B.S., Funkhouser, W.K., Gulley, M.L., Hackman, T.G., Hayward, M.C., Huang, M., Rathmell, W.K., Salazar, A.H., Shockley, W.W., Shores, C.G., Thorne, L., Weissler, M.C., Wrenn, S., Zanation, A.M., Brown, B.T., Pham, M., 2015. Comprehensive genomic characterization of head and neck squamous cell carcinomas. *Nature* 517, 576–582. <https://doi.org/10.1038/nature14129>
- Li, H., 2013. Aligning sequence reads, clone sequences and assembly contigs with BWA-MEM. *Bioinformatics* (Oxford, England) 29, 175–176. <https://doi.org/10.1093/bioinformatics/btt109>
- Liberzon, A., Birger, C., Thorvaldsdóttir, H., Ghandi, M., Mesirov, J.P., Tamayo, P., 2015. The Molecular Signatures Database Hallmark Gene Set Collection. *Cell Systems* 1, 417–425. <https://doi.org/10.1016/J.CELS.2015.12.004>
- McGranahan, N., Favero, F., De Bruin, E.C., Birkbak, N.J., Szallasi, Z., Swanton, C., 2015. Clonal status of actionable driver events and the timing of mutational processes in cancer evolution. *Science Translational Medicine*. <https://doi.org/10.1126/scitranslmed.aaa1408>
- Messerschmidt, C., Foddis, M., Blumenau, S., Müller, S., Bentele, K., Holtgrewe, M., Kun-Rodrigues, C., Alonso, I., do Carmo Macario, M., Morgadinho, A.S., Velon, A.G., Santo, G., Santana, I., Mönkäre, S., Kuuluvainen, L., Schleutker, J., Pöyhönen, M., Myllykangas, L., Senatore, A., Berchtold, D., Winek, K., Meisel, A., Pavlovic, A., Kostic, V., Dobricic, V., Lohmann, E., Hanagasi, H., Guven, G., Bilgic, B., Bras, J., Guerreiro, R., Beule, D., Dirnagl, U., Sassi, C., 2021. PHACTR1 genetic variability is not critical in small vessel ischemic disease patients and PcomA recruitment in C57BL/6J mice. *Scientific Reports* 11, 1–11. <https://doi.org/10.1038/s41598-021-84919-x>
- Messerschmidt, C., Holtgrewe, M., Beule, D., 2017. HLA-MA: simple yet powerful matching of samples using HLA typing results. *Bioinformatics* (Oxford, England) 33, 2241–2242. <https://doi.org/10.1093/BIOINFORMATICS/BTX132>
- Messerschmidt, C., Obermayer, B., Klinghammer, K., Ochsenreither, S., Treue, D., Stenzinger, A., Glimm, H., Fröhling, S., Kindler, T., Brandts, C.H., Others, 2020. Distinct immune evasion in APOBEC-enriched, HPV-negative HNSCC. *International Journal of Cancer*.
- Miao, D., Margolis, C.A., Vokes, N.I., Liu, D., Taylor-Weiner, A., Wankowicz, S.M., Adeegbe, D., Keliher, D., Schilling, B., Tracy, A., Manos, M., Chau, N.G., Hanna, G.J., Polak, P., Rodig, S.J., Signoretti, S., Sholl, L.M., Engelman, J.A., Getz, G., Jänne, P.A., Haddad, R.I., Choueiri, T.K., Barbie, D.A., Haq, R., Awad, M.M., Schadendorf, D., Hodi, F.S., Bellmunt, J., Wong, K.-K., Hammerman, P., Van Allen, E.M., 2018. Genomic correlates of response to immune checkpoint blockade in microsatellite-stable solid tumors. *Nature Genetics* 50, 1271–1281. <https://doi.org/10.1038/s41588-018-0200-2>
- Miller, D.M., Thomas, S.D., Islam, A., Muench, D., Sedoris, K., 2012. c-Myc and cancer metabolism. *Clinical Cancer Research* 18, 5546–5553. <https://doi.org/10.1158/1078-0432.CCR-12-0977>
- Mlakar, V., Morel, E., Mlakar, S.J., Ansari, M., Gumy-Pause, F., 2021. A review of the biological and clinical implications of RAS-MAPK pathway alterations in neuroblastoma. *Journal of Experimental and Clinical Cancer Research* 40, 1–16. <https://doi.org/10.1186/s13046-021-01967-x>
- Molina, J.R., Adjei, A.A., 2006. The Ras/Raf/MAPK Pathway. *Journal of Thoracic Oncology* 1, 7–9. [https://doi.org/10.1016/s1556-0864\(15\)31506-9](https://doi.org/10.1016/s1556-0864(15)31506-9)
- Nguyen, L., Papenhausen, P., Shao, H., 2017. The Role of c-MYC in B-Cell Lymphomas: Diagnostic and Molecular Aspects. *Genes* 8, 2–22. <https://doi.org/10.3390/GENES8040116>

- Nowell, P.C., 1976. The clonal evolution of tumor cell populations. *Science* 194, 23–28. <https://doi.org/10.1126/science.959840>
- Oliva, M., Spreafico, A., Taberna, M., Alemany, L., Coburn, B., Mesia, R., Siu, L.L., 2019. Immune biomarkers of response to immune-checkpoint inhibitors in head and neck squamous cell carcinoma. *Annals of Oncology* 30, 57–67. <https://doi.org/10.1093/ANNONC/MDY507>
- Otto, R., Rössler, J.N., Sers, C., Mamlouk, S., Leser, U., 2019. Robust in-silico identification of Cancer Cell Lines based on RNA and targeted DNA sequencing data. *Scientific Reports* 9. <https://doi.org/10.1038/s41598-018-36300-8>
- Park, J.R., Eggert, A., Caron, H., 2008. Neuroblastoma: Biology, Prognosis, and Treatment. *Pediatric Clinics of North America* 55, 97–120. <https://doi.org/10.1016/j.pcl.2007.10.014>
- Patel, S.J., Sanjana, N.E., Kishton, R.J., Eidizadeh, A., Vodnala, S.K., Cam, M., Gartner, J.J., Jia, L., Steinberg, S.M., Yamamoto, T.N., Merchant, A.S., Mehta, G.U., Chichura, A., Shalem, O., Tran, E., Eil, R., Sukumar, M., Guijarro, E.P., Day, C.-P., Robbins, P., Feldman, S., Merlino, G., Zhang, F., Restifo, N.P., 2017. Identification of essential genes for cancer immunotherapy. *Nature* 548, 537–542. <https://doi.org/10.1038/nature23477>
- Patro, R., Duggal, G., Love, M.I., Irizarry, R.A., Kingsford, C., 2017. Salmon provides fast and bias-aware quantification of transcript expression. *Nature Methods* 14, 417–419. <https://doi.org/10.1038/nmeth.4197>
- Peifer, M., Hertwig, F., Roels, F., Drexler, D., Gartlgruber, M., Menon, R., Krämer, A., Roncaioli, J.L., Sand, F., Heuckmann, J.M., Ikram, F., Schmidt, R., Ackermann, S., Engesser, A., Kahlert, Y., Vogel, W., Altmüller, J., Nürnberg, P., Thierry-Mieg, J., Thierry-Mieg, D., Mariappan, A., Heynck, S., Mariotti, E., Henrich, K.O., Gloeckner, C., Bosco, G., Leuschner, I., Schweiger, M.R., Savelyeva, L., Watkins, S.C., Shao, C., Bell, E., Höfer, T., Achter, V., Lang, U., Theissen, J., Volland, R., Saadati, M., Eggert, A., De Wilde, B., Berthold, F., Peng, Z., Zhao, C., Shi, L., Ortmann, M., Büttner, R., Perner, S., Hero, B., Schramm, A., Schulte, J.H., Herrmann, C., O’Sullivan, R.J., Westermann, F., Thomas, R.K., Fischer, M., 2015. Telomerase activation by genomic rearrangements in high-risk neuroblastoma. *Nature* 526, 700–704. <https://doi.org/10.1038/nature14980>
- Perlman, R.L., 2016. Mouse Models of Human Disease: An Evolutionary Perspective. *Evolution, Medicine, and Public Health* 2016, eow014. <https://doi.org/10.1093/emph/eow014>
- Prinz, F., Schlange, T., Asadullah, K., 2011. Believe it or not: how much can we rely on published data on potential drug targets? *Nature Reviews Drug Discovery* 10:9 10, 712–712. <https://doi.org/10.1038/nrd3439-c1>
- Prior, I.A., Hood, F.E., Hartley, J.L., 2020. The frequency of ras mutations in cancer. *Cancer Research* 80, 2669–2974. <https://doi.org/10.1158/0008-5472.CAN-19-3682>
- Puram, S.V., Tirosh, I., Parikh, A.S., Patel, A.P., Yizhak, K., Gillespie, S., Rodman, C., Luo, C.L., Mroz, E.A., Emerick, K.S., Deschler, D.G., Varvares, M.A., Mylvaganam, R., Rozenblatt-Rosen, O., Rocco, J.W., Faquin, W.C., Lin, D.T., Regev, A., Bernstein, B.E., 2017. Single-Cell Transcriptomic Analysis of Primary and Metastatic Tumor Ecosystems in Head and Neck Cancer. *Cell* 171, 1611–1624.e24. <https://doi.org/10.1016/J.CELL.2017.10.044>
- Rae, J.M., Creighton, C.J., Meck, J.M., Haddad, B.R., Johnson, M.D., 2007. MDA-MB-435 cells are derived from M14 Melanoma cells - A loss for breast cancer, but a boon for melanoma research. *Breast Cancer Research and Treatment* 104, 13–19. <https://doi.org/10.1007/s10549-006-9392-8>
- Rieke, D.T., Klinghammer, K., Keilholz, U., 2016. Targeted Therapy of Head and Neck Cancer.

- Oncology Research and Treatment 39, 780–786. <https://doi.org/10.1159/000452432>
- Roberts, S.A., Lawrence, M.S., Klimczak, L.J., Grimm, S.A., Fargo, D., Stojanov, P., Kiezun, A., Kryukov, G.V., Carter, S.L., Saksena, G., Harris, S., Shah, R.R., Resnick, M.A., Getz, G., Gordenin, D.A., 2013. An APOBEC cytidine deaminase mutagenesis pattern is widespread in human cancers. <https://doi.org/10.1038/ng.2702>
- Saez-Rodriguez, J., Blüthgen, N., 2020. Personalized signaling models for personalized treatments. *Molecular Systems Biology* 16, e9042. <https://doi.org/10.15252/MSB.20199042>
- Schimke, R.T., Kaufman, R.J., Alt, F.W., Kellems, R.F., 1978. Gene Amplification and Drug Resistance in Cultured Murine Cells. *Science* 202, 1051–1055. <https://doi.org/10.1126/SCIENCE.715457>
- Schubert, M., Klinger, B., Klünemann, M., Sieber, A., Uhlitz, F., Sauer, S., Garnett, M.J., Blüthgen, N., Saez-Rodriguez, J., 2018. Perturbation-response genes reveal signaling footprints in cancer gene expression. *Nature Communications* 9, 20. <https://doi.org/10.1038/s41467-017-02391-6>
- Schumann, F., Blanc, E., Messerschmidt, C., Blankenstein, T., Busse, A., Beule, D., 2019. SigsPack, a package for cancer mutational signatures. *BMC Bioinformatics* 20. <https://doi.org/10.1186/s12859-019-3043-7>
- Sechidis, K., Papangelou, K., Metcalfe, P.D., Svensson, D., Weatherall, J., Brown, G., 2018. Distinguishing prognostic and predictive biomarkers: an information theoretic approach. *Bioinformatics* 34, 3365–3376. <https://doi.org/10.1093/BIOINFORMATICS/BTY357>
- Seiwert, T.Y., Burtneß, B., Mehra, R., Weiss, J., Berger, R., Eder, J.P., Heath, K., McClanahan, T., Luceford, J., Gause, C., Cheng, J.D., Chow, L.Q., 2016. Safety and clinical activity of pembrolizumab for treatment of recurrent or metastatic squamous cell carcinoma of the head and neck (KEYNOTE-012): an open-label, multicentre, phase 1b trial. *The Lancet. Oncology* 17, 956–965. [https://doi.org/10.1016/S1470-2045\(16\)30066-3](https://doi.org/10.1016/S1470-2045(16)30066-3)
- Shlien, A., Malkin, D., 2009. Copy number variations and cancer. *Genome Medicine* 1, 62. <https://doi.org/10.1186/GM62>
- Skloot, R., 2011. *The immortal life of henrietta lacks*, APLS book club. Broadway Paperbacks.
- Son, E., Panwar, A., Mosher, C.H., Lydiatt, D., 2018. Cancers of the Major Salivary Gland. *Journal of oncology practice* 14, 99–108. <https://doi.org/10.1200/JOP.2017.026856>
- Stampe, H., Jakobsen, K.K., Bendtsen, S.K., Grønhøj, C., Buchwald, C. von, 2021. Systematic review on the current knowledge and use of single-cell RNA sequencing in head and neck cancer. *APMIS* 129, 619–625. <https://doi.org/10.1111/APM.13173>
- Su, Y.Y., Chien, C.Y., Luo, S.D., Huang, T.L., Lin, W.C., Fang, F.M., Chiu, T.J., Chen, Y.H., Lai, C.C., Hsu, C.M., Li, S.H., 2016. Betel nut chewing history is an independent prognosticator for smoking patients with locally advanced stage IV head and neck squamous cell carcinoma receiving induction chemotherapy with docetaxel, cisplatin, and fluorouracil. *World Journal of Surgical Oncology* 14, 1–9. <https://doi.org/10.1186/s12957-016-0844-2>
- Subramanian, A., Tamayo, P., Mootha, V.K., Mukherjee, S., Ebert, B.L., Gillette, M.A., Paulovich, A., Pomeroy, S.L., Golub, T.R., Lander, E.S., Mesirov, J.P., 2005. Gene set enrichment analysis: A knowledge-based approach for interpreting genome-wide expression profiles. *Proceedings of the National Academy of Sciences* 102, 15545–15550. <https://doi.org/10.1073/PNAS.0506580102>
- Talevich, E., Shain, A.H., Botton, T., Bastian, B.C., 2016. CNVkit: Genome-Wide Copy Number Detection and Visualization from Targeted DNA Sequencing. *PLoS Computational Biology* 12. <https://doi.org/10.1371/journal.pcbi.1004873>
- Tang, K.-W., Alaei-Mahabadi, B., Samuelsson, T., Lindh, M., Larsson, E., 2013. The

- landscape of viral expression and host gene fusion and adaptation in human cancer. *Nature communications* 4, 2513. <https://doi.org/10.1038/ncomms3513>
- Tate, J.G., Bamford, S., Jubb, H.C., Sondka, Z., Beare, D.M., Bindal, N., Boutselakis, H., Cole, C.G., Creatore, C., Dawson, E., Fish, P., Harsha, B., Hathaway, C., Jupe, S.C., Kok, C.Y., Noble, K., Ponting, L., Ramshaw, C.C., Rye, C.E., Speedy, H.E., Stefancsik, R., Thompson, S.L., Wang, S., Ward, S., Campbell, P.J., Forbes, S.A., 2019. COSMIC: The Catalogue Of Somatic Mutations In Cancer. *Nucleic Acids Research* 47, D941–D947. <https://doi.org/10.1093/nar/gky1015>
- The german human genome-phenome archive [WWW Document], 2020. URL <https://www.ghga.de/about-us/mission>
- The nobel prize in physiology or medicine 2018 [WWW Document], 2018. URL <https://www.nobelprize.org/prizes/medicine/2018/summary/> (accessed 6.17.2022).
- Tian, X., Pelton, A., Shahsafaei, A., Dorfman, D.M., 2016. Differential expression of enhancer of zeste homolog 2 (EZH2) protein in small cell and aggressive B-cell non-Hodgkin lymphomas and differential regulation of EZH2 expression by p-ERK1/2 and MYC in aggressive B-cell lymphomas. *Modern Pathology* 29, 1050–1057. <https://doi.org/10.1038/modpathol.2016.114>
- Trenner, A., Sartori, A.A., 2019. Harnessing DNA Double-Strand Break Repair for Cancer Treatment. *Frontiers in Oncology* 9, 1388. <https://doi.org/10.3389/fonc.2019.01388>
- Trigg, R.M., Turner, S.D., 2018. ALK in neuroblastoma: Biological and therapeutic implications. *Cancers* 10. <https://doi.org/10.3390/cancers10040113>
- Uriu, K., Kosugi, Y., Ito, J., Sato, K., 2021. The Battle between Retroviruses and APOBEC3 Genes: Its Past and Present. *Viruses* 13. <https://doi.org/10.3390/V13010124>
- Van Allen, E.M., Miao, D., Schilling, B., Shukla, S.A., Blank, C., Zimmer, L., Sucker, A., Hillen, U., Foppen, M.H.G., Goldinger, S.M., Utikal, J., Hassel, J.C., Weide, B., Kaehler, K.C., Loquai, C., Mohr, P., Gutzmer, R., Dummer, R., Gabriel, S., Wu, C.J., Schadendorf, D., Garraway, L.A., 2015. Genomic correlates of response to CTLA-4 blockade in metastatic melanoma. *Science* 350, 207–211. <https://doi.org/10.1126/science.aad0095>
- Vandewalle, P., 2012. Code sharing is associated with research impact in image processing. *Computing in Science and Engineering* 14, 42–47. <https://doi.org/10.1109/MCSE.2012.63>
- Vasan, N., Baselga, J., Hyman, D.M., 2019. A view on drug resistance in cancer. *Nature* 575, 299–309. <https://doi.org/10.1038/s41586-019-1730-1>
- Wang, S., Jia, M., He, Z., Liu, X.-S., 2018. APOBEC3B and APOBEC mutational signature as potential predictive markers for immunotherapy response in non-small cell lung cancer. *Oncogene* 37, 3924–3936. <https://doi.org/10.1038/s41388-018-0245-9>
- Warren, C.J., Santiago, M.L., Pyeon, D., 2022. APOBEC3: Friend or Foe in Human Papillomavirus Infection and Oncogenesis? <https://doi.org/10.1146/annurev-virology-092920-030354> 9, 375–395. <https://doi.org/10.1146/ANNUREV-VIROLOGY-092920-030354>
- Wilkinson, M.D., Dumontier, M., Aalbersberg, I.J., Appleton, G., Axton, M., Baak, A., Blomberg, N., Boiten, J.W., da Silva Santos, L.B., Bourne, P.E., Bouwman, J., Brookes, A.J., Clark, T., Crosas, M., Dillo, I., Dumon, O., Edmunds, S., Evelo, C.T., Finkers, R., Gonzalez-Beltran, A., Gray, A.J.G., Groth, P., Goble, C., Grethe, J.S., Heringa, J., Hoen, P.A.C. t, Hooft, R., Kuhn, T., Kok, R., Kok, J., Lusher, S.J., Martone, M.E., Mons, A., Packer, A.L., Persson, B., Rocca-Serra, P., Roos, M., Schaik, R. van, Sansone, S.A., Schultes, E., Sengstag, T., Slater, T., Strawn, G., Swertz, M.A., Thompson, M., Van Der Lei, J., Van Mulligen, E., Velterop, J., Waagmeester, A., Wittenburg, P., Wolstencroft, K., Zhao, J., Mons, B., 2016. The FAIR Guiding Principles for scientific data management

- and stewardship. *Scientific Data* 2016 3:1 3, 1–9. <https://doi.org/10.1038/sdata.2016.18>
- Yan, L., Rosen, N., Arteaga, C., 2011. Targeted cancer therapies. *Chinese Journal of Cancer* 30, 1–4. <https://doi.org/10.5732/cjc.010.10553>
- Yarkoni, T., 2022. The generalizability crisis. *Behavioral and Brain Sciences* 45. <https://doi.org/10.1017/S0140525X20001685>
- Yim, E.-K., Park, J.-S., 2005. The Role of HPV E6 and E7 Oncoproteins in HPV-associated Cervical Carcinogenesis. *Cancer Research and Treatment* 37, 319. <https://doi.org/10.4143/crt.2005.37.6.319>
- Young, D., Xiao, C.C., Murphy, B., Moore, M., Fakhry, C., Day, T.A., 2015. Increase in head and neck cancer in younger patients due to human papillomavirus (HPV). *Oral oncology* 51, 727–730. <https://doi.org/10.1016/J.ORALONCOLOGY.2015.03.015>

Eidesstattliche Versicherung

Ich, Clemens Messerschmidt, versichere an Eides statt durch meine eigenhändige Unterschrift, dass ich die vorgelegte Dissertation mit dem Thema:

“Understanding treatment resistance in head and neck cancer, lymphoma and neuroblastoma through omics data analysis in a translational oncology setting.”

(Charakterisierung der Behandlungsresistenz bei Kopf- und Halskrebs, Lymphomen und Neuroblastomen durch die Analyse von Omics-Daten.)

selbstständig und ohne nicht offengelegte Hilfe Dritter verfasst und keine anderen als die angegebenen Quellen und Hilfsmittel genutzt habe.

Alle Stellen, die wörtlich oder dem Sinne nach auf Publikationen oder Vorträgen anderer Autoren/innen beruhen, sind als solche in korrekter Zitierung kenntlich gemacht. Die Abschnitte zu Methodik (insbesondere praktische Arbeiten, Laborbestimmungen, statistische Aufarbeitung) und Resultaten (insbesondere Abbildungen, Graphiken und Tabellen) werden von mir verantwortet.

Ich versichere ferner, dass ich die in Zusammenarbeit mit anderen Personen generierten Daten, Datenauswertungen und Schlussfolgerungen korrekt gekennzeichnet und meinen eigenen Beitrag sowie die Beiträge anderer Personen korrekt kenntlich gemacht habe (siehe Anteilserklärung). Texte oder Textteile, die gemeinsam mit anderen erstellt oder verwendet wurden, habe ich korrekt kenntlich gemacht.

Meine Anteile an etwaigen Publikationen zu dieser Dissertation entsprechen denen, die in der untenstehenden gemeinsamen Erklärung mit dem/der Erstbetreuer/in, angegeben sind. Für sämtliche im Rahmen der Dissertation entstandenen Publikationen wurden die Richtlinien des ICMJE (International Committee of Medical Journal Editors; www.icmje.org) zur Autorenschaft eingehalten. Ich erkläre ferner, dass ich mich zur Einhaltung der Satzung der Charité – Universitätsmedizin Berlin zur Sicherung Guter Wissenschaftlicher Praxis verpflichte.

Weiterhin versichere ich, dass ich diese Dissertation weder in gleicher noch in ähnlicher Form bereits an einer anderen Fakultät eingereicht habe.

Die Bedeutung dieser eidesstattlichen Versicherung und die strafrechtlichen Folgen einer unwahren eidesstattlichen Versicherung (§§156, 161 des Strafgesetzbuches) sind mir bekannt und bewusst.

Datum, Unterschrift des Doktoranden/der Doktorandin

Anteilserklärung an den aufgelisteten Publikationen

Clemens Messerschmidt hatte folgenden Anteil an den folgenden Publikationen:

Publikation 1

Messerschmidt, C., Obermayer, B., Klinghammer, K., Ochsenreither, S., Treue, D., Stenzinger, A., Glimm, H., Fröhling, S., Kindler, T., Brandts, C.H., Schulze-Osthoff, K., Weichert, W., Tinhofer, I., Klauschen, F., Keilholz, U., Beule, D., Rieke, D.T., 2020. Distinct immune evasion in APOBEC-enriched, HPV-negative HNSCC. *Int. J. Cancer* 147, 2293–2302.

Beitrag im Einzelnen:

- Ich habe zur Konzeption und Planung des Projekts beigetragen.
- Ich habe die hauseigene Bioinformatik-Pipeline namens snappy für die Analyse von Hochdurchsatz-Sequenzierungsdaten mitentwickelt.
- Ich habe die komplette bioinformatische Analyse aller Daten aus den TCGA- und DKTK-Masterkohorten durchgeführt.
- Ich habe an der Einzelzell-Transkriptomik-Analyse mitgewirkt.
- Ich habe die Abbildungen 1A, 1B, 2, 3, 4, 5A und 6 erstellt.
- Ich habe Tabelle 1 erstellt.
- Ich habe das Manuskript mitverfasst und war für die gesamte Kommunikation mit dem Editor während der Einreichung und dem Überarbeitungsprozess verantwortlich.

Publikation 2

Akpa, C.A., Kleo, K., Oker, E., Tomaszewski, N., **Messerschmidt, C.**, López, C., Wagener, R., Oehl-Huber, K., Dettmer, K., Schoeler, A., Lenze, D., Oefner, P.J., Beule, D., Siebert, R., Capper, D., Dimitrova, L., Hummel, M., 2020. Acquired resistance to DZNep-mediated apoptosis is associated with copy number gains of *AHCY* in a B-cell lymphoma model. *BMC Cancer* 20, 1–12.

Beitrag im Einzelnen:

- Ich analysierte die Daten der Whole-Exome-Sequenzierung, einschließlich der Qualitätskontrolle der Rohdaten und des Alignments mit der Genomreferenz GRCh37.
- Ich analysierte genomweit Kopienzahlvarianten (CNV), annotierte sie und schlug die *AHCY*-Amplifikation als den wahrscheinlichsten Kandidaten für den Erwerb der DZNep-Resistenz vor.

- Ich erstellte Abbildung 2A und schrieb die Manuskriptabschnitte, in denen die Whole-Exome-Analyse beschrieben wird, und überprüfte das finale Manuskript.

Publikation 3

Dorel, M., Klinger, B., Mari, T., Toedling, J., Blanc, E., **Messerschmidt, C.**, Nadler-Holly, M., Ziehm, M., Sieber, A., Hertwig, F., Beule, D., Eggert, A., Schulte, J.H., Selbach, M., Blüthgen, N., 2021. Neuroblastoma signalling models unveil combination therapies targeting feedback-mediated resistance. PLOS Comput. Biol. 17, e1009515.

Beitrag im Einzelnen:













- Ich analysierte die Daten der Whole-Exome-Sequenzierung, einschließlich der Qualitätskontrolle der Rohdaten der Sequenzierung, Alignment mit der Genomreferenz GRCh37, Variantcalling, Variantenannotation und Priorisierung der Varianten.
- Ich lud diese Ergebnisse auf unsere selbst gehostete cbioportal-Instanz, um sie für Mitarbeiter bequem zugänglich zu machen.
- Ich verglich das Mutationsprofil jeder Zelllinie mit öffentlichen Datenbanken, um sicherzustellen, dass die Identitäten der Zelllinien korrekt waren und mit dem bisherigen Wissen über Treibermutationen übereinstimmten.

Unterschrift, Datum und Stempel des/der erstbetreuenden Hochschullehrers/in

Unterschrift des Doktoranden/der Doktorandin

**Druckexemplar der Publikation
Messerschmidt et al. 2020**

Distinct immune evasion in APOBEC-enriched, HPV-negative HNSCC

Clemens Messerschmidt^{1,2}  | Benedikt Obermayer^{1,2}  | Konrad Klinghammer³  |
 Sebastian Ochsenreither^{3,4,5}  | Denise Treue⁶  | Albrecht Stenzinger^{5,7}  |
 Hanno Glimm^{5,8,9} | Stefan Fröhling^{5,10}  | Thomas Kindler^{5,11,12} |
 Christian H. Brandts^{5,13,14}  | Klaus Schulze-Osthoff^{5,15} | Wilko Weichert^{5,16} |
 Ingeborg Tinhofer^{5,17}  | Frederick Klauschen^{5,6} | Ulrich Keilholz^{4,5}  |
 Dieter Beule^{1,2,18}  | Damian T. Rieke^{3,4,19} 

¹Core Unit Bioinformatics, Berlin Institute of Health (BIH), Berlin, Germany

²Charité – Universitätsmedizin Berlin, Corporate Member of Freie Universität Berlin, Humboldt-Universität zu Berlin, and Berlin Institute of Health, Berlin, Germany

³Department of Hematology and Oncology, Campus Benjamin Franklin, Charité – Universitätsmedizin Berlin, Corporate Member of Freie Universität Berlin, Humboldt-Universität zu Berlin, and Berlin Institute of Health, Hindenburgdamm 30, Berlin, 12203, Germany

⁴Charité Comprehensive Cancer Center, Charité – Universitätsmedizin Berlin, Corporate Member of Freie Universität Berlin, Humboldt-Universität zu Berlin, and Berlin Institute of Health, Berlin, Germany

⁵German Cancer Consortium (DKTK) and German Cancer Research Center (DKFZ), Heidelberg, Germany

⁶Institute of Pathology, Charité – Universitätsmedizin Berlin, Corporate Member of Freie Universität Berlin, Humboldt-Universität zu Berlin, and Berlin Institute of Health, Berlin, Germany

⁷Institute of Pathology, Heidelberg University Hospital, Heidelberg, Germany

⁸Department of Translational Medical Oncology, National Center for Tumor Diseases (NCT) Dresden and German Cancer Research Center (DKFZ), Dresden, Germany

⁹University Hospital Carl Gustav Carus, Technische Universität Dresden, Dresden, Germany

¹⁰Department of Translational Medical Oncology, National Center for Tumor Diseases (NCT) Heidelberg and German Cancer Research Center (DKFZ), Heidelberg, Germany

¹¹Department of Hematology, Medical Oncology & Pneumology, University Medical Center, Mainz, Germany

¹²University Cancer Center Mainz (UCT), Johannes Gutenberg-University, Mainz, Germany

¹³University Cancer Center Frankfurt (UCT), Goethe University Frankfurt, Frankfurt, Germany

¹⁴Department of Medicine, Hematology/Oncology, Goethe University, Frankfurt, Germany

¹⁵Interfaculty Institute of Biochemistry, Tübingen University, Tübingen, Germany

¹⁶Institute of Pathology, Technical University Munich, Munich, Germany

¹⁷Department of Radiooncology and Radiotherapy, Charité – Universitätsmedizin Berlin, Corporate Member of Freie Universität Berlin, Humboldt-Universität zu Berlin, and Berlin Institute of Health, Berlin, Germany

¹⁸Max Delbrück Center for Molecular Medicine in the Helmholtz Association, Berlin, Germany

¹⁹Berlin Institute of Health (BIH), Berlin, Germany

Abbreviations: APOBEC, apolipoprotein B mRNA editing enzyme, catalytic polypeptide-like; BLCA, urothelial bladder carcinoma; CDKN2A, cyclin-dependent kinase inhibitor 2A; CRISPR, clustered regularly interspaced short palindromic repeats; CTLA4, cytotoxic T-lymphocyte-associated protein 4; DKTK MASTER, Deutsches Konsortium für translationale Krebsforschung Molecular aided stratification for tumor eradication research; DNA, deoxyribonucleic acid; ECOG, eastern co-operative oncology group; GDC, genomic data commons; HLA-A, human leukocyte antigen A; HNSCC, head and neck squamous cell carcinoma; HPV, human papilloma virus; ICI, immune checkpoint inhibition; IFNG, interferon gamma; LAG3, lymphocyte-activation gene 3; LSCC, lung squamous cell carcinoma; LUAD, lung adenocarcinoma; PDCD1, Programmed cell death protein 1; PD-L1, programmed cell death 1 ligand 1; RNA, ribonucleic acid; SBS, single base substitution; SNV, single nucleotide variation; SYCP2, synaptonemal complex protein 2; TCGA, the cancer genome atlas; t-SNE, t-distributed stochastic neighbor embedding; VAF, variant allele frequency; VTCN1, V-set domain-containing T-cell activation inhibitor 1.

This is an open access article under the terms of the Creative Commons Attribution License, which permits use, distribution and reproduction in any medium, provided the original work is properly cited.

© 2020 The Authors. *International Journal of Cancer* published by John Wiley & Sons Ltd on behalf of UICC

Correspondence

Dieter Beule, Core Unit Bioinformatics, Berlin Institute of Health, Charitéplatz 1, 10117 Berlin, Germany.
 Email: dieter.beule@bihealth.de and Damian T. Rieke, Charité Comprehensive Cancer Center, Charitéplatz 1, 10117 Berlin, Germany.
 Email: damian.rieke@charite.de

Funding information

Berliner Krebsgesellschaft e.V.; Deutsches Konsortium für translationale Krebsforschung (DKTK)

Abstract

Immune checkpoint inhibition leads to response in some patients with head and neck squamous cell carcinoma (HNSCC). Robust biomarkers are lacking to date. We analyzed viral status, gene expression signatures, mutational load and mutational signatures in whole exome and RNA-sequencing data of the HNSCC TCGA dataset (n = 496) and a validation set (DKTK MASTER cohort, n = 10). Public single-cell gene expression data from 17 HPV-negative HNSCC were separately reanalyzed. APOBEC3-associated TCW motif mutations but not total single nucleotide variant burden were significantly associated with inflammation. This association was restricted to HPV-negative HNSCC samples. An APOBEC-enriched, HPV-negative subgroup was identified, that showed higher T-cell inflammation and immune checkpoint expression, as well as expression of APOBEC3 genes. Mutations in immune-evasion pathways were also enriched in these tumors. Analysis of single-cell sequencing data identified expression of APOBEC3B and 3C genes in malignant cells. We identified an APOBEC-enriched subgroup of HPV-negative HNSCC with a distinct immunogenic phenotype, potentially mediating response to immunotherapy.

KEYWORDS

immune checkpoint inhibition, head and neck cancer, APOBEC, mutational signature, tumor inflammation

1 | INTRODUCTION

Cancer is a disease of the genome in that cancer cells have acquired somatic variants that prove advantageous for their growth. These mutations lead to changes in affected proteins and eventually cellular transformation. Altered proteins can be recognized by the immune system through presentation of peptides by the major histocompatibility complex (MHC), which allows for eradication of the tumor. Immune evasion is therefore considered one of the hallmarks of cancer.¹ Immune checkpoint inhibitors (ICI), improving immune recognition and T-cell activation, are an effective treatment option in a subgroup of patients in several cancer types including head and neck squamous cell carcinoma (HNSCC).² The presence of an interferon-gamma inflamed gene expression signature (IFNG signature or T-cell inflamed phenotype^{3,4}), expression of immune checkpoint PD-L1² and tumor mutational burden are associated with response.^{5,6} However, effective predictive biomarkers to guide ICI treatment in the clinic are lacking to date.

HNSCC is a common cancer type worldwide. It is mainly caused by tobacco and alcohol consumption, as well as infection with the human papilloma virus (HPV).⁷ These two groups (HPV-positive and HPV-negative) are distinct entities with different outcome and different tumor biology.⁸ A better responsiveness of HPV-associated tumors to ICI has been suggested by early clinical data³ but not confirmed in other studies.^{2,9} Immune activation due to immunological “foreignness” in virally induced cancers is a potential mechanism of differential immune activation.¹⁰ Additionally, an intracellular antiviral

What's new?

Head and neck squamous cell carcinoma (HNSCC) is sometimes susceptible to immune checkpoint inhibitors, and biomarkers are needed to help identify which tumors are most likely to respond. Using the Cancer Genome Atlas, these authors evaluated 496 HSNCCs by HPV status, gene expression signatures, mutational load, and mutational signatures. They found that increased inflammation was associated with APOBEC3-induced mutations in HPV-negative cancers. This newly identified APOBEC-enriched, HPV-negative subgroup showed higher immune checkpoint expression, and also more mutations in immune-evasion pathways, suggesting this may be a way to identify candidates for immune checkpoint inhibitor therapy.

response mediated by the APOBEC3-family of proteins leads to the accumulation of mutations and tumorigenesis.¹¹ In several cancer types, APOBEC-mediated tumorigenesis is increasingly recognized as an important mechanism, even when independent of viral infections.^{12,13} APOBEC activity can be inferred from an analysis of mutational signatures in the tumor genome. A so-called TCW motif has been identified as an APOBEC-specific mutational signature.¹⁴ The role of APOBEC-induced mutations in HPV-negative HNSCC and its

association with immune activation is unclear. We analyzed mutational signatures to uncover mechanisms driving tumor inflammation in HNSCC.

2 | MATERIALS AND METHODS

2.1 | TCGA datasets

TCGA mutation data sets were downloaded for HNSCC¹⁵ (n = 502), lung adenocarcinoma¹⁶ (LUAD, n = 542), urothelial bladder carcinoma¹⁷ (BLCA, n = 395) and lung squamous cell carcinoma¹⁸ (LUSCC, n = 178) from BROAD firehose in MAF format.

2.2 | Identification of an APOBEC-induced subgroup and APOBEC mutational signature

Somatic mutation data in a MAF file was split into separate VCF files, one per TCGA sample. To annotate putative APOBEC induced mutations, we used the method described by Roberts et al,¹⁹ annotating C>T and C>G variants in TCW (TCA, TCT) motifs and their reverse complements, respectively. The number of cytosine mutations in the TCW motif and outside of it in each sample were compared to the respective occurrences of C/G and the TCW motif on chr1 of the human genome with Fisher's exact test.

Values of *P* were subsequently Holm-Bonferroni corrected and all cases with *P*' < .05 were labeled APOBEC-enriched.

COSMIC single base substitution (SBS) signature contributions for the mutational profile of each tumor sample were downloaded from msigndb.²⁰ Samples were grouped and a Wilcoxon rank test was used to test for differences between groups.

2.3 | HPV status

HPV status was assigned based on the number of reads mapping to HPV genomes, which are included as separate contigs in the bam files (genome release 38) available from GDC Portal. We used a cutoff of 3500 reads to label a sample as HPV-positive. Results were checked against the HPV expression signature described by Buitrago-Pérez et al²¹ and a derived reduced signature containing only gene CDKN2A and SYCP2 as well as prior results by Tang et al²² and TCGA clinical annotation for consistency.

2.4 | Expression data analysis and IFNG signature

Expression data for sets of genes ("RNA Seq V2 RSEM") was downloaded from the HNSCC TCGA provisional cohort¹⁵ from cbioPortal.org.²³ Samples that lacked either mutational or expression data were excluded. The IFNG signature was computed as the mean of the log2-transformed RSEM v2 expression values per sample.

2.5 | Identification of gene expression subtypes

HNSCC samples were attributed to gene expression subtypes. Basal, Classical and Inflamed/Mesenchymal cluster centroids were downloaded from the supplementary material of Keck et al.⁸ Normalized RSEM expression values from TCGA were log2-transformed and scaled. The nearest centroid in terms of Euclidean distance was then assigned as the label of a sample. To test for independence of variables between Keck classes and APOBEC groups Fisher's exact test was used.

2.6 | Immune population metagene analysis

Gene expression signatures, also called metagenes, for tumor-infiltrating immune populations were acquired from The Cancer Immunome Database²⁴ (TCIA.at). Enrichment of signatures was computed for each immune population in each sample with the R package GSVA using the method *gsva*²⁵. Differential metagene expression was assessed with *limma*.²⁶

2.7 | Analysis of immunotherapy-essential genes

We analyzed mutations in 554 genes which have been shown to be essential for cancer immunotherapy in a CRISPR assay.²⁷ To identify enrichment of mutations in these genes, we used a Fisher exact test considering the number of cases in HPV-negative/APOBEC-enriched and HPV-negative/APOBEC-negative respectively, and the number of mutated genes from the aforementioned gene set in each group. Variant effect was annotated with Jannovar.²⁸

2.8 | Analysis of APOBEC timing

Variant allele fractions (VAF) of TCW mutations compared to all other variants were used to infer the timing of APOBEC activity. Patients harboring significantly distinct variant allele fractions for TCW variants compared to all other variants of a given case were classified as early APOBEC activation, if the TCW variants had higher VAF, or as late activation, if they had lower overall VAF compared to all other variants. Patients with no difference or too few variants were grouped as "no preference". The false-positive rate was controlled with the R package *q* value,²⁹ using a threshold of 0.2.

2.9 | Single-cell expression

This analysis was based on the digital expression matrix, holding the expression values of 23 686 genes for 5902 cells of 17 tumor samples (GSE103322), together with a classification into malignant and various nonmalignant cell types provided by the authors.³⁰ Data were projected into tSNE coordinates using the standard Seurat workflow³¹ and visualized using feature plots and violin plots.

2.10 | Independent validation of IFNG signature scores

Patients with advanced cancers, an ECOG performance status of 0–1 and an age < 50 years were eligible for enrollment in the DTKK-MASTER program across cancer centers in Germany. The DTKK-MASTER trial was approved by local ethics committees (Heidelberg and Berlin). Written informed consent was obtained from all participating patients. Whole-exome and RNA sequencing were performed on fresh-frozen tissues. From RNA-seq data for all cases, HPV status was predicted as described above. IFNG signature was computed as described above after generating transcript abundances with salmon³² against

ENSEMBL v75. The mapping of gene symbols used and their respective ENSEMBL ids are shown in Table S1.

3 | RESULTS

3.1 | Identification of inflammation-associated mutational signatures

Mutation and gene expression data from head and neck squamous cell carcinoma samples were downloaded from The Cancer Genome Atlas (n = 496). The presence of a T-cell inflamed microenvironment was

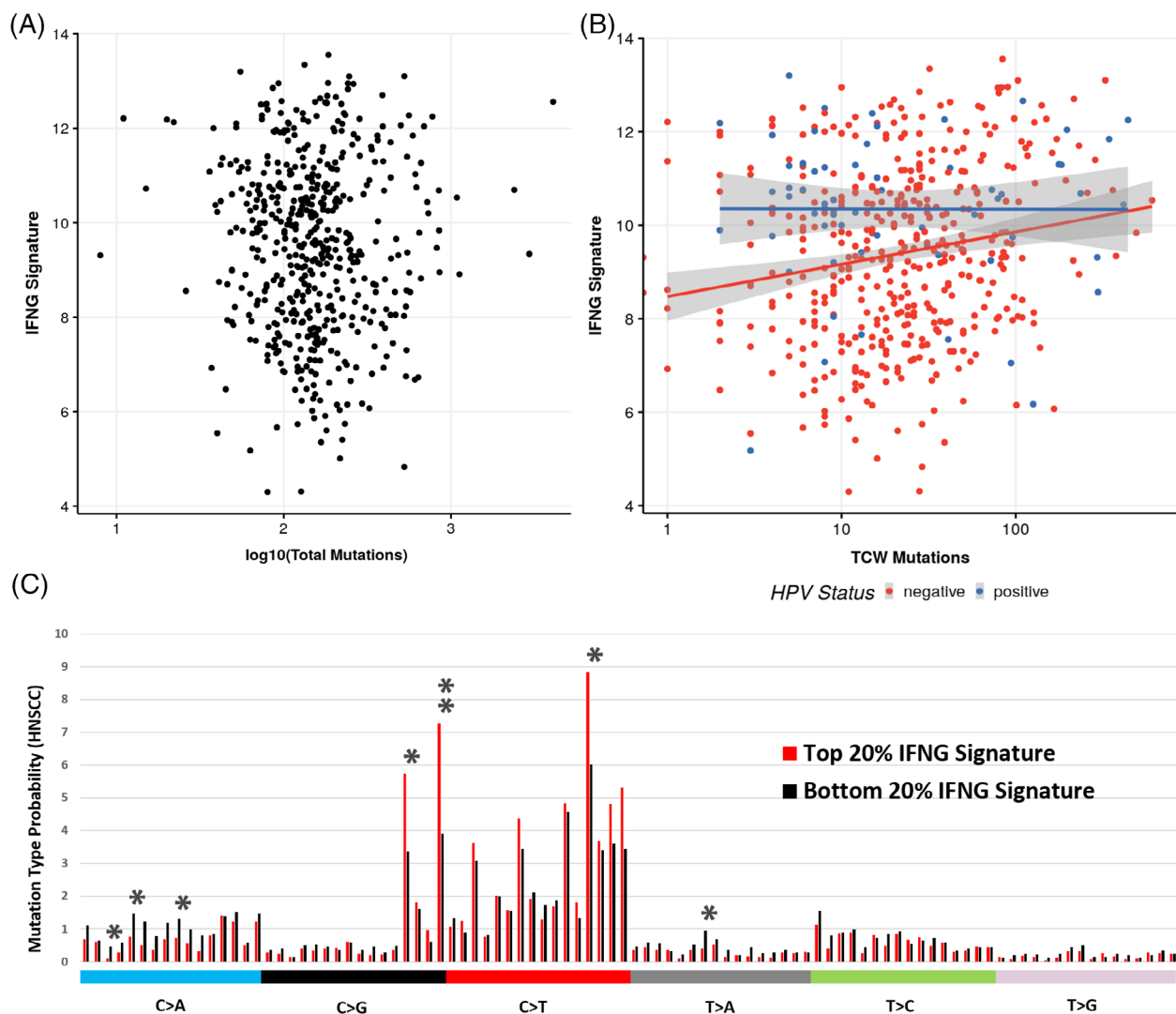


FIGURE 1 Inflammation as measured by an Interferon-gamma signature score is associated with APOBEC activity, not total variant count. A, Relationship between total single nucleotide variant count and the six-gene IFNG signature. No significant correlation was found between these measures ($R = -0.03 \pm 0.08$). B, Relationship between the six-gene IFNG signature and the number of C>T and C>G mutations in TCW motifs. Colors indicate HPV-status (red: HPV-negative, n = 432, blue: HPV-positive, n = 64). A significant correlation between TCW mutations and the IFNG signature was identified in HPV negative cases ($R = 0.18$, $P = 1 \times 10^{-4}$). C, The frequency of base exchange motifs (eg. C>A substitution with incorporation of the bases at the 5' and 3' end, thus allowing 96 potential mutation types) was compared between the patients with the highest and lowest IFNG signature within the TCGA cohort. The top 20% of inflamed cases showed a significant enrichment of variants in the APOBEC3-associated TCW context (* $P < .05$, ** $P < .01$, all P values were Bonferroni corrected) [Color figure can be viewed at wileyonlinelibrary.com]

assessed in the samples by analysis of a six-gene IFNG signature.³³ Total count of single nucleotide variants (SNV) did not correlate significantly with the IFNG signature (Figure 1A). Next, we analyzed associations between the T-cell inflamed gene expression phenotype and mutational signatures. C>T and C>G mutations are referred to as TCW mutations, as they preferentially occur in TCA and TCT contexts (TCW motif), indicating APOBEC3-induced mutagenesis. TCW mutations were significantly enriched in patients with high expression of the IFNG signature (Figure 1C).

3.2 | Analysis of HPV-status on inflammation and mutational signatures

HNSCC consists of biologically distinct HPV-positive and -negative subgroups. We identified 64 HPV-positive (53 HPV16, 8 HPV33 and 3 HPV35) and 432 HPV-negative samples in the TCGA dataset.

IFNG signature score, total SNV count, counts of TCW mutations and the ratio of the number of TCW mutations compared to the number of total mutations (TCW ratio) were assessed in both groups. Mutational load was significantly more pronounced in HPV-negative samples than in HPV-positive (Figure 2A, $P = 1.7 \times 10^{-4}$), whereas the IFNG signature was significantly higher in HPV-positive samples (Figure 2B, $P = 3.7 \times 10^{-5}$). Further, we compared the ratio of the number of TCW mutations/number of total mutations as a surrogate measure for APOBEC3 mutational activity, which was significantly higher in HPV-positive tumors (Figure 2C, $P = 2.6 \times 10^{-3}$). We then analyzed the association between TCW mutations and inflammation in HPV-positive and HPV-negative HNSCC and found a significant correlation only among HPV-negative HNSCC (Figure 1B). An association between APOBEC-induced TCW-mutations and the IFNG signature could be validated in independent LSCC, LUAD and BLCA datasets (Figure S1).

3.3 | Identification of an APOBEC-enriched HPV-negative subgroup

Since the association between APOBEC-induced mutations (TCW mutations) and the T-cell inflamed phenotype was restricted to HPV-negative samples, we grouped the HPV-negative samples into APOBEC-enriched ($n = 84$) and APOBEC-negative ($n = 348$) cases. This newly defined HPV-negative, APOBEC-enriched subgroup showed a higher relative contribution for both APOBEC-associated mutational Signatures 2 and 13 (Figure S2A). Further, the scores of Signatures 2 and 13 ranked higher in the APOBEC-enriched group when compared among the other COSMIC SBS signatures per sample (Figure S2B).

We observed that the HPV-negative subgroup with an enrichment of APOBEC-induced mutations showed a significantly higher IFNG signature score compared to all other HPV-negative cases (HPV-negative, APOBEC-negative; Figure 3A). To exclude the possibility that this signal came from samples falsely classified as HPV-negative, we repeated the analysis by removing all HPV-negative cases with more than five reads mapping to any of the HPV contigs without a change in results (Figure S4).

In addition to differences observed regarding overall inflammation, HPV-negative, APOBEC-enriched cases also exhibited higher predicted infiltration of myeloid-derived suppressor cells (MDSC), Type 17T-helper cell and effector memory CD8+ cell gene expression signatures (Figure S5). Further, differential expression of immune checkpoints was analyzed between groups. A significantly higher gene expression was identified for CD274 (PD-L1), CTLA4, LAG3 and PDCD1 (PD-1) in APOBEC-enriched cases. Only VTCN1 showed a significantly lower gene expression in APOBEC-enriched cases (Figure 3B).

Previous analyses have established different HNSCC subgroups based on gene expression.⁸ The APOBEC-enriched HPV-negative samples were assigned to these subgroups and were significantly enriched in the inflamed/mesenchymal cluster (Table S2).

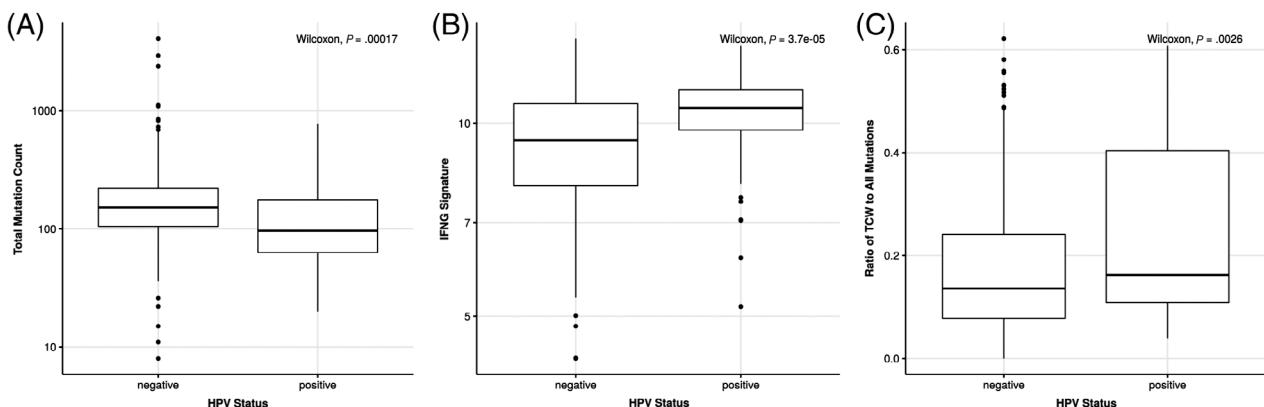


FIGURE 2 HPV status is an important variable in HNSCC. A, Boxplot of total single nucleotide variant count, grouped by HPV status. Total single nucleotide variant count was significantly higher in HPV-negative cases ($P = 1.7 \times 10^{-4}$). B, Boxplot of INFG signature score, grouped by HPV status. The six-gene IFNG signature score was significantly higher in HPV-positive samples ($P = 3.7 \times 10^{-5}$). C, Boxplot of ratio of TCW variants to total single nucleotide variant count, grouped by HPV status. The TCW-ratio was significantly higher in HPV-positive samples ($P = 2.6 \times 10^{-3}$)

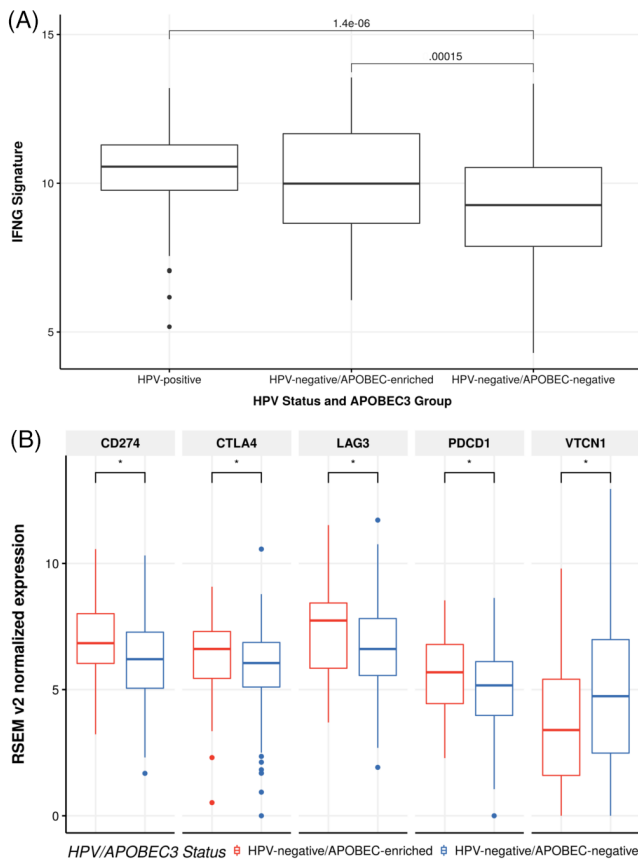


FIGURE 3 HPV-negative, APOBEC-enriched tumors exhibit higher inflammation, higher immune checkpoint expression. A, IFNG signature scores, grouped by HPV status and APOBEC enrichment for HPV-negative cases. HPV negative, APOBEC-enriched HNSCC showed a significantly higher IFNG signature than APOBEC-negative samples ($P = 1.5 \times 10^{-4}$). No significant difference between HPV-positive and HPV-negative/APOBEC-enriched samples was found. B, Gene expression of five immune checkpoints was significantly different between APOBEC-enriched and APOBEC-negative HPV-negative samples ($P < .05$ after Benjamini-Hochberg correction). All but VTCN1 showed significantly higher expression among APOBEC-enriched cases [Color figure can be viewed at wileyonlinelibrary.com]

We additionally analyzed mutations in immunotherapy-relevant genes.²⁷ The APOBEC-enriched subgroup showed significantly more variants with functional impact in immunotherapy-essential genes (Table 1, $P = 1.8 \times 10^{-4}$). Among those genes, HLA-A showed the highest relative enrichment among APOBEC-enriched cases and remained significant after correcting for multiple testing (Table S3).

Among HPV-negative samples, smokers were significantly under-represented ($P = .02$, Table S4) in the APOBEC-enriched group, no significant differences were observed for alcohol consumption. Further, we observe nonrandom associations between tumor site and HPV/APOBEC group ($P < .05$, Table S5) with an enrichment of APOBEC-associated cases in tumor arising from the oral cavity and alveolar ridge but an underrepresentation of laryngeal tumors and tumors of the oral tongue. No difference in overall survival was identified between HPV-negative APOBEC-enriched and APOBEC-negative groups (Figure S3).

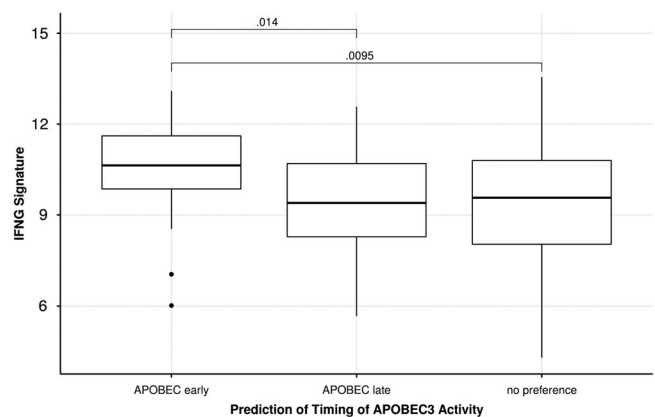


FIGURE 4 Cases with early APOBEC-activation show higher inflammation. IFNG signature score in HPV-negative cases for each group of APOBEC3 activity timing. n (APOBEC early) = 15, n (APOBEC late) = 50, n (no preference) = 367

TABLE 1 HPV-negative APOBEC-enriched and APOBEC-negative groups with counts of hits in gene set identified by Patel et al

	HPV-negative/APOBEC-enriched	HPV-negative/APOBEC-negative	P value
No. of cases	84	348	
No. of hits (collapsed to genes)/No. of cases	7.6 (638 total)	4.7 (1643 total)	1.8E-4
No. of hits with functional impact (collapsed to genes)/No. of cases	5.7 (476 total)	3.7 (1277 total)	8.8E-4
No. of hits (collapsed to genes), without HLA genes/No. of cases	7.3 (617 total)	4.7 (1623 total)	4.1E-4
No. of hits with functional impact (collapsed to genes), without HLA genes/No. of cases	5.5 (461 total)	3.6 (1259 total)	1.6E-3

Note: Two sets of Fisher exact tests were carried out, first considering a gene mutated if any variant was found. Second, only mutations with putative functional impact (MODERATE, HIGH flags as returned by Jannovar, eg, missense or stop gain variants) were considered. Both times, the APOBEC-enriched group showed a significant enrichment for mutations in immunotherapy related genes compared to the APOBEC-negative group. Tests were re-done without variants in HLA genes to exclude possible false-positive calls from variant calling.

3.4 | APOBEC activation is an early event in some HNSCC

To identify temporal patterns of APOBEC activation during tumor evolution, we analyzed the variant allele frequency (VAF) of TCW mutations in HNSCC. Cases with early TCW variants exhibited a significantly higher IFNG signature score compared to late TCW activation (Figure 4). We repeated the analysis for the TCGA cohorts of BLCA and LUAD. For BLCA, we did not observe any difference between the groups. However, in LUAD, we observed the opposite effect. Cases with early APOBEC activation were found to exhibit lower inflammation scores than the other two groups, which has been described before³⁴ (Figure S6).

3.5 | Identification of APOBEC3B and APOBEC3C expression in HNSCC

Gene expression of APOBEC3 family genes was analyzed in the TCGA cohort. HPV-positive samples exhibited significantly higher total APOBEC3 gene expression than HPV-negative samples (Figure 5A). Among HPV-negative samples, the APOBEC-enriched subgroup showed significantly higher expression of APOBEC genes than the APOBEC-negative subgroup. When analyzing APOBEC gene expression by gene, APOBEC3A was most prominently overexpressed in HPV-negative, APOBEC-enriched samples (Figure S7). Since bulk gene expression analyses do not differentiate between tumor and stroma, we analyzed gene expression data in single-cell transcriptome data of HPV-negative HNSCC³⁰ (GSE103322).

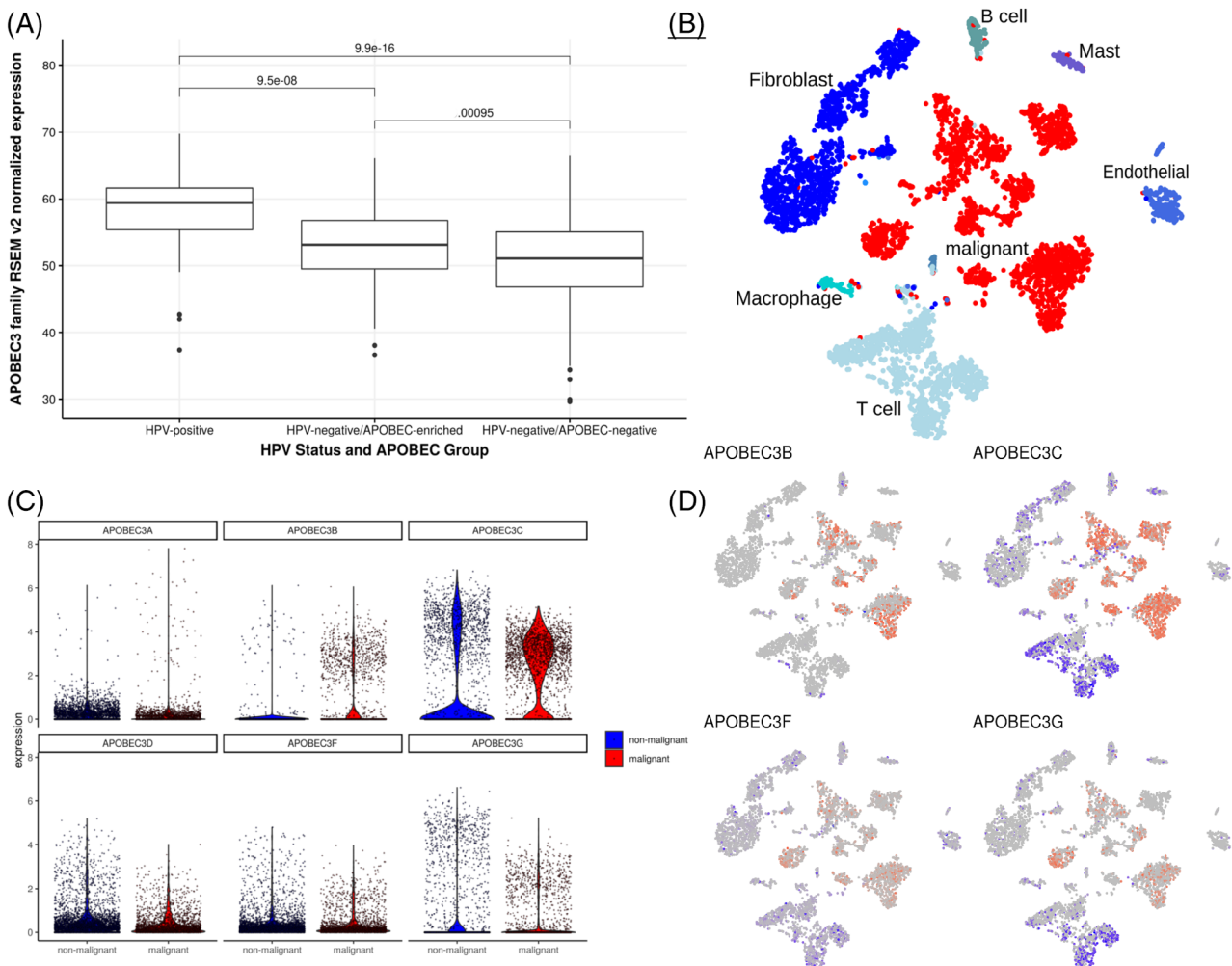


FIGURE 5 Independent single-cell expression data demonstrates the expression of APOBEC3C and APOBEC3B in tumor cells. A, Aggregated expression of APOBEC3 family genes for the three groups HPV-positive, HPV-negative/APOBEC-enriched, HPV-negative/APOBEC-negative. HPV-positive cases show significantly higher APOBEC3 expression than HPV-negative cases. Among those, the APOBEC-enriched subgroup exhibits significantly higher APOBEC3 gene expression. B, tSNE projection of all cells from 17 single-cell transcriptomics-profiled cases,³⁰ grouped into cell types. C, Violin plots of APOBEC3 gene expression between malignant (red) and nonmalignant cells (blue). APOBEC3B and APOBEC3C gene expression were detected in tumor cells. D, tSNE plots with projected expression of genes in the APOBEC3 family in 17 single-cell data sets of HPV-negative cases.³⁰ Biomarker-based groups of malignant (red) and nonmalignant cells (blue). Expression strength indicated by color intensity, with gray indicating that no expression was detected [Color figure can be viewed at wileyonlinelibrary.com]

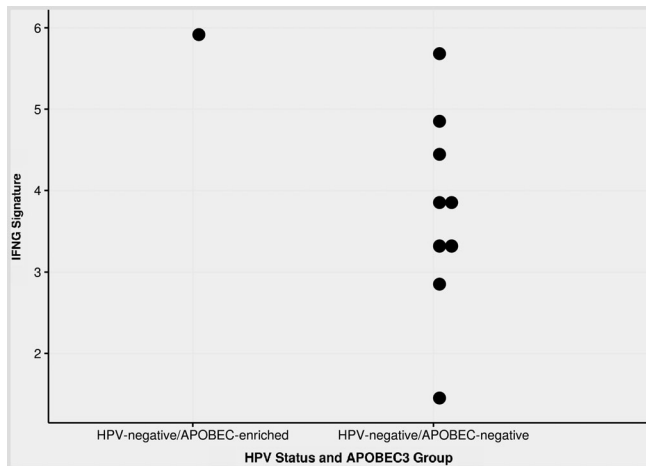


FIGURE 6 Independent analysis in a clinical cohort. IFNG signature score in the head-and-neck DTK Master cohort grouped by APOBEC status for all HPV-negative cases. The only identified HPV-negative/APOBEC-enriched sample harbored the highest IFNG gene expression signature score

Among those, APOBEC3B and APOBEC3C gene expression were highest in malignant cells (Figure 5B-D).

3.6 | Independent validation of findings

In an independent cohort of 10 HPV-negative cases of HNSCC, sequenced for the DTK MASTER program from six cancer centers in Germany, we set out to validate these findings. We identified one HPV-negative patient with an APOBEC-enriched mutational signature. Again, we computed the IFNG signature score and compared it between the already defined groups (Figure 6). The HPV-negative case with APOBEC enrichment (Figure S8, data available in Table S6) showed the highest inflammation in this cohort.

4 | DISCUSSION

Immune checkpoint inhibition has become an important treatment option in HNSCC, providing a benefit in a subset of patients.³⁵ The predictive value of a T-cell inflamed phenotype, as defined by an IFNG expression signature, has been shown in HNSCC and other tumor types.^{3,4} Additionally, a high mutational load is correlated with response to immune checkpoint inhibition.⁵ Yet, in our and other analyses, no clinically useful correlation between those two predictive markers was shown.⁶

To better understand differential immune activation and evasion in HNSCC, we analyzed the relationship between different mutational signatures and inflammation in HNSCC. An APOBEC-induced TCW mutational signature was significantly associated with a T-cell inflamed phenotype. This association could be validated in other tumor types, including lung and bladder cancer. Previous studies also support the

role of APOBEC-induced mutational signatures in immune activation in several cancer types.^{36,37} Among tumors with a high APOBEC mutational burden, Faden et al described HNSCC to have the highest IFNG levels, especially among HPV-positive cases.³⁸ In addition to these analyses, we show that, despite overall high levels of inflammation and APOBEC mutagenesis in HPV-positive HNSCC, a dose-dependent association between TCW mutations and inflammation is restricted to HPV-negative cases, thus leading to the establishment of an APOBEC-associated subgroup with differential immune activation among HPV-negative samples. We attribute the difference between HPV-positive and HPV-negative cases to the overall high impact of APOBEC-induced tumorigenesis in HPV-positive HNSCC¹¹ and a generally higher level of IFNG activation in these tumors. The activation of APOBEC in non-virally associated tumors has also been shown across cancer types.¹⁴ This signature has been proposed to occur later in tumorigenesis and to induce branched evolution in lung cancer.^{34,39}

Our own analyses in HNSCC rather suggest an early APOBEC activation in a subset of HPV-negative HNSCC with an immunogenic phenotype, thus proposing a different oncogenic mechanism in HNSCC, further supporting the idea of a distinct subgroup. It is currently unclear what drives this APOBEC activation. Previous analyses have suggested a link with single strand exposure and DNA repair defects.^{40,41} It is also conceivable that short-term viral exposure induces APOBEC activation and carcinogenesis without genomic viral integration in some patients. Faden et al also suggested a potential role of germline APOBEC polymorphisms in mutagenesis.³⁸

A subgroup of HPV-negative oral squamous cell carcinoma patients in never-smokers, never-drinkers with high tumor inflammation has been described in the literature.⁴² This agrees with our observation, since smokers were underrepresented in the APOBEC-associated subgroup that was also enriched for tumors arising from the oral cavity. Further research focusing on the impact of short-term viral exposure and APOBEC-activation or virus-independent mechanisms of APOBEC-activation, especially in this hard-to-treat subgroup, are of interest.

We were not able to immunohistochemically analyze APOBEC protein expression in HNSCC and HNSCC patient-derived xenograft models, a well-known problem with currently available APOBEC3 antibodies.¹² In the TCGA data, APOBEC3A was most prominently expressed in the APOBEC-enriched subgroup. However, the tumor microenvironment poses a challenge in the analysis of bulk data. Inflammatory signatures, such as the IFNG signature, are associated with more immune infiltration and lower tumor purity. We therefore resorted to a re-analysis of publicly available single-cell gene expression data. Doing so, we were able to circumvent the bias of measuring APOBEC3 activity in the tumor microenvironment.⁴³ Here, expression of APOBEC3 subtypes 3B and 3C was most prominent among malignant cells. APOBEC3B has also been identified in previous publications on APOBEC activation in cancer, including HNSCC,^{13,37} whereas the role of APOBEC3C remains less well defined. Since transient expression of APOBEC3 subtypes has been described,⁴⁴ short term activity of other APOBEC3-subtypes might cause mutations in the absence of APOBEC gene expression in later analyses, thus potentially explaining the observed differences. The observed different

contributions of APOBEC mutational Signatures 2 and 13 between HPV-positive and HPV-negative samples might also reflect different underlying APOBEC3-activity.

It is currently unclear what causes the T-cell inflamed phenotype in APOBEC-induced cancers. We were able to show that these tumors, despite harboring the same overall mutational load, show a distinct immune escape, represented by an enrichment for mutations in immunotherapy-essential genes (such as HLA-A), expression of regulatory immune signatures, including myeloid-derived, as well as expression of immune checkpoint molecules. Furthermore, these samples cluster in the immunogenic mesenchymal/inflamed subgroup.⁸ It is possible that APOBEC-induced mutations are more prone to detection by the immune system, due to their association with viral infections. Yet, our own analyses in APOBEC-induced cancers did not show an increase in bioinformatically predicted neo-antigens (data not shown). Therefore, the reasons for the different mechanisms of immune evasion in APOBEC-associated HPV-negative HNSCC are not known but might also be relevant in other tumor types including urothelial^{45,46} or lung cancer.³⁷ Does APOBEC-activity translate into differential response to immune checkpoint inhibition? Early studies suggest that APOBEC-associated tumors might indeed respond better to ICI therapy.^{37,47} We were able to find some supporting evidence for the differential immune activation also within the recurrent/metastatic DTKK-MASTER cohort. However, this cohort is small and does not represent the demographics of the majority of HNSCC patients. Thus, further research is required to analyze this association, especially in patient cohorts treated with immune checkpoint inhibition. Mutational signatures inferred from DNA sequencing and specifically APOBEC3-associated motifs should be further investigated as a potentially predictive biomarker for immune checkpoint inhibition in HPV-negative HNSCC.

ACKNOWLEDGEMENTS

This work was funded by a grant awarded by Berliner Krebsgesellschaft e.V. to DTR, FK and DB. DTR is a participant in the Berlin Institute of Health - Charité Clinical Scientist Program funded by the Charité - Universitätsmedizin Berlin and the Berlin Institute of Health. The DTKK MASTER trial is funded by the German Cancer Consortium (DKTK). The results shown here are in part based upon data generated by the TCGA Research Network: <http://cancergenome.nih.gov/>

CONFLICT OF INTEREST

A. S. reports receiving research funding from Chugai, BMS, Ventana Roche and honoraria from Bayer, Novartis, BMS, AstraZeneca, Roche, Takeda, ThermoFisher, Illumina (Advisory Board) and Takeda, Roche, BMS, Illumina, AstraZeneca, Novartis, ThermoFisher, Bayer, MSD, Lilly (Speaker). W. W. reported honoraria unrelated to the current work (speaker's bureau and advisory board) from AstraZeneca, MSD, BMS, Bayer, Roche, Pfizer, Merck, Lilly, Novartis, Takeda, Amgen, Astellas and Research Funding from Bruker, MSD, BMS and Roche. The other authors report no potential conflict of interest that is relevant to this work.

DATA ACCESSIBILITY

Data sources and handling of the publicly available data used in our study are described in the Materials and Methods. The other data and further details are available from the corresponding author upon request.

ETHICS STATEMENT

The DTKK MASTER trial was approved by the local ethics committees. Written, informed consent was obtained from all participating patients.

ORCID

Clemens Messerschmidt  <https://orcid.org/0000-0001-8632-656X>

Benedikt Obermayer  <https://orcid.org/0000-0002-9116-630X>

Konrad Klinghammer  <https://orcid.org/0000-0001-6425-4833>

Sebastian Ochsenreither  <https://orcid.org/0000-0001-6024-4312>

Denise Treue  <https://orcid.org/0000-0002-0657-5505>

Albrecht Stenzinger  <https://orcid.org/0000-0003-1001-103X>

Stefan Fröhling  <https://orcid.org/0000-0001-7907-4595>

Christian H. Brandts  <https://orcid.org/0000-0003-1732-2535>

Ingeborg Tinhofer  <https://orcid.org/0000-0002-0512-549X>

Ulrich Keilholz  <https://orcid.org/0000-0001-6773-9406>

Dieter Beule  <https://orcid.org/0000-0002-3284-0632>

Damian T. Rieke  <https://orcid.org/0000-0003-0027-7977>

REFERENCES

- Hanahan D, Weinberg RA. Hallmarks of cancer: the next generation. *Cell*. 2011;144:646-674.
- Ferris RL, Blumenschein G, Fayette J, et al. Nivolumab for recurrent squamous-cell carcinoma of the head and neck. *N Engl J Med*. 2016; 375:1856-1867.
- Seiwert TY, Burtneß B, Mehra R, et al. Safety and clinical activity of pembrolizumab for treatment of recurrent or metastatic squamous cell carcinoma of the head and neck (KEYNOTE-012): an open-label, multicentre, phase 1b trial. *Lancet Oncol*. 2016;17:956-965.
- Ayers M, Luceford J, Nebozhyn M, et al. IFN- γ -related mRNA profile predicts clinical response to PD-1 blockade. *J Clin Invest*. 2017;127: 2930-2940.
- van Allen EM, Miao D, Schilling B, et al. Genomic correlates of response to CTLA-4 blockade in metastatic melanoma. *Science (80-)*. 2015;350:207-211.
- Cristescu R, Mogg R, Ayers M, et al. Pan-tumor genomic biomarkers for PD-1 checkpoint blockade-based immunotherapy. *Science (80-)*. 2018;362:eaar3593.
- Rieke DT, Klinghammer K, Keilholz U. Targeted therapy of head and neck cancer. *Oncol Res Treat*. 2016;39:780-786.
- Keck MK, Zuo Z, Khattri A, et al. Integrative analysis of head and neck cancer identifies two biologically distinct HPV and three non-HPV subtypes. *Clin Cancer Res*. 2015;21:870-881.
- Mehra R, Seiwert TY, Gupta S, et al. Efficacy and safety of pembrolizumab in recurrent/metastatic head and neck squamous cell carcinoma: pooled analyses after long-term follow-up in KEYNOTE-012. *Br J Cancer*. 2018;119:153-159.
- Blank CU, Haanen JB, Ribas A, Schumacher TN. The cancer immunogram. *Science (80-)*. 2016;352:658-660.
- Henderson S, Chakravarthy A, Su X, Boshoff C, Fenton TR. APOBEC-mediated cytosine deamination links PIK3CA helical domain mutations to human papillomavirus-driven tumor development. *Cell Rep*. 2014;7(6):1833-1841. <https://doi.org/10.1016/j.celrep.2014.05.012>

12. Venkatesan S, Rosenthal R, Kanu N, et al. Perspective: APOBEC mutagenesis in drug resistance and immune escape in HIV and cancer evolution. *Ann Oncol*. 2018;29:563-572.
13. Burns MB, Temiz NA, Harris RS. Evidence for APOBEC3B mutagenesis in multiple human cancers. *Nat Genet*. 2013;45:977-983.
14. Alexandrov LB, Nik-Zainal S, Wedge DC, et al. Signatures of mutational processes in human cancer. *Nature*. 2013;500:415-421.
15. Lawrence MS, Sougnez C, Lichtenstein L, et al. Comprehensive genomic characterization of head and neck squamous cell carcinomas. *Nature*. 2015;517:576-582.
16. Collisson EA, Campbell JD, Brooks AN, et al. Comprehensive molecular profiling of lung adenocarcinoma. *Nature*. 2014;511:543-550.
17. Weinstein JN, Akbani R, Broom BM, et al. Comprehensive molecular characterization of urothelial bladder carcinoma. *Nature*. 2014;507(7492):315-322. <https://doi.org/10.1038/nature12965>
18. Hammerman PS, Voet D, Lawrence MS, et al. Comprehensive genomic characterization of squamous cell lung cancers. *Nature*. 2012;489:519-525.
19. Roberts SA, Lawrence MS, Klimczak LJ, et al. An APOBEC cytidine deaminase mutagenesis pattern is widespread in human cancers. *Nat Genet*. 2013;45:970-976.
20. Huang PJ, Chiu LY, Lee CC, et al. MSignatureDB: a database for deciphering mutational signatures in human cancers. *Nucleic Acids Res*. 2018;46(D1):D964-D970. <https://doi.org/10.1093/nar/gkx1133>
21. Buitrago-Pérez A, Garaulet G, Vázquez-Carballo A, Paramio JM, García-Escudero R. Molecular signature of HPV-induced carcinogenesis: pRb, p53 and gene expression profiling. *Curr Genomics*. 2009;10:26-34.
22. Tang K-W, Alaei-Mahabadi B, Samuelsson T, Lindh M, Larsson E. The landscape of viral expression and host gene fusion and adaptation in human cancer. *Nat Commun*. 2013;4:2513.
23. Gao J, Aksoy BA, Dogrusoz U, et al. Integrative analysis of complex cancer genomics and clinical profiles using the cBioPortal. *Sci Signal*. 2013;6:pl1-pl1.
24. Charoentong P, Finotello F, Angelova M, et al. Pan-cancer Immunogenomic analyses reveal genotype-Immuno-phenotype relationships and predictors of response to checkpoint blockade. *Cell Rep*. 2017;18:248-262.
25. Hänzelmann S, Castelo R, Guinney J. GSVA: gene set variation analysis for microarray and RNA-Seq data. *BMC Bioinformatics*. 2013;14:7. <https://doi.org/10.1186/1471-2105-14-7>
26. Ritchie ME, Phipson B, Wu D, et al. Limma powers differential expression analyses for RNA-sequencing and microarray studies. *Nucleic Acids Res*. 2015;43(7):e47. <https://doi.org/10.1093/nar/gkv007>
27. Patel SJ, Sanjana NE, Kishton RJ, et al. Identification of essential genes for cancer immunotherapy. *Nature*. 2017;548:537-542.
28. Jäger M, Wang K, Bauer S, Smedley D, Krawitz P, Robinson PN. Jannovar: a Java library for exome annotation. *Hum Mutat*. 2014;35:548-555.
29. Storey J. qvalue: Q-Value estimation for false discovery rate control. R package version 2.0.0. 2015. DOI: <https://doi.org/10.18129/B9.bioc.qvalue>
30. Puram SV, Tirosh I, Parkhi AS, et al. Single-cell transcriptomic analysis of primary and metastatic tumor ecosystems in head and neck cancer. *Cell*. 2017;171:1611-1624.e24.
31. Butler A, Hoffman P, Smibert P, Papalexi E, Satija R. Integrating single-cell transcriptomic data across different conditions, technologies, and species. *Nat Biotechnol*. 2018;36:411-420.
32. Patro R, Duggal G, Love MI, Irizarry RA, Kingsford C. Salmon provides fast and bias-aware quantification of transcript expression. *Nat Methods*. 2017;14:417-419.
33. Chow LQM, Mehra R, Haddad RI, et al. Biomarkers and response to pembrolizumab (pembro) in recurrent/metastatic head and neck squamous cell carcinoma (R/M HNSCC). *J Clin Oncol*. 2016;34:6010-6010.
34. McGranahan N, Favero F, de Bruin EC, Birkbak NJ, Szallasi Z, Swanton C. Clonal status of actionable driver events and the timing of mutational processes in cancer evolution. *Sci Transl Med*. 2015;7:283ra54.
35. Burtress B, Harrington KJ, , et al. KEYNOTE-048: phase III study of first-line pembrolizumab (P) for recurrent/metastatic head and neck squamous cell carcinoma (R/M HNSCC). *Ann Oncol*. 2018;29(Suppl. 8):viii729-viii729. <https://doi.org/10.1093/annonc/mdy424.045>
36. Budczies J, Seidel A, Christopoulos P, et al. Integrated analysis of the immunological and genetic status in and across cancer types: impact of mutational signatures beyond tumor mutational burden. *Oncimmunology*. 2018;7:e1526613. <https://doi.org/10.1080/2162402X.2018.1526613>
37. Wang S, Jia M, He Z, Liu X-S. APOBEC3B and APOBEC mutational signature as potential predictive markers for immunotherapy response in non-small cell lung cancer. *Oncogene*. 2018;37:3924-3936.
38. Faden DL, Ding F, Lin Y, et al. APOBEC mutagenesis is tightly linked to the immune landscape and immunotherapy biomarkers in head and neck squamous cell carcinoma. *Oral Oncol*. 2019;96:140-147.
39. Swanton C, McGranahan N, Starrett GJ, Harris RS. APOBEC enzymes: mutagenic fuel for cancer evolution and heterogeneity. *Cancer Discov*. 2015;5:704-712.
40. Chen J, Miller BF, Furano AV. Repair of naturally occurring mismatches can induce mutations in flanking DNA. *Elife*. 2014;3:e02001. <https://doi.org/10.7554/eLife.02001>
41. Taylor BJ, Nik-Zainal S, Wu YL, et al. DNA deaminases induce break-associated mutation showers with implication of APOBEC3B and 3A in breast cancer kataegis. *Elife*. 2013;2:e00534. <https://doi.org/10.7554/eLife.00534>
42. Foy J-P, Bertolus C, Michallet M-C, et al. The immune microenvironment of HPV-negative oral squamous cell carcinoma from never-smokers and never-drinkers patients suggests higher clinical benefit of IDO1 and PD1/PD-L1 blockade. *Ann Oncol*. 2017;28:1934-1941.
43. Leonard B, Starrett GJ, Maurer MJ, et al. APOBEC3G expression correlates with T-cell infiltration and improved clinical outcomes in high-grade serous ovarian carcinoma. *Clin Cancer Res*. 2016;22:4746-4755.
44. Petljak M, Alexandrov LB, Brummel JS, et al. Characterizing mutational signatures in human cancer cell lines reveals episodic APOBEC mutagenesis. *Cell*. 2019;176:1282-1294.e20. <https://doi.org/10.1016/j.cell.2019.02.012>
45. Mullane SA, Werner L, Rosenberg J, et al. Correlation of Apobec Mrna expression with overall survival and pd-11 expression in urothelial carcinoma. *Sci Rep*. 2016;6:27702.
46. Glaser AP, Fantini D, Wang Y, et al. APOBEC-mediated mutagenesis in urothelial carcinoma is associated with improved survival, mutations in DNA damage response genes, and immune response. *Oncotarget*. 2018;9:4537-4548.
47. Miao D, Margolis CA, Vokes NI, et al. Genomic correlates of response to immune checkpoint blockade in microsatellite-stable solid tumors. *Nat Genet*. 2018;50:1271-1281.

SUPPORTING INFORMATION

Additional supporting information may be found online in the Supporting Information section at the end of this article.

How to cite this article: Messerschmidt C, Obermayer B, Klinghammer K, et al. Distinct immune evasion in APOBEC-enriched, HPV-negative HNSCC. *Int. J. Cancer*. 2020;147:2293-2302. <https://doi.org/10.1002/ijc.33123>

Druckexemplar der Publikation Akpa et al. 2020

RESEARCH ARTICLE

Open Access



Acquired resistance to DZNep-mediated apoptosis is associated with copy number gains of *AHCY* in a B-cell lymphoma model

Chidimma Agatha Akpa^{1,2*}, Karsten Kleo¹, Elisabeth Oker¹, Nancy Tomaszewski¹, Clemens Messerschmidt³, Cristina López⁴, Rabea Wagener⁴, Kathrin Oehl-Huber⁴, Katja Dettmer⁵, Anne Schoeler^{6,7}, Dido Lenze¹, Peter J. Oefner², Dieter Beule³, Reiner Siebert⁴, David Capper^{2,6,7}, Lora Dimitrova¹ and Michael Hummel^{1,2}

Abstract

Background: Enhancer of zeste homolog 2 (EZH2) is considered an important driver of tumor development and progression by its histone modifying capabilities. Inhibition of EZH2 activity is thought to be a potent treatment option for eligible cancer patients with an aberrant EZH2 expression profile, thus the indirect EZH2 inhibitor 3-Deazaneplanocin A (DZNep) is currently under evaluation for its clinical utility. Although DZNep blocks proliferation and induces apoptosis in different tumor types including lymphomas, acquired resistance to DZNep may limit its clinical application.

Methods: To investigate possible mechanisms of acquired DZNep resistance in B-cell lymphomas, we generated a DZNep-resistant clone from a previously DZNep-sensitive B-cell lymphoma cell line by long-term treatment with increasing concentrations of DZNep (ranging from 200 to 2000 nM) and compared the molecular profiles of resistant and wild-type clones. This comparison was done using molecular techniques such as flow cytometry, copy number variation assay (OncoScan and TaqMan assays), fluorescence in situ hybridization, Western blot, immunohistochemistry and metabolomics analysis.

Results: Whole exome sequencing did not indicate the acquisition of biologically meaningful single nucleotide variants. Analysis of copy number alterations, however, demonstrated among other acquired imbalances an amplification (about 30 times) of the *S*-adenosyl-L-homocysteine hydrolase (*AHCY*) gene in the resistant clone. *AHCY* is a direct target of DZNep and is critically involved in the biological methylation process, where it catalyzes the reversible hydrolysis of *S*-adenosyl-L-homocysteine to L-homocysteine and adenosine. The amplification of the *AHCY* gene is paralleled by strong overexpression of *AHCY* at both the transcriptional and protein level, and persists upon culturing the resistant clone in a DZNep-free medium.

(Continued on next page)

* Correspondence: chidimma.akpa@charite.de

¹Department of Experimental Hematopathology, Institute of Pathology, Charité Medical University, Berlin, Charitéplatz 1, 10117 Berlin, Germany

²Berlin School of Integrative Oncology, Charité - Medical University of Berlin, Berlin, Germany

Full list of author information is available at the end of the article



© The Author(s). 2020 **Open Access** This article is licensed under a Creative Commons Attribution 4.0 International License, which permits use, sharing, adaptation, distribution and reproduction in any medium or format, as long as you give appropriate credit to the original author(s) and the source, provide a link to the Creative Commons licence, and indicate if changes were made. The images or other third party material in this article are included in the article's Creative Commons licence, unless indicated otherwise in a credit line to the material. If material is not included in the article's Creative Commons licence and your intended use is not permitted by statutory regulation or exceeds the permitted use, you will need to obtain permission directly from the copyright holder. To view a copy of this licence, visit <http://creativecommons.org/licenses/by/4.0/>. The Creative Commons Public Domain Dedication waiver (<http://creativecommons.org/publicdomain/zero/1.0/>) applies to the data made available in this article, unless otherwise stated in a credit line to the data.

(Continued from previous page)

Conclusions: This study reveals one possible molecular mechanism how B-cell lymphomas can acquire resistance to DZNep, and proposes AHCY as a potential biomarker for investigation during the administration of EZH2-targeted therapy with DZNep.

Keywords: 3- Deazaneplanocin a (DZNep), B-cell lymphoma, Enhancer of zeste homolog 2 (EZH2), S-adenosyl-L-homocysteine hydrolase (AHCY)

Background

The development of drug resistance to cancer chemotherapeutics remains a major concern in most treatment regimens. Several epigenetic-based therapies are under investigation or being employed for treatment of patients with lymphomas of B-cell origin. This is due to the important role that epigenetic alterations play in promoting tumor development and progression via downregulation of tumor suppressor genes [1]. These epigenetic modifications may involve covalent post-translational modifications at the N-termini of histones or changes in the methylation pattern of cytosine bases within the DNA, especially at CpG sites [2]. Histones are important structural components of the cell that package and organize DNA into nucleosomal units and various post-translational modifications of histones are known to contribute to transcriptional gene activity in conjunction with other mechanisms [3–8].

Enhancer of zeste homolog 2 (EZH2) is a histone methyltransferase that is involved in cellular differentiation and development in both health and disease. EZH2 promotes transcriptional repression by catalyzing the trimethylation of lysine 27 on histone 3 (H3K27me3) - a repressive histone mark. In lymphoma and other malignancies, *EZH2* gain-of-function mutations and overexpression are considered important drivers of oncogenesis because of their role in silencing tumor suppressor genes regulating apoptosis, cell cycle regulation, proliferation, migration and differentiation [9–14]. Due to its oncogenic role, the targeting of EZH2 might be a promising approach for lymphoma therapy. 3-Deazaneplanocin A (DZNep) is an indirect inhibitor of EZH2 currently in the pre-clinical phase of drug development and has been shown to promote apoptosis in various primary tumor cells and cancer cell lines [15–20]. The apoptotic effects mediated by DZNep application are more pronounced in cancer cells, with minimal effects on normal cells, and are fostered by the inhibition of the repressive H3K27me3 mark [15, 18, 21].

DZNep directly inhibits the enzyme S-adenosyl-L-homocysteine hydrolase (AHCY) that catalyzes the reversible hydrolysis of S-adenosyl-L-homocysteine (SAH) to L-homocysteine and adenosine. The direct inhibition of AHCY by DZNep leads to the build-up of the substrate SAH, which in turn causes a negative feedback inhibition of methyltransferases such as EZH2 [22]. Proper

functioning of AHCY is essential for the efficient maintenance of histone methylation levels in the cell [23]. Alterations in AHCY function have been linked to cancer with varying outcomes depending on the cancer entity involved. For example, with lowered AHCY activity, the invasiveness of breast cancer and glioblastoma cell lines decreases [24, 25]. Furthermore, in hepatocellular carcinoma cells, reduced AHCY activity is associated with cell cycle inhibition and a lowered proliferation rate [23]. In esophageal squamous cell carcinoma, however, elevated AHCY levels had no effect on cell proliferation but promoted apoptosis and inhibited cell migration and adhesion [26]. Besides, aberrant AHCY expression has been observed with the transformation of follicular lymphoma to diffuse large B-cell lymphoma [27].

In this study, we investigated the underlying molecular mechanism of resistance of a B-cell lymphoma model to DZNep using a DZNep-resistant clone generated from a DZNep-sensitive cell line. We identified *AHCY* as a potential biomarker that could be of predictive relevance for therapeutic inhibition of EZH2 using DZNep.

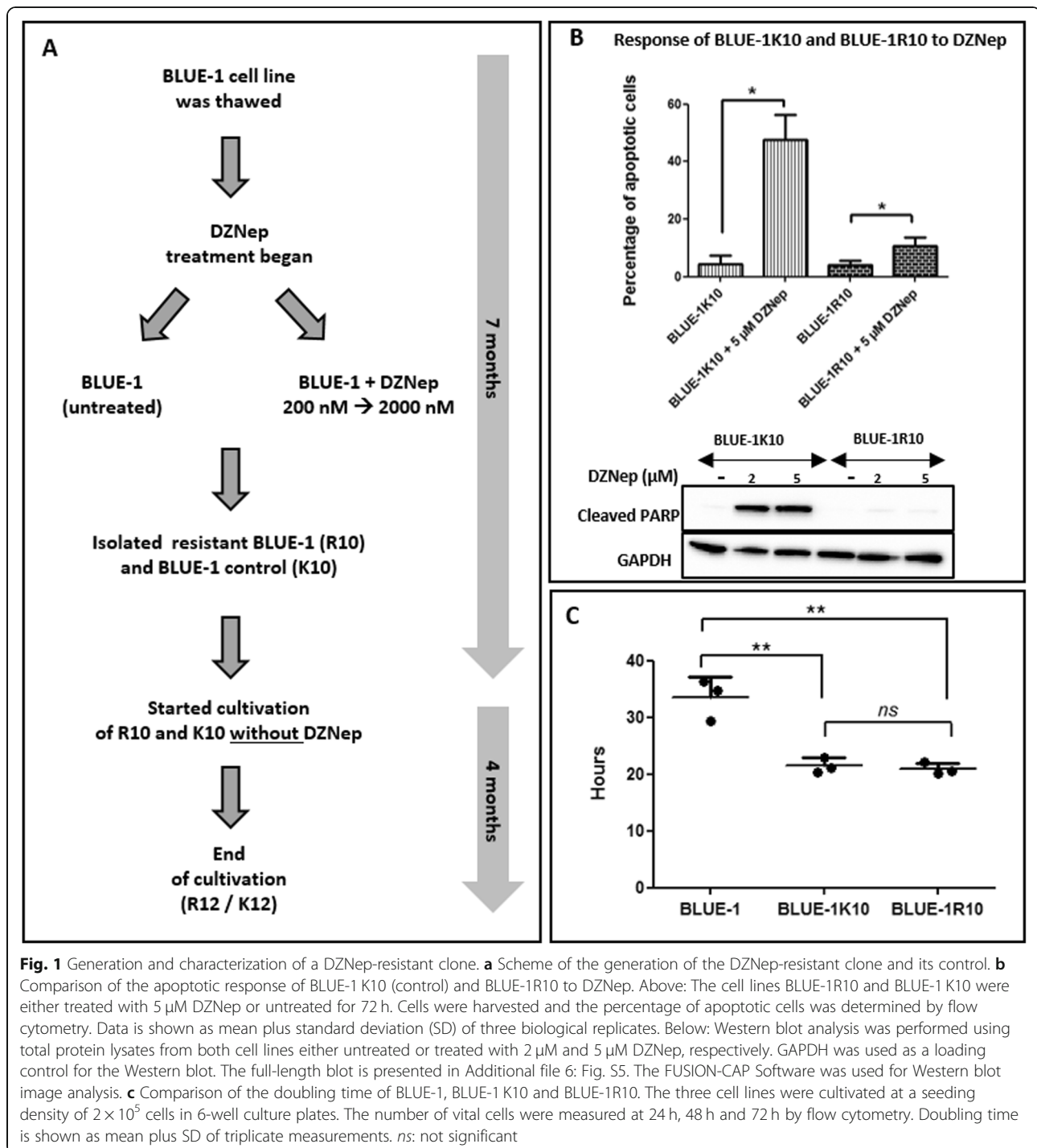
Methods

Drug, cell lines and culture conditions

DZNep (Selleckchem, Germany) was dissolved in sterile water following the manufacturer's recommendation as previously described [20].

The sporadic Burkitt lymphoma cell line BLUE-1 (ACC-594, from German Collection of Microorganisms and Cell Cultures (DSMZ) Germany) was cultured in RPMI 1640 (ThermoFisher Scientific, Germany) medium enriched with 20% fetal calf serum (PAN-Biotech, Germany). Cell lines were tested and confirmed mycoplasma negative with the MycoAlert Mycoplasma Detection kit (Lonza, Germany). All cell lines were incubated at 37 °C at 5% CO₂.

Generation of a DZNep resistant clone was achieved by splitting the BLUE-1 culture into a control group and a treatment group (Fig. 1a). The treated group received increasing concentrations of DZNep starting from 200 nM up to 2000 nM over a period of 7 months. The cells were split 3 times a week and fresh medium without or with DZNep was added to the control and treated cells, respectively. Vital cells were counted each time by flow cytometry before the cells were split. Cryostocks were



made every third to fourth week from both cell cultures. At 7 months, DZNep pressure on cultures of the treated group was removed by growing both untreated (BLUE-1 K10) and treated (BLUE-1R10) cells in medium without DZNep. About 4 months later, both cell cultures were harvested (BLUE-1 K12 and BLUE-1R12) and frozen. Prior to further use, frozen cells were thawed and maintained in a DZNep-free medium for at least 1 week.

Flow cytometry

The BD Accuri C6 flow cytometer (Becton Dickinson Biosciences, USA) was used for the measurement of apoptotic cells and determination of the doubling time of cells. Measurement of apoptosis was performed after staining 3×10^5 cells from the cell cultures with a mixture of Annexin V (Biolegend, USA) and propidium iodide (Biolegend, USA). Doubling time was determined by

seeding the cells in 6-well plates at a cell density of 2×10^5 cells/ml. The number of vital cells were counted after 24 h, 48 h and 72 h by flow cytometry. The doubling time during the exponential growth phase was subsequently calculated using the formula $DT = T \ln 2 / \ln(Xe/Xb)$ (https://www.atcc.org/~media/PDFs/Culture%20Guides/AnimCellCulture_Guide.ashx), where DT represents the doubling time (in hours), T symbolizes the incubation time (in hours), Xe indicates the cell number at the end of the incubation time, and Xb is the cell number at the beginning of the incubation time.

Western blotting, RNA isolation and real-time reverse transcriptase polymerase chain reaction (RT-PCR)

Cell lysis and Western blot were carried out as described previously [20]. Twelve percent Expedeon RunBlue SDS protein gels (Biozol Diagnostica Vertrieb GmbH, Germany) were utilized for the run. The primary and secondary antibodies used for Western blot are shown in Table 1.

RNA was isolated using the RNeasy Midi Kit (Qiagen, Germany) adhering to the manufacturer's recommendations and reverse transcribed to cDNA using TaqMan Reverse Transcription reagents (ThermoFisher Scientific, Germany) on a T3 thermocycler (Biometra GmbH, Germany). Real-time RT-PCR was carried out using TaqMan Gene Expression Assays and TaqMan Gene Expression Master Mix (ThermoFisher Scientific, Germany) following the manufacturer's protocol on the StepOnePlus Real-Time PCR System (ThermoFisher Scientific, Germany). Beta-2 microglobulin (*B2M*) and succinate dehydrogenase (*SDHA*) genes were used as endogenous controls and the $\Delta\Delta C_t$ method [28] was followed for relative mRNA quantification. Details of the respective TaqMan assays used are listed in Table 2.

DNA isolation, whole exome sequencing (WES), copy number variation (CNV) assay and OncoScan CNV assay

Genomic DNA was isolated from the cell lines using QIAamp DNA Mini Kit (Qiagen, Germany), following

Table 2 TaqMan assays used for gene expression and copy number variation (CNV) analysis

TaqMan Assays				
	Targets	Assay ID	Type	Company
cDNA target	AHCY	Hs00898137_g1	Gene expression assay	ThermoFisher Scientific
	B2M	Hs00984230_m1	Gene expression assay	ThermoFisher Scientific
	SDHA	Hs00417200_m1	Gene expression assay	ThermoFisher Scientific
gDNA target	AHCY	Hs02422126_cn	CNV assay	ThermoFisher Scientific

the manufacturer's instructions. WES was performed on genomic DNA at the Berlin Institute of Health core facility Genomics, Berlin, Germany. Sequencing libraries were prepared with the SureSelect^{XT} Human All Exon v4 library kit (Agilent, Germany) following the manufacturer's instructions. Cluster Generation was done with the aid of TruSeq PE Cluster Kit v4 (Illumina, USA) and the resulting templates sequenced on an Illumina HiSeq2000 sequencer (at least 150 million reads with a sequencing depth of greater than 160x) using the Illumina HiSeq SBS 250 cycle kit v4.

Data analysis was performed using BWA-MEM [29] to map each whole-exome data set against the reference genome GRCh37. Samblaster [30] was used to mark duplicates. To detect copy number changes, DNA profiles from the respective cell lines were compared (BLUE-1R10 against BLUE-1 K10) with CNVkit [31]. The copy number changes were prioritized according to their log₂ fold-change and custom plots of amplified regions created using CNVkit plotting functions.

CNV analysis was performed on genomic DNA from the respective BLUE-1 cell lines, controls and patient samples by applying the TaqMan copy number assay (assay ID: Hs02422126_cn) to the *AHCY* gene on chromosome 20. The assay covers intron 7 and exon 8 on the reference genome GRCh37 and was performed according to the manufacturer's recommendations. Data

Table 1 List of antibodies

Target Protein	Primary antibody		Company	Clone name / catalogue number
	Application			
	Western blot	Immunohistochemistry		
GAPDH	✓		Cell Signaling Technology	14C10
Histone 3	✓		Cell Signaling Technology	96C10
Cleaved PARP	✓		Cell Signaling Technology	Asp214
AHCY	✓	✓	OriGene	TA332593
Secondary antibody				
Anti-rabbit HRP-conjugated	✓		GE Healthcare	NA934V
Anti-mouse HRP-conjugated	✓		Agilent	P0447

analysis was done using the CopyCaller software version 2.1 (ThermoFisher Scientific, Germany).

OncoScan CNV assay Kit was also used to perform copy number analysis according to standard protocols (Affymetrix) [32]. The Chromosome Analysis Suite 4.0 (ChAS) (ThermoFisher, Germany) software was used to visualize, analyze and summarize the chromosomal aberrations, including gains, losses, and loss of heterozygosity (LOH). The non-FFPE analysis work-flow was applied. Criteria for copy number alterations include chromosomal changes encircling at least 20 informative probes, with a minimum size event of at least 100 kb, with median $\log_2\text{Ratio} \pm 0.3$, and showing a CNN-LOH more than 5 Mb. Individual copy number analysis for each BLUE-1 cell line, as well as, comparative analysis between the three cell lines (BLUE-1, BLUE-1 K10, and BLUE-1R10) was done. In addition, we manually inspected all the aberrations filtered out due to the criteria described above and included only those aberrations showing differences in the B-allele frequency (BAF).

Clonality studies

B-cell clonality studies were performed to determine the immunoglobulin heavy chain (IGH) rearrangements for BLUE-1, BLUE-1 K10 and BLUE-1R10 using a multiplex PCR method developed within the EuroClonality/BIOMED-2 collaborative study, BMH4-CT98–3936 [33] for all three IGH frame work regions. After PCR on the ProFlex PCR Thermocycler (ThermoFisher Scientific, Germany), gel electrophoresis was performed to check the amplification of PCR products. For single base pair resolution, GeneScan analysis (capillary electrophoresis) of the IGH PCR products was performed with the 3500 series Genetic Analyser (ThermoFisher Scientific, Germany). The sizes of the various PCR products were determined using the GeneMapper 4.0 software (ThermoFisher Scientific, Germany).

Immunohistochemistry and fluorescence in situ hybridization (FISH) analysis

Immunohistochemistry (IHC) was performed using sections of formalin-fixed paraffin-embedded (FFPE) cell line blocks as described [34]. The primary antibody used in this case was anti-AHCY antibody (Table 1). FISH was performed on sections of formalin-fixed paraffin-embedded (FFPE) cell line blocks as described [35, 36]. This was carried out using orange-labeled *AHCY* gene-specific probes (product name: AHCY-20-OR) and green-labeled chromosome 20-control (centromeric) probes (product name: CHR20–10-GR) (both purchased from Empire Genomics, USA). DakoCytomation Hybridizer (Dako/Agilent, Germany) was used for FISH probe hybridization, while nuclear counterstaining was

done with the aid of Dako fluorescence mounting medium containing DAPI (Dako/Agilent, Germany). Visualization and analysis (of at least 50 intact nuclei) were performed with the Zeiss Axio Imager Z1 (Zeiss, Germany) and the Isis imaging software version 5.3.1 (Metasystems, Germany).

Cytogenetics, metabolomics and global DNA methylation analysis

Profiling of short tandem repeats (STR) for authentication of the cell lines BLUE-1, BLUE-1 K10 and BLUE-1R10 using the StemElite kit (Promega) was performed as previously described [32]. Conventional cytogenetic analysis was performed as reported [37] and the karyotypes were described according to ISCN guidelines (2013).

The intermediates of methionine and polyamine metabolism in BLUE-1, BLUE-1 K12 and BLUE-1R12 cell extracts were measured by liquid chromatography-tandem mass spectrometry following an established protocol [38]. Genome-wide DNA methylation analysis was done on BLUE-1, BLUE-1 K10 and BLUE-1R10 using the Infinium MethylationEPIC BeadChip (Illumina, USA) as described [39]. Copy number plots were generated from the raw output data (*.idat* files) using the 'conumee' R package in Bioconductor [39, 40].

Statistical analysis

Statistical analysis was done using the GraphPad Prism 5 software (GraphPad Software, California, USA). Statistical significance was evaluated using the Mann-Whitney U test (two-tailed) for pairwise comparisons, and one-way ANOVA with the Tukey post-hoc test for group comparisons. *p* values less than 0.05 were considered significant.

Results

Generation and characterization of a DZNep-resistant cell line clone

We generated a DZNep-resistant clone by subjecting the DZNep-sensitive Burkitt lymphoma cell line BLUE-1 [20] to progressively increasing concentrations of DZNep for up to 7 months (Fig. 1a and Methods section). Analyses were performed with the resistant BLUE-1 subclones (BLUE-1R10 or BLUE-1R12) and their respective controls. To analyze the response of the generated DZNep-resistant clone to DZNep, we treated the clone and its corresponding control with 5 μM DZNep for 72 h and then measured the percentage of apoptotic cells. The control cell line, BLUE-1 K10, exhibited strong apoptosis with about 50% apoptotic cells in comparison to the resistant BLUE-1R10 clone, which displayed only about 10% apoptotic cells following treatment with DZNep (Fig. 1b). Furthermore, Western blot analysis

performed on total protein lysate obtained after treatment of both cell lines with 2 μ M and 5 μ M DZNep revealed an increase in the expression of cleaved PARP, indicating apoptosis in the DZNep-treated cells of BLUE-1 K10 in relation to BLUE-1R10 (Fig. 1b). The doubling time of the DZNep-resistant clone BLUE-1R10 was also compared with that of the corresponding control BLUE-1 K10 and the parent cell line BLUE-1. This revealed that both BLUE-1R10 and BLUE-1 K10 had shorter doubling times than BLUE-1 (Fig. 1c).

To determine the identity of the generated clone, we explored the STR profile and determined the clonality of BLUE-1R10. The results were then compared with those of its corresponding control BLUE-1 K10 and the parent cell line BLUE-1. The STR profile analysis for the three cell lines when compared with the DSMZ STR profiling database revealed an STR profile of a BLUE-1 cell line, confirming their authenticity. Furthermore, the IGH chain gene rearrangement patterns for the three cell lines were identical (Additional file 1: Figure S1). We also performed genomic characterization of the cell lines using conventional cytogenetics and copy number analysis by OncoScan CNV assay. Only minor differences in the karyotype were observed upon analysis of the three cell lines (Additional file 2: Figure S2). Upon further examination the copy number data, we detected genomic aberrations exclusive to each of the three BLUE-1 cell lines (Additional file 5: Table S1). We detected three abnormalities only present in BLUE-1R10 as compared to the parental BLUE-1 and BLUE-1 K10 cell lines. These include one loss in 4q12q12, one high copy gain in 6q14.3q14.3, and one LOH in 20p12.2p13. Moreover, we observed aberrations solely in the parental BLUE-1 cell line, including gains in 6p22.1p25.3, 19p13.11p13.3, and 19p13.11q13.43, which may have been lost due to prolonged culture conditions. We also distinguished common copy number aberrations in BLUE-1 and BLUE-1R10 cell lines, but not shown in the BLUE-1 K10 (Additional file 5: Table S1).

Identification of biomarkers for resistance to DZNep

To probe the underlying mechanism of resistance of BLUE-1R10 to DZNep, we performed WES of genomic DNA obtained from BLUE-1R10 and its corresponding control BLUE-1 K10. Additional copy number variant analysis was performed on the WES data using the software tool CNVkit. This analysis identified a small focal, approximately 30-fold copy number gain in the region spanning the *AHCY* gene and the proximal part of the *ITCH* gene on chromosome 20 (Fig. 2a). Upon manual inspection of this specific genomic region in the OncoScan data, we confirmed the presence of this high copy number gain including the *AHCY* gene (Additional file 3: Figure S3). It was not called in the initial analysis due

to applied detection criteria for the analysis which filtered the amplicon out due to its small genomic size and low marker content (see material and method sections for more details).

We validated this *AHCY* gain on the DNA level using two methods. First, we used the TaqMan Copy Number Assay to analyze DNA obtained from cryostocks collected at the various time-points during the generation of the resistant clone, including BLUE-1 as the reference cell line. We noted a clear copy number gain in *AHCY* beginning with BLUE-1R6 (preserved after almost 5 months of treatment with DZNep) and increasing thereafter (Fig. 2b). The *AHCY* copy number gain was further confirmed by a CNV analysis using global DNA-methylation data from BLUE-1R10, and comparing it with data from BLUE-1 K10 and BLUE-1. Here, the gain in *AHCY* copy number on chromosome 20 was also obvious in the resistant clone in comparison to the respective control and the parent cell line (Fig. 2c).

AHCY copy number gain at the chromosomal and transcriptional level

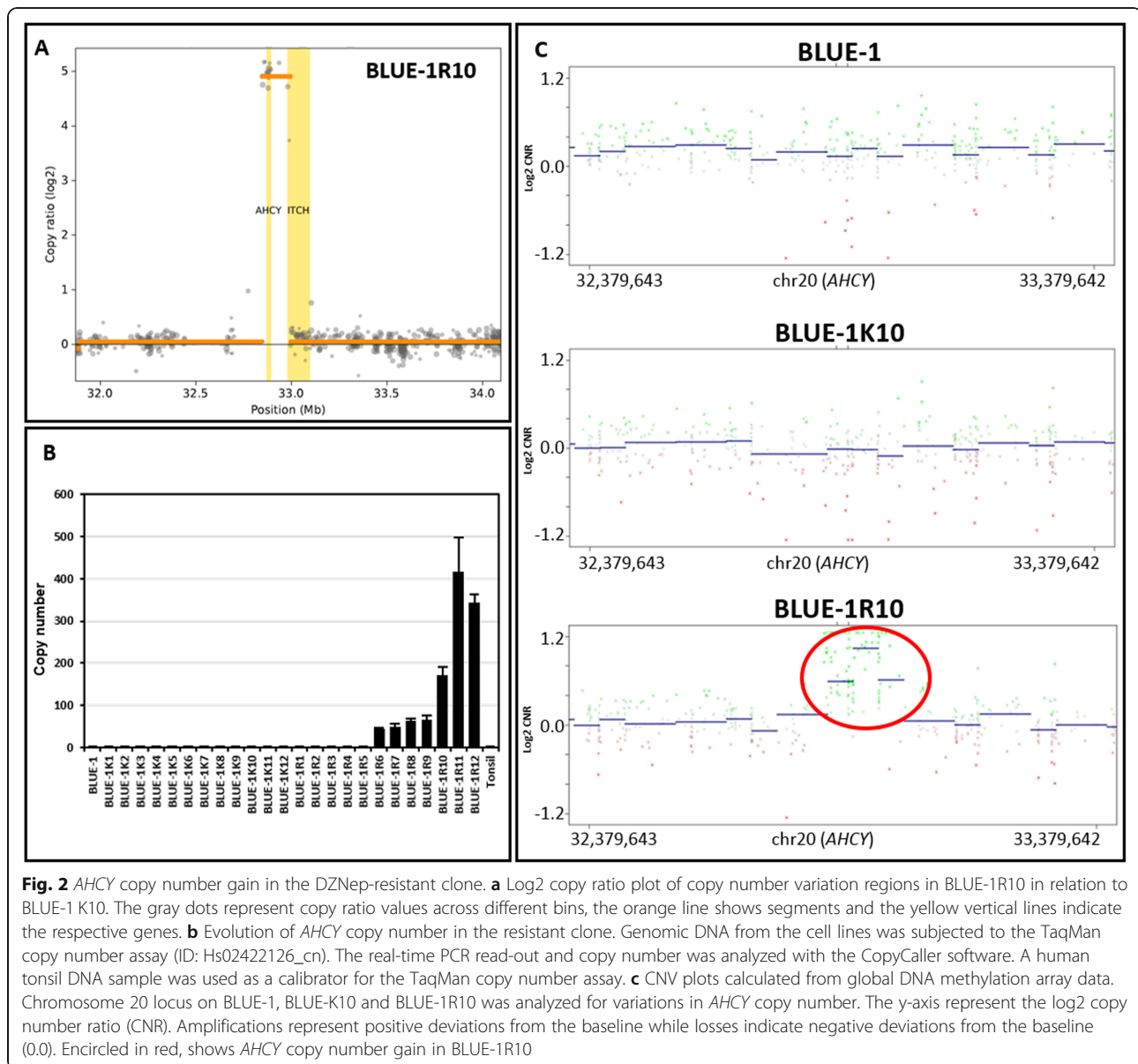
On the chromosomal level, we confirmed *AHCY* amplification in BLUE-1R10 and BLUE-1R12, by performing a FISH study using target-specific probes for *AHCY* on chromosome 20q11.22. Our FISH data (Fig. 3a) revealed cluster-type amplification and large *AHCY*-gene clusters in form of dense clouds of labeled regions suggestive for hsr-regions in cells of BLUE-1R10, when compared with its control BLUE-1 K10 and BLUE-1.

To ascertain the expression of *AHCY*, we performed a real-time PCR using the TaqMan gene expression assay on cDNA from the resistant clone, the respective controls and the parent cell line BLUE-1. The results display overexpression of *AHCY* in the resistant clone BLUE-1R10 and a further increase in BLUE-1R12 (Fig. 3b).

AHCY gain at the protein level and metabolomics studies

AHCY expression at the protein level was determined using two different methods, IHC and Western blot. The IHC results show increased *AHCY* expression in the resistant clone in comparison to its control and the parent cell line (Fig. 4a). The Western blot result (Fig. 4b) confirmed that *AHCY* is overexpressed in BLUE-1R10, with a higher expression in BLUE-1R12. The respective controls and parent BLUE-1 cell line had a similar level of *AHCY* expressed.

To understand the dynamics of the concentrations of methionine intermediates in the resistant clone, its control and the parent cell line, we employed a high performance liquid chromatography-tandem mass spectrometry method. We notice a similar distribution pattern for *S*-adenosyl-L-homocysteine (SAH), adenine and adenosine in BLUE-1 and the control cell line



BLUE-1 K12. The resistant clone (BLUE-1R12), however, displayed a significant increase ($p < 0.05$) in the level of both adenine and adenosine in comparison to its control BLUE-1 K12 (Fig. 4c).

AHCY copy number gain in primary lymphoma samples

We examined the frequency of *AHCY* copy number gains in a small series of B-cell lymphomas by examining 12 primary lymphoma samples consisting of Burkitt lymphoma, diffuse large B-cell lymphoma, follicular lymphoma, primary mediastinal B-cell lymphoma and anaplastic large cell lymphoma. We performed the TaqMan CNV assay using genomic DNA isolated from these samples. Subsequent analysis of the *AHCY* copy number with the CopyCaller software revealed a predicted *AHCY* copy number

of 2 for all but one sample, which had a predicted copy number of 1 (Additional file 4: Figure S4). In addition, we checked the frequency of *AHCY* copy number alterations in B-cell lymphoma by analyzing published genomic data from 1295 B-cell lymphoma samples curated from 5 different studies on the cBio Cancer Genomics Portal [41, 42] but no *AHCY* genomic alterations were detected.

Discussion

Acquired resistance to small molecule inhibitors used in cancer treatment remains a huge problem in cancer therapy. Although many cancer types respond to initial therapy, there is the uncertainty of resistance arising against the utilized drug [43]. Various molecular

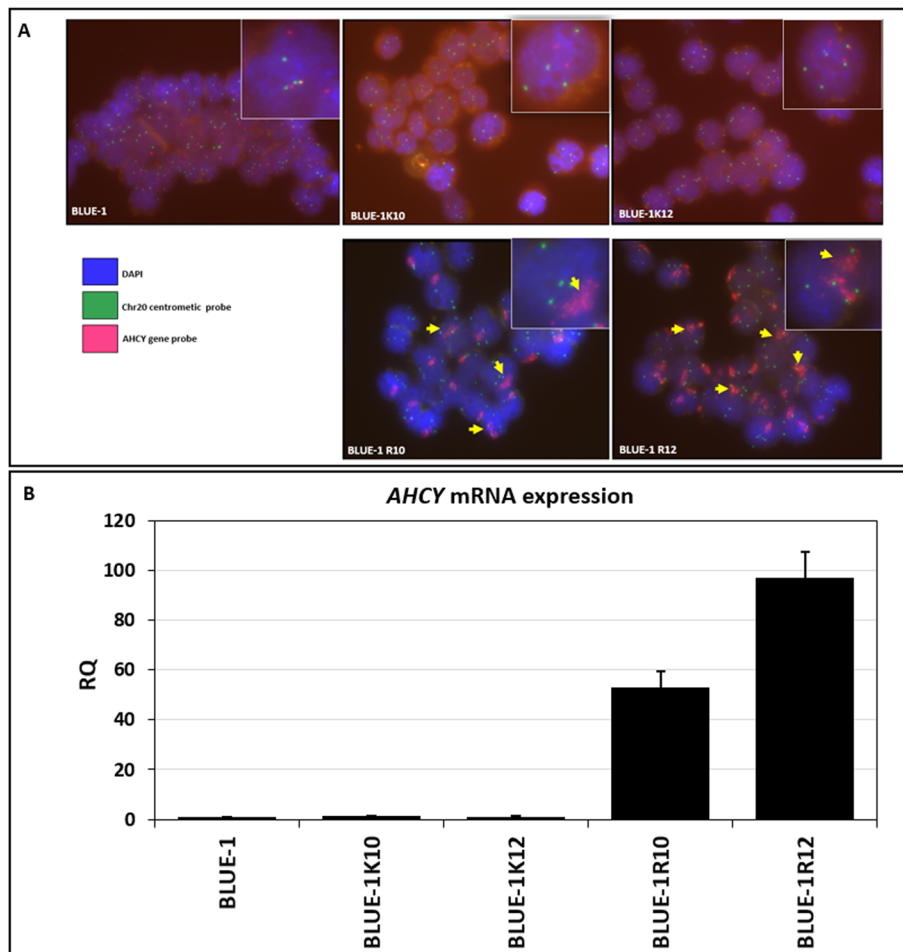
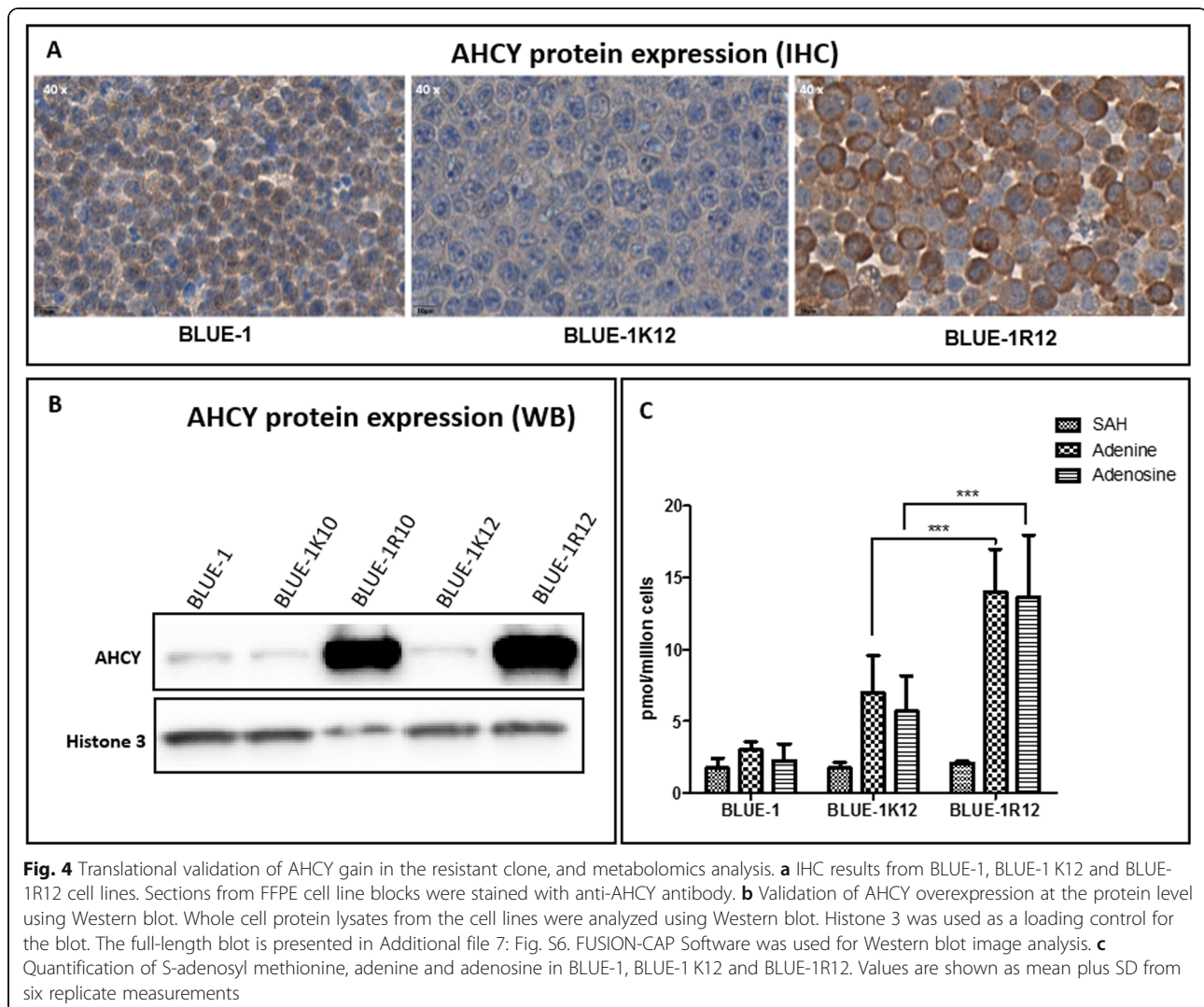


Fig. 3 *AHCY* copy number gain in the DZNep-resistant clone: chromosomal and transcriptional validation. **a** FISH analysis using *AHCY* target-specific probes in the resistant clone and its control. Yellow arrows show in pink color a cluster-type amplification of *AHCY*. Green dots represent the centromere of chromosome 20. **b** Transcriptional expression of *AHCY*. cDNA was synthesized from the RNA of all cell lines. Relative gene expression (shown on the y-axis) was quantified using the *AHCY* gene expression assay, with B2M and SDHA used as an endogenous control. RQ is shown as mean plus SD of triplicate measurements

mechanisms are involved in the resistance of tumor cells to therapy [44–46]. DZNep - an indirect EZH2 inhibitor - is known to be efficacious against many different types of cancer and, hence, may make its way into clinical trials. Already, genetic determinants of sensitivity to DZNep-mediated apoptosis have been described for gastric cancer and multiple myeloma tumor cells respectively [47, 48]. In this study, we aimed to investigate the molecular mechanism underlying acquired resistance to DZNep in B-cell lymphoma, and to identify biomarkers predictive of the therapeutic success of EZH2 inhibition with DZNep. To achieve this, we generated and investigated a DZNep-resistant clone. The continued resistance of the clone (BLUE-1R10) to DZNep following treatment with DZNep as well as upon cultivation in a DZNep-free medium implies that a permanent change has occurred on the genomic level in this clone. We analyzed the

proliferation rate of BLUE-1R10, comparing its doubling time with that of BLUE-1 K10 and BLUE-1. The shorter doubling time observed in the resistant clone and its control in relation to the parent cell line is in contrast to a previous report of an increased doubling time in two colon cancer cell lines that acquired drug resistance upon prolonged cultivation with irinotecan [49]. Since the reduction in doubling time was also observed in the control cell line BLUE-1 K10, the increased growth rate of both BLUE-1R10 and BLUE-1 K10 cannot be attributed to the effect of DZNep on the cells. Perhaps, some changes in genes responsible for cell cycle regulation and proliferation could have occurred during the long-term cultivation of the clone and its control. This is not surprising because, we already know the extent of genetic and transcriptional heterogeneity that occur in cell lines during evolution [50]. Besides, in other cell types



such as human embryonic stem cells, the effect of prolonged cultivation on the proliferative capacity is evident as an increase in the proliferative capacity of these cells [51].

It was crucial to confirm the identity of the DZNep-resistant clone to ensure that it certainly originated from the parent cell line BLUE-1. To achieve this, the STR profile and clonality of BLUE-1R10 was explored together with that of BLUE-1 K10 and BLUE-1. The identical STR profile and IGH chain gene rearrangement patterns indicate that both cell lines indeed originate from the same parent. Nevertheless, the differences observed between BLUE-1, BLUE-1 K10 and BLUE-1R10 upon genomic interrogation using the OncoScan CNV assay could suggest a divergent genomic evolution between BLUE-1 K10 and BLUE-1R10 cell lines in culture.

Since AHCY is a direct target of DZNep-mediated EZH2 inhibition, we focused on validating the identified AHCY gain in the resistant clone. Using the TaqMan

Copy Number Assay, which measures gene copy numbers by incorporating the TaqMan copy number assay with the TaqMan copy number reference assay in a single real-time PCR run, validation of AHCY amplification was achieved on the DNA level. The progressive increase in the AHCY copy number observed from BLUE-1R6 confirms that the gain in copy number is continual in the DZNep-resistant clone. It is noteworthy that at the point of DZNep withdrawal from the clone (from BLUE-1R9 to BLUE-1R10), there was an almost two-fold increase in the AHCY copy number. This copy number gain doubled following continuous cultivation of the clone in a DZNep-free medium (from BLUE-1R10 to BLUE-1R11 and BLUE-1R12). This implies that the AHCY copy number gain, once initiated, does not require DZNep pressure to persist. Although this copy number event may reflect a sort of genomic compensation in the resistant clone due to prolonged AHCY inhibition, it is unlikely that this genomic aberration

would decrease to baseline levels upon prolonged withdrawal of DZNep pressure.

Moreover, the FISH data which revealed that the *AHCY* amplification was more pronounced in BLUE-1R12 in comparison to BLUE-1R10 further affirms the persistence of *AHCY* copy number gain. The chromosome 20 polysomy observed in the cells of each cell line may reflect the level of genomic instability usually occurring in cancer cells [52, 53]. The overexpression of *AHCY* on the transcriptional and protein level in the DZNep-resistant clone is consistent with the knowledge of drug resistance in cancer stemming from alterations in the drug target, particularly, alterations involving modified enzyme expression [46, 54]. Alterations in the apoptotic machinery did not appear to be involved in the resistance of the resistant clone to apoptosis based on its RNA expression profile.

The results of our metabolomics studies which revealed an analogous distribution for SAH, adenine and adenosine in both BLUE-1 and BLUE-1 K12 signifies that following long-term culture of BLUE-1, there is no peculiar alteration of the balance exerted by these intermediates within the cell. The increase in adenine and adenosine levels of the resistant clone (BLUE-1R12) when compared to BLUE-1 K12 is in line with the increased expression of *AHCY*, which catalyzes the hydrolysis of SAH to adenosine and L-homocysteine.

Previous works have linked copy number gains on chromosome 20q with the pathogenesis of tumors such as colon cancer [55], colorectal cancer [56], and cervical cancer [57], with significant gains of the *AHCY* gene among others. However, little is known about the role of *AHCY* copy number gain in driving B-cell lymphomas. For this reason, we analyzed the *AHCY* copy number of 12 primary lymphoma samples using the TaqMan CNV assay. The absence of *AHCY* copy number gain in the patient samples analyzed implies that it is unlikely that *AHCY* copy number gains play a driving role in B-cell lymphoma pathogenesis. In addition, the absence of *AHCY* copy number alterations from in silico studies signifies that alterations in *AHCY* are rare in primary B-cell lymphoma however, in solid tumors, the frequency of *AHCY* amplification can be as high as 20% [41, 42].

Conclusion

Acquired drug resistance poses a great challenge in cancer therapy. It is important to recognize mechanisms of resistance for novel drugs about to enter clinical trials so that one can monitor for early signs of development of drug resistance. DZNep is a promising epigenetic drug that is in the pre-clinical phase of clinical approval, but has shown promising effects for selected cancer patients. We show that copy number gain of *AHCY* is one possible mechanism of acquired resistance to DZNep-

mediated apoptosis and propose *AHCY* as a potential biomarker to stratify patients during the use of DZNep. Although *AHCY* alterations are rare in primary B-cell lymphomas, it may still be important to screen for modifications of this gene in patients prior to the initiation of EZH2 based therapy with DZNep. These findings might be valuable in predicting patients, who will benefit from EZH2 inhibition using DZNep once it progresses into clinical studies.

Supplementary information

Supplementary information accompanies this paper at <https://doi.org/10.1186/s12885-020-06937-8>.

Additional file 1: Figure S1. Confirmation of the identical B-cell clonality of BLUE-1K10 and BLUE-1R10.

Additional file 2: Figure S2. Karyotypes of the cell lines BLUE-1, BLUE-1R10 and BLUE-1K10.

Additional file 3: Figure S3. OncoScan Copy number analysis in the of BLUE-1 cell lines.

Additional file 4: Figure S4. Analysis of *AHCY* copy number in primary lymphoma samples.

Additional file 5: Table S1. Comparative copy number analysis in the BLUE-1 cell lines as determined by OncoScan assay.

Additional file 6: Figure S5. Full-length blot for Western blot image presented in Fig. 1.

Additional file 7: Figure S6. Full-length blot for Western blot image presented in Fig. 4.

Abbreviations

AHCY: S-adenosyl-L-homocysteine hydrolase; B2M: Beta 2 microglobulin; BAF: B-allele frequency; ChAS: Chromosome analysis suite; CN-LOH: Copy neutral loss of heterozygosity; CNR: Copy number ratio; CNV: Copy number variation; DZNep: 3-Deazaneplanocin A; DSMZ: German Collection of Microorganisms and Cell Cultures; EZH2: Enhancer of zeste homolog 2; FFPE: Formalin-fixed paraffin-embedded; FISH: Fluorescence in situ hybridization; H3K27me3: Lysine 27 trimethylation on histone 3; IGH: Immunoglobulin heavy chain; IHC: Immunohistochemistry; LOH: Loss of heterozygosity; RT-PCR: Reverse transcriptase polymerase chain reaction; SAH: S-adenosyl-L-homocysteine; SDHA: Succinate dehydrogenase; STR: Short tandem repeat; WES: Whole exome sequencing

Acknowledgements

We thank Anke Sommerfeld, Edda von der Wall, Erika Berg, Lisa Ellmann and the team of the tumor genetics group of the Institute of Human Genetics in Ulm for their technical support. We also appreciate Dr. Elena Myelona and Prof. Claudia Baldus for their constructive advice during this work.

Authors' contributions

CAA, KK, LD, MH took part in study conceptualization and design, CAA, KK, EO, NT, KD, DL performed data curation. Data analysis and interpretation was carried out by CAA, KK, CM, CL, RW, KO, AS, DC, RS, LD and MH. CAA, PJO, DB, RS, DC and MH acquired funding and resources. KK, RS, LD and MH supervised the project. CAA wrote the manuscript, and CAA, KK, CM, CL, RW, KO, KD, AS, PJO, DB, RS, DC and MH edited the manuscript. All authors read and approved the final manuscript.

Funding

This work, including personnel funding and acquisition of materials and reagents was supported by the Berlin School of Integrative Oncology (BSIO), Berlin, Germany. Infrastructural support by the KinderKrebsInitiative Buchholz Holm-Seppensen to the Institute of Human Genetics in Ulm is gratefully acknowledged.

Availability of data and materials

The datasets supporting the conclusions of this article are included within the article and its additional files.

Ethics approval and consent to participate

Permission for the use of human primary samples was granted by the Institutional Review Board Charité – Berlin (EA4/104/11).

Consent for publication

Not applicable.

Competing interests

MH is a member of the editorial board (Associate Editor) of BMC cancer journal. All other authors declare that they have no competing interests.

Author details

¹Department of Experimental Hematopathology, Institute of Pathology, Charité Medical University, Berlin, Charitéplatz 1, 10117 Berlin, Germany. ²Berlin School of Integrative Oncology, Charité - Medical University of Berlin, Berlin, Germany. ³Berlin Institute of Health, Charité Core Unit Bioinformatics, Berlin, Germany. ⁴Institute of Human Genetics, Ulm University and Ulm University Medical Center, Ulm, Germany. ⁵Institute of Functional Genomics, University of Regensburg, Regensburg, Germany. ⁶Department of Neuropathology, Charité, Medical University of Berlin, corporate member of Free University Berlin, Humboldt-University Berlin, and Berlin Institute of Health, Berlin, Germany. ⁷German Cancer Consortium (DKTK); Partner Site Berlin, German Cancer Research Center (DKFZ), Heidelberg, Germany.

Received: 15 November 2019 Accepted: 7 May 2020

Published online: 14 May 2020

References

- Hu XT, He C. Recent progress in the study of methylated tumor suppressor genes in gastric cancer. *Chin J Cancer*. 2013;32(1):31–41.
- Ghavifekr Fakhri M, Farshdousti Hagh M, Shانهbandi D, Baradaran B. DNA methylation pattern as important epigenetic criterion in cancer. *Genet Res Int*. 2013;2013:317569. <https://doi.org/10.1155/2013/317569>.
- Martin C, Zhang Y. The diverse functions of histone lysine methylation. *Nat Rev Mol Cell Bio*. 2005;6(11):838–49.
- Zhang Y, Reinberg D. Transcription regulation by histone methylation: interplay between different covalent modifications of the core histone tails. *Genes Dev*. 2001;15(18):2343–60.
- Greer EL, Shi Y. Histone methylation: a dynamic mark in health, disease and inheritance. *Nat Rev Genet*. 2012;13(5):343–57.
- Sadakierska-Chudy A, Filip M. A comprehensive view of the epigenetic landscape. Part II: histone post-translational modification, nucleosome level, and chromatin regulation by ncRNAs. *Neurotox Res*. 2015;27(2):172–97.
- Grant PA. A tale of histone modifications. *Genome Biol*. 2001;2:4.
- Barnes CE, English DM, Cowley SM. Acetylation & co: an expanding repertoire of histone acylations regulates chromatin and transcription. *Essays Biochem*. 2019;63(1):97–107.
- Alzrigat M, Jernberg-Wiklund H, Licht JD. Targeting EZH2 in Multiple Myeloma-Multifaceted Anti-Tumor Activity. *Epigenomes*. 2018;2(3):16.
- Wang CX, Liu ZH, Woo CW, Li ZJ, Wang LF, Wei JS, et al. EZH2 mediates epigenetic silencing of neuroblastoma suppressor genes CASZ1, CLU, RUNX3, and NGFR. *Cancer Res*. 2012;72(1):315–24.
- Yamaguchi H, Hung MC. Regulation and role of EZH2 in Cancer. *Cancer Res Treat*. 2014;46(3):209–22.
- Gan L, Yang YN, Li Q, Feng Y, Liu TS, Guo WJ. Epigenetic regulation of cancer progression by EZH2: from biological insights to therapeutic potential. *Biomark Res*. 2018;6.
- Kim KH, Roberts CWM. Targeting EZH2 in cancer. *Nat Med*. 2016;22(2):128–34.
- Marchesi I, Bagella L. Targeting enhancer of Zeste homolog 2 as a promising strategy for cancer treatment. *World J Clin Oncol*. 2016;7(2):135–48.
- Tan J, Yang XJ, Zhuang L, Jiang X, Chen W, Lee PL, et al. Pharmacologic disruption of polycomb-repressive complex 2-mediated gene repression selectively induces apoptosis in cancer cells. *Genes Dev*. 2007;21(9):1050–63.
- Fiskus W, Wang YC, Sreekumar A, Buckley KM, Shi HD, Jillella A, et al. Combined epigenetic therapy with the histone methyltransferase EZH2 inhibitor 3-deazaneplanocin a and the histone deacetylase inhibitor panobinostat against human AML cells. *Blood*. 2009;114(13):2733–43.
- Zhou J, Bi C, Cheong LL, Mahara S, Liu SC, Tay KG, et al. The histone methyltransferase inhibitor, DZNep, up-regulates TXNIP, increases ROS production, and targets leukemia cells in AML. *Blood*. 2011;118(10):2830–9.
- Fiskus W, Rao R, Balusu R, Ganguly S, Tao J, Sotomayor E, et al. Superior efficacy of a combined epigenetic therapy against human mantle cell lymphoma cells. *Clin Cancer Res*. 2012;18(22):6227–38.
- Crea F, Hurt EM, Mathews LA, Cabarcas SM, Sun L, Marquez VE, et al. Pharmacologic disruption of Polycomb repressive complex 2 inhibits tumorigenicity and tumor progression in prostate cancer. *Mol Cancer*. 2011;10.
- Akpa CA, Kleo K, Lenze D, Oker E, Dimitrova L, Hummel M. DZNep-mediated apoptosis in B-cell lymphoma is independent of the lymphoma type, EZH2 mutation status and MYC, BCL2 or BCL6 translocations. *PLoS One*. 2019;14(8):e0220681.
- Girard N, Bazille C, Lhuissier E, Benateau H, Llobart-Bosch A, Boumediene K, et al. 3-Deazaneplanocin A (DZNep), an Inhibitor of the Histone Methyltransferase EZH2, Induces Apoptosis and Reduces Cell Migration in Chondrosarcoma Cells. *Plos One*. 2014;9:5.
- Miranda TB, Cortez CC, Yoo CB, Liang GN, Abe M, Kelly TK, et al. DZNep is a global histone methylation inhibitor that reactivates developmental genes not silenced by DNA methylation. *Mol Cancer Ther*. 2009;8(6):1579–88.
- Beluzic L, Grbesa I, Beluzic R, Park JH, Kong HK, Kopjar N, et al. Knock-down of AHCY and depletion of adenosine induces DNA damage and cell cycle arrest. *Sci Rep*. 2018;8(1):14012.
- Park SJ, Kong HK, Kim YS, Lee YS, Park JH. Inhibition of S-adenosylhomocysteine hydrolase decreases cell mobility and cell proliferation through cell cycle arrest. *Am J Cancer Res*. 2015;5(7):2127–38.
- Kim JH, Kim JH, Kim SC, Yi YS, Yang WS, Yang Y, et al. Adenosine dialdehyde suppresses MMP-9-mediated invasion of cancer cells by blocking the Ras/Raf-1/ERK/AP-1 signaling pathway. *Biochem Pharmacol*. 2013;86(9):1285–300.
- Li QH, Mao LH, Wang RL, Zhu LQ, Xue LX. Overexpression of S-adenosylhomocysteine hydrolase (SAHH) in esophageal squamous cell carcinoma (ESCC) cell lines: effects on apoptosis, migration and adhesion of cells. *Mol Biol Rep*. 2014;41(4):2409–17.
- Martinez-Climent JA, Alizadeh AA, Segraves R, Blesa D, Rubio-Moscardo F, Albertson DG, et al. Transformation of follicular lymphoma to diffuse large cell lymphoma is associated with a heterogeneous set of DNA copy number and gene expression alterations. *Blood*. 2003;101(8):3109–17.
- Bookout AL, Mangelsdorf DJ. Quantitative real-time PCR protocol for analysis of nuclear receptor signaling pathways. *Nucl Recept Signal*. 2003;1:e012.
- Li H. Aligning sequence reads, clone sequences and assembly contigs with BWA-MEM. *arXiv.org > q-bio > arXiv:13033997v2*; 2013.
- Faust GG, Hall IM. SAMBLASTER: fast duplicate marking and structural variant read extraction. *Bioinformatics*. 2014;30(17):2503–5.
- Talevich E, Shain AH, Botton T, Bastian BC. CNVkit: genome-wide copy number detection and visualization from targeted DNA sequencing. *PLoS Comput Biol*. 2016;12(4):e1004873.
- Wagener R, Lopez C, Kleinheinz K, Bausinger J, Aukema SM, Nagel I, et al. IG-MYC-positive neoplasms with precursor B-cell phenotype are molecularly distinct from Burkitt lymphomas. *Blood*. 2018;132:2280.
- van Dongen JJM, Langerak AW, Bruggemann M, Evans PAS, Hummel M, Lavender FL, et al. Design and standardization of PCR primers and protocols for detection of clonal immunoglobulin and T-cell receptor gene recombinations in suspect lymphoproliferations: report of the BIOMED-2 concerted action BMH4-CT98-3936. *Leukemia*. 2003;17(12):2257–317.
- Kleo K, Dimitrova L, Oker E, Tomaszewski N, Berg E, Taruttis F, et al. Identification of ADGRE5 as discriminating MYC target between Burkitt lymphoma and diffuse large B-cell lymphoma. *BMC Cancer*. 2019;19(1):322.
- Horn H, Ziepert M, Wartenberg M, Staiger AM, Barth TFE, Bernd HW, et al. Different biological risk factors in young poor-prognosis and elderly patients with diffuse large B-cell lymphoma. *Leukemia*. 2015;29(7):1564–70.
- Horn H, Ziepert M, Becher C, Barth TFE, Bernd HW, Feller AC, et al. MYC status in concert with BCL2 and BCL6 expression predicts outcome in diffuse large B-cell lymphoma. *Blood*. 2013;121(12):2253–63.
- Schlegelberger B, Zwingers T, Harder L, Nowotny H, Siebert R, Vesely M, et al. Clinicopathogenetic significance of chromosomal abnormalities in patients with blastic peripheral B-cell lymphoma. *Kiel-Wien-Lymphoma Study Group*. *Blood*. 1999;94(9):3114–20.
- Stevens AP, Dettmer K, Kirovski G, Samejima K, Hellerbrand C, Bosserhoff AK, et al. Quantification of intermediates of the methionine and polyamine

- metabolism by liquid chromatography-tandem mass spectrometry in cultured tumor cells and liver biopsies. *J Chromatogr A*. 2010;1217(19):3282–8.
39. Capper D, Stichel D, Sahm F, Jones DTW, Schrimpf D, Sill M, et al. Practical implementation of DNA methylation and copy-number-based CNS tumor diagnostics: the Heidelberg experience. *Acta Neuropathol*. 2018;136(2):181–210.
 40. Hovestadt V, Zapatka M. Conumee: enhanced copy-number variation analysis using Illumina DNA methylation arrays. R package <http://bioconductor.org/packages/conumee/>.
 41. Cerami E, Gao JJ, Dogrusoz U, Gross BE, Sumer SO, Aksoy BA, et al. The cBio Cancer genomics portal: an open platform for exploring multidimensional Cancer genomics data. *Cancer Discov*. 2012;2(5):401–4.
 42. Gao JJ, Aksoy BA, Dogrusoz U, Dresdner G, Gross B, Sumer SO, et al. Integrative Analysis of Complex Cancer Genomics and Clinical Profiles Using the cBioPortal. *Sci Signal*. 2013;6(269):pl1.
 43. Gottesman MM. Mechanisms of cancer drug resistance. *Annu Rev Med*. 2002;53:615–27.
 44. Pan ST, Li ZL, He ZX, Qiu JX, Zhou SF. Molecular mechanisms for tumour resistance to chemotherapy. *Clin Exp Pharmacol P*. 2016;43(8):723–37.
 45. Iglesias VS, Giuranno L, Dubois LJ, Theys J, Vooijs M. Drug resistance in non-small cell lung Cancer: a potential for NOTCH targeting? *Front Oncol*. 2018;8.
 46. Mansoori B, Mohammadi A, Davudian S, Shirjang S, Baradaran B. The different mechanisms of Cancer drug resistance: a brief review. *Adv Pharm Bull*. 2017;7(3):339–48.
 47. Cheng LL, Itahana Y, Lei ZD, Chia NY, Wu Y, Yu Y, et al. TP53 genomic status regulates sensitivity of gastric cancer cells to the histone methylation inhibitor 3-deazaneplanocin a (DZNep). *Clin Cancer Res*. 2012;18(15):4201–12.
 48. Xie ZG, Bi CL, Cheong LL, Liu SC, Huang GF, Zhou JB, et al. Determinants of Sensitivity to DZNep Induced Apoptosis in Multiple Myeloma Cells. *Plos One*. 2011;6:6.
 49. Petitprez A, Poindessous V, Ouaret D, Regairaz M, Bastian G, Guerin E, et al. Acquired irinotecan resistance is accompanied by stable modifications of cell cycle dynamics independent of MSI status. *Int J Oncol*. 2013;42(5):1644–53.
 50. Ben-David U, Siranosian B, Ha G, Tang H, Oren Y, Hinohara K, et al. Genetic and transcriptional evolution alters cancer cell line drug response. *Nature*. 2018;560(7718):325.
 51. Bin Park Y, Kim YY, Oh SK, Chung SG, Ku SY, Kim SH, et al. Alterations of proliferative and differentiation potentials of human embryonic stem cells during long-term culture. *Exp Mol Med*. 2008;40(1):98–108.
 52. Pikor L, Thu K, Vucic E, Lam W. The detection and implication of genome instability in cancer. *Cancer Metast Rev*. 2013;32(3–4):341–52.
 53. Asatryan AD, Komarova NL. Evolution of genetic instability in heterogeneous tumors. *J Theor Biol*. 2016;396:1–12.
 54. Housman G, Byler S, Heerboth S, Lapinska K, Longacre M, Snyder N, et al. Drug resistance in cancer: an overview. *Cancers (Basel)*. 2014;6(3):1769–92.
 55. Loo LWM, Tiirikainen M, Cheng I, Lum-Jones A, Seifried A, Church JM, et al. Integrated analysis of genome-wide copy number alterations and gene expression in microsatellite stable, CpG island methylator phenotype-negative colon cancer. *Gene Chromosome Canc*. 2013;52(5):450–66.
 56. Hassan NZA, Mokhtar NM, Sin TK, Rose IM, Sagap I, Harun R, et al. Integrated Analysis of Copy Number Variation and Genome-Wide Expression Profiling in Colorectal Cancer Tissues. *Plos One*. 2014;9(4):e92553.
 57. Scotto L, Narayan G, Nandula S, Arias-Pulido H, Subramaniam S, Schneider A, et al. Identification of copy number gain and overexpressed genes on chromosome arm 20q by an integrative genomic approach in cervical cancer: potential role in progression. *Gene Chromosome Canc*. 2008;47(9):755–65.

Publisher's Note

Springer Nature remains neutral with regard to jurisdictional claims in published maps and institutional affiliations.

Ready to submit your research? Choose BMC and benefit from:

- fast, convenient online submission
- thorough peer review by experienced researchers in your field
- rapid publication on acceptance
- support for research data, including large and complex data types
- gold Open Access which fosters wider collaboration and increased citations
- maximum visibility for your research: over 100M website views per year

At BMC, research is always in progress.

Learn more biomedcentral.com/submissions



Druckexemplar der Publikation Dorel et al. 2021

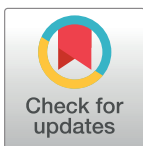
RESEARCH ARTICLE

Neuroblastoma signalling models unveil combination therapies targeting feedback-mediated resistance

Mathurin Dorel^{1,2}, Bertram Klinger^{1,2,5,6}, Tommaso Mari⁸, Joern Toedling³, Eric Blanc⁴, Clemens Messerschmidt⁴, Michal Nadler-Holly⁸, Matthias Ziehm⁸, Anja Sieber^{1,2,5}, Falk Hertwig³, Dieter Beule⁴, Angelika Eggert^{3,5,6,7}, Johannes H. Schulte^{3,5,6,7}, Matthias Selbach⁸, Nils Blüthgen^{1,2,4,6,7*}

1 Institute of Pathology, Charité-Universitätsmedizin Berlin, Berlin, Germany, 2 Integrative Research Institute for the Life Sciences and Institute for Theoretical Biology, Humboldt-Universität zu Berlin, Berlin, Germany, 3 Department of Pediatric, Division of Oncology and Haematology, Charité-Universitätsmedizin Berlin, Berlin, Germany, 4 Berlin Institute of Health, Berlin, Germany, 5 German Cancer Consortium (DKTK), partner site Berlin, Germany, 6 German Cancer Research Center (DKFZ), Heidelberg, Germany, 7 Berlin Institute of Health (BIH), Berlin, Germany, 8 Max Delbrück Center for Molecular Medicine, Berlin, Germany

* nils.bluehgen@charite.de



OPEN ACCESS

Citation: Dorel M, Klinger B, Mari T, Toedling J, Blanc E, Messerschmidt C, et al. (2021) Neuroblastoma signalling models unveil combination therapies targeting feedback-mediated resistance. *PLoS Comput Biol* 17(11): e1009515. <https://doi.org/10.1371/journal.pcbi.1009515>

Editor: Inna Lavrik, OvGU; Medical Faculty, GERMANY

Received: June 7, 2021

Accepted: October 1, 2021

Published: November 4, 2021

Peer Review History: PLOS recognizes the benefits of transparency in the peer review process; therefore, we enable the publication of all of the content of peer review and author responses alongside final, published articles. The editorial history of this article is available here: <https://doi.org/10.1371/journal.pcbi.1009515>

Copyright: © 2021 Dorel et al. This is an open access article distributed under the terms of the [Creative Commons Attribution License](https://creativecommons.org/licenses/by/4.0/), which permits unrestricted use, distribution, and reproduction in any medium, provided the original author and source are credited.

Data Availability Statement: The data and analysis packages are available at these repositories: RNA-Seq data: ENA PRJEB40670 (<https://www.ebi.ac.uk/ena/browser/view/PRJEB40670>) STASNet

Abstract

Very high risk neuroblastoma is characterised by increased MAPK signalling, and targeting MAPK signalling is a promising therapeutic strategy. We used a deeply characterised panel of neuroblastoma cell lines and found that the sensitivity to MEK inhibitors varied drastically between these cell lines. By generating quantitative perturbation data and mathematical modelling, we determined potential resistance mechanisms. We found that negative feedbacks within MAPK signalling and via the IGF receptor mediate re-activation of MAPK signalling upon treatment in resistant cell lines. By using cell-line specific models, we predict that combinations of MEK inhibitors with RAF or IGFR inhibitors can overcome resistance, and tested these predictions experimentally. In addition, phospho-proteomic profiling confirmed the cell-specific feedback effects and synergy of MEK and IGFR targeted treatment. Our study shows that a quantitative understanding of signalling and feedback mechanisms facilitated by models can help to develop and optimise therapeutic strategies. Our findings should be considered for the planning of future clinical trials introducing MEKi in the treatment of neuroblastoma.

Author summary

Only few targeted therapies are currently available to treat high-risk neuroblastoma. To address this issue we characterized the drug response of high risk neuroblastoma cell lines and correlated it with genomic and transcriptomic data. Particularly for MEK inhibition, we saw that our panel could be nicely separated into two groups of resistant and sensitive cell lines. Genomic and transcriptomic markers alone did not help to discriminate between responders and non-responders. We used signalling perturbation data to build

package: GitHub (<https://github.com/molsysbio/STASNet/releases/tag/Dorel2020>)
Phosphoproteomics: https://itbgit.biologie.hu-berlin.de/dorel/phosphoproteomics_tnb_perturbations.

Funding: We acknowledge funding from the Berlin Institute of Health (CRG1 Terminate NB) and from the Federal Ministry of Education and Research /BMBF/ (grant MSTARs, to NB and MS). The funders had no role in study design, data collection and analysis, decision to publish, or preparation of the manuscript.

Competing interests: The authors have declared that no competing interests exist.

cell line specific signalling models. Our models suggest that negative feedbacks within MAPK signalling lead to a stronger reactivation of MEK in MEKi resistant cell lines after MEK inhibition. Model analysis suggested that combining MEK inhibition with IGF1R or RAF inhibition could be an effective treatment and we characterised this combination using phosphoproteomics by mass-spectrometry and growth assays. Our study confirms the importance of quantitative understanding of signalling and may help plan future clinical trials involving MEK inhibition for the treatment of neuroblastoma.

Introduction

Neuroblastoma is the most common and devastating extracranial childhood solid tumour, accounting for 15% of all childhood cancer deaths. The 5-year survival rate is 75% overall, but it is below 45% for so-called high-risk neuroblastoma that represent about 40% of patients [1–3]. Telomere maintenance is a central hallmark of high-risk neuroblastoma [4], and approximately 50% of high-risk neuroblastoma harbour amplification of the MYCN oncogene [5]. Mutations activating the RAS/MAPK signalling pathway are frequent in high-risk and relapsed neuroblastoma [6, 7], with relapsed neuroblastoma being almost always fatal. Most recently, mutations in the p53/MDM2 or RAS/MAPK pathway in the presence of telomere maintenance mechanisms were shown to define a subgroup of ultra-high risk neuroblastoma with a 5-year survival below 20%. Therefore, development of novel therapies for patients with high risk or relapsed neuroblastoma is an urgent clinical need. Mutations of anaplastic lymphoma kinase (ALK), present in 8% of all patients at diagnosis [8, 9], are the most common mutations activating the RAS/MAPK pathway in neuroblastoma. In addition, mutations in PTPN11, NF1, Ras and other RAS/MAPK pathway signalling elements occur in neuroblastoma [7, 10].

This makes RAS/MAPK pathway inhibition a promising treatment option for neuroblastoma, and ALK and MEK inhibitors are already being tested in early clinical trials [11]. However, tumour responses to targeted inhibitors were inconsistent, and early progression pointed towards development of resistance, giving a strong incentive to understand mechanisms of primary and secondary resistance and how to overcome these mechanisms.

Resistance to targeted therapies of signalling pathways are often mediated by feedbacks that re-wire or re-activate signalling. For example, resistance to PI3K/mTOR inhibition in breast cancer is often mediated by feedbacks that lead to activation of JAK/STAT signalling [12]. Similarly, in colon cancer, MAPK-directed therapy is counteracted by a negative feedback that leads to hyper-sensitisation of the EGF receptor and ultimately reactivation of MAPK and AKT signalling [13, 14]. Additionally, a very strong feedback from ERK to RAF leads to reactivation of MAPK signalling upon MEK inhibition in many cancer types [15–17]. One approach to overcome feedback-mediated resistance is by combinatorial therapy that co-targets the feedback [18].

We report here how a more quantitative understanding of feedback mechanisms might help to optimise combinatorial treatment. We used a neuroblastoma cell line panel representing the class of very high-risk neuroblastoma, which we profiled for drug sensitivity, genomic and transcriptomic alterations. We observed strong differences in the sensitivity to MEK inhibition. To arrive at a mechanistic understanding of resistance to MEK inhibition, we generated systematic perturbation data and quantified signalling using data-driven models. By this we described qualitative and quantitative differences in feedback structures that might confer the observed robustness to MEK inhibition. We then identified potential combinations capable of

sensitising highly resistant cell lines to MEK inhibition, and tested these combinations systematically.

Results

Drug sensitivity in a panel of very-high-risk neuroblastoma cell lines

We collected a panel of 9 neuroblastoma cell lines (CHP212, LAN6, NBEB1, SKNAS, NGP, SKNSH, N206, KELLY and IMR32) and performed molecular profiling of these cells (RNA-sequencing and exome sequencing, see Fig 1A and S1 File). We noticed that all cell lines harbour a mutation in at least one of the RAS pathway genes with all cell lines having a mutation in either KRAS, NRAS, NF1, BRAF or ALK. One cell line (IMR32) had two mutations in the pathway: a mutation in KRAS and an atypical BRAF mutation. Most cell lines also have a mutation in one of the p53 pathway genes: ATRX, ATM, ATR, PRKDC, CDKN2A and TP53. Additionally, all express telomerase as seen by TERT expression, except for LAN6 which is known to have an alternative mechanism to lengthen the telomeres (ALT) [4]. We saw strong variability in the expression of MYCN, with 4 cell lines expressing low levels of MYCN, and 5 cell lines displaying high levels of MYCN. When considering mutations of individual genes, we found a strong heterogeneity within our panel, but overall the frequency of mutations in individual genes reflects that of high risk tumours [6]. Taken together, those data indicate that the chosen cell line panel can be seen as representative for the group of very-high risk neuroblastoma.

To further characterise the cell line panel, we measured drug sensitivity for 6 inhibitors that target components of the pathways shown to be affected by mutations (MAPK/PI3K/mTOR), using live cell imaging and computing growth rates from confluency measurements (Fig 1B). In this panel of cell lines, there was no notable difference in the sensitivity to the AKT inhibitor MK2206 or to the RAF/pan-tyrosine kinase-inhibitor Sorafenib. In contrast, pronounced variation in IC₅₀ across the panel can be seen for mTORC1 inhibitor Rapamycin and MEK inhibitor AZD6244. When comparing to published drug sensitivity data, the IC₅₀ for AZD6244 largely correlate with those derived for a different MEK inhibitor (binimetinib) [19]. All 6 NRAS wild type cell lines showed similar sensitivity to Rapamycin while the 3 NRAS mutant cell lines exhibited either strong resistance (SKNSH and SKNAS) or sensitivity (CHP212). This is only partly in agreement with previous literature that described CHP212 but also SKNAS as sensitive to sub-nanomolar concentrations of Everolimus, a Rapamycin analog [20]. AZD6244 is the drug with the most variable drug response, with a subset of 6 cell lines being very resistant to AZD6244 (IC₅₀ >10 μM, Fig 1C and S1 Fig) and another subset of 3 cell lines showing extreme sensitivity (IC₅₀ ≈ 10–100 nM). When correlating inhibitor sensitivity with mutations, we found no notable correlation for AZD6244 and Rapamycin (S2 Fig). Drug sensitivities also did not correlate significantly with selected expression data (adjusted p > 0.93 for the 1000 most variable genes and adjusted p > 0.94 for GO signal transduction genes, S3 Fig). Also a PCA analysis could not separate cells according to MEKi sensitivity for those two expression groups (S4 and S5 Figs). For instance, previous reports showed that NF1 expression is linked to sensitivity to MEK inhibitors [19], however we only found a weak and non-significant correlation with AZD6244 sensitivity ($R^2 = 0.34$, $p = 0.10$, S6 Fig). Taken together, this data establishes that this cell line panel represents a heterogeneous group of very high risk neuroblastoma that differ in drug sensitivity, most prominently against MEK inhibitors. Furthermore, it suggests that the difference cannot be explained by single mutations or expression of marker genes alone.

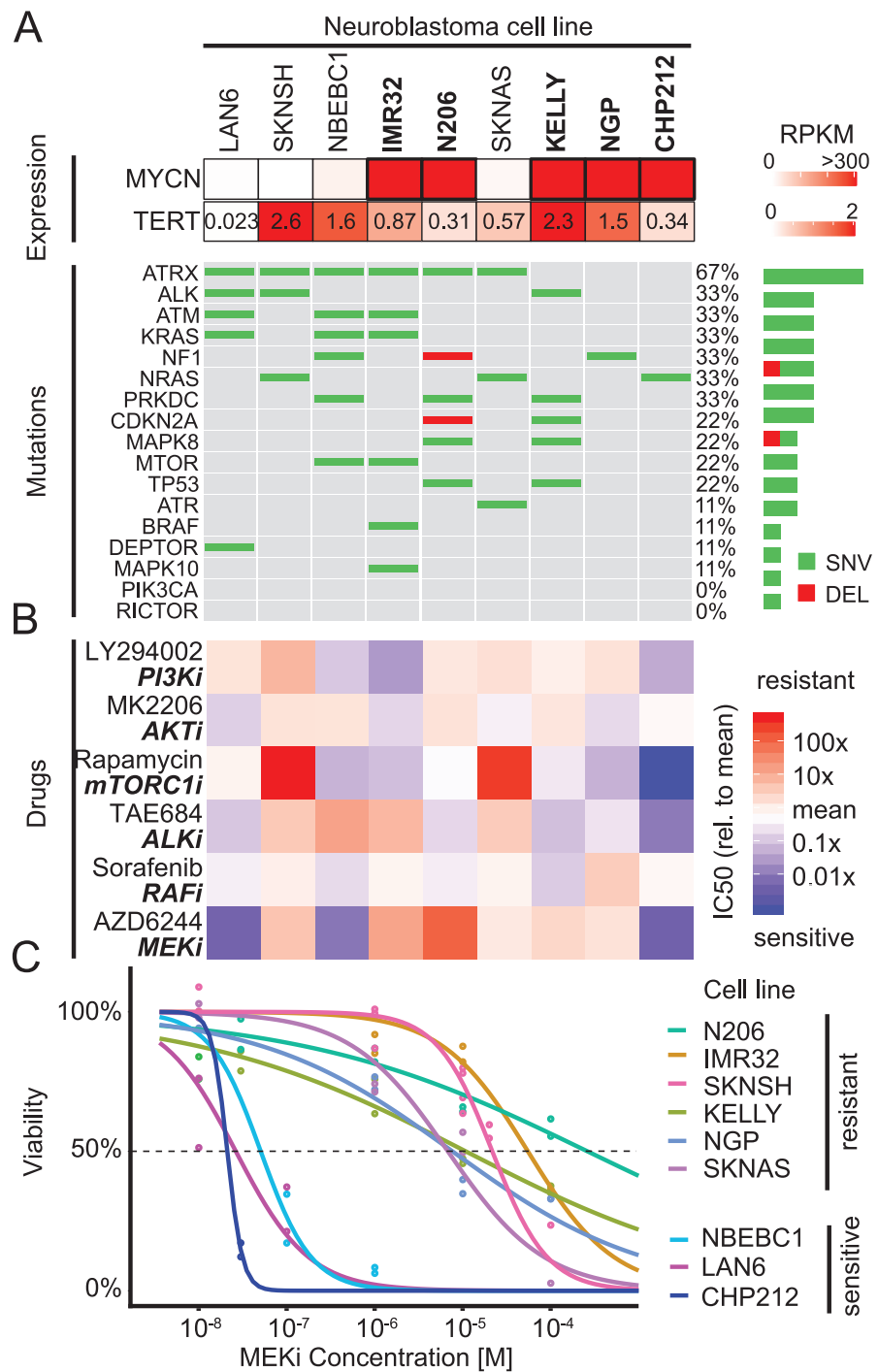


Fig 1. Mutations are insufficient to explain sensitivity variations to RAS/PI3K drugs in neuroblastoma cell line panel. Panel A: Oncoprint of 9 neuroblastoma cell lines for RAS/p53/PI3K related genes along with MYCN and TERT mRNA expression. Bold font indicates MYCN-amplified cell lines. B: Relative IC50 of the same 9 neuroblastoma cell lines as in A for drugs targeting the PI3K and MAPK pathways (n = 2). C: Viability concentration curves for the MEKi inhibitor AZD6244 on the neuroblastoma cell line panel along with the calculated IC50 (intersection with dotted line). Points represent measurements (n = 2).

<https://doi.org/10.1371/journal.pcbi.1009515.g001>

Perturbation-response data unveils heterogeneity in signalling

To get insights into the underlying mechanisms of resistance to the MEK inhibitor AZD6244, we selected 6 neuroblastoma cell lines that represented the spectrum of sensitivity to MEK inhibition (sensitive: CHP212, LAN6; resistant: SKNAS, SKNSH, KELLY and IMR32). Using these cell lines, we performed perturbation experiments, in which we stimulated the cells by growth factors for 30 minutes, and additionally inhibited specific pathways for 90 minutes (Fig 2A). After perturbation, we then monitored pathway activity by measuring phosphoproteins.

We designed the experiments such that they probe the AKT/mTOR and MAPK signalling pathways (Fig 2B). Specifically, we selected ligands that might activate those pathways based on the expression of growth factor receptors in the cell lines. As expression of receptors was heterogeneous (S7 and S8 Figs), we chose a set of growth factors such that each cell line had robust expression of receptors for at least two provided ligands. Inhibitors were chosen such that they block key steps of the pathway. The position of perturbations and readouts in the signalling network is shown in Fig 2B. We perturbed the 6 cell lines with 4 ligands (PDGF, EGF, IGF1 and NGF, shown in blue) and 7 inhibitors (GS4997 (ASK1i), MK2206 (AKTi), Rapamycin (mTORC1i), AZD6244/Selumetinib (MEKi), Sorafenib (RAFi), TAE684 (ALKi) and GDC0941 (PI3Ki), shown in red) alone or in combinations. Subsequently, we measured 6 phosphoproteins (MEK, ERK, AKT, S6K, p38 and cJUN, yellow background) for each perturbation using a sandwich ELISA where a first bead-bound antibody captures the protein and a second recognises the phosphosite of interest. All experiments were performed in two biological replicates.

Overall, the perturbation experiments yielded 240 data points per cell line, which are visualised in a heatmap in Fig 2C. Inspection of the heatmap shows that the perturbation-response data has similar patterns in different cell lines, but there are also clear differences. For instance, inhibition of mTOR leads to down-regulation of phospho-S6K across all cell lines, but inhibition of AKT and PI3K has diverging effects on S6K. Similarly, application of MEKi leads to an increase of phospho-MEK across all cell lines, but ALK inhibition had varying effects in different cell lines.

To get further insights into this high-dimensional data set, we performed principal component analysis (PCA) on the perturbation data (Fig 2D top and S9 Fig). The PCA highlights 3 groups of cell lines. The first component (42% of variance) separates the cell lines according to the effect of Sorafenib and TAE684 on AKT and S6K. The second component (26%) separates IMR32 and KELLY based mainly on the MEK response to MEK inhibition. The third component (18%) contains the effects of IGF1, GS4997 and Rapamycin on AKT and S6K and mainly separates KELLY and IMR32 (S10 Fig).

When we applied hierarchical clustering on the cell line panel, SKNSH was clustered separately, suggesting that it has a very atypical response to the perturbations, with a generally very high response to all ligands, and an especially strong response to PDGF (Fig 2D bottom). This atypical status of SKNSH is also present in the mRNA expression, with a PCA on the most variable genes or on the genes in the GO term “signal transduction” separating it from the other cell lines. Interestingly, CHP212 also separated from the other cell lines in a PCA based on gene expression data, but not when considering the response to the perturbations. When grouping cells by MEK inhibitor sensitivity, we noticed that simple multivariate analysis by PCA does not separate cells into groups that correspond to sensitive or resistant cells (Fig 2D top and S9 Fig), and also hierarchical clustering does not separate sensitive from resistance cell lines (Fig 2D bottom).

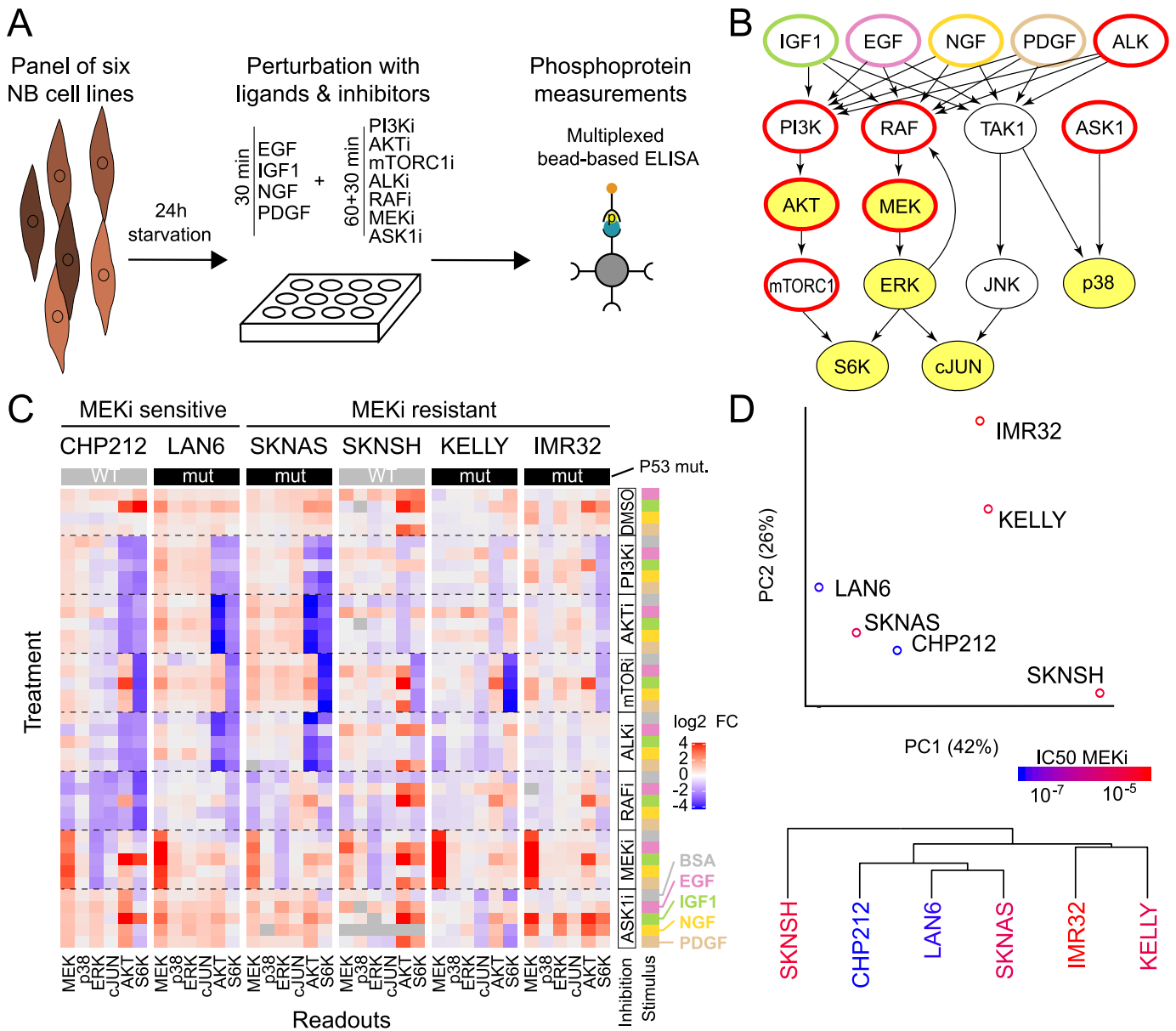


Fig 2. Neuroblastoma cell lines show heterogeneous responses to signalling perturbations. A: Outline of the perturbation experiments. A panel of cell lines was treated with growth factors and small molecule inhibitors, and the resulting effect on selected phosphoproteins was measured using multiplexed bead-based ELISAs. B: Graphical representation of the perturbation scheme on a literature signalling network. Blue and red contour highlights ligand stimulation and kinase inhibition, respectively; yellow filling shows measured phosphoproteins. C: Perturbation data obtained from applying all combinations of 4 ligands or BSA control and 7 inhibitors or DMSO control to 6 neuroblastoma cell lines. Each measurement is normalised by the BSA+DMSO control of the corresponding cell line and represents at least 2 biological replicates. Readouts are phospho-proteins p-MEK1^{S217/S221}, p-p38^{T180/Y182}, p-ERK1^{T202/Y204}, p-cJUN^{S63}, p-AKT^{S473} and p-S6K^{T389}. D: Global non-mechanistic analysis of the perturbation data presented in C: TOP first two components of a principal component analysis and BOTTOM hierarchical clustering. Colour scale corresponds to the IC50 for AZD6244 treatment (see also Fig 1C).

<https://doi.org/10.1371/journal.pcbi.1009515.g002>

Signalling models highlight differential feedback regulation of MEK

To get further, more mechanistic, insights into potential resistance mechanisms, we used the perturbation data to parameterise signalling models. We applied our previously developed method that has been derived from Modular Response Analysis (MRA, implemented as R

package STASNet, [21]) to fit signalling network models to each cell line. This modelling procedure requires a literature network and the perturbation data as input, and then estimates response coefficients corresponding to link strengths using a maximum likelihood estimate (see Fig 3A, first step). By using the statistical framework of the likelihood ratio test, the modelling procedure then allows to test if any extension of the literature network is required to describe the data (see Fig 3A, second step). To compare parameters between cell lines, it is essential to harmonise parameters between all cells that can practically not be identified alone, i.e. parameters for inhibitors (see Fig 3A, third step). This finally yields a parameter map that allows to compare signalling strength between cell lines (see Fig 3A, final step).

When starting with a canonical literature network (see Materials and methods), we obtained reasonable fits for 4 of the 6 cell lines, as judged by the sum of weighted squared residuals that is in the order of number of data points (Fig 3B, red bars), and the normal distribution of residuals (S11 Fig). When we systematically tested if extensions of the network improve the fit using a likelihood ratio test, we found that significant improvements were still possible for most cell lines. We therefore performed successive rounds of extensions for each cell line independently (Fig 3A and S3 File). While SKNSH required no extension of the literature network, CHP212, LAN6, SKNAS required two or three extensions. KELLY and IMR32, the two cell lines that initially had the poorest fit, required four extensions (Fig 3C). After the extension the sum of weighted squared residuals was in the order of the number of data points for all cell lines except KELLY (Fig 3B green bar). The high residuals still exhibited by KELLY could be narrowed down to uncertainties in individual data points (see S3 File). Two network extensions (ASK1→MEK and p38→S6K) were significant in at least 3 cell lines and correspond to an effect of the ASK1 inhibitor GS4997 on the MEK/ERK MAPK pathway and S6K. Both links are negative which suggests an antagonism between the p38 MAPK and the MEK/ERK MAPK pathways in neuroblastoma cell lines. This negative crosstalk from p38 to MEK/ERK has also been described in other cell systems, e.g. after p38 knockdown in HeLa cells [22].

All extended models had similar, but different, parameters for the inhibitor strength. However, there is a strong interdependence of the inhibitor strength and link strength downstream of the inhibitor which render comparison between those link strengths in different cells difficult (see S3 File). As all cell lines received the same inhibitor concentration we therefore harmonised the inhibitor parameters by fixing them to the mean value between all models (Fig 3A, fixed inhibitor parameters). The resulting harmonised models maintained a good agreement with the data (Fig 3B, blue bars) and were used for inter-model comparisons (Fig 3D and 3E).

When inspecting the parameters for ligand-induced pathway activation, we noticed that they reflected a strong heterogeneity in ligand response between the cell lines. Reassuringly, they matched the expression of the corresponding receptors in many cases (Fig 3D and S12 Fig). The parameters for pathways downstream of NGF correlated mostly with NTRK1 expression and not with NGFR expression, which might indicate that NGF signalling is mediated mostly via NTRK1 in those cell lines. The parameters for IGF-induced signals correlated with IGF1R or IGF2R for MEK and AKT, respectively, indicating that both receptors mediate IGF1 signalling independently. Interestingly, the parameters for the pathway from EGF to MEK did not correlate with EGFR expression, but they do for EGF to AKT, which might suggest that differences in adaptor protein expression shape routing into downstream signalling in the various cell lines. Indeed, the expressions of GAB2 and SRC are very different between the cell lines and could explain that IMR32 and LAN6 are activated by EGF as strongly as SKNAS and SKNSH despite their lower EGFR expression (Fig 2C and S6 Fig). Another potential cause for the attenuated activation of MEK/ERK is that in NRAS mutant cell lines (CHP212, SKNAS and SKNSH), MEK/ERK activity is less inducible by receptors, as also parameter values of the

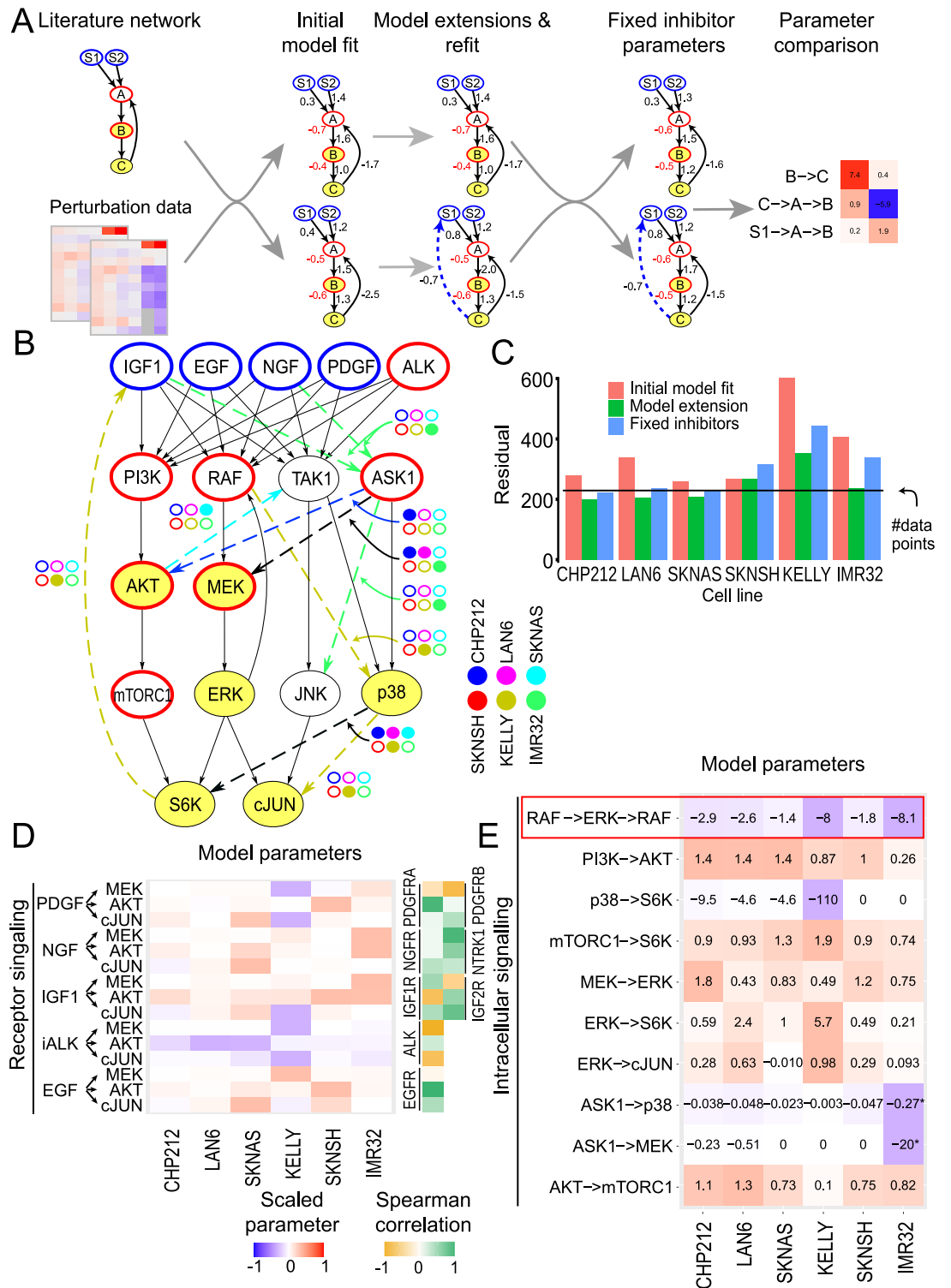


Fig 3. Receptor expression and topology variations explain the heterogeneity in perturbation response. A: Starting from a literature-derived network, a model was fitted for each cell line (Initial model fit) and extended following suggestions from the model (Model extensions and refit). Those models with different network structures were then harmonised by fixing the inhibition parameters to a consensus value (Fixed inhibitor parameters) to make the parameters directly comparable (Parameter comparison). B: Model residuals before and after model extension and harmonisation. The black line represents the number of data points, which

is equal to the expected mean of the error if the model explains all the data. C: Cell-line-specific network extensions (dashed arrows) relative to the literature network. Colour of the extended link was matched to cell line colour if required in only one cell line model and black otherwise. D: Model paths from the receptors to the first measured downstream node and correlation with the corresponding receptor expression. The colours correspond to the value of the path scaled by the maximum absolute value of that path between all cell lines. E: Model paths between non-receptor perturbed nodes and measured nodes for routes present in at least 2 cell lines. Colour scale is the same as in D. Cells are ordered from left to right from most sensitive to most resistant to the MEK inhibitor AZD6244. Due to the absence of ASK1 basal activity in IMR32, ASK1->p38 and ASK1->MEK represent in this cell line NGF->ASK1->p38 and NGF->ASK1->MEK, respectively.

<https://doi.org/10.1371/journal.pcbi.1009515.g003>

routes from PDGF, EGF, NGF and IGF into MAPK signalling are lower in those cell lines. Conversely, these cell line models display a slightly more inducible PI3K pathway. This observation is in agreement with a recent comparative study of G12V-mutated RAS isoforms in colorectal SW48 cells, where the NRAS-mutated cell line showed a weaker coupling of receptors to MEK and a stronger coupling to PI3K than in the parental cell line [23]. This would suggest that an activation of the MEK/ERK pathway is relayed predominantly by NRAS while the PI3K pathway activation is mediated by other proteins [24]. Taken together, this shows that the wiring and routing of ligand induced signalling in these cell lines is varying and is mostly explainable by the expression of the corresponding receptor and RAS mutation status.

In contrast to the receptor-associated parameters, the strength of intra-cellular kinase paths are less variable, and most paths are comparable between cell lines (Fig 3E). The most prominent exception is the negative feedback in MAPK signalling from ERK to RAF. When compared to the other cell lines, this feedback appears to be 3 to 4 times stronger in KELLY and IMR32, which are two cell lines that are highly resistant to AZD6244. A strong RAF-mediated feedback is a known resistance mechanism against MEK inhibitors [15–17], where relieve of inhibition of upstream components post inhibition can partially reactivate signalling. This suggests that AZD6244 resistance could be mediated by a differential regulation of this feedback.

Apart from the RAF-mediated feedback, MAPK signalling is also controlled by receptor-mediated feedbacks. In the KELLY cell line, our modelling procedure extended the model by a negative feedback from S6K to IGF1R that could then explain the strong accumulation of pMEK by IGF following AZD6244 treatment (Fig 3C and S3 File). Receptor-mediated feedbacks are also known to mediate resistance, notably to MAPK inhibitions [13, 18, 25–27], by reactivating this pathway and other parallel pathways.

In summary, the signalling parameters derived from the perturbation data by our models show that cell lines diverge in receptor expression and feedback regulation, with strong multi-layered feedbacks for some of the resistant cell lines.

Differential quantitative wiring of resistant cell lines

A hallmark of negative feedbacks is that they lead to re-activation of the pathway after pathway inhibition. In agreement with this, we observe an increase of phosphorylated MEK upon MEKi treatment (AZD6244) that is more pronounced in the cell lines IMR32 and KELLY compared to the other cell lines modelled, including the most sensitive cell lines CHP212 and LAN6 (Fig 4A and S13 Fig). We also tested the most resistant cell line in our panel, N206, which also showed a strong feedback response (Fig 4A). To more precisely dissect the feedback wiring, we generated additional focused perturbation data for those cells with high feedback (KELLY, IMR32 and N206) to MEK inhibition. We stimulated cells with different growth factors (IGF and NGF or EGF), and blocked MAPK signalling with MEK and RAF inhibitors, and subsequently monitored six phosphoproteins (Fig 4B). Subsequently, we used this data to parameterise a focused MRA model that additionally either contained or did not contain the only receptor-mediated feedback found in the first modelling round from S6K→IGF1 (Figs

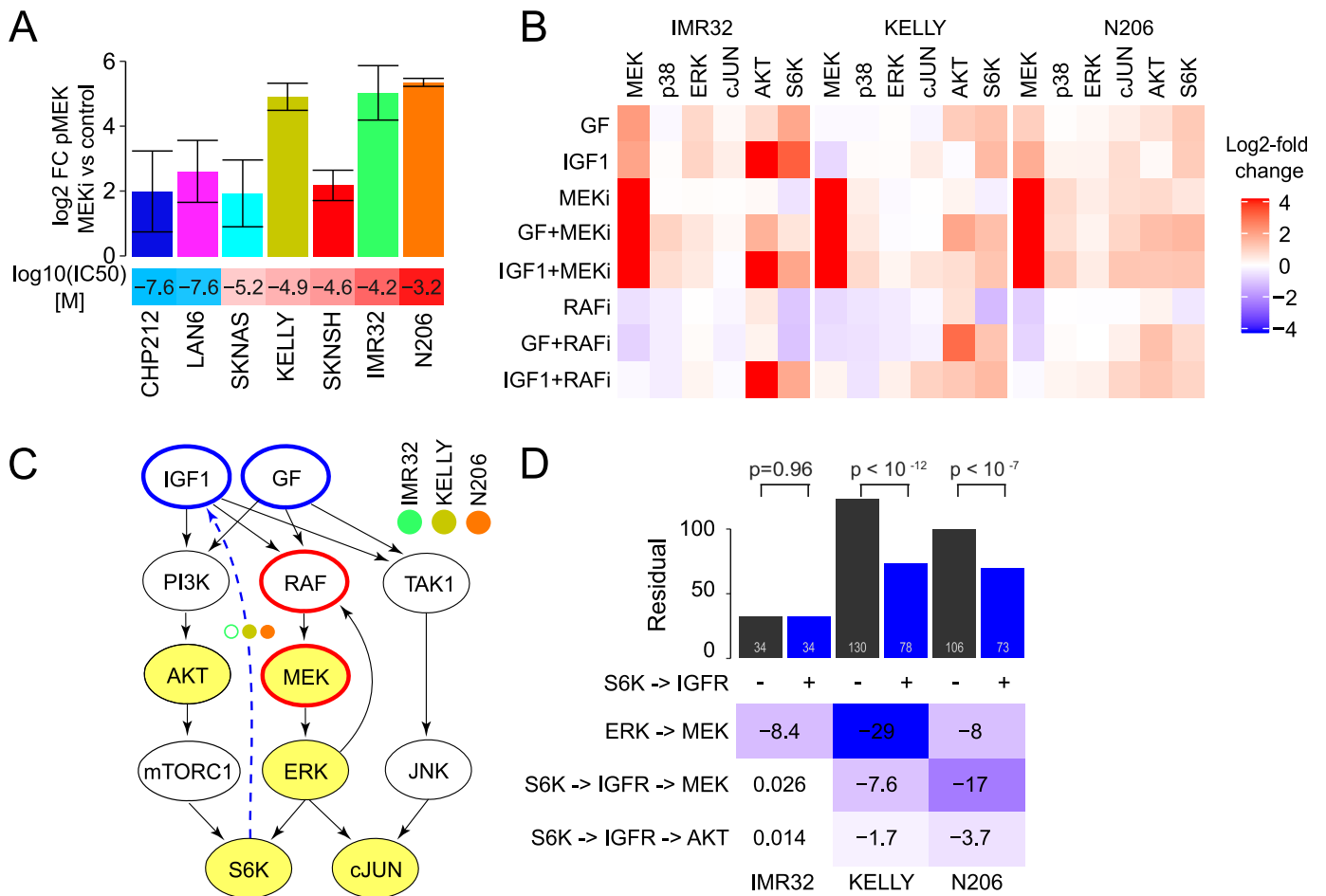


Fig 4. AZD6244 resistant cell lines have strong feedback control of MAPK signalling. A: Mean pMEK log₂-fold change relative to control after AZD6244 treatment in 7 neuroblastoma cell lines measured with bead-based ELISAs. Error bars represent 95% confidence interval. B: Measurement of 6 phosphoproteins (columns) after perturbation of N206, IMR32 and KELLY by either EGF (KELLY, N206) or NGF (IMR32) (together referred to as GF), IGF1, or control BSA in combination with Sorafenib (RAFi), AZD6244 (MEKi) or control DMSO. Values are expressed in log₂-fold change to BSA+DMSO control. C: Starting model and S6K→IGF1 receptor extension for the high pMEK responder cell lines. D: (top panel) Model residuals for N206, IMR32 and KELLY models with (black) or without (blue) an S6K→IGF1 receptor feedback link and corresponding p-value (χ^2 test with df = 1). (bottom panel) Parameter values of the high pMEK responder models including the S6K→IGF1 receptor link.

<https://doi.org/10.1371/journal.pcbi.1009515.g004>

3C and 4A). Inclusion of the IGF receptor-mediated feedback led to a significantly better fit of the data for N206 and KELLY (χ^2 p<0.05), but did not improve the IMR32 model (Fig 4C and 4D). Interestingly, the S6K→IGF1→RAF→MEK feedback is stronger in the N206 models, but the pathway-intrinsic feedback (ERK→RAF→MEK) is stronger in KELLY (Fig 4D). This highlights that all these cells display negative feedback regulation, but the strengths of the two layers of feedbacks are different between cell lines.

Parallel inhibition of MEK and IGFR leads to synergistic effects on the phosphoproteome

To gain a more systematic understanding of the effect of MEK and IGFR inhibition on the signalling states of the cells, we generated deep (phospho-)proteomics profiles using tandem mass-tag (TMT) based mass spectrometry [28, 29]. We reasoned that inhibition of IGFR in

combination with MEK should have a synergistic effect in N206 compared to IMR32. We measured the phospho- and total protein levels in IMR32 and N206 cells after 4h treatment with MEK and/or IGFR inhibitors and control cells. Although a similar number of phosphosites were dis-regulated in both cell lines (448 in IMR32, 615 in N206, FDR < 0.05), there was little overlap in the phospho-peptides differentially regulated between the two cell lines (Fig 5A), and this overlap was mostly limited to phospho-peptides affected by MEK inhibition (S14 Fig). In IMR32, IGFR inhibition had little effect, while the presence of MEK inhibition strongly affected the phosphoproteome (Fig 5B left). Moreover the effect of the combination of MEK and IGFR inhibitors was dominated by the effect of the MEK inhibition, with about two thirds of the differential phosphopeptides (96/149) being also regulated by MEK inhibitor alone. Accordingly, differentially phosphorylated peptides in IMR32 are enriched in MAPK targets (S15 Fig). In contrast, both MEK as well as IGFR inhibition induce strong alterations in the phosphoproteome in N206 (S14 Fig), affecting both mTOR and MAPK signalling targets (S15 Fig), and the combination exhibits a synergistic effect (Fig 5B right). Overall, 24 differentially phosphorylated sites in N206 show synergistic regulation, as defined by a significant deviation of the combination from the sum of the individual treatment effects. Of these, 17 phosphosites were synergistically down-regulated, and 7 sites showed up-regulation. Moreover, 10 of those synergistically downregulated phosphosites are known or putative targets of the PI3K/AKT signalling axis. This suggests that MEK/ERK signalling influences AKT signalling in a IGFR dependant way. In contrast, only two sites showed synergy in IMR32 (Fig 5C). Among the synergistically downregulated phospho-sites in N206 was S425 of the Eukaryotic translation initiation factor 4B (EIF4B), a protein involved in regulation of translation and a known nexus between AKT and MAPK signalling [30]. We performed a kinase substrate enrichment analysis [31] to explore how the signalling networks were affected by the inhibitions (Fig 5D). For IMR32 cells, this analysis showed a decreased phosphorylation of MEK and JAK targets and an increased phosphorylation of ARAF and BRAF targets in response to MEK inhibition. Interestingly, in combination with IGFR inhibition the RAF activation is partially reversed whereas other kinase targets seem rather unaffected. Overall this indicates a feedback activation of RAF that does not totally compensate the loss of MEK activity. In N206 cells, the response to MEK inhibition and the attenuation of the activation of RAF targets following double inhibitor treatment is similar to the response in IMR32. However, in IMR32 cells IGFR inhibitor treatment had little impact on the kinome whereas a massive down-regulation of targets of a range of kinases occurred in N206 cells, covering the PI3K/AKT/mTOR pathway (SGK1–3, AKT1, p70S6K), MAPK pathway (p90RSK) and many members of the Protein Kinase C Family. This suggests a central role of IGFR signalling on central growth and survival pathways.

When we investigated the phosphorylation of components of the MAPK pathway more closely, we found many RAF negative feedback/crosstalk sites to be down-regulated after MEK inhibition (BRAF: T401, S750, T753; RAF1: S29, S642, S259) in both cell lines (Fig 5E). MEK1 S222/S226 phosphorylation is increased and pERK S204 decreased in both cell lines after MEK inhibition, in line with corresponding measurements using bead-based ELISAs. Among those down-regulated phosphosites that were only significant in the combination in N206 we detected many MYCN-phosphosites, notably MYCN S62, which is regulated by MAPK via CDK1 [32]. Interestingly, this loss of S62 phosphorylated MYCN is associated with reduced MYCN levels (Fig 5F) despite the association of MYCN S62 with increased MYCN degradation [33]. The decreased detection of MYCN S62 might be a consequence of the loss of total MYCN protein but is likely not causing this loss itself. This downregulation was observed in IMR32 and N206 cells upon single inhibition (IGFRi for N206 and MEKi for both cell lines), but only in N206 cells an even stronger downregulation could be observed upon double

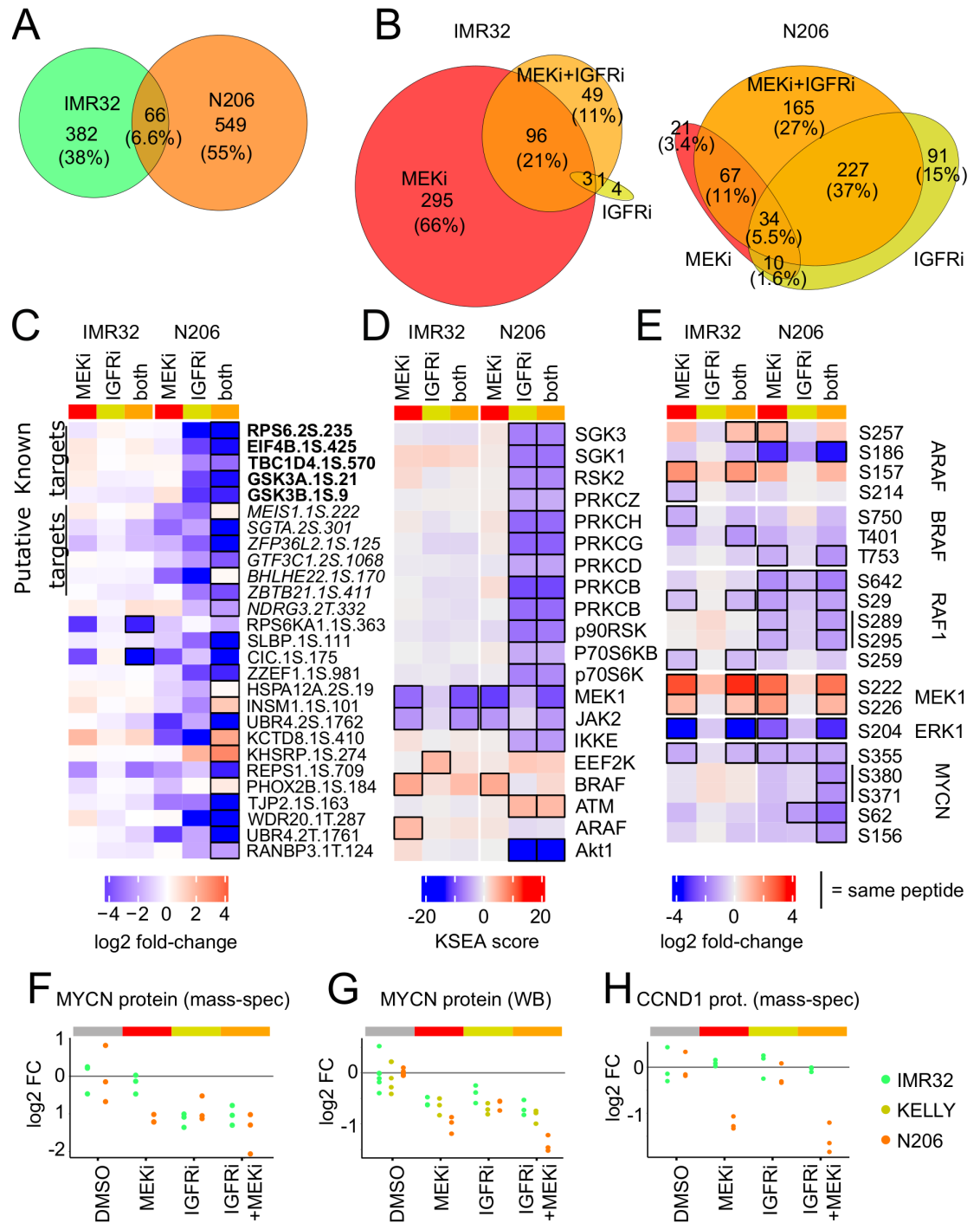


Fig 5. Phosphoproteomics analysis reveals important variations in the response to combination treatment. A-B: Venn diagrams showing the overlap in differentially regulated phosphosites A: between IMR32 and N206 or B: between treatments for each cell line. C: Phosphopeptides synergistically altered by MEKi+IGFRi combination (black outline) when compared to the sum of individual inhibitor treatments. AKT, mTOR or P70S6K *bona fide* targets (bold font) and putative targets (italic font; top 5 predicted kinases by PhosphoNET Kinase Predictor www.phosphonet.ca) are indicated. D: Kinase substrate enrichment score using PhosphoSitePlus annotations. E: Log-fold change to DMSO for RAF/MAPK and MYCN phosphopeptides. C-E: Black outline highlights significant changes in activity (limma moderated t-test, FDR<5%) F-H: Relative levels compared to control of the total proteins levels for MYCN (F) and CCND1 (H) measured with mass spectrometry and MYCN measured with Western blot (G).

<https://doi.org/10.1371/journal.pcbi.1009515.g005>

inhibition (Fig 5F). We confirmed these effects in Western blots for IMR32 and N206 cells (Fig 5G), and also found downregulation of MYCN upon IGFRi as well as MEKi treatment but no synergetic decrease after the combination treatment (Fig 5G). Another interesting protein that is regulated synergistically in N206 is Cyclin D1 (Fig 5H), a protein that is involved in cell cycle progression and whose loss likely mediates MYCN loss. It should be noted that only 5 proteins (PHGDH, DERL1, AMPD3, ARHGEF16 and CCND1) were found differentially affected with an FDR < 10%, highlighting that on this time scale phospho-protein changes dominated.

Taken together, the proteomics data is coherent with the model that MAPK signalling in N206 is controlled by a dual feedback structure involving RAF and IGFR, whereas it is mainly controlled by a RAF-mediated feedback in IMR32. It furthermore supports the notion that treatment with MEK and IGFR inhibitors would show synergy in N206.

Vertical inhibition can break feedback-mediated resistance

Feedback regulation is often a central aspect for drug resistance that could be overcome by a vertical inhibition strategy, where an inhibition of an upstream node prevents pathway reactivation. Based on our models, we tested if the additional application of an inhibitor targeting the feedback nodes (RAF and IGFR) would sensitise resistant cells toward MEK inhibition (Fig 6A). We quantified growth reduction after inhibiting IMR32, KELLY and N206 with different dose combinations of inhibitors against MEK (AZD6244), IGFR (AEW541) and RAF (LY3009120) (Fig 6B). In agreement with our model predictions of strong IGFR-mediated feedback in N206 (Fig 4D), there was a strong synergistic effect as evaluated by the Bliss score [34] of the combination of MEK and IGFR inhibitions on growth in N206 but little in KELLY or IMR32 (Fig 6C and see S16 Fig for Loewe score).

When trying to overcome the model-derived strong ERK-RAF feedback found in all three cell lines with a combination of MEK and RAF inhibition we only found a synergistic effect for two of the three cell lines (N206 and KELLY), whereas IMR32 remained resistant and no synergy could be detected. We hypothesised that this observed resistance in IMR32 might be either because the vertical inhibition by MEKi and RAFi was molecularly not effective or that IMR32 might no longer depend on ERK signalling for survival and growth. To distinguish the former from the latter we decided to compare model simulation and measurements for perturbation effects of selected inhibitor combinations on pMEK and pERK in IMR32 and KELLY cells.

Based on the model simulations, in both cell lines the vertical inhibition of MEK + RAF inhibitor was predicted to suppress MAPK signalling much stronger than MEK inhibitor alone or in combination with an ERK inhibitor. Moreover, the suppressive effect was predicted to be even more profound in IMR32 than in KELLY (Fig 6D left). We then measured the effect on pMEK and pERK of MEK inhibitor alone and in combination with the RAF inhibitor LY3009120 or ERK inhibitor SCH772984 (Fig 6D right). The measurements qualitatively supported the model simulations showing that RAF inhibitor suppressed MEK feedback activation by AZD6244, and that this suppression is stronger in IMR32. Addition of the ERK inhibitor neither suppressed this feedback activation nor could it decrease ERK phosphorylation more than RAF inhibition, as also predicted by the model. This suggests that in agreement with the model simulations the combination of RAFi and MEKi is most effective in IMR32 to effectively suppress ERK activation and feedback-mediated re-activation. However, since the growth is least affected by this combination IMR32 seems not to depend on ERK activity.

As both KELLY and N206 have strong multi-layered feedbacks (Fig 4D), we also tried triple combinations of IGFRi, RAFi and MEKi. We observed that only in KELLY, triple inhibitor

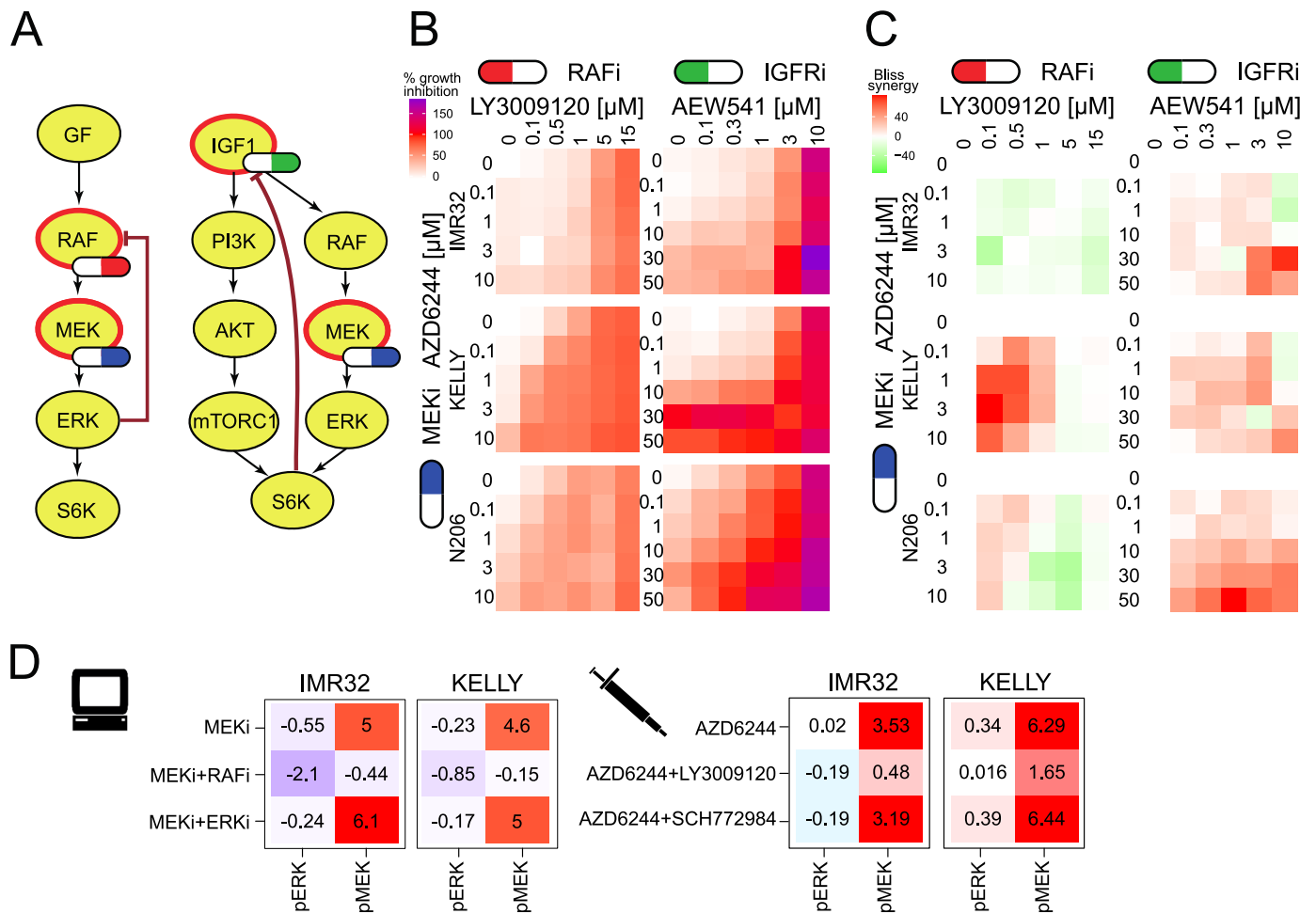


Fig 6. AZD6244 resistant cell lines can be sensitised with combined inhibition with the IGFR inhibitor AEW541 or the RAF inhibitor LY3009120. A: Model-inferred targeting strategy of dual inhibition. B: Growth inhibition measurements for various combinations of the MEK inhibitor AZD6244 with the RAF inhibitor LY3009120 or the IGFR inhibitor AEW541. Values over 100 indicate cell death. n = 2. C: Bliss synergy corresponding to the measurements in B. D: LEFT: Model predictions of pERK and pMEK activity for MEK inhibition alone and in combination with inhibition of upstream kinase RAF or downstream kinase ERK for KELLY and IMR32. Values are log-fold changes to IGF1 condition with inhibitor strength set to -1. D: RIGHT: pERK and pMEK plex measurements in KELLY and IMR32 after 90min treatment of the MEK inhibitor AZD6244 in combination with either DMSO, SCH772984 (ERKi, 10µM) or LY3009120 (RAFi, 5µM) in cells grown with 10% FCS. Values are log-fold change to FCS medium condition.

<https://doi.org/10.1371/journal.pcbi.1009515.g006>

treatment seems to have an additional benefit compared to the best combination of two inhibitors. (S17 Fig and S2 File).

Discussion

Neuroblastoma is a complex disease with distinct subtypes that display radically different outcomes, ranging from spontaneous regression in low-risk groups to only 50% survival of patients in the high risk neuroblastoma group. Mutations in RAS/MAPK signalling are a hallmark of high risk neuroblastoma, and also define a subgroup of patients with ultra-high-risk neuroblastoma and an even worse survival. Therefore targeted treatment might be a valid strategy to treat those patients. However, response to MEK inhibitors are very variable, and it is thus important to understand mechanisms of resistance and how to circumvent these.

In this work, we explored how a more quantitative understanding of signalling can be used to design combinatorial treatments to counteract drug resistance. We used a panel of deeply profiled cell lines representing high risk neuroblastoma and showed that the response to MEK inhibitors is variable, with some cell lines responding at low doses in the nM range, whereas others are highly resistant. By using signalling perturbation-response data, we characterised the signalling network surrounding MAPK. Analysis of that perturbation data with the modelling framework of modular response analysis unveiled that MAPK signalling is controlled by a multi-layered feedback with variable strength. A central finding was that MEK-inhibitor sensitive cells are controlled by low feedbacks within the MAPK cascade, whereas a subset of resistant cell lines shows strong multi-layered feedbacks that may be causal for resistance. Simulation of cell-line specific models suggested that different combinations of inhibitors can be used to overcome resistance, and experiments could confirm these predictions in two out of three cell lines.

Our work highlights that systematic perturbation data are a powerful source to probe intracellular signalling pathways. The connectivity of signalling pathways implies that minor quantitative alterations of the network can lead to many changes in response, not all of which alter the phenotype. In this work, we saw that multivariate analysis of the perturbation data alone was not fruitful to separate cell lines with respect to their drug sensitivity. In contrast, integration of data by models highlighted that variations of only a few links is enough to explain the differences between those cell lines. Modelling was therefore key to integrate the data and to unveil feedback loops as potential sources of resistance.

In our work we used a maximum likelihood version of MRA, but there are multiple other methods that might be suited to reconstruct semi-quantitative signalling networks from perturbation data. [35] proposed a bayesian variant which overcomes the linearity assumption of MRA using chemical kinetics to guide the inference and fuzzy-logic models such as used by [36] also show good performance to reconstruct network topology from signalling data. However getting quantitative values for the interactions between components of a signalling network from a small set of perturbations requires MRA variants [21, 37] or necessitates time-resolved perturbation data which limits the number of perturbations that can be studied simultaneously [38]. While boolean models are very good strategies to model large signalling networks and complex synergies [39], they would be unable to capture quantitative differences in feedback regulation, which are the key resistance mechanisms uncovered in this work.

Drug resistance to targeted therapies have been attributed to negative feedback loops in multiple tumours. Most importantly, sensitivity to MEK inhibitors is strongly influenced by a pathway-intrinsic feedback, where ERK phosphorylates RAF at multiple sites [15–17]. This feedback has been shown to be very strong in epithelial cells leading to pathway robustness [16], which can be overcome by vertical inhibition of RAF [17]. Another mode of feedback regulation is the inhibition of receptors by pathways. An example is the inhibitory regulation of EGFR by the MAPK pathway [13, 14]. When inhibiting MAPK signalling by MEK or RAF inhibitors, this feedback leads to hyper-sensitisation of EGFR, which in turn reactivates MAPK signalling and additionally activates other downstream pathways such as PI3K/AKT signalling. Also in this case vertical inhibition can help to overcome this mode of resistance, by co-targeting the MAPK pathway and the upstream receptor.

Our modelling analysis suggested that some neuroblastoma cell lines possess two major layers of feedback in MAPK signalling. One of these feedbacks is pathway-intrinsic (from ERK to RAF) and one is a feedback to the IGF receptor. Interestingly, different cell lines show different relative strength of feedbacks from ERK to RAF and IGF, and simulations show that those require different strategies for vertical inhibition. For the cell line KELLY, modelling unveiled an extremely strong negative feedback from ERK to RAF. This suggests that a combination of

MEK and RAF inhibitor will be more potent than a combination of MEK and IGFR inhibitor. In contrast, in the cell line N206, both feedbacks have similar strength, suggesting that both combinations might be potent. In line with these predictions, experiments showed that in KELLY indeed the combination of MEK and RAF inhibitors is much more potent to reduce growth compared to the combination of MEK and IGFR. In contrast, in N206 both combinations reduce growth.

Our phospho-proteomics analysis shows that the combination of MEK and IFGR also has different effects in the two cell lines: Whereas it shows clearly synergistic effects of the combination in N206, there is no sign of synergy in IMR32. By aggregating the phosphoproteome to kinase activities using kinase enrichment scores, one can also get insights into the re-wiring of signalling after perturbation. In our case, it clearly shows how the re-activation of RAF after MEK inhibition is inhibited by the treatment with IGFR inhibitors, and IGFR and MEK inhibitors synergize in reducing AKT activity in N206. The phosphoproteome also showed that the dual treatment of IGFR and MEK manifests itself in synergistic downregulation of important proteins that are regulated by convergent signalling of MEK and AKT, such as MYCN and EIF4B.

Interestingly, a third resistant cell line, IMR32, showed no response in growth to MEK inhibitor in vertical combination with either RAF and/or IGFR inhibitor on growth, even though it's cellular ERK signalling was strongly responsive. This highlights that cancer cells might lose ERK-mediated cell cycle control, suggesting that coupling of cellular phenotype to signalling pathways is not necessarily strict [40, 41]. To more directly model changes on cellular phenotypes such as growth or viability, models of signalling would need to be connected to phenotypic readouts [42]. In addition, it might be beneficial to include downstream readouts such as cyclin levels or CDK activation that are more directly involved in cell cycle progression and can be deregulated in cancer [43, 44]. Our model attributes signalling differences between cell lines to an apparent feedback from MAPK signalling to IGFR and/or RAF. However, our model is too coarse-grained to distinguish feedback regulation from other, potentially non-linear mechanisms of cross-talk. Ultimately, only mechanistic studies that e.g. include the use of cell lines that have mutant feedback will unveil if the feedbacks are responsible for the observed signalling phenotypes and inhibitor synergies. It should be also pointed out that our measurements only encompass one time point and that later dynamics of the MAPK pathway, such as transcriptional feedbacks, could also explain IMR32 resistance to vertical inhibition.

In summary, our results show that a quantitative understanding of differences in signalling networks can be very helpful to rationalize resistance, and to derive effective treatments. Future work should investigate if those feedback mechanisms exist in tumours *in vivo* and whether they could explain relapses. Our description of the wiring of the RAS/MAPK pathway in neuroblastoma will support the design of clinical trials using combinatorial treatments to prevent or overcome therapy resistance. In addition, the framework described here could be used to analyse signalling in tumours of individual patients. While it will be technically challenging to assess signalling network responses in tumour patients, *ex vivo* cultures—so-called avatars—could be an option [45, 46]. We envision that learning features of robustness and vulnerability of tumours from signalling models on cell line panels might greatly reduce the required set of perturbations in those avatars that are sufficient to inform a model, and allow reliable stratification and prediction of treatment options.

Materials and methods

Cell lines

The neuroblastoma cell lines were obtained by courtesy of the Deubzer lab (Charité, Berlin) as part of the Terminate-NB consortium. The identity of the cell lines was confirmed with STR

profiling (see S2 Table), which were generated by Eurofins Cell Line Authentication Test and matched with the Cellosaurus STR similarity research tool [47]. All cell lines were grown in DMEM (Gibco, Life Technologies) with 3.5 g/L glucose (Sigma), 5 mM glutamine (Gibco, Life Technologies) and 10% FCS (Pan Biotech).

Whole exome sequencing

DNA was extracted from the human neuroblastoma cell lines (see above), using the NucleoSpin Tissue kit (Macherey-Nagel) according to the manufacturer's protocol. From the DNA, libraries for whole-exome sequencing were prepared using the SureSelect Human All Exon V7 kit (Agilent) and the Illumina TruSeq Exome kit. The libraries were sequenced on Illumina HiSeq 4000 and Illumina NovaSeq 6000 sequencers. The read sequences and base quality scores were demultiplexed and stored in Fastq format using the Illumina bcl2fastq software v2.20. Adapter remnants and low-quality read ends were trimmed off using custom scripts. The quality of the sequence reads was assessed using the FastQC software. Reads were aligned to the human genome, assembly GRCh38, using the bwa mem software version 0.7.10 [48], and duplicate read alignments were removed using samblaster version 0.1.24 [49]. Copy-number alterations were determined using cnvkit version 0.1.24 [50]. Single-nucleotide variants (SNVs) were identified using strelka version 2.9.10 [51]. Afterwards, potential germline variants were filtered out by excluding all SNVs that had also been observed in at least 1% of samples in cohorts of healthy individuals, namely the 1000 Genomes Project [52] and the NHLBI GO Exome Sequencing Project [53] cohorts. The raw data are available on ENA under the accession number PRJEB40670.

RNA sequencing

The cell lines were sequenced in 3 separate batches. The IMR32, KELLY, SKNAS, LAN6, NBEB1 cell lines were prepared in triplicate, using a paired-end stranded protocol with 2x75 cycles per fragment and 2 more cell lines (NGP, SKNSH) were prepared in duplicate, using a paired-end stranded protocol with 2x150 cycles. Two more libraries (CHP212 and N206) were prepared using a paired-end stranded protocol with 2x75 cycles per fragment.

Raw sequencing data were rigorously checked for quality using FastQC. The reads were aligned to the human genome GRCh38 (without patches or haplotypes) and the GENCODE transcript annotation set using the STAR aligner software [54]. The read counts per gene were obtained using the featurecounts [55] method from the subread software package. The raw data are available on ENA under the accession number PRJEB40670.

Drug sensitivity assay

Cells grown for 1 day in full medium were treated with the indicated drugs in 4 different concentrations (0.1, 1, 10 and 100 μ M Fig 1B) along with the corresponding DMSO controls on the same plate. The growth of the cells was tracked by phase contrast imaging for 72h with 4 images per well taken every 2h using the Incucyte Zoom instrument (Essen BioScience) and the confluency estimated using the Incucyte Zoom Analysis software (Essen BioScience). The growth rate was estimated with a linear fit on the log-transformed confluency, and the IC50 was determined by fitting a sigmoid of the form:

$$V = \frac{1}{1 + \exp(-\log(C) + IC50) \times S)}$$

to normalised growth rates (implemented in <https://github.com/MathurinD/drugResistance>). V is the growth rate relative to DMSO control, C is the concentration and the parameters $IC50$

and slope S are fitted. See [S1 Table](#) for the fitted parameters and [S2 File](#) for the raw data and analysis scripts, as well as [S18](#) and [S19](#) Figs for example images.

Synergy estimation

For the synergy assay, cells seeded the day before were treated with different concentrations of AZD6244 (0.1, 1, 10, 30 and 50 μM , Selleck Chemicals) in combination with NVP-AEW541 (0.1, 0.3, 1, 3 and 10 μM , Cayman Chemical) or LY3009120 (0.1, 0.3, 1, 3 and 15 μM , Selleck Chemicals). The synergy scores were determined using the R package synergyfinder [56] with the relative growth rates thresholded between 0 and 1 as input (0 meaning no growth or cell death and 1 meaning growth as fast as the DMSO control).

Perturbation assay

Cells were seeded in 24 well plates and grown for 2 days in full medium followed by 24h in FCS-free medium before treatment with the same concentrations of ligands and inhibitors.

All inhibitors were dissolved in DMSO and cells were treated for 90 minutes at the following concentrations: GDC0941 (1 μM , Selleck Chemicals), AZD6244/Selumetinib (10 μM , Selleck Chemicals), MK2206 2HCl (10 μM , Selleck Chemicals), Rapamycin (10 μM , Selleck Chemicals), Sorafenib (10 μM , Selleck Chemicals), GS-4997 (10 μM , Selleck Chemicals) and TAE684 (10 μM , Selleck Chemicals).

The cells were treated for 30 minutes (60 minutes after inhibitor treatment) with ligands in a 0,1% PBS/BSA carrier solution at the following concentrations: EGF (25 ng/mL, Peprotech), PDGF (10 ng/mL, Peprotech), NGF (50 ng/mL, Peprotech) and IGF1 (100 ng/mL, Peprotech).

The cells were then lysed using BioRad Bio-Plex Cell Lysis Kit and measured using the Bio-Plex MAGPIX Multiplex Reader with a custom kit from ProtAtOnce with analytes p-cJUN (S63), p-p38 (T180/Y182), p-AKT (S473), p-ERK1/2 (T202/Y204, T185/Y187), p-MEK1 (S217/S221), p-S6K (T389) and p-RSK1 (S380). The p-RSK1 (S380) readout was discarded because of a low dynamic range.

The same procedure and analytes were used for the other perturbation assays in this paper. Refer to the main text for the exact inhibitors and concentrations used for each experiment.

Signalling models

The model for each cell line was fitted separately from the corresponding perturbation data with the *createModel* function from the R package STASNet [21]. STASNet implements the variation of Modular Response Analysis (MRA) described in [13] and [21] that implements a dual effect of inhibitors as both a negative stimulus and a disruption of signal propagation. Under the hypothesis of pseudo-steady-state and locally linear dependencies between nodes, MRA models the response to a perturbation as

$$R = -\tilde{r}^k * S \quad (1)$$

where R_{ij} is the global response of node j after perturbation of node i , \tilde{r}_{ij}^k is the local response of node j after perturbation of node i taking into account the effect of inhibition of node k , and S_{ik} is the sensitivity of node i to perturbation k . The pAKT readout was systematically removed if AKT inhibition was present because the AKT inhibitor MK2206 blocks AKT autophosphorylation [57], i.e acts upstream of the AKT node, while STASNet expects inhibitors to act downstream of their annotated target.

We designed a literature network consisting of the MAPK and PI3K/AKT signalling pathway as annotated in KEGG (<https://www.genome.jp/kegg/pathway/hsa/hsa04010.html> and

https://www.genome.jp/kegg-bin/show_pathway?hsa04151) with intermediate nodes suppressed, the addition of the well documented ERK->RAF feedback and all receptors corresponding to RTK. Each cell line was fitted first on the literature network, then we extended the networks independently using a greedy hill climbing approach, until no significant link could be added. We then performed successive rounds of reduction to identify the non-significant links. Most removed links relate to receptor connections. Only three connections not related to receptors were removed during this procedure, each for one cell line only. To facilitate model comparison, these links were ultimately retained in the model, as otherwise the model parameters would not be comparable. Those models with final topology yielded similar values for the inhibition parameters so we generated new models with those parameters fixed to the mean value across all 6 models and re-fitted each cell line with inhibitor values fixed. With this fitting strategy the links between models became directly comparable as the non-identifiability induced by the inhibitor parameters was removed (Fig 3A). The high pMEK responder cell line models were fitted using the same procedure.

Western blot

Cells were grown to confluency for 3 days in full medium and treated with AEW541 10 μ M and/or AZD6244 10 μ M or control DMSO for 4h then lysed using BioRad Bio-Plex Cell Lysis Kit. The lysates were run for 3h at a constant 45 mA in 10% acrylamid gels and blotted for 45 minutes at 400 mA on nitrocellulose. The membranes were stained for total protein using Pierce Reversible Protein Stain (ThermoFischer 24580) and blocked for 30 minutes in 1:1 PBS: Odyssey blocking buffer. The primary antibodies were incubated overnight at 4C one at a time and the corresponding secondary during the following day for 2h at room temperature in 1:1 PBST/Odyssey. We used the following primary antibodies: pIGF1R beta^{Y1135/Y1136} 1:1000 (CST 3024), pAKT^{S473} 1:2000 (CST 4060), total MYCN 1:200 (Santa Cruz sc-53993) and pMEK^{S217/S221} 1:1000 (CST 9154).

TMT (phospho-)proteomics

For the proteomics and phosphoproteomics cells were grown to confluency for 3 days in full medium and treated with AEW541 10 μ M and/or AZD6244 10 μ M or control DMSO for 4h.

We used an adapted version of the TMT workflow [28]: samples were reduced, alkylated and digested with a combination of LysC (Wako) and Trypsin (Promega) using the single-pot, solid-phase-enhanced sample preparation [58]. For each sample, an equal amount of peptide was then chemically labelled with TMTpro reagents [29]. Samples were randomly assigned to one of the first 15 TMT channels, while the 16th channel was composed of a superset of all the samples to allow multi-plex normalisation. Equal amounts of the labelling reactions were combined in two TMT16 plexes, desalted via SepPak columns (Waters) and fractionated via high-pH fractionation [59] on a 96 minutes gradient from 3 to 55% acetonitrile in 5 mM ammonium formate, each fraction collected for 1 minute then combined into 24 fractions. From each fraction, an aliquot was used to measure the total proteome while the remaining peptides were combined into 12 fractions and used as input for an immobilised metal affinity chromatography using an Agilent Bravo system. For the total proteome analysis, peptides were on-line fractionated on a multi-step gradient from 0 to 55% acetonitrile in 0.1% formic acid prior injection in a QExactive HF-x mass spectrometer. Samples were acquired using a data dependent acquisition strategy with MS1 scans from 350 to 1500 m/z at a resolution of 60 000 (measured at 200 m/z), maximum injection time (IT) of 10 ms and an automatic gain control (AGC) target value of 3×10^6 . The top 20 most intense precursor ions with charges from +2 to +6 were selected for fragmentation with an isolation window of 0.7 m/z. Fragmentation was

done in an HCD cell with a normalised collision energy of 30% and analysed in the detector with a resolution of 45 000 (200 m/z), AGC target value of 10^5 , maximum IT of 86 ms. We used the same parameters for phosphoproteome analysis with the exception of MS2 maximum IT that was set to 240 ms.

The acquired raw files were analysed using MaxQuant v1.6.10.43 [60], with TMTpro tags manually added as fixed modifications and used for quantitation. The correction factors for purity of isotopic labels was set according to vendor specification and minimum reporter precursor intensity fraction was set to 0.5. The resulting protein groups were filtered for potential protein contaminants, protein groups only identified via peptides decorated with modification or hits in the pseudo-reverse database used for FDR control. The resulting intensities of each sample channel were normalised to the intensity of the 16th reference channel, then median-centered and normalised according to the median-absolute deviation. Identified phosphopeptides were similarly filtered, with the exception of filtering based on modified sites, and normalised using the same strategy.

Differentially expressed phosphopeptides were called using the *limma* package [61] with a false discovery rate of 0.05 on treatment minus control contrasts. Synergies were computed using a contrast fit of the combination minus the sum of single treatments. Kinase substrate activity was implemented in R using the ratio of the mean z-score as described in [31] and computed for kinase-substrate sets from PhosphoSitePlus [62]. The normalised intensities and scripts used for the analysis can be found at https://itbgit.biologie.hu-berlin.de/dorel/phosphoproteomics_tnb_perturbations.

Supporting information

S1 Fig. Annotated IC50 of all measured drugs and cell lines with MYCN and TERT expression information.

(PDF)

S2 Fig. IC50 and mutations. t-test comparison of the IC50 in mutant (Mut) versus wild type (WT) for RAS/P53 and associated genes with mutation frequency between 30% and 70% in our panel.

(PDF)

S3 Fig. IC50 and gene expression. Top correlation between IC50 and mRNA transcript per million for the 1000 most variable genes (top, adjusted $p > 0.93$) and GO signal transduction genes (bottom, adjusted $p > 0.94$).

(PDF)

S4 Fig. PCA on the 1000 most variable genes. Principal component analysis of the 1000 most variable genes. All components up to the first one explaining less than 10% of the variance are shown.

(PDF)

S5 Fig. PCA on the signal transduction genes. Principal component analysis of the 5262 signal transduction genes. All components up to the first one explaining less than 10% of the variance are shown.

(PDF)

S6 Fig. Selected gene-drug correlations. Correlation of NF1 expression with AZD6244 IC50 and ALK expression with TAE684 IC50.

(PDF)

S7 Fig. Receptors RNA expression (TPM).

(PDF)

S8 Fig. Adaptors and ERBB receptor family RNA expression (TPM).

(PDF)

S9 Fig. Perturbation data PCA. Pair-plot of the principal components from the perturbation in 2. All components up to the first one explaining less than 10% of the variance are shown.

(PDF)

S10 Fig. Perturbation PCA loadings. Main loadings in the first 3 principal components of the perturbation data PCA. Colors correspond to the component for which the condition has the highest absolute weight. Table indicates the weight for the top 10 conditions of the first 3 principal components.

(PDF)

S11 Fig. Models qq-plots. Quantile-quantile plots of the initial models using the (A) literature topology and (B) the final model after extension.

(PDF)

S12 Fig. Correlation of signaling and receptor expression. Correlation between the fitted path value from ligands to readouts and the expression of the matching receptor or receptor family. IGFRsum and PDGFRsum are the sum of the isoforms expression for IGFR and PDGFR respectively.

(PDF)

S13 Fig. AZD6244 perturbation versus IC50. Linear model fit of AZD6244 IC50 response to perturbations including AZD6244. Points are independent replicates, $n = 2$.

(PDF)

S14 Fig. Differential phosphopeptides. Differentially measured phosphopeptides in IMR32 and N206 after 4h inhibition ($FDR < 0.05$, $n = 3$) classified by treatment(s) where the phosphosite is differentially expressed.

(PDF)

S15 Fig. KEGG enrichment of phosphoproteomics. KEGG enrichment of unique genes corresponding to phosphopeptides differentially expressed after MEKi, IGFRi or MEKi+IGFRi treatment in (A) IMR32, (B) N206 or (C) both strictly. Enrichment was computed using the R package `enrichKEGG`.

(PDF)

S16 Fig. Loewe synergy. Loewe synergy for the combinations of AZD6244 with (A) AEW541 or (B) LY3009120 shown in 6B. Synergy scores were computed with the R package `synergyfinder`. Positive scores indicate synergy, negative scores indicate antagonism.

(PDF)

S17 Fig. Viability to combination treatments. Relative viability of IMR32, KELLY and N206 after treatment with AZD6244, AEW541 and RO5126766 alone or in combination. Confluency was tracked for 72h using the Incucyte Zoom. Growth rate was fitted to the confluency curve and normalised to the average growth rate of the corresponding DMSO controls. black crosses indicate the mean value for each cell line for the corresponding treatment.

(PDF)

S18 Fig. Incucyte CHP212. Incucyte image of the AZD6244-sensitive cell line CHP212 immediately after and 72h after DMSO or AZD6244 treatment.

(PDF)

S19 Fig. Incucyte IMR32. Incucyte image of the AZD6244-resistant cell line IMR32 immediately after and 72h after DMSO or AZD6244 treatment.

(PDF)

S1 Table. IC50 data.

(CSV)

S2 Table. STR profiling results.

(XLSX)

S1 File. Sequencing data and related analysis scripts.

(ZIP)

S2 File. Dose response data and related analysis scripts.

(ZIP)

S3 File. Model data and fitting summary.

(ZIP)

Acknowledgments

We thank Alexandria McGearey for technical assistance with preparing the whole-exome sequencing libraries, Martha Hergesekke for help in cell culture, as well as Jasmin Wünschel for providing the cell lines.

Author Contributions

Conceptualization: Bertram Klinger, Nils Blüthgen.

Data curation: Mathurin Dorel, Tommaso Mari, Joern Toedling, Eric Blanc, Clemens Messerschmidt, Michal Nadler-Holly, Matthias Ziehm, Falk Hertwig.

Funding acquisition: Angelika Eggert, Matthias Selbach, Nils Blüthgen.

Investigation: Mathurin Dorel, Tommaso Mari.

Methodology: Bertram Klinger, Anja Sieber.

Project administration: Nils Blüthgen.

Resources: Matthias Ziehm, Falk Hertwig, Johannes H. Schulte.

Software: Mathurin Dorel, Bertram Klinger, Nils Blüthgen.

Supervision: Bertram Klinger, Dieter Beule, Angelika Eggert, Johannes H. Schulte, Matthias Selbach, Nils Blüthgen.

Visualization: Mathurin Dorel.

Writing – original draft: Mathurin Dorel.

Writing – review & editing: Bertram Klinger, Nils Blüthgen.

References

1. De Bernardi B, Nicolas B, Boni L, Indolfi P, Carli M, Di Montezemolo LC, et al. Disseminated neuroblastoma in children older than one year at diagnosis: Comparable results with three consecutive high-dose protocols adopted by the Italian Co-Operative Group for Neuroblastoma. *Journal of Clinical Oncology*. 2003; 21(8):1592–1601. <https://doi.org/10.1200/JCO.2003.05.191> PMID: 12697885
2. Maris JM, Hogarty MD, Bagatell R, Cohn SL. Neuroblastoma. *Lancet*. 2007; 369(9579):2106–2120. [https://doi.org/10.1016/S0140-6736\(07\)60983-0](https://doi.org/10.1016/S0140-6736(07)60983-0) PMID: 17586306
3. Kyo Y, Tanaka T, Hayashi K, Iehara T, Kaneko M, Hosoi H, et al. Identification of therapy-sensitive and therapy-resistant neuroblastoma subtypes in stages III, IVs and IV. *Cancer Letters*. 2011; 306(1):27–33. <https://doi.org/10.1016/j.canlet.2011.02.016> PMID: 21486686
4. Peifer M, Hartwig F, Roels F, Dreidax D, Gartlgruber M, Menon R, et al. Telomerase activation by genomic rearrangements in high-risk neuroblastoma. *Nature*. 2015; 526(7575):700–704. <https://doi.org/10.1038/nature14980> PMID: 26466568
5. Barone G, Anderson J, Pearson ADJ, Petrie K, Chesler L. New strategies in neuroblastoma: Therapeutic targeting of MYCN and ALK. *Clinical cancer research: an official journal of the American Association for Cancer Research*. 2013; 19(21):5814–21. <https://doi.org/10.1158/1078-0432.CCR-13-0680> PMID: 23965898
6. Ackermann S, Cartolano M, Hero B, Welte A, Kahlert Y, Roderwieser A, et al. A mechanistic classification of clinical phenotypes in neuroblastoma. *Science*. 2018; 362(6419):1165–1170. <https://doi.org/10.1126/science.aat6768> PMID: 30523111
7. Eleveld TF, Oldridge DA, Bernard V, Koster J, Daage LC, Diskin SJ, et al. Relapsed neuroblastomas show frequent RAS-MAPK pathway mutations. *Nature genetics*. 2015; 47(8):864–71. <https://doi.org/10.1038/ng.3333> PMID: 26121087
8. Bresler SC, Weiser DA, Huwe PJ, Park JH, Krytska K, Ryles H, et al. ALK Mutations Confer Differential Oncogenic Activation and Sensitivity to ALK Inhibition Therapy in Neuroblastoma. *Cancer Cell*. 2014; 26(5):682–694. <https://doi.org/10.1016/j.ccell.2014.09.019> PMID: 25517749
9. Hallberg B, Palmer RH. The role of the ALK receptor in cancer biology. *Annals of Oncology*. 2016; 27(suppl3):iii4–iii15. <https://doi.org/10.1093/annonc/mdw301> PMID: 27573755
10. Pugh TJ, Morozova O, Attiyeh EF, Asgharzadeh S, Wei JS, Auclair D, et al. The genetic landscape of high-risk neuroblastoma. *Nature Genetics*. 2013; 45(3):279–284. <https://doi.org/10.1038/ng.2529> PMID: 23334666
11. Johnsen JI, Dyberg C, Fransson S, Wickström M. Molecular mechanisms and therapeutic targets in neuroblastoma. *Pharmacological Research*. 2018; 131:164–176. <https://doi.org/10.1016/j.phrs.2018.02.023> PMID: 29466695
12. Britschgi A, Andraos R, Brinkhaus H, Klebba I, Romanet V, Müller U, et al. JAK2/STAT5 Inhibition Circumvents Resistance to PI3K/mTOR Blockade: A Rationale for Cotargeting These Pathways in Metastatic Breast Cancer. *Cancer Cell*. 2012; 22(6):796–811. <https://doi.org/10.1016/j.ccr.2012.10.023> PMID: 23238015
13. Klinger B, Sieber A, Fritsche-Guenther R, Witzel F, Berry L, Schumacher D, et al. Network quantification of EGFR signaling unveils potential for targeted combination therapy. *Molecular Systems Biology*. 2013; 9(1):673. <https://doi.org/10.1038/msb.2013.29> PMID: 23752269
14. Prahallad A, Sun C, Huang S, Di Nicolantonio F, Salazar R, Zecchin D, et al. Unresponsiveness of colon cancer to BRAF(V600E) inhibition through feedback activation of EGFR. *Nature*. 2012; 483(7387):100–104. <https://doi.org/10.1038/nature10868> PMID: 22281684
15. Friday BB, Yu C, Dy GK, Smith PD, Wang L, Thibodeau SN, et al. BRAF V600E disrupts AZD6244-induced abrogation of negative feedback pathways between extracellular signal-regulated kinase and Raf proteins. *Cancer Research*. 2008; 68(15):6145–6153. <https://doi.org/10.1158/0008-5472.CAN-08-1430> PMID: 18676837
16. Fritsche-Guenther R, Witzel F, Sieber A, Herr R, Schmidt N, Braun S, et al. Strong negative feedback from Erk to Raf confers robustness to MAPK signalling. *Molecular Systems Biology*. 2011; 7(1):489–489. <https://doi.org/10.1038/msb.2011.27> PMID: 21613978
17. Sturm OE, Orton R, Grindlay J, Birtwistle M, Vyshemirsky V, Gilbert D, et al. The mammalian MAPK/ERK pathway exhibits properties of a negative feedback amplifier. *Science Signaling*. 2010; 3(153):ra90–undefined. <https://doi.org/10.1126/scisignal.2001212> PMID: 21177493
18. Klinger B, Blüthgen N. Consequences of feedback in signal transduction for targeted therapies. *Biochemical Society Transactions*. 2014; 42(4):770–775. <https://doi.org/10.1042/BST20140130> PMID: 25109956

19. Woodfield SE, Zhang L, Scorsone KA, Liu Y, Zage PE. Binimetinib inhibits MEK and is effective against neuroblastoma tumor cells with low NF1 expression. *BMC cancer*. 2016; 16:172. <https://doi.org/10.1186/s12885-016-2199-z> PMID: 26925841
20. Kiessling MK, Curioni-Fontecedro A, Samaras P, Lang S, Scharl M, Aguzzi A, et al. Targeting the mTOR complex by everolimus in NRAS mutant neuroblastoma. *PLoS ONE*. 2016; 11(1):e0170851–undefined. <https://doi.org/10.1371/journal.pone.0147682> PMID: 26821351
21. Dorel M, Klinger B, Gross T, Sieber A, Prahallad A, Bosdriesz E, et al. Modelling signalling networks from perturbation data. *Bioinformatics*. 2018; 34(23):4079–4086. <https://doi.org/10.1093/bioinformatics/bty473>
22. Finch AR, Caunt CJ, Perrett RM, Tsaneva-Atanasova K, McArdle CA. Dual specificity phosphatases 10 and 16 are positive regulators of EGF-stimulated ERK activity: Indirect regulation of ERK signals by JNK/p38 selective MAPK phosphatases. *Cellular Signalling*. 2012; 24(5):1002–1011. <https://doi.org/10.1016/j.cellsig.2011.12.021> PMID: 22245064
23. Hood FE, Klinger B, Newlaczyk AU, Sieber A, Dorel M, Oliver SP, et al. Isoform-specific Ras signaling is growth factor dependent. *Molecular Biology of the Cell*. 2019; 30(9):1108–1117. <https://doi.org/10.1091/mbc.E18-10-0676> PMID: 30785867
24. Yang HW, Shin MG, Lee S, Kim JR, Park WS, Cho KH, et al. Cooperative Activation of PI3K by Ras and Rho Family Small GTPases. *Molecular Cell*. 2012; 47(2):281–290. <https://doi.org/10.1016/j.molcel.2012.05.007> PMID: 22683270
25. Corcoran RB, Ebi H, Turke AB, Coffee EM, Nishino M, Cogdill AP, et al. EGFR-mediated reactivation of MAPK signaling contributes to insensitivity of BRAF-mutant colorectal cancers to RAF inhibition with vemurafenib. *Cancer Discovery*. 2012; 2(3):227–235. <https://doi.org/10.1158/2159-8290.CD-11-0341> PMID: 22448344
26. Rozengurt E, Soares HP, Sinnett-Smith J. Suppression of feedback loops mediated by pi3k/mTOR induces multiple overactivation of compensatory pathways: An unintended consequence leading to drug resistance. *Molecular Cancer Therapeutics*. 2014; 13(11):2477–2488. <https://doi.org/10.1158/1535-7163.MCT-14-0330> PMID: 25323681
27. Lake D, Corrêa SAL, Müller J. Negative feedback regulation of the ERK1/2 MAPK pathway; 2016. Available from: <http://link.springer.com/10.1007/s00018-016-2297-8>.
28. Mertins P, Tang LC, Krug K, Clark DJ, Gritsenko MA, Chen L, et al. Reproducible workflow for multiplexed deep-scale proteome and phosphoproteome analysis of tumor tissues by liquid chromatography-mass spectrometry. *Nature Protocols*. 2018; 13(7):1632–1661. <https://doi.org/10.1038/s41596-018-0006-9> PMID: 29988108
29. Li J, Van Vranken JG, Pontano Vaites L, Schweppe DK, Huttlin EL, Etienne C, et al. TMTpro reagents: a set of isobaric labeling mass tags enables simultaneous proteome-wide measurements across 16 samples. *Nature Methods*. 2020; 17(4):399–404. <https://doi.org/10.1038/s41592-020-0781-4> PMID: 32203386
30. Shahbazian D, Roux PP, Mieulet V, Cohen MS, Raught B, Taunton J, et al. The mTOR/PI3K and MAPK pathways converge on eIF4B to control its phosphorylation and activity. *The EMBO Journal*. 2006; 25(12):2781–2791. <https://doi.org/10.1038/sj.emboj.7601166> PMID: 16763566
31. Casado P, Rodriguez-Prados JC, Cosulich SC, Guichard S, Vanhaesebroeck B, Joel S, et al. Kinase-substrate enrichment analysis provides insights into the heterogeneity of signaling pathway activation in leukemia cells; 2013. Available from: <http://www.ncbi.nlm.nih.gov/pubmed/23532336>.
32. Sjöstrom SK, Finn G, Hahn WC, Rowitch DH, Kenney AM. The Cdk1 complex plays a prime role in regulating N-myc phosphorylation and turnover in neural precursors. *Developmental Cell*. 2005; 9(3):327–338. <https://doi.org/10.1016/j.devcel.2005.07.014> PMID: 16139224
33. Gustafson WC, Meyerowitz JG, Nekritz EA, Chen J, Benes C, Charron E, et al. Drugging MYCN through an Allosteric Transition in Aurora Kinase A. *Cancer Cell*. 2014; 26(3):414–427. <https://doi.org/10.1016/j.ccr.2014.07.015> PMID: 25175806
34. Tang J, Wennerberg K, Aittokallio T. What is synergy? The Saarisekä agreement revisited; 2015. Available from: <http://journal.frontiersin.org/article/10.3389/fphar.2015.00181>.
35. Oates CJ, Hennessy BT, Lu Y, Mills GB, Mukherjee S. Network inference using steady-state data and goldbeter-koshland kinetics. *Bioinformatics*. 2012; 28(18):2342–2348. <https://doi.org/10.1093/bioinformatics/bts459> PMID: 22815361
36. Terfve CDA, Wilkes EH, Casado P, Cutillas PR, Saez-Rodriguez J. Large-scale models of signal propagation in human cells derived from discovery phosphoproteomic data. *Nature Communications*. 2015; 6(1):1–11. <https://doi.org/10.1038/ncomms9033> PMID: 26354681
37. Santra T, Kolch W, Kholodenko BN. Integrating Bayesian variable selection with Modular Response Analysis to infer biochemical network topology. *BMC systems biology*. 2013; 7:57. <https://doi.org/10.1186/1752-0509-7-57> PMID: 23829771

38. Invergo BM, Beltrao P. Reconstructing phosphorylation signalling networks from quantitative phosphoproteomic data. *Essays in Biochemistry*. 2018; 62(4):525–534. <https://doi.org/10.1042/EBC20180019> PMID: 30072490
39. Niederdorfer B, Touré V, Vazquez M, Thommesen L, Kuiper M, Lægred A, et al. Strategies to Enhance Logic Modeling-Based Cell Line-Specific Drug Synergy Prediction. *Frontiers in Physiology*. 2020; 11:862. <https://doi.org/10.3389/fphys.2020.00862> PMID: 32848834
40. Cerezo A, Guadamillas MC, Goetz JG, Sánchez-Perales S, Klein E, Assoian RK, et al. The Absence of Caveolin-1 Increases Proliferation and Anchorage-Independent Growth by a Rac-Dependent, Erk-Independent Mechanism. *Molecular and Cellular Biology*. 2009; 29(18):5046–5059. <https://doi.org/10.1128/MCB.00315-09> PMID: 19620284
41. Castro AF, Campos T, Babcock JT, Armijo ME, Martínez-Conde A, Pincheira R, et al. M-Ras induces Ral and JNK activation to regulate MEK/ERK-independent gene expression in MCF-7 breast cancer cells. *Journal of Cellular Biochemistry*. 2012; 113(4):1253–1264. <https://doi.org/10.1002/jcb.23458> PMID: 22121046
42. Korkut A, Wang W, Demir E, Aksoy BA, Jing X, Molinelli EJ, et al. Perturbation biology nominates upstream-downstream drug combinations in RAF inhibitor resistant melanoma cells. *eLife*. 2015; 4:e04640. <https://doi.org/10.7554/eLife.04640> PMID: 26284497
43. Keyomarsi K, Pardee AB. Redundant cyclin overexpression and gene amplification in breast cancer cells. *Proceedings of the National Academy of Sciences of the United States of America*. 1993; 90(3):1112–1116. <https://doi.org/10.1073/pnas.90.3.1112> PMID: 8430082
44. Sung WW, Lin YM, Wu PR, Yen HH, Lai HW, Su TC, et al. High nuclear/cytoplasmic ratio of cdk1 expression predicts poor prognosis in colorectal cancer patients. *BMC Cancer*. 2014; 14(1):951. <https://doi.org/10.1186/1471-2407-14-951> PMID: 25511643
45. Brandt R, Sell T, Lüthen M, Uhlitz F, Klinger B, Riemer P, et al. Cell type-dependent differential activation of ERK by oncogenic KRAS in colon cancer and intestinal epithelium. *Nature Communications*. 2019; 10(1):2919. <https://doi.org/10.1038/s41467-019-10954-y> PMID: 31266962
46. Saez-Rodríguez J, Blüthgen N. Personalized signaling models for personalized treatments. *Molecular Systems Biology*. 2020; 16(1):e9042–undefined. <https://doi.org/10.15252/msb.20199042> PMID: 32129942
47. Robin T, Capes-Davis A, Bairoch A. CLASTR: The Cellosaurus STR similarity search tool—A precious help for cell line authentication. *International Journal of Cancer*. 2019; 146(5):1299–1306. <https://doi.org/10.1002/ijc.32639> PMID: 31444973
48. Li H. Aligning sequence reads, clone sequences and assembly contigs with BWA-MEM. *arXiv.org*. 2013;.
49. Faust GG, Hall IM. SAMBLASTER: fast duplicate marking and structural variant read extraction. *Bioinformatics*. 2014; 30(17):2503–2505. <https://doi.org/10.1093/bioinformatics/btu314> PMID: 24812344
50. Talevich E, Shain AH, Botton T, Bastian BC. CNVkit: Genome-Wide Copy Number Detection and Visualization from Targeted DNA Sequencing. *PLOS Computational Biology*. 2016; 12(4):e1004873. <https://doi.org/10.1371/journal.pcbi.1004873> PMID: 27100738
51. Kim S, Scheffler K, Halpern AL, Bekritsky MA, Noh E, Källberg M, et al. Strelka2: fast and accurate calling of germline and somatic variants. *Nature Methods*. 2018; 15(8):591–594. <https://doi.org/10.1038/s41592-018-0051-x> PMID: 30013048
52. Auton A, Abecasis GR, Altshuler DM, Durbin RM, Bentley DR, Chakravarti A, et al. A global reference for human genetic variation; 2015. Available from: <http://www.nature.com/articles/nature15393>.
53. Fu W, O'Connor TD, Jun G, Kang HM, Abecasis G, Leal SM, et al. Analysis of 6,515 exomes reveals the recent origin of most human protein-coding variants. *Nature*. 2013; 493(7431):216–220. <https://doi.org/10.1038/nature11690> PMID: 23201682
54. Dobin A, Davis CA, Schlesinger F, Drenkow J, Zaleski C, Jha S, et al. STAR: Ultrafast universal RNA-seq aligner. *Bioinformatics*. 2013; 29(1):15–21. <https://doi.org/10.1093/bioinformatics/bts635> PMID: 23104886
55. Liao Y, Smyth GK, Shi W. FeatureCounts: An efficient general purpose program for assigning sequence reads to genomic features. *Bioinformatics*. 2014; 30(7):923–930. <https://doi.org/10.1093/bioinformatics/btt656> PMID: 24227677
56. Ianevski A, He L, Aittokallio T, Tang J. SynergyFinder: A web application for analyzing drug combination dose-response matrix data. *Bioinformatics*. 2017; 33(15):2413–2415. <https://doi.org/10.1093/bioinformatics/btx162> PMID: 28379339
57. Yan L. MK-2206: A potent oral allosteric AKT inhibitor. *Cancer Research*. 2009; 69(9 Supplement): DDT01–1.

58. Hughes CS, Moggridge S, Müller T, Sorensen PH, Morin GB, Krijgsveld J. Single-pot, solid-phase-enhanced sample preparation for proteomics experiments. *Nature Protocols*. 2019; 14(1):68–85. <https://doi.org/10.1038/s41596-018-0082-x> PMID: 30464214
59. Bath TS, Francavilla C, Olsen JV. Off-line high-pH reversed-phase fractionation for in-depth phospho-proteomics. *Journal of Proteome Research*. 2014; 13(12):6176–6186. <https://doi.org/10.1021/pr500893m> PMID: 25338131
60. Tyanova S, Temu T, Cox J. The MaxQuant computational platform for mass spectrometry-based shotgun proteomics. *Nature Protocols*. 2016; 11(12):2301–2319. <https://doi.org/10.1038/nprot.2016.136> PMID: 27809316
61. Ritchie ME, Phipson B, Wu D, Hu Y, Law CW, Shi W, et al. Limma powers differential expression analyses for RNA-sequencing and microarray studies. *Nucleic Acids Research*. 2015; 43(7):e47. <https://doi.org/10.1093/nar/gkv007> PMID: 25605792
62. Hornbeck PV, Zhang B, Murray B, Kornhauser JM, Latham V, Skrzypek E. PhosphoSitePlus, 2014: Mutations, PTMs and recalibrations. *Nucleic Acids Research*. 2015; 43(D1):D512–D520. <https://doi.org/10.1093/nar/gku1267> PMID: 25514926

Lebenslauf

Mein Lebenslauf wird aus datenschutzrechtlichen Gründen in der elektronischen Version meiner Arbeit nicht veröffentlicht.

Komplette Publikationsliste

- Akpa, C.A., Kleo, K., Oker, E., Tomaszewski, N., **Messerschmidt**, C., López, C., Wagener, R., Oehl-Huber, K., Dettmer, K., Schoeler, A., Lenze, D., Oefner, P.J., Beule, D., Siebert, R., Capper, D., Dimitrova, L., Hummel, M., 2020. Acquired resistance to DZNep-mediated apoptosis is associated with copy number gains of AHCY in a B-cell lymphoma model. *BMC Cancer* 20, 1–12. <https://doi.org/10.1186/s12885-020-06937-8> (Impact factor 2019: 3.150)
- Blanc, E., Holtgrewe, M., Dhamodaran, A., **Messerschmidt**, C., Willimsky, G., Blankenstein, T., Beule, D., 2019. Identification and ranking of recurrent neo-epitopes in cancer. *BMC Med. Genomics* 12, 171. <https://doi.org/10.1101/389437> (Impact factor 2019: 2.570)
- Dorel, M., Klinger, B., Mari, T., Toedling, J., Blanc, E., **Messerschmidt**, C., Nadler-Holly, M., Ziehm, M., Sieber, A., Hertwig, F., Beule, D., Eggert, A., Schulte, J.H., Selbach, M., Blüthgen, N., 2021. Neuroblastoma signalling models unveil combination therapies targeting feedback-mediated resistance. *PLOS Comput. Biol.* 17, e1009515. <https://doi.org/10.1371/journal.pcbi.1009515> (Impact factor 2020: 4.475)
- Holtgrewe, M., **Messerschmidt**, C., Nieminen, M., Beule, D., 2019. Digestiflow: from BCL to FASTQ with ease. *Bioinformatics* 36, 1983–1985. <https://doi.org/10.1093/bioinformatics/btz850> (Impact factor 2019: 5.610)
- Lamping, M., Benary, M., Leyvraz, S., **Messerschmidt**, C., Blanc, E., Kessler, T., Schütte, M., Lenze, D., Jöhrens, K., Burock, S., Klinghammer, K., Ochsenreither, S., Sers, C., Schäfer, R., Tinhofer, I., Beule, D., Klauschen, F., Yaspo, M.L., Keilholz, U., Rieke, D.T., 2020. Support of a molecular tumour board by an evidence-based decision management system for precision oncology. *Eur. J. Cancer* 127, 41–51. <https://doi.org/10.1016/j.ejca.2019.12.017> (Impact factor 2020: 9.162)
- Messerschmidt**, C., Foddiss, M., Blumenau, S., Müller, S., Bentele, K., Holtgrewe, M., Kun-Rodrigues, C., Alonso, I., do Carmo Macario, M., Morgadinho, A.S., Velon, A.G., Santo, G., Santana, I., Mönkäre, S., Kuuluvainen, L., Schleutker, J., Pöyhönen, M., Myllykangas, L., Senatore, A., Berchtold, D., Winek, K., Meisel, A., Pavlovic, A., Kostic, V., Dobricic, V., Lohmann, E., Hanagasi, H., Guven, G., Bilgic, B., Bras, J., Guerreiro, R., Beule, D., Dirnagl, U., Sassi, C., 2021. PHACTR1 genetic variability is not critical in small vessel ischemic disease patients and PcomA recruitment in C57BL/6J mice. *Sci. Rep.* 11, 1–11. <https://doi.org/10.1038/s41598-021-84919-x> (Impact factor 2021: 4.996)
- Messerschmidt**, C., Holtgrewe, M., Beule, D., 2017. HLA-MA: simple yet powerful matching of samples using HLA typing results. *Bioinformatics* 33, 2241–2242. <https://doi.org/10.1093/BIOINFORMATICS/BTX132> (Impact factor 2017: 5.481)
- Messerschmidt**, C., Obermayer, B., Klinghammer, K., Ochsenreither, S., Treue, D.,

- Stenzinger, A., Glimm, H., Fröhling, S., Kindler, T., Brandts, C.H., Schulze-Osthoff, K., Weichert, W., Tinhofer, I., Klauschen, F., Keilholz, U., Beule, D., Rieke, D.T., 2020. Distinct immune evasion in APOBEC-enriched, HPV-negative HNSCC. *Int. J. Cancer* 147, 2293–2302. <https://doi.org/10.1002/ijc.33123> (Impact factor 2019: 5.145)
- Obermayer, B., Holtgrewe, M., Nieminen, M., **Messerschmidt, C.**, Beule, D., 2020. SCelVis: Exploratory single cell data analysis on the desktop and in the cloud. *PeerJ* 8. <https://doi.org/10.7717/PEERJ.8607> (Impact factor 2020: 2.379)
- Peitz, C., Sprüssel, A., Linke, R.B., Astrahantseff, K., Grimaldi, M., Schmelz, K., Toedling, J., Schulte, J.H., Fischer, M., **Messerschmidt, C.**, Beule, D., Keilholz, U., Eggert, A., Deubzer, H.E., Lodrini, M., 2020. Multiplexed Quantification of Four Neuroblastoma DNA Targets in a Single Droplet Digital PCR Reaction. *J. Mol. Diagnostics* 22, 1309–1323. <https://doi.org/10.1016/j.jmoldx.2020.07.006> (Impact factor 2020: 5.568)
- Quinn, H.M., Vogel, R., Popp, O., Mertins, P., Lan, L., **Messerschmidt, C.**, Landshammer, A., Lisek, K., Château-Joubert, S., Marangoni, E., Koren, E., Fuchs, Y., Birchmeier, W., 2021. YAP and β -Catenin cooperate to drive oncogenesis in basal breast cancer. *Cancer Res.* 81, 2116–2127. <https://doi.org/10.1158/0008-5472.CAN-20-2801> (Impact factor 2021: 13.312)
- Schumann, F., Blanc, E., **Messerschmidt, C.**, Blankenstein, T., Busse, A., Beule, D., 2019. SigsPack, a package for cancer mutational signatures. *BMC Bioinformatics* 20. <https://doi.org/10.1186/s12859-019-3043-7> (Impact factor 2019: 3.242)
- Seidel, E., Walenda, G., **Messerschmidt, C.**, Obermayer, B., Peitzsch, M., Wallace, P., Bahethi, R., Yoo, T., Choi, M., Schrade, P., Bachmann, S., Liebisch, G., Eisenhofer, G., Beule, D., Scholl, U.I., 2020. Generation and characterization of a mitotane-resistant adrenocortical cell line. *Endocr. Connect.* 9, 122–134. <https://doi.org/10.1530/EC-19-0510> (Impact factor 2020: 2.592)
- Thole, T.M., Toedling, J., Sprüssel, A., Pfeil, S., Savelyeva, L., Capper, D., **Messerschmidt, C.**, Beule, D., Groeneveld-Krentz, S., Eckert, C., Gambará, G., Henssen, A.G., Finkler, S., Schulte, J.H., Sieber, A., Bluethgen, N., Regenbrecht, C.R.A., Künkele, A., Lodrini, M., Eggert, A., Deubzer, H.E., 2020. Reflection of neuroblastoma intratumor heterogeneity in the new OHC-NB1 disease model. *Int. J. Cancer* 146, 1031–1041. <https://doi.org/10.1002/ijc.32572> (Impact factor 2020: 7.396)

Danksagung

An dieser Stelle möchte ich allen Menschen danken, die mich bei der Anfertigung meiner Dissertation unterstützt haben. Insbesondere gilt mein Dank Prof. Dieter Beule, ohne den diese Arbeit nicht möglich gewesen wäre. Desweiteren danke ich Prof. Nils Blüthgen, Prof. Ulf Leser und Prof. Christine Sers für die Unterstützung während meiner Zeit im Graduiertenkolleg compcancer. Danken möchten ich außerdem allen KollegInnen und FreundInnen, die mich auf diesem Weg begleitet haben.

Meiner Frau danke ich für ihre Unterstützung und ihre Geduld, welche ich manchmal überstrapaziert habe. Ebenso gilt meiner ganzen Familie großer Dank dafür, dass sie mich geerdet und nach Rückschlägen wieder aufgebaut hat.

